Development and Characterization of a Co-culture Model of Head and Neck Cancer Using Bioprintable Decellularized Extracellular Matrix Bioinks

Jacqueline Kort Mascort

Bioengineering Department, Faculty of Engineering, McGill University, Montreal

April 2023

A thesis submitted to McGill University in partial fulfillment of the requirements of the degree of Ph.D. in Biological and Biomedical Engineering

Table of Contents

Abstract

To fully understand the mechanistic synergy of the tumor microenvironment (TME) and improve current therapeutic strategies, diverse approaches have been used to recapitulate cancer *in-vivo* and *in-vitro*. The development of 3D *in-vitro* models has been conducive to a diverse collection of 3D cultures that, using multiple fabrication techniques, biomaterials, and cells, have been able to recreate one or several aspects of the TME such as the 3D architecture, the inclusion of stromal and neoplastic components, and a mechanically and biologically relevant extracellular matrix (ECM). The ECM has been reported as a critical component in the development and progression of neoplastic diseases. Hence, having an accurate biomechanically fitting representation of it in *in-vitro* cancer models is crucial to promote a tissue-like environment in culture. Several materials, both natural and synthetic, have been proposed to fulfill this need. Decellularized extracellular matrices (dECMs) in particular, have been of great interest for their bioactive properties. dECMs have been shown to promote cell development, differentiation, cell-matrix interactions, and can be processed into thermo-sensitive gels that can encapsulate cells. Here, we have formulated a composite bioink containing dECM derived from porcine tongue and alginate and gelatin as rheological modifiers to develop a highly bioprintable material that can be used to fabricate head and neck cancer (HNSCC) models *in-vitro* using extrusion bioprinting techniques. We have fully characterized this bioink's mechanical properties and proven that our material has a comparable Young's modulus to that observed in HNSCC tumors *in-vivo*. We also quantified its biochemical composition and cellular encapsulation capabilities. We have bioprinted monoculture constructs with UM-SCC-12 and UM-SCC-38 head and neck

cancer cell lines and vocal fold fibroblasts (HVFFs). Monocultures have shown relevant morphology and cell development over 19 days with high cell viability. The cancer models have been used to perform drug testing experiments with cisplatin and 5-fluorouracil, relevant standard-of-care chemotherapeutic drugs. A significant increase in IC_{50} was observed in the 3D printed cultures compared to the traditional 2D culture assay.

In efforts to complement the monoculture cancer model with a stromal component, we developed and characterized a co-culture model with both UM-SCC-38 cancer cells and HVFFs. Over 19 days, morphology evolves into tightly packed cancer spheroids that are sheathed by HVFFs that tend to position in the periphery. Having cancer cells in the center and the stroma in the perimeter is a behavior commonly reported *in-vivo*. We also observed significant changes in collagen and MMP (matrix metalloproteinase) expression for 22 days of co-culture, which can be attributed to the presence of fibroblasts. These changes reinforce the dependency on the stromal component during cancer development and prove the importance of developing *in-vitro* cancer models that mimic the complexity and heterogeneity of the TME.

Résumé

Pour comprendre la synergie mécaniste du microenvironment tumoral et améliorer les techniques thérapeutiques actuelles, différentes approches ont été mise en oeuvre pour reproduire un modèle de cancer *in-vivo* et *in-vitro*. Grâce à l'utilisation de biomatériaux, cellules et diverses techniques de fabrication, différents modèles de culture 3D *in-vitro* ont été élaboré. Ces modèles ont permis de reproduire un ou plusieurs aspects du microenvironnement tumoral en reproduisant l'architecture 3D, une matrice extracellulaire (MEC) possédant des propriétés mécaniques et biologiques d'intérêts, et en incorporant des composants du stroma et caractéristiques de la néoplasie. La MEC ayant été identifiée comme élément clé dans le développement et la progression des maladies néoplasiques, il est essentiel d'avoir une représentation biomécanique précise de celle-ci dans les modèles de cancer *in-vitro* afin de reproduire fidèlement l'environnement tissulaire en culture. Pour répondre à ce besoin, différents matériaux, naturels ou synthétiques, ont été étudié. Les matrices extracellulaires décellularisées sont particulièrement prometteuses en raison de leurs propriétés bioactives qui favorisent le développement, la differentiation ainsi que les interactions cellulaires, et peuvent également être transformées en gel thermosensibles pouvant encapsuler des cellules.

Ici, nous avons élaboré une bio-encre composée d'une matrice extracellulaire decéllularisée dérivée de langue de porc, associée à de l'alginate et de la gélatine pour modifier ses propriétés rhéologiques. Ce matériau permet de créer des modèles de cancers des voies aérodigestives supérieures *in-vitro* en utilisant une technique d'impression par extrusion. Nous avons étudié les propriétés mécaniques de cette bio-encre et montré que notre matériau présente un module élastique de Young similaire à celui observé dans les

tumeurs de cancers des voies aérodigestives supérieures. Nous avons également quantifié sa composition biochimique et son potentiel d'encapsulation cellulaire. Nous avons bio-imprimé des monocultures avec des lignées cellulaires de cancers des voies aérodigestives supérieures UM-SCC-12 et UM-SCC-38 et des fibroblastes des cordes vocales (HVFFs). Au cours d'une période de 19 jours, le développement cellulaire et morphologique des monocultures a été favorable, avec une viabilité cellulaire élevée. Des expériences ont été réalisé afin de tester les effets du cisplatine et du 5-flurouracil, médicaments chimio-thérapeutiques standards, sur les modèles de cancer élaborés. Une différence significative a pu être observée entre la concentration inhibitrice médiane CI50 des cultures imprimées en 3D et celle des cultures cellulaires en 2D.

Afin de compléter le modèle de monoculture cancéreuse avec un composant du stroma, nous avons développé et caractérisé un modèle de co-culture de cellules cancéreuses UM-SCC-38 et de fibroblastes des cordes vocales. Au cours de 19 jours, la morphologie a évolué vers des sphéroïdes cancéreux compacts enveloppés par des fibroblastes des cordes vocales se positionnant en périphérie; cette répartition spatiale est un phénomène commun *in-vivo*. Au cours de 22 jours de co-culture, nous avons également observé des changements significatifs dans l'expression de collagène et des métalloprotéinases matricielles, qui peuvent être expliqués par la présence des fibroblastes. Ces changements renforcent la dépendance du développement des modèles de cancer *in-vitro* à l'égard du stroma et démontrent l'importance de développer des modèles reproduisant la complexité et l'hétérogénéité du microenvironnement tumoral.

Acknowledgments

I want to thank my family, particularly my mom, who has always reassured me that I can complete any objective I set for myself. For her unconditional love and support throughout my degree and academic career and for always trusting my decisions, which sometimes meant keeping us apart. To my brother and my sister, who cheered me up and were always very proud of me and curious about my Ph.D. project.

Next, I thank Salvador, my husband, and my colleague. He was my constant support in this journey and always provided good insight and feedback during difficult times and cheered for me. I could not have done this without you.

Also, I want to thank Matt, my primary supervisor, who gave me the opportunity to dedicate several years to science. He helped me become the researcher and scientist I am today and gave me insights and support when needed. Thank you for believing in me and giving me the freedom to pursue my project on topics I was passionate about.

I want also to thank Simon, my co-supervisor. I appreciate all your assistance and help throughout these years.

Additionally, I thank the members of my Ph.D. committee, Satya Prakash, Nicole Li-Jessen, and Showan Nazhat. I appreciated your insights, suggestions, and willingness to help me and my project succeed.

Also, I thank all my friends and colleagues Tao Jiang, Gil Munguia, Omar Peza, Joyce Jang, Molly Shen, Guangyu Bao, Michelle Tran, Maria Orjuela-Laverde, Linda Balabanian, Haruka Yoshie, Mahsa Jalali, Juanjuan Liu, this experience would not have been the same without you.

I thank all the technicians, staff members, and collaborators, including Denis Flipo, Greg Bonnamour, Xavier Elisseeff, Audrey Ferlatte, Cleber Silveira Moraes, Kelly Sears, Luc Arsenault, Kurt Dejgaard.

I want to finally thank all the funding sources that made my project possible. FRQNT (Fonds de recherche du Québec), McGill University, NSERC (Natural Sciences and Engineering Research Council of Canada), CIHR (Canadian Institutes of Health Research)

Contribution to original knowledge

During my doctoral studies, I established novel methodologies, material formulations, and processes leading to the development of a bioprinted *in-vitro* co-culture model of tumor epithelial cells and stromal fibroblasts in a mechanically defined decellularized ECM hydrogel. My original contributions based on the publications that resulted from this project are presented below.

In my first peer-reviewed article (Chapter 3), I formulated a composite hydrogel containing dECM components, alginate, a seaweed-derived polysaccharide, and gelatin, denatured collagen. This material was used to bioprint cell-laden HNSCC constructs compatible with drug testing experiments. I developed methods to decellularize and solubilize tongue tissue to form an extrudable dECM hydrogel. This bioink permitted the reseeding with new cells, showing the processing protocol's success. I reinforced this material with alginate and gelatin as rheological modifiers to make the hydrogel compatible with extrusion bioprinting. I tested several formulations until I found a combination that allowed successful fabrication of 3D cultures, stability during long-term culture, permitted cell development with high cell viability, and had similar mechanical characteristics to the tissue of study. Cell viability remained above 90% over the three weeks of culture. This setup produced spheroids of at least 3000μm^2 of cross-sectional area by day 15 of culture. This composite was designed to replicate head and neck cancer (HNSCC) tumors, but its mechanics can be tuned by changing the w/v ratio of its constituents for other applications or requirements. The bioink was thoroughly characterized mechanically and biochemically using rheology, atomic force microscopy, mass spectrometry, etc. The 3D monoculture allowed the testing of chemotherapeutic

drugs (cisplatin and 5-fluorouracil), showing higher IC_{50} levels in 3D cultures against the 2D culture groups. A 4-fold increase in the IC_{50} of cisplatin and an 80-fold increase for 5-fluorouracil were observed in the 3D constructs compared to monolayer cultures.

In my second research article (Chapter 4), I developed a heterogenous HNSCC model using neoplastic cells (UM-SCC-38) and fibroblasts (HVFF) to promote and observe cancer-stromal interactions and their influence on spheroid growth, changes in matrix collagen and the regulation of matrix proteases. This model was fabricated using extrusion bioprinting and showed morphological changes and development over time. I took the time to characterize this model in detail since it is crucial to comprehend its behavior before its use for drug discovery, personalized therapy, or translational studies. This model provides the tools to recapitulate characteristics of HNSCC *in-vitro* and allows us to study its evolution through time. Contributions of the stroma and ECM leading to chemotherapeutic resistance caused by the acellular and cellular components of the stroma are directly observable or can be obtained by sampling secreted factors. Following the deposition of the co-culture model, we observed UM-SCC-38 spheroid formation that began during the first week in culture and continued over a three-week period in which the fibroblasts settled directly surrounding each spheroid. It is compatible with commonly used quantification techniques such as confocal and scanning electron microscopy, colorimetric assays, and fluorescent labeling. Using a Luminex assay to quantify matrix metalloproteases in co-cultures compared to monocultures, we observed significant differences in MMP-9 and MMP-10 expression corresponding to periods of the culture in which collagen underwent remodeling. It is an in-between scenario between 2D cultures and animal models that permits modification and tailoring according to the

needs of the study. It has the possibility to be tuned for other types of cancer and is proposed as an alternative tool to test novel drug treatments for HNSCC.

Finally, I had the opportunity to publish a literature review focused on dECM hydrogels (Section 2.2). The intent of writing it was to provide a basic but thorough understanding of dECM hydrogels, their characteristics, considerations to have before using them, and how several groups across the globe have used them in different applications. This article focuses on use cases and provides practical knowledge to engineer dECM hydrogels for the desired application. I propose these processed tissues as materials we can tailor, characterize, and use in diverse applications. I view this contribution as a timely addition to the literature since dECM hydrogels appeal to groups with interdisciplinary backgrounds. I envision this article being a guide for someone who is not an expert in the field but is interested in it and would like to know all the critical characteristics of dECM hydrogels before working with them.

Contribution of authors

For the three articles included in this thesis, the contribution of the authors is listed below:

1. **Review Article: Decellularized ECM hydrogels: Prior Use Considerations, Applications, and Opportunities in Tissue Engineering and Biofabrication**

   Jacqueline Kort-Mascort, Salvador Flores-Torres, Omar Peza-Chavez, Joyce Jang, Lucas Antonio Pardo, Simon D. Tran, Joseph Kinsella

   JKM, as the first author, proposed the topic, did an in-depth literature review, proposed a table of contents, and wrote the first draft. She also revised the final version and modified it according to the reviewers' comments when submitted for publication.

   SFT collaborated with the section "Instabilities if dECM Hydrogels" and helped with the final draft's careful revision and section arrangement.

   OPC collaborated with the section "Mechanically Stable dECM Hydrogels" and helped with a detailed revision final draft.

   JJ assisted with the "Applications of dECM hydrogels" section and revised the article before publication.

   LAP helped with the section "Physical Characteristics of dECM Hydrogels" and revised the article prior to publication.

   SDT and **JK,** as the supervisors of this project, contributed with their insight in planning the article, its scope, and the topics included. They also were constantly revising the manuscript until ready for publication.

2. Research Article No. 1: Decellularized extracellular matrix composite hydrogel bioinks for the development of 3D bioprinted head and neck *in-vitro* tumor models

Jacqueline Kort-Mascort, Guangyu Bao, Osama Elkashty, Salvador Flores-Torres, Jose G. Munguia-Lopez, Tao Jiang, Allen J. Ehrlicher, Luc Mongeau, Simon D. Tran, Joseph M. Kinsella

JKM as the first author, designed and performed all the experiments, analysis, and writing of this manuscript except for the contributions listed for other authors below. She did the literature review, revised the final version, and modified it according to the reviewers' comments when submitted for publication.

GB assisted with the atomic force microscopy experiments and revised the manuscript in detail prior to publication.

OE aided with the histological processing, staining, and pathological assessment.

SFT, JGML, and TJ aided with experimental design and reviewed the first final draft.

AJE, and LM complemented the manuscript with their expertise and reviewed the final version of the manuscript.

SDT and **JK,** as the supervisors of this project, contributed with their insights, experimental design, and constant revising of the manuscript until ready for publication.

3. Research Article No. 2: Bioprinted cancer-stromal *in-vitro* models in a decellularized ECM-based bioink exhibit progressive remodeling and maturation.

Jacqueline Kort-Mascort, Molly L. Shen, Emma Martin, Salvador Flores-Torres, Lucas Antonio Pardo, Peter M. Siegel, Simon D. Tran, Joseph Kinsella.

JKM as the first author, designed and performed all the experiments, analysis, and writing of this manuscript except for the contributions listed for other authors below. She did the literature review, revised the final version, and modified it according to the reviewers' comments when submitted for publication.

MLS assisted with the cell transduction and reviewed the first final draft.

EM helped with the topographical characterization of the materials and revised the manuscript in detail before submission.

SFT aided with experimental design and reviewed the first final draft.

LAP collaborated on the microscopy acquisition and detailed revision of the manuscript.

PMS complemented the manuscript with his expertise and reviewed the final version of the manuscript.

SDT and **JK,** as the supervisors of this project, contributed with their insights, experimental design, and constant revising of the manuscript until ready for submission.

Lists of figures and tables

Figures and tables are grouped by article.

Decellularized ECM hydrogels: Prior Use Considerations, Applications, and Opportunities in Tissue Engineering and Biofabrication

List of Figures

List of Tables

Decellularized extracellular matrix composite hydrogel bioinks for the development of 3D bioprinted head and neck in-vitro tumor models

List of Figures

List of Tables

Bioprinted cancer-stromal in-vitro models in a decellularized ECM-based bioink exhibit progressive remodeling and maturation.

List of Figures

Thesis abbreviations

- 2D, two dimensional
- 3D, three dimensional
- 4D, four dimensional
- 5-FU, 5-fluorouracil
- ACN, acetonitrile
- ANOVA, analysis of variance
- AV, aortic valve
- bFGF, basic fibroblast growth factor
- BSA, bovine serum albumin
- CAFs, cancer-associated fibroblasts
- C-ES, cell-electrospinning
- CM, cardiomyocytes
- CN, cellulose nanoparticles
- CPCs, cardiac progenitor cells
- DAPI, 4′,6-diamidino-2-phenylindole
- dECM, decellularized extracellular matrix
- dECMT, decellularized extracellular matrix from tongue
- DLP, digital Light Processing
- DMEM, Dulbecco's modified Eagle medium
- DMMB, dimethylmethylene blue; DNAse, deoxyribonuclease
- DNA, deoxyribonucleic acid
- DPBS, Dulbecco′s phosphate buffered saline

- EBB, extrusion-based bioprinting
- ECM, extracellular matrix
- EMT, epithelial-mesenchymal transition
- EVs, extracellular vesibles
- FBGCs, foreign body giant cells
- FBR, foreign body reaction
- FDA, Food and Drug Asministration
- FGF, fibroblast growth factor
- FWHM, full width at half maximum
- GA, glutaraldehyde
- GAG, glycosaminoglycans
- GelMA, gelatin methacryloyl
- GLP, Good Laboratory Practices
- GMP, Good Manufacturing Practices
- H&E, hematoxylin and eosin
- hASCs, human adipose-derived stem cells
- hBMSCs, human bone mesenchymal stem cells
- HCD, higher-energy C-trap dissociation
- HFIP, hexafluoro-2-propanol
- HIFs, hypoxia-inducible factors
- hiPSC, human induced pluripotent stem cell (hiPSC)
- HMEC human dermal microvascular endothelial cells
- HNSCC, head and neck squamous cell carcinomas
- HPV, human papillomavirus (HPV)

- HT, high throughput
- HTK, histidine-tryptophan-ketoglutarate
- HVFF, human vocal fold fibroblast
- IC50, half-maximal inhibitory concentration
- iCM, induced pluripotent stem cell derived cardiomyocytes
- IL4, interleukin 4
- LC/MS/MS, liquid Chromatography with tandem mass spectrometry
- LOX, lysyl oxidase
- LVR, linear viscoelastic region
- MAA, methacrylic anhydride
- MelHA, methacrylated hyaluronic acid
- MI, myocardial infarction
- MMP, matrix metalloproteinases
- MS/MS, tandem mass spectrometry
- MSCs, mesenchymal stem cells
- PBS, phosphate buffered saline
- PBT, polybutylene terephthalate
- PCL, polycaprolactone
- PCL, polycaprolactone;
- PD-1, programmed cell death protein 1
- PEG, polyethylene glycol
- PEG-DA , poly(ethylene glycol) diacrylate
- PEO, polyethylene oxide
- PERV, porcine endogenous retrovirus

- PLGA, poly(lactic-co-glycolic acid)
- PVA, polyvinyl alcohol
- RFP, red fluorescent protein
- RNAse, ribonuclease
- ROI, region of interest
- RRX, rhodamine red-X
- SCAP, human apical papilla derived mesenchymal stem cells
- SDS, sodium dodecyl sulfate
- SEM, scanning electron microscopy
- sGAG, sulfated glycosaminoglycans
- SIS, small intestinal submucosa
- STR, short tandem repeat
- TGF-β1, transforming growth factor beta 1
- TIMP, tissue inhibitor of metalloproteinase
- TME, tumor microenvironment
- TSP-1, thrombospondin 1
- UHPLC, ultra-high-performance liquid chromatography
- UV, ultraviolet radiation
- UVA, ultraviolet radiation A
- UW, University of Wisconsin
- VEGF, Vascular endothelial growth factor
- WST, water soluble tetrazolium salts

1. Introduction

Squamous cancer of the head and neck (HNSCC) is a family of cancers often associated with tobacco and alcohol use but can also occur in the presence of human papillomavirus (HPV).[1,2] In its early stages, HNSCC is treated with chemotherapy, surgery, and radiotherapy. Still, in late stages, traditional treatment methods result in 50% cancer relapse after two years of treatment, poor prognosis, and secondary effects such as mucositis, dermatitis, and dysphagia, etc.[3] Conventional *in-vitro* cell culture systems, and preclinical small animal models, that mechanistically study cancer biology suffer from restricted outputs due to the lack of interactions between the tumor epithelial and tumor-associated stromal cells and the tumor microenvironment (TME) present in human tumors.[4,5] Furthermore, research in preclinical small animal models has been proven to be an important but incomplete tool due to species-dependent physiological differences, compromised immune response, and dissimilar protein expression profiles.[6-9]

Alternative tools such as tissue-engineered *in-vitro* tumor models[10] have been developed, including 3D hydrogel culture systems,[5,11,12] spheroid, and organoid culture,[13] and organ-on-a-chip[10,13,14] platforms. 3D bioprinting offers the potential to create models with the user-defined placement of cell types, cell density, and scaffold materials (bioinks).[15,16] Several bioinks have been proposed using synthetic hydrogels.[17,18] Still, these often fail to replicate the biochemical and biomechanical complexity found in native ECM, resulting in a lack of intrinsic physiological function.[19] dECM is a tissue-derived material that has shown bioactive (inductive) behaviour[19], including the promotion of cell proliferation, differentiation,[20] cell-ECM,[21] and cell-cell interactions.

Extrusion bioprinting has shown the capability to create 3D constructs at a scale and time that is relevant for clinical and biomedical applications,[22] and for dECM hydrogels, is a very popular biofabrication method.[23] Extrusion of dECM hydrogels has been successfully used to develop different healthy and pathological tissue constructs,[24-27] cancer models,[28] grafts,[29] and organ-on-a-chip models[30] *in-vitro*. dECM hydrogels tend to have reduced mechanical properties when compared to the tissue of origin due to the decellularization and solubilization process required to fabricate them. To overcome the lack of mechanical and structural stability of dECM hydrogels, many strategies have been developed to improve their interaction between chains, molecular structure, and formulations, [31-33] making them more compatible materials for extrusion bioprinting.

In this thesis, my main aim is to develop a heterogenous HNSCC model using extrusion bioprinting techniques. I hypothesize that co-cultures of epithelial and stromal cells encapsulated within a bioink containing dECM will provide an environment with crucial characteristics found *in-vivo*. This model will result in a biomimetic *in-vitro* platform that can be used for drug discovery and translational research.

To accomplish this, I divided my project into three aims:

- **Aim 1:** Develop and characterize an extrudable physiologically relevant cell-laden hydrogel bioink.
- **Aim 2:** Fabricate and validate a three-dimensional printed (3DP) monoculture *in-vitro* model of HNSCC and evaluate tumor response to chemotherapeutic treatment.
- **Aim 3:** Fabricate and validate a three-dimensional (3D) bioprinted co-culture *in-vitro* model of HNSCC.

In the next chapter (Chapter 2), a review of relevant literature is presented before moving into the findings obtained in this project.

In Chapter 3, the article goes over the completion of Aims 1 and 2. I formulate and characterize a bioprintable ink that contains reinforced dECM hydrogel with alginate and gelatin as rheological modifiers. I encapsulated HNSCC cells and developed the cultures for several weeks until they were challenged with standard-of-care chemotherapeutic agents for HNSCC. In Chapter 4, the article focuses on Aim 3. To replicate the cancer-stromal environment, I fabricated a heterogenous HNSCC model containing both HNSCC cells and fibroblasts. I made sure to characterize this model to present it as a tool for drug discovery and translational studies. Each scientific article has a connecting section to ensure a logical progression and linking the findings to the project's primary goal. Chapter 5 includes the discussions and conclusions of the project.

2. Literature review

2.1. Head and neck cancer

Head and neck cancer (HNSCC) is a family of neoplastic diseases that arise from the head and neck region.[34] In 2018, HNSCC was the 11th cancer by incidence in Canada.[35] Worldwide, it is estimated that 800,000 patients were diagnosed with this disease in 2020.[36] The majority of HNSCC are squamous cell carcinomas that arise from the mucosa or four main sites: the pharynx, larynx, sinonasal cavity, and oral cavity.[34] In Canada, these cancers are three times more prevalent in men than women.[35] Their incidence in old adults is associated with heavy use of tobacco and alcohol.[37,38] Cases caused by contact with toxic substances are slowly declining in developed countries but continue to increase in non-developed countries.[39] The presence of human papillomavirus (HPV), especially HPV type 16, has also been linked to the development of oropharyngeal cancer.[40] HPV-associated HNSCC cases have risen in adults located in North America and Europe.[39] The population can be protected from HPV-16 with the HPV vaccines so it is possible that vaccination could also prevent the development of oropharyngeal cancer.[41]

Treatment must be chosen according to the stage, surgical accessibility, and anatomical site since vital organs are very close together in the head and neck region. Structure, function preservation, quality of life, age, and preferences of the patient are also considered. Surgery and radiotherapy have successfully treated and controlled early-stage (stage I and II) HNSCC with long-term survival rates of 70 to 90% of patients. However, more than 60% of patients arrive at the clinic with locally advanced tumors (stage III and IV). Tumors have invaded locally, and metastasis to regional nodes can be present. In these cases, there is a risk of up to 40% of local recurrence and less than 50% 5-year

overall survival. Advanced head and neck cancer treatment generally includes surgery followed by radiotherapy or chemotherapy. When surgery is not feasible, chemotherapy has been used as the standard of care approach for HNSCC. Concomitant radiotherapy with chemotherapy has been reported to decrease the 5-year mortality by 6.5% compared with chemotherapy alone.

Cisplatin is the standard chemotherapeutic agent to treat HNSCC.[42] High-dose cisplatin is generally administered to young patients with no additional complications, while carboplatin is used for patients with existing conditions, but it is less effective than cisplatin.[43] Both drugs are taxane-based and prevent DNA replication of highly proliferative cells, such as cancer cells. Other chemotherapeutic agents, such as 5-fluorouracil, and docetaxel have been used to treat HNSCC.[43] In 2006, Cetuximab, a targeted therapy antibody that binds to the epidermal growth factor receptor, was approved for clinical use when administered with radiotherapy since it improved patients' survival compared to radiotherapy alone.[44] Anti-PD-1 immunotherapies such as pembrolizumab and nivolumab were approved by the Food and Drug Administration (FDA) in 2016 for showing improvements in patients with metastatic HNSCC that have received platinum treatments.[44,45] Despite the progress in correctly diagnosing and treating patients with several approaches, 50-60% of late-stage HNSCC patients present recurrence or distant metastasis.[43,46] Hence, efforts to find more efficient therapies are crucial to treat this and other neoplastic diseases.

Novel approaches to treat cancer are still being developed, and targeted therapies such as immunotherapy are still in their infancy. However, robust and biomimetic pre-clinical models are required to test these therapies before moving forward with clinical trials. In

2022 the FDA passed the FDA Modernization Act 2.0, which allows the use of alternative pre-clinical models, such as cell assays and computational models, to prove the effectiveness and safety of a drug. Previously, 3D *in-vitro* cancer models have been proposed as alternatives to animal pre-clinical models. These models can be used in a semi or high-throughput manner, allowing the testing of multiple treatments in parallel and being an intermediate model between the simplified 2D cultures and animal models, which can recapitulate relevant aspects of the disease *in-vitro*. With these regulation changes, technologies such as microfluidic systems, tumor spheroids, and bioprinted models become even more relevant to accelerate the discovery and approval process to later proceed with clinical trials. *In-vitro* models, when correctly characterized and designed, can help shorten the current 8-year bottleneck between drug discovery and approval, providing more options with hopefully better outcomes for patients.[47]

In this thesis, we used 3D extrusion printing techniques to fabricate a heterogenous head and neck cancer model. To simulate the extracellular matrix (ECM) *in-vitro,* we propose using dECM hydrogels. In the upcoming chapter, a review article presents in detail what dECM hydrogels are, the considerations before use, advantages, limitations, and applications for tissue engineering and building microenvironments *in-vitro*.

2.2. Decellularized ECM hydrogels: Prior Use Considerations, Applications, and Opportunities in Tissue Engineering and Biofabrication

This article was published in Biomaterials Science, Royal Society of Chemistry, on the 2nd of December 2020. DOI: **https://doi.org/10.1039/D2BM01273A**

Authors: Jacqueline Kort-Mascort[a], Salvador Flores-Torres[a], Omar Peza-Chavez[a], Joyce Jang[a], Lucas Antonio Pardo[a], Simon D. Tran[b], Joseph Kinsella[a*]

joseph.kinsella@mcgill.ca

[a] Department of Bioengineering, McGill University, Montreal, Quebec, Canada.

[b] Faculty of Dental Medicine and Oral Health Sciences, McGill University, Montreal, Quebec, Canada.

ABSTRACT

Tissue development, wound healing, pathogenesis, regeneration, and homeostasis rely upon coordinated and dynamic spatial and temporal remodeling of extracellular matrix (ECM) molecules. ECM reorganization and normal physiological tissue function, require the establishment and maintenance of biological, chemical, and mechanical feedback mechanisms directed by cell-matrix interactions. To replicate the physical and biological environment provided by the ECM *in-vivo,* methods have been developed to decellularize and solubilize tissues which yield organ and tissue-specific bioactive hydrogels. While these biomaterials retain several important traits of the native ECM, the decellularizing process, and subsequent sterilization, and solubilization result in fragmented, cleaved, or partially denatured macromolecules. The final product has decreased viscosity, moduli, and yield strength, when compared to the source tissue, limiting the compatibility of

isolated decellularized ECM (dECM) hydrogels with fabrication methods such as extrusion bioprinting. This review describes the physical and bioactive characteristics of dECM hydrogels and their role as biomaterials for biofabrication. In this work, critical variables when selecting the appropriate tissue source and extraction methods are identified. Common manual and automated fabrication techniques compatible with dECM hydrogels are described and compared. Fabrication and post-manufacturing challenges presented by the dECM hydrogels decreased mechanical and structural stability are discussed as well as circumvention strategies. We further highlight and provide examples of the use of dECM hydrogels in tissue engineering and their role in fabricating complex *in-vitro* 3D microenvironments.

2.2.1. Introduction

The extracellular matrix is a complex three-dimensional array of macromolecular components. In mammals, this non-cellular environment is composed by an organ-dependant combination of approximately 300 different types of proteins, which are referred as the core matrisome.(1) This collection of proteins includes collagens, proteoglycans, and glycoproteins. Additionally, other molecules such as carbohydrates, growth factors, cytokines, and ECM-modifying enzymes may also be present in the ECM.(1) Apart from providing structural support to tissues, the ECM develops and remodels in cooperation with cells, sustaining a biomolecular balance that dictates cell survival, function, differentiation, motility, and polarity to maintain tissue homeostasis.(1, 2) Given the critical functions imparted by the ECM, it is an indispensable component for simulating the tissue microenvironment *in-vitro*.

Attempts to replicate the ECM for *in-vitro* 3D cell culture, or as a tissue engineering scaffold, have yielded a multitude of novel materials both synthetic and naturally derived(3). However, due to the structural and macromolecular complexity and ongoing reorganization characteristic of the ECM it is challenging to create analogous materials.(4) Synthetic materials, although scalable and easily reproducible, often do not contain the complete spectrum of protein domains that mediate cell-matrix adhesions or the signaling molecules that regulate and promote the distribution, activation, polarization, and proliferation of cells.(2) The lack of these ECM ligands can negatively impact cell development since several pathways are dependent on ligand specific cell-ECM adhesions.(5, 6) Naturally derived materials, in particular ECM-hydrogels, retain an array of bioactive components which allow cell-matrix interactions. ECM hydrogels are tissue-derived and can be prepared by decellularizing the organ of interest, and solubilizing it to form a hydrogel, which preserves the intrinsic biochemical complexity of the tissue of origin.(7) This top-down approach suggests being a suitable alternative to biochemically mimic the ECM *in-vitro* because of ECM hydrogel's capacity to influence remodelling, differentiation, and cell behavior. However, challenges related to batch-to-batch variability and the lack of structural integrity due to the enzymatic or mechanical processes when preparing ECM-hydrogels have to be assessed as these materials possess reduced mechanical and viscoelastic properties.(8)

Here, we review the defining characteristics of dECM hydrogels, their physical and bioinductive properties, the variables that must be considered when developing dECM-hydrogels, techniques commonly used to fabricate dECM-constructs and how this material has been proposed for tissue engineering applications and to build

microenvironments *in-vitro* to recapitulate aspects present in the tissue microenvironment *in-vivo*. (Fig. 1). Commercial possibilities of these materials and the current challenges of translating ECM derived materials are also addressed. Lastly, we present the emerging potential of dECM-hydrogels as a promising alternative to current biomaterials used in biofabrication. For a more detailed review of non-hydrogel decellularized extracellular matrices, we invite the reader to refer to these publications.(9-13)

2.2.2. ***Decellularized ECM hydrogels***

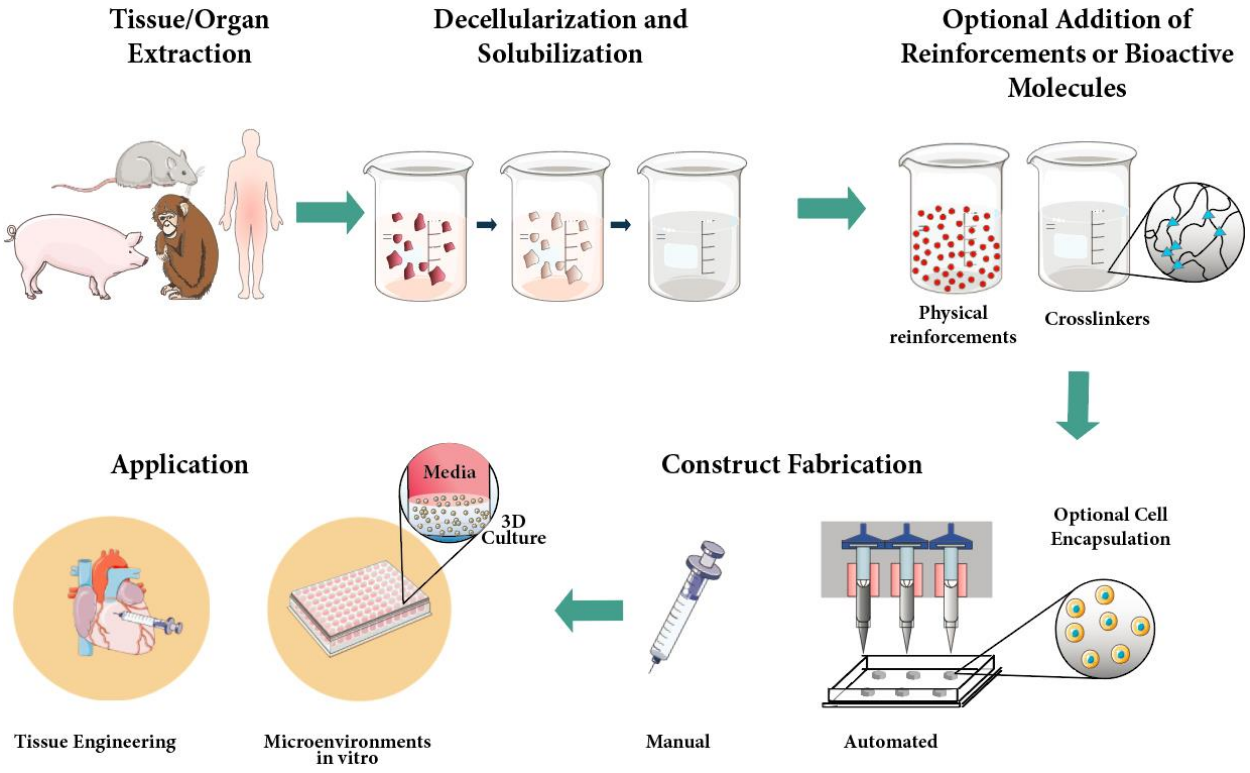

Fig. 1: Preparation and Applications of dECM Hydrogels *dECM hydrogels are prepared by extracting tissue which is decellularized and solubilized to form a thermosensitive hydrogel which can be mechanically reinforced or complemented with bioactive molecules. These hydrogels can be used to fabricate 3D constructs with manual and/or automatic techniques which allow cell encapsulation if desired. The constructs can be used for tissue engineering*

applications or to create 3D microenvironments in-vitro for applications in discovery or translational medicine. The Figure was partly generated using Servier Medical Art, provided by Servier, licensed under a Creative Commons Attribution 3.0 unported license.

Tissue decellularization consists of removing native cells from the tissue or organ of interest while preserving the structure and composition of the ECM.(14) It can be done by perfusing whole organs or by constantly agitating small pieces of tissue.(15) Briefly, decellularization consists in a combination of physical, enzymatic, and chemical processes that can include washes with detergents, enzymes, and buffers.(10, 14) The decellularized tissue is commonly solubilized by enzymatic digestion(16, 17) or more recently by ultrasonic cavitation.(18) Solubilization results in a gel that physically crosslinks at physiological temperature, attributed by collagen self-assembly mechanisms.(7, 19, 20) The final reconstituted product of the decellularization and solubilization process results in a bioactive and cytocompatible hydrogel.(21)

Some tissues require additional steps prior to decellularization since some native tissue components can make ECM isolation more challenging. For example, tissues with significant fat content are generally subjected to a delipidation step to extract the lipid components while maintaining the proteins.(22) Chloroform, acetone, and methanol have been reported as solvents for lipid extraction.(23, 24) Triton X-100, a non-ionic detergent, has also been used to disturb the lipid-lipid and lipid-protein interactions.(9, 25) Another example is bone tissue which is often exposed to a demineralization step, generally performed by acid extraction, to remove mineral content from the tissue.(26) Hydrochloric acid (HCl) and EDTA are commonly used as decalcifying agents.(22, 26) The demineralization of bone has been shown to not affect the osteoconductive properties

of the tissue and there are even commercially available products approved for clinical use.(27)

Physical characteristics of dECM hydrogels

Decellularization and solubilization protocols may have substantial effects on the native extracellular matrix (ECM) resulting in changes in the physical properties of the final product (Fig. 2 a.-b). Decellularized kidneys,(28) corneas,(8) cardiac tissue,(29) and bone(30) have reported significant structural changes in the final acellular material when processed using different protocols. dECM hydrogels have a randomly oriented fibrillar structure, characterized by an angular network alignment close to 0%, and interconnecting pores comparable to the morphology present in collagen I gels.(8, 26, 31) The density of fiber intersections is directly correlated to the storage modulus of the dECM hydrogel, and it is significantly different depending on the tissue source and processing methods.(31)

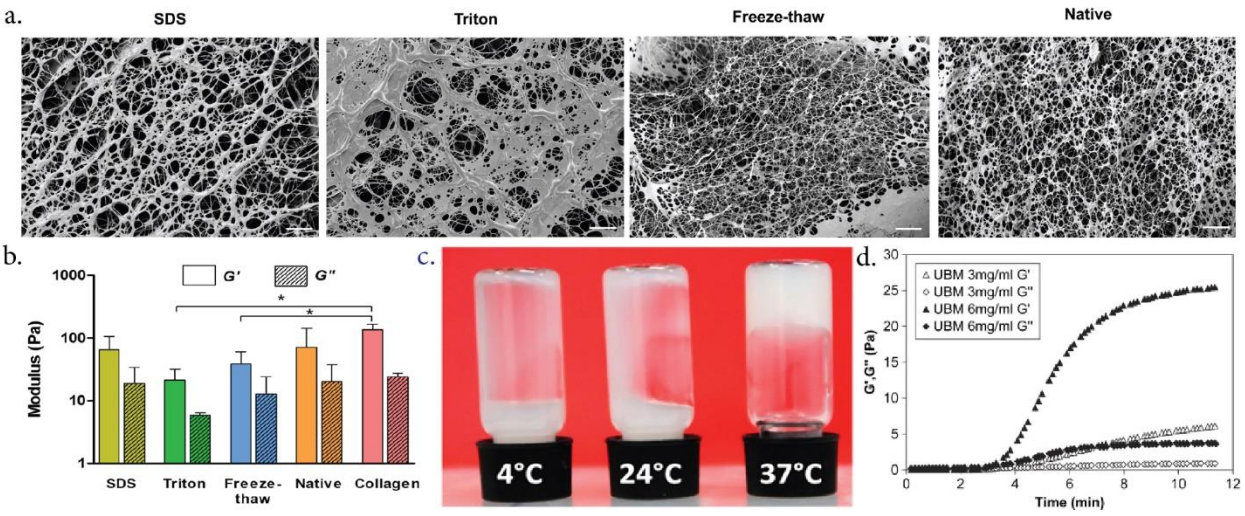

Fig. 2: Physical Characteristics of dECM Hydrogels

a. CryoSEM micrographs and b. Storage and loss moduli of corneal dECM hydrogels that were processed with different decellularization methods. Reproduced from ref. (8) with permission from Springer Nature, Copyright 2019. -1000x Scale bar:10μm. c. Inversion test of tongue dECM hydrogel at different temperatures. Reproduced from ref.(32) with permission from American Chemistry Society, Copyright 2021. d. Gelation kinetics of urinary bladder dECM hydrogels at two different concentrations.(33) Gels were loaded on the rheometer at 15°C. Temperature was set to 37°C for the test. Reproduced from ref. (33) with permission from Elsevier, Copyright 2008.

In addition to the fiber orientation and topography, the characteristics of the pores created or retained during processing becomes increasingly important as pore size and pore volume can influence cell infiltration, migration and organization.(34, 35) Due to size exclusion, pores greater than 100 μm can contribute to cell infiltration and attachment.(36) They are also useful for the transport of nutrients, metabolites, and large biomolecules, but may compromise mechanical properties.(37)

When incubated at physiological temperature and pH, an increase in the turbidity of dECM hydrogels is observed(38, 39) as a result of polymerization of soluble ECM into an

insoluble hydrogel network.(38) Turbidity changes have been reported to plateau after 24h of incubation at 37 °C for dECM hydrogels indicating completion of the sol-to-gel transition within this timescale.(38) Similar turbidity changes reported in pure collagen I and fibrin hydrogels have been attributed to the fibril and network formation of these proteins during and following gelation.(40, 41) As turbidity influences the optical characteristics of the gels, thus adequate controls and calibration must be considered when performing quantitative assays or imaging.

dECM hydrogels are viscoelastic and display shear-thinning behavior resulting in a decrease in viscosity when high shear stress is applied.(42) This property makes them compatible with extrusion-based bioprinting and other fabrication techniques as the reduced viscosity allows for extrusion at lower pressures. The shear thinning property is also beneficial when cells are encapsulated since the pressure required to extrude a shear thinning material is lower than a shear thickening material.(43) Lower printing pressures can retain cellular viability during the printing process.(44) Increasing the dECM concentration in a gel can increase the viscosity of the material, without losing its shear-thinning property.(45)

Fabrication techniques benefit from materials that have a fast recovery after shear since it promotes shape retention and structural fidelity.(46) It has been reported that concentrated dECM hydrogels have an increased viscosity recovery after high shear stress is applied.(47) Viscosity recovery is attributed to the reforming of the fibril network after the high shear stress is removed.(48) Studies have shown that incorporating rheological modifiers such as silk fibroin, methylcellulose, or alginate can shorten the material's recovery time.(49-51)

The magnitude of the complex modulus of dECM hydrogels depends on the tissue source and it is deeply impacted by the selected decellularization and solubilization techniques.(8, 32, 42, 45) Biofabrication techniques often rely on viscoelastic hydrogels with thermal dependencies. dECM hydrogels exhibit distinctive rheological features at different temperatures. Higher storage moduli have been observed in dECM hydrogels at temperatures between 4 °C – 37 °C degrees when compared to loss moduli. Moreover, a decrease in the loss factor can be observed when the material is heated from 4 °C to 37 °C.(32, 42, 52) This difference can be attributed to thermal crosslinking and gelation processes. Collagen self-assembles as temperature rises, thus increasing the stiffness of the gel (Fig. 2 d.).(7, 33) Thermal crosslinking can be easily observed when performing an inversion test under different temperature conditions (Fig. 2 c.).(32, 42) dECM hydrogel stabilization after thermal crosslinking at 37 °C should occur in a time frame that is compatible with cell culture and fabrication techniques. Faster gelation time increases the shape fidelity during fabrication but can also lead to instrument clogging, thus controlling this property influences the fabrication process.(53) Due to the naturally slow gelation of dECM-hydrogels,(53) supplementing with materials such as gelatin,(54) alginate,(55) and poly (ethylene glycol)-diacrylate(56) have been devised to control gelation kinetics of dECM-containing gels. This fine tuning enables cells to be dispersed within the material in its weaker state followed by thermal crosslinking of the dECM resulting in high cell viability after encapsulation. Alternatively, photopolymerizers such as vitamin B2(57) or PEG-DA(56) have been used to photocrosslink and polymerize dECM hydrogels when exposed to long-wavelength UVA light during the 3D fabrication process, increasing the mechanical properties and allowing dECM gels to be utilized in photolithographic fabrication methods.(58)

Through the use of the stress-strain curves obtained from rheological studies, it is possible to calculate the compressive or elastic moduli of dECM hydrogels.(59-61) The concentration of dry weight of dECM in the hydrogel is directly proportional to the magnitude of its elastic modulus.(45) Studies have compared both the compressive and Young's moduli of dECM hydrogels derived from various sources such as the liver(60), cardiac tissue,(59) and bone.(61) A significant difference in moduli can be observed when comparing dECM containing biomaterials versus the native tissue.(60)

dECM hydrogels from different sources have been physically characterized and even though some properties such as shear-thinning and thermal crosslinking capabilities are consistent among differently prepared materials, characteristics such as elastic modulus, porosity, and viscosity are heavily influenced by the tissue source, the protocol and reagents used to decellularize and solubilize the hydrogel, and the concentration at which it was prepared. For that reason, every batch should be properly characterized to successfully understand and optimize the material for the desired application and fabrication technique.

Bioactive characteristics of dECM hydrogels

Composition

The processes used to decellularize and solubilize the tissue can significantly impact the preservation of the intrinsic properties of the native tissue. dECM hydrogels are composed of structural and functional proteins, glycosaminoglycans, and proteoglycans with a distinctive biomolecular fingerprint.(62) This collection of proteins can vary significantly between different species, donor's health, age, and other pre-existing

conditions. The impact of these variables in the final dECM product is covered in detail in section 3. However, there are some ECM components commonly present in dECM hydrogels regardless of the tissue source(63) which are discussed in this section.

Liquid chromatography-tandem mass spectroscopy (LC-MS/MS) has been used to obtain the protein profile of the ECM and dECM hydrogels(7). In general, dECMs are high in collagen,(62) the most abundant protein in animals and one of the main components of the basal lamina. In tissues, collagen serves as a structural component and regulates tissue development and migration.(64) There are more than 28 types of collagens identified in animals and their relative concentration within a specific tissue can contribute to physical and biological properties providing environmental conditions that promote cellular development.(65, 66) The Badylak lab, has compared the biochemical characteristics of several tissue sources in decellularized powders, sheets, and gels.(62) When looking at the presence of soluble collagen between dermis, spinal cord, brain, and urinary bladder ECM, the dermis contained significantly higher concentrations when compared to the other samples.(31, 67)

dECM also contains fibronectin, a dimeric glycoprotein that binds to cells through integrins, which are transmembrane cell-surface receptors, and simultaneously to other ECM molecules such as collagen, heparin, and fibrin.(68) These interactions make fibronectin a key contributor in cell modulations within the ECM and its activity has been linked to cell migration, growth, adhesion, and differentiation.(65, 68, 69)

Laminins are cross-shaped glycoproteins which are heavily present in the basal lamina and mediate the adhesion between cells and the ECM via integrin-binding.(65) *In-vitro*, laminin aggregates and forms mesh-like structures which are cation induced and are

attributed to the calcium binding sites present in this glycoprotein.(70, 71) A study comparing decellularized porcine subcutaneous and visceral adipose tissue observed the presence of laminin, collagen I, and collagen VI in both samples(72). Collagen I expression was higher in the subcutaneous adipose tissue, but collagen VI and laminin expression were higher in the visceral adipose tissues.(72) Decellularization methods frequently diminish the integrity and functionality of isolated laminins as they are highly crosslinked and suffer from degradation under the ionic, pH, and mechanical conditions employed. Ionic detergents such as sodium dodecyl sulfate (SDS) are considered effective, but harsh since they can denature important ligands and proteins in the dECM(73).

Glycosaminoglycans (GAGs) (7, 16, 31) are linear and negatively charged polysaccharides that when sulfated and covalently attached to a core protein are called proteoglycans (PGs).(74) The GAG region of these proteoglycans interacts with several structural proteins including laminin, collagen, and fibronectin(74) thus, contributing to the organization and formation of the ECM. Due to their conformation and secondary structure, GAGs occupy a significant volume attracting and retaining large amounts of water due to the negative charge of the sulfate or carboxyl groups present in these molecules.(75, 76) They attract osmotically active ions such as Na^+ creating a swelling structure that allows the ECM to withstand compressive forces.(75) They also interact with chemokines, cytokines, growth factors, and cell surface receptors making them active participants during development, cell migration and differentiation(77). They are also present in the basement membrane of mammalian tissues where they influence its permeability and architecture.(74) The content of GAGs in decellularized tissue is dependent on the source tissue. Differences in sulfated glycosaminoglycan (sGAG)

concentrations between tissues may contribute to differences in the mechanical properties of dECM gels as has been reported when comparing tissues with lower GAG in their ECM such as dermal tissue relative to tissues with higher GAG content such as the urinary bladder.(7, 31) A depletion of GAGs has been reported in dECM samples relative to the source tissue; this reduction is generally attributed to the detergent processing.(78, 79) Examples of decellularized tissues that have reported the presence of GAGs include the lung,(80) small intestinal submucosa,(16) pericardium,(79) cartilage,(81) tracheal mucosa,(82) intervertebral discs,(83) adipose tissue,(84) liver,(85) spinal cord,(86) bone,(86)dentine,(86) and umbilical cord.(87)

Other bioactive molecules reported in dECMs include cytokines, growth factors, and vesicles. Even though they do not directly provide structural or mechanical support, these remain biologically active, and can contribute to the regulation of multiple biochemical and mechanotransduction pathways that modulate immune response, wound healing, cell proliferation, remodelling, and differentiation.(21) Presence of active molecules such as vascular endothelial growth factor (VEGF), an angiogenic inducing molecule, has been reported in decellularized small intestinal submucosa and it allowed tube formation on human dermal microvascular endothelial cells (HMEC)(88). Angiogenesis-related proteins have been detected in decellularized aortic tissue and small intestinal submucosa. All 55 proteins were detected in the samples with fibroblast growth factor (FGF)1 and FGF being more abundant in the small intestinal submucosa sample.(89) Thrombospondin-1 (TSP1), an ECM glycoprotein with antiangiogenic properties,(90) was significantly more abundant in all samples when compared to the rest of the proteins in the array.(89) Another study used decellularized human adipose tissue and extracted

transforming growth factor beta (TGF-β1), insulin-like growth factor 1 (IGF-1), basic fibroblast growth factor (bFGF) , and VEGF from the matrix.(91) Other decellularized tissues reporting the presence of growth factors include nerve grafts,(92) pancreas,(93) kidney,(94) placenta,(95) brain(95), liver,(96) etc.

Extracellular matrix vesicles (EVs) are membrane carriers between 40 and 5000 nm in size that are released by cells.(97) EVs contain biologic material such as proteins or nucleic acids, and can be categorized as microvesicles, exosomes and apoptotic bodies depending on their size, site of origin, releasing mechanism, and morphology.(98, 99) EVs have been shown to play an active role in communication by transferring cargo between cells (100) and influence several healthy and pathological processes such as angiogenesis,(101) cell differentiation,(102) cancer progression,(103, 104) immune response,(105, 106) and epithelial to mesenchymal transition.(107) Matrix-bound nanovesicles have been found in acellular decellularized extracellular matrices derived from urinary bladder, sub-intestinal submucosa, and dermis.(108) These EVs were present in the matrix after being in contact with enzymatic, chemical, detergent chemicals, and protected genetic material from the nucleases used when decellularizing. These vesicles contained microRNA, which is known for having phenotypical and functional effects in cells and can recapitulate some of the biologic characteristics of the source tissue. In this study the microRNA affected macrophage surface marker expression and neural cell differentiation.

Cell-ECM interactions

For the microenvironment to function harmoniously, a synergy between the encapsulated cells and the ECM is required.(6) Cells create connections to the ECM through integrins,

a family of transmembrane proteins, that later mature into stable focal adhesion (FA) sites.(109, 110) These connections serve to sense the biophysical cues that drive cell behaviour.(6, 110) This bidirectional interaction between cells and ECM is referred to as dynamic reciprocity.(111) Integrins are the bridge that connects cells with different ECM proteins including collagen and fibronectin(110). Traction forces generated by cells during migration can affect the conformation of fibronectin promoting its elongation, bundling and fibril formation stiffening the ECM causing a resistance to yield.(6, 112) Fibronectin can elongate more than 8-fold increasing the fiber stiffness from 50 kPa to 1-2 MPa.(113) This can be attributed to the exposure of cryptic sites which form cryptic bonds increasing the fiber's resistance.(113) Collagen reorganization can also be triggered by cells actively generating forces to shift and realign the fibers.(114) Cell-secreted factors can also alter and remodel the ECM. The lysyl oxidase (LOX) enzyme family can mediate collagen crosslinking increasing matrix rigidity.(115) Cells can detect these changes in matrix resistance which results in changes in cell morphology, proliferation, and rearrangement of actin fibers.(116) On the other hand, matrix metalloproteinases (MMPs), such as collagenases and gelatinases are enzymes secreted by cells that can cleave collagens unfolding regions of the triple helix.(117) An upregulation of MMPs has been associated with disease progression since it allows cancer cell invasion by breaking cell-cell and cell-ECM adhesions, degrading ECM proteins, and promoting angiogenesis; allowing founder cells to move out into the stroma and distant tissues.(118-120) Presence of non-structural proteins involved in cell-ECM interactions such as MMPs, tenascins, and thrombospondins has been reported in decellularized tissues.(80, 121) However, more research is needed to verify how viable are these molecules after the decellularization process and how they influence the reseeding of the dECM tissues.

Cellular differentiation

Stem cells are a progeny of cells that have a pluripotent nature that allows them to transform into any cell lineages when specific cues are present in the environment.(122, 123) This plasticity helps maintain tissue homeostasis by replenishing cells when needed for tissue growth, regeneration, or wound healing.(122) With the growing interest of developing stem-cell therapies for applications such as cancer, degenerative diseases, tissue regeneration etc., understanding their function and how to successfully culture and efficiently differentiate them *in-vitro* is of critical importance.(123) *In-vivo*, the bioinductive properties of the ECM play a major role in guiding differentiation and lineage maintenance due to the dynamic biophysical and biochemical characteristics during development, wound healing, and regeneration.(123, 124) Hence, to replicate and drive a controlled differentiation *in-vitro,* a 3D culture with cell-cell and cell-ECM interactions are a requisite.(124) dECM materials used to encapsulate stem cells should contain bioactive molecules that allow cell attachment, induce signal transduction, and have a mechanical integrity similar to the tissue of interest.(124)

Neural stem/progenitor cells (NSPCs) encapsulated in a porcine dECM hydrogel derived from spinal cord have shown a higher degree of differentiation into neurons after one week compared to cells embedded in porcine dECM hydrogel from peripheral nerves and in collagen I.(125) Differentiation could be attributed either to the higher porosity in the spinal cord dECM that promoted higher viability, proliferation, and migration in the early stage of the 3D culture or to the modulation of integrin α2, α9, and β1 expression profiles and protein kinase B (Akt) /extracellular signal-regulated kinase (ERK) signaling pathways.(125) Also, a significant increase in the expression of differentiation genes was

quantified in human bone mesenchymal stem cells (hBMSCs) cultured on annulus fibrosus dECM hydrogel compared to the collagen I group.(126) Human apical papilla derived mesenchymal stem cells (SCAP) were encapsulated in bone, spinal cord, and dentine dECM hydrogels and only bone and spinal cord groups expressed neural lineage markers with a higher response in the spinal cord group.(86) Other examples of dECM tissue hydrogels that promoted differentiation of cells include human umbilical cord,(87) porcine urinary bladder,(33, 67) spinal cord,(67) brain,(67) heart,(127, 128), cartilage,(42) and adipose tissue(33)

Nature has evolved the ECM to coordinate with the cellular components of tissues via a series of biochemical, biophysical and regulatory networks based on sensing, transducing, and adapting the composition, spatial, and temporal properties known as dynamic reciprocity. This foundational characteristic enables the complex composition of ECM to be adaptive to its environment. When source tissues with known characteristics are used to create dECM hydrogels, they can retain several key elements that drive dynamic reciprocity (binding domains, focal adhesion complexes, etc.) that can influence mechanical or biochemical responses. More research must be done to fully understand the potential that dECM hydrogels have in modulating and mediating cell behaviour.

2.2.3. Selecting the appropriate ECM

Tissue and organ specific bioactive components found within dECM hydrogels create a physiological-like extracellular microenvironment that can encapsulate several types of cells while considering important biological and physical properties of the desired tissue. dECM materials can induce directed differentiation towards specific cell types by

mimicking the *in-vivo* developmental conditions or the biological and biophysical properties experienced during regeneration or disease. When considering the application of dECM as a tissue engineering matrix or bioink, specific criteria of the source ECM including tissue age, species of origin, and health must be considered. These factors may have significant effects on the function, viability, growth, and morphology of cells being encapsulated or cultured.

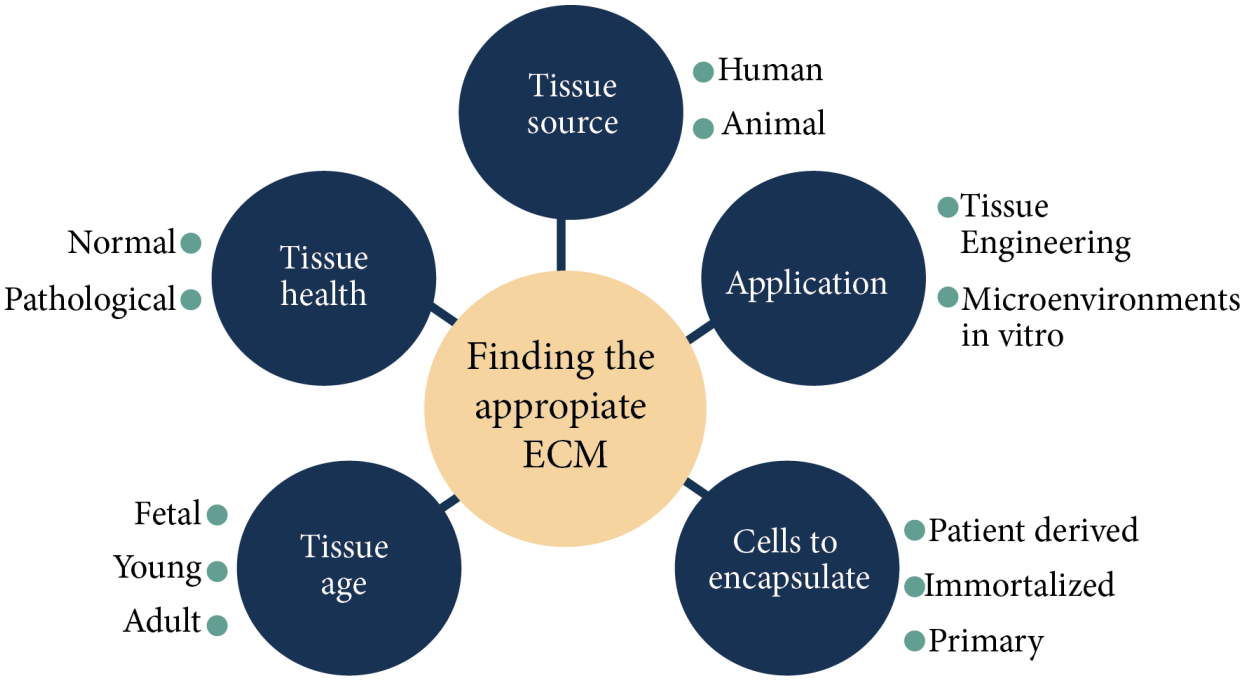

Fig. 3: Variables to consider when selecting the appropriate ECM to fabricate dECM hydrogels.

Tissue source

It is ideal to decellularize autologous or allogenic tissue, but specifically for human tissues, availability can be limiting. However, several groups have reported the use of human-derived dECM obtained from donated, damaged, diseased, or cadaveric tissues. These

include skin,(129, 130) teeth,(131) lungs,(132) liver,(133, 134) kidney,(135) heart,(136) cartilage,(137) ovarian,(138) among others. (62, 139)

Xenografts have been a suitable solution to the shortage of human tissue for research or clinical applications. A major source of tissue for dECM applications comes from pigs due to their availability, size, and genetic relatedness.(140) To date more than 80 FDA-approved products are animal derived and have been successfully used over the past decades including porcine liver, dermis, small intestine, and urinary bladder.(63) Decellularization of several porcine organs has been reported including skin,(141) heart,(142) liver,(143) small intestinal submucosa,(144) bladder,(145) etc. It is important to mention that due to pig's genomic similarity, there is a risk of acquiring infectious diseases including porcine endogenous retrovirus (PERV).(146) Rodent tissue has also been decellularized, but the low yield of tissue per animal makes it challenging to acquire dECM hydrogels at scale. Other species such as cow(147) and goat(148) have been successfully decellularized.

After decellularization, ECM of the same organ or tissue, but sourced from a different species (i.e., porcine vs human), has been reported to have similarities including ECM protein composition, shear thinning behaviour and self-assembly while presenting significant differences apart from the genetic disparity such as sGAG content and complex moduli.(149) Comparing decellularized human umbilical cord hydrogels with porcine bladder, brain, and spinal cord hydrogels resulted in materials with similar mechanical and biological properties.(87) Mesenchymal stem cells (MSCs) cultured in each of these sources of dECM gels display similar migration patterns and guided differentiation of

neural stem cells with axonal outgrowth *in-vitro*. However, higher proliferation rates and higher sGAG content were observed in the umbilical cord samples.(87)

Successfully decellularized tissues have a decreased number of antigenic epitopes compared to the tissue prior to decellularization (150) which allows the material to be used clinically with limited rejection. Implantation of ECM products to reconstruct or repair injured, or missing tissues is an approach that requires the implantable material to promote an immune response that facilitates an anti-inflammatory macrophage response. The main limitation of dECM is the presence of foreign antigens present in allogenic and xenogeneic tissues that can trigger an inflammatory immune response when implanted. Macrophages are known to be among the first respondents in the host response to pathogens, injury, or implantation of foreign biomaterials and are key players in tissue-remodelling. Activated macrophages can present either the M1-phenotype, which is associated with a pro-inflammatory response, or the M2-phenotype which is linked with the anti-inflammatory response, tissue repair and wound healing.(150) Macrophage's response to ECM hydrogels can vary greatly depending on the differences in the decellularization process and residual detergents. A study reported that in general, ECM induces an M2-like phenotype, but studies of M1-phenotype expression of macrophages exposed to liver ECM and skeletal muscle ECM have been reported.(151)

Tissue age

When selecting source ECM, it is necessary to consider the age, condition, and organ of interest. It has been shown that ECM from the same organ has significantly different composition and characteristics dependant on the age of the mammal and differences in ECM crosslinking, fibrosis, growth factor and sGAG content may be substantial and

impact cell development and function.(152, 153) The Badylak group compared the structural, mechanical, and compositional properties of small intestinal submucosa (SIS) derived from pigs and found that depending on the desired characteristics of the ECM, the age of the animal should be considered.(153) They found that for the best mechanical properties, the SIS tissue should be harvested from an animal of at least 12 weeks of age but no more than 52 weeks. If an abundance of sGAG content is of interest, ECM between 3 and 12 weeks of age should be considered as the ECM expression is greatest in younger specimens. Increased metabolic activity was observed in all ECM groups when compared to the non-ECM containing control group. However, stem cells showed equivalent migration towards ECM samples between 2 to 26 weeks of age, but in lower amount towards the 52-week-old samples.(153) Decellularized monkey kidneys also determined that the age of the donor is a key factor on the efficient recellularization where the youngest group outperformed older donors. Higher cell infiltration and repopulation in younger kidneys can be attributed to the ECM remodelling that occurs as the animals develop(154). Differences in ECM composition, such as higher concentration of adipose tissue, ECM crosslinking, and fibrosis has also been reported in aged human hearts.(149, 155) These ECM changes can be indicators of the increased tissue stiffness as the source ages.(155) Another study created hydrogels containing dECM from rat hearts at three different stages of development and reported significant differences in MSCs ability to create traction forces depending on the dECM's age and hydrogel stiffness.(156) They also showed increased stiffness in the adult group when compared with the neonatal and fetal samples.(156) If human tissue is repurposed into dECM hydrogels, there may be important differences from aged, mature, and young donors. Apart from age, the storage conditions of the tissue and collection time before decellularization can also impact its

mechanical properties. Especially with human samples, a significant amount of time may pass between the death and the harvesting of the tissue for decellularization. Rheological studies done on porcine liver stored in three different preservation solutions for periods between 5 and 53 hours show good preservation in all solutions for the first 11 hours. An increase in complex moduli over time is observed when samples are stored in Lactated Ringer or University of Wisconsin (UW) solutions, but no significant increase when stored in Histidine-Tryptophan-Ketoglutarate (HTK) solution.(157) These examples showing significant changes in matrix composition and mechanics should not be generalized to all tissues, but it is important to consider that human cadaveric donors are often older than animal sources and storing and harvesting conditions can deeply impact sample's stiffness.

Normal vs pathological tissue

The ECM is a dynamic structure that is constantly modified due to changes in the environment. Cells react to their environmental stimuli and may remodel the ECM by promoting protein synthesis, degradation, post-translational modifications, and crosslinking.(158) When the tissue is healthy, the cells and ECM components function harmoniously promoting tissue homeostasis.(4) However, when using unhealthy tissue, pathological characteristics present in the ECM can activate pathological cell behaviour.(159) Upregulation or downregulation of structural protein expression and small bioactive molecules can be driven by ECM conditions that significantly impact cellular behaviour.(4, 159)

Several diseases including cancer,(160) emphysema,(161) Alport syndrome,(162) and infarct (163) present an overexpression of ECM molecules causing tissue fibrosis and as a result a different dECM hydrogel when compared to normal tissues. Apart from mechanical differences, additional biochemical and biological variations are observed. Beyond the structural proteins providing the mechanical properties of the decellularized ECM, it can also act as a reservoir of growth factors and other bioactive molecules characteristic of the state and health of the tissue source.

ECM composition and structure is different even in patients that have been diagnosed with the same cancer(164) and those discrepancies can cause a dysregulation of signaling pathways that can promote the expression of epithelial-to-mesenchymal (EMT) markers.(165) Healthy and cancerous breast dECM were recellularized with MCF-7 (human breast adenocarcinoma cell lines) and normal dECM inhibited the EMT by inducing cell apoptosis while the cancerous ECM promoted EMT.(165) Decellularized colorectal cancer mucosa was also compared with its healthy counterpart and significant differences were found not only in structural and secreted proteins, but also in their angiogenic potential.(166) The cancerous group, after being recellularized with cancer epithelial cells, induced an overexpression of IL-8 in less than one week of culture, a chemokine associated with cell growth and proliferation.(166)

Other pathologies such as emphysema have also been studied by culturing normal and emphysematous decellularized human lungs with fibroblasts, epithelial, endothelial, and bone marrow-derived MSCs. Results showed that both groups (healthy and pathological) supported initial binding, but cells seeded in emphysematous ECM did not survive for more than one week.(161) They also solubilized the decellularized tissue to create ECM

hydrogels. Both groups permitted comparable cell attachment and proliferation and no significant differences in cell viability were observed.(161) The authors of this study concluded that further evaluation is needed to assess how useful these matrices would be for clinical applications since the implications remain unclear. Genomic characterization of encapsulated cells could provide additional insights on gene expression differences between the healthy and pathological groups, focusing on emphysema-associated genes. Another study comparing dECM derived from healthy and Alport syndrome mice kidneys saw significant differences in the fibrous protein content; the Alport syndrome groups had elevated levels of collagen I, collagen IV, fibronectin, and in cytokine content.(162) Additionally, when macrophages were reseeded, both groups induced an M2 phenotype which is favorable for healing and repair. Later they homogenized these tissues and both groups promoted an M1 phenotype suggesting that the 3D structure is key and plays a significant role during cell differentiation.(162) Studies for cardiac applications have incorporated dECM hydrogels from healthy and infarcted rats into a polyacrylamide gel to create an *in-vitro* model to evaluate cell therapy.(163) The materials were engineered to match the mechanical properties of both groups before seeding with three different c-kit+ cardiac progenitor cells. The group containing healthy ECM had higher cell adhesion and proliferation while the infarct group showed a significant increase in pro-survival and angiogenic cytokines and minimal differentiation potential.(163)

Lifestyle habits can also influence the composition and mechanics of tissue. These variables, although difficult to standardize and even to quantify, may impact the final dECM hydrogel and material. The organisms' diet, daily activities, and contact with hazardous compounds such as tobacco, heavy metals, or alcohol can significantly affect

its health. For example, lung fibrosis is known to occur in heavy smokers,(167) bone density has been reported higher in older sprinters and runners when compared with the non-athletic groups(168), and increased heart wall thickness is a cardiovascular adaptation to exercise presented in elite athletes.(169) Obesity has been suggested as a driver in cancer cell progression due to abnormal levels in cytokines, hormones and growth factors in adipocytes.(170) In particular for breast cancer, a group used decellularized obese mammary glands to identify full-length collagen VI as a new driver of triple negative breast cancer (TNBC) invasion.(171) The abundance of this molecule is directly proportional to the body mass index in TNBC patients.(171) This study highlights the importance of selecting relevant materials for translational studies and new target discoveries for cancer and other pathologies. We expect future research to provide answers as for how lifestyle habits affect the final decellularized product due to differences in the tissue composition could help us understand the implications of factors such diet and activity levels in cellular response when using dECM hydrogels for tissue engineering or *in-vitro* applications. Since significant changes between healthy and pathological tissue that may influence cell behaviour and phenotype are conserved even after tissue decellularization, solubilization, and dECM hydrogel preparation, the selection of the appropriate source ECM for the desired outcome is a critical element of proper experimental design.

Cells

The expected structure and function of the tissue outcome is dependent upon the cell type and its ability to properly develop, function, and interact with an appropriately selected dECM source. Even when using terminally differentiated cells, their phenotype may still

be plastic, allowing for de-differentiation. For instance, muscle cells can lose expression of actin when cultured in gels with high concentrations of collagen, whereas the supplementation of laminin can stabilize their phenotype.(172) Force production by muscle cells is directly related to the stiffness of their environment, as the force is transferred through ECM. (173) Thus, it is important to not only account for the phenotypic effects of the dECM but also how it will influence the dynamic activity of cells upon encapsulation and throughout the duration of the experiment.

Ideally, the source of dECM will correspond to the cell type, which will increase the cytocompatibility as the ECM composition will match that of the native environment from which the cells originated.(174) It has been shown that human MSCs cultured on hydrogel mats previously populated by chondrocytes or osteocytes induced differentiation into those same cell types. (175) Furthermore, matching tissue type, without considering the species, can yield unwanted results and may introduce a degree of unpredictability in the system as the differences of ECM from other species, however small, may be enough to promote divergent results.(176) A study defined the ECM phenome of humans, mice, zebrafish, Drosophila, and C. elegans, and provided a phenotype grouping strategy that showed cross-species interferences.(176) Differences in gene expression and proliferation were observed in endothelial cells seeded in decellularized tissue slices derived from human, primate, pig and rat lungs suggesting the presence of species-dependent biologic cues.(177) This study is an example of how significant differences in gene expression can be observed in cells seeded in matching tissue type from different sources.

Additionally, immune cell function is known to be affected by interactions with dECM from foreign species as immune responses can be triggered by the recognition of foreign antigens within the dECM.(178, 179) Apart from ECM, paracrine signaling and matrix remodelling by supportive cells, such as fibroblasts, can be a necessary aid to both the maintenance of phenotype and execution of cellular functions. (180) The inclusion of cardiac fibroblasts in 3D culture with stem cells, lead to a greater population of functional cardiomyocytes demonstrating alignment of muscle fibers and beating activity.(181, 182) Fibroblasts are known to mediate the maintenance and remodelling of the ECM during development and wound healing of various tissues including the heart, however their paracrine signaling through growth factors may be sufficient to aid in cardiomyocyte differentiation.(183) Indirect co-cultures using hanging inserts were capable of enhancing expression of cardiomyocyte genes and beating activity. (181)

In summary, one must ask: what is the expected function of the cells or tissue? What phenotypic state do the cells require for that action? What type of signaling is needed to both induce and maintain that state? With answers to these questions, the optimal source of dECM that will best fit the requirements can be explored.

2.2.4. Fabrication techniques

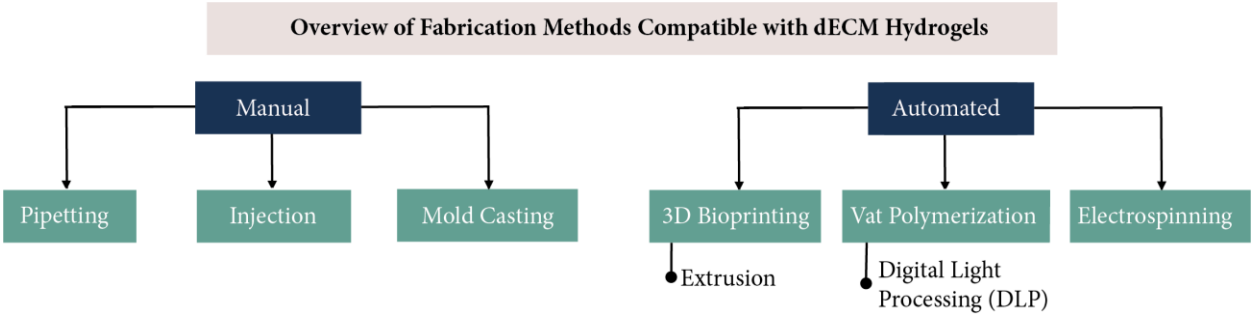

Fig. 4: Overview of fabrication methods compatible with dECM hydrogels.

Manual and automatic methods have been reported compatible with dECM hydrogels or dECM hydrogel-containing bioinks.

Manual

Engineered tissues and organs need to replicate the structure, geometry, and organization of the tissue organ being emulated in order to achieve their intended biological or physiological function. Ideally the engineered model replicates the tissue organization across scales, from the orientation of molecules to the structure of tissues within functional organs. Several fabrication techniques have been developed to create structurally defined tissue-scale models using dECM hydrogels or bioinks by engineering the mechanics of the dECM via cross-linking or by including rheological modifying co-gels to enable the use of automated additive manufacturing methods such as extrusion or photopolymerization.

When dECM is used to model 3D cell-matrix interactions during limited culture periods, where the structural complexity of the tissue is not needed, the most commonly used method is to deposit the cell-laden gel into a dome or cast the gel into a simple mold. These experiments are routinely performed when evaluating the biochemical or molecular biological functions of mono or co-culture systems using reconstituted basement membrane or dECM. Manual techniques are appealing because they do not require complex or expensive equipment to fabricate small and simple 3D constructs.(184) These methods also allow for viscous gels with low yield strengths, which would otherwise not maintain the 3D complex organ scale structure without external

support systems, to be used. However, opportunity for user error and inconsistencies between samples present challenges in replicating studies when using these techniques.(185, 186) Pipetting has been used to culture cells and to grow organoids or spheroids in a 3D environment using dECM hydrogels derived from liver (187) and placenta.(188)

Injectable dECM hydrogels have been developed as therapeutic approaches for intervertebral disc degeneration,(189) stroke,(190, 191) ischemia,(192) meniscus repair,(193) cardiac regeneration,(194, 195) repair of temporomandibular joint disc,(196) etc. Mold casting has been used by researchers for *in-vitro* applications including substrate coating for cell culture(197-199) and organoid formation.(39, 200) Manual techniques have been proven very useful, but there are disadvantages that make them not as attractive for complex construct fabrication. With these methods, it is not possible to control cell location and it is challenging to work with multiple materials or cell lines at once. Hence, the community has turned to automated fabrication techniques to create intricate structures of the desired size and architecture.

Automated

Automated deposition, or fabrication techniques have specific material requirements such as viscosity, response to shear, and yield stress that must be obtained by dECM gels in order to create reproducible models.

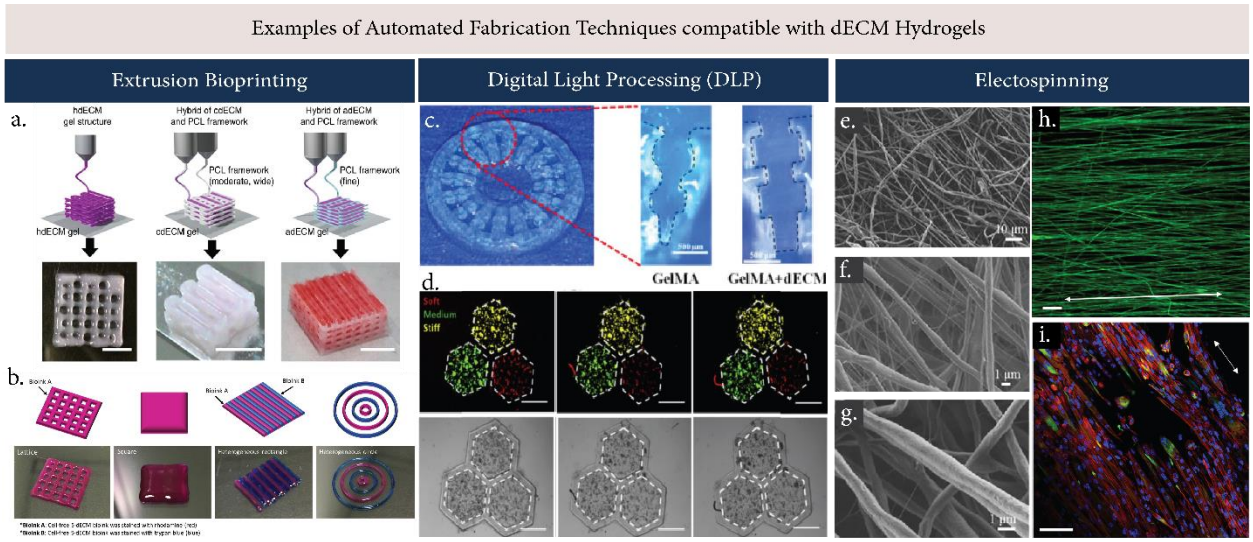

Fig. 5: Examples of Automated Fabrication Techniques compatible with dECM Hydrogels. ***a.-b. Extrusion Bioprinting:*** *a. Printed heart (hdECM), and a combination of either cartilage (cdECM) or adipose (adECM) with PCL. Reproduced from ref. (42) with permission from Springer Nature, Copyright 2014. b. Red and blue stained porcine skin dECM. Reproduced from ref. (141) with permission from Elsevier, Copyright 2018.* ***c.-d. Digital Light Processing:*** *c. DLP printed GelMA/dECM and GelMA scaffolds. dECM derived from porcine liver. Reproduced from ref. (60) with permission from Elsevier, Copyright 2020. d. Bioprinted liver cancer tissue platform with varied scaffold stiffness.(58) Day 0, 3, and 7 respectively. Reproduced from ref. (58) with permission from Elsevier, Copyright 2018.* ***e.-i. Electrospinning:*** *e.-g. Scanning electron microscopy of electrospun porcine cardiac dECM. Reproduced from ref. (201) with permissions from John Wiley and Sons, Copyright 2017. Scale bars e.10 µm f.-g. 1 µm. h. Confocal images of electrospun dECM fibers fabricated on a collector rotating at 3000 rpm.(202) Scale bar 50 µm. i. Aligned myotubes formed on dECM scaffolds after 7 days of culture.(202) Scale bar 100 µm. Desmin (green), actin (red), and nuclei (blue). Reproduced from ref. (202) with the permission from AAAS, Copyright 2021.*

Extrusion printing

Extrusion bioprinting, or extrusion-based bioprinting (EBB), is an additive manufacturing technique that has been immensely popular for tissue engineering and biomedical applications. It allows the serial fabrication of hydrogel constructs out of Computer Aided Design (CAD) models in a layer-by-layer fashion.(203) The material or bioink is loaded into cartridges and mounted on a XYZ stage where it is extruded through a nozzle following parameters provided by a computer. Extruding cells encapsulated in bioinks is possible with this technique(204) and when pressure is adequate to limit shear stress, viability above 80% can be achieved.(205) An ideal material for this technique should have shear thinning properties,(206) which is the case for dECM hydrogels(32, 42) but their behavior might change if additional materials are incorporated to reinforce the bioink. Extrusion printing supports bioinks with viscosities of 30 mPa/s to $>6 \times 10^7$ mPa/s(207) with print resolution in the hundreds of micrometer range. Moreover, this technique allows the fabrication of complex geometries and heterogeneous models since incorporation of different materials and/or cells in the same structure can be achieved if the printer has multiple cartridges.(203) Extrusion of dECM hydrogels has been successfully used to develop *in-vitro* healthy and disease tissue constructs,(141, 208-210) cancer models,(32) grafts,(211) and organ-on-a-chip models(212).

Digital light processing (DLP)

Digital light processing techniques makes use of photopolymerizable or photocrosslinkable materials that can be cured, or crosslinked, upon the exposure of patterned UV or visible projected light.(213) The 3D structure is achieved layer-by-layer as the projector exposes the curable material progressively as per the user-defined model

geometry(213) To photo-crosslink dECM hydrogels, a photoinitiator must be added, as the mechanism of photopolymerization produces reactive species that may be cytotoxic if used in high concentrations, care must be used in determining experimental conditions used and the potential for detrimental reactivity or photosensitivity of the cells selected.(214, 215) Additionally, using long UV exposure times to crosslink each layer of the 3D structure can affect cell viability and functionality of bioactive molecules of dECM hydrogels.(214) However, several groups have successfully reported the fabrication of dECM hydrogel constructs using this technique.(58, 60, 216) Heart and liver dECM hydrogels combined with GelMA were used to create cell-laden constructs with human induced pluripotent stem cell (hiPSC)-derived cardiomyocytes (hiPSC-CMs) and hiPSC-hepatocytes (hiPSC-Heps), respectively maintaining high cell viability.(216) DLP printing allowed the fabrication of structures as fine as 30 μm and the modification of the mechanical properties of the materials by varying the UV-exposure times while bioprinting.(216) The same group performed growth and invasion studies of hepatocellular carcinoma in DLP printed liver hydrogel constructs with varied scaffold stiffnesses.(58) Another group created a microtissue with a liver dECM-GelMA hydrogel and encapsulated hepatic cells that showed an increase in albumin and urea secretion, to demonstrate the retention of hepatocyte specific functions.(60)

Electrospinning

Electrospinning is a high throughput (HT) technique that allows the fabrication of porous scaffolds with controlled fiber orientation using a charged material.(217) In general, a solvent is needed to dissolve the polymer to the desired concentration to promote fibers with desired characteristics. Filaments are formed when an electric field is applied to a

liquid droplet which elongates forming a conical shape called the “Taylor cone” from which a charged jet is ejected.(217, 218) The fiber’s path starts in a straight line, but it later follows a whipping pattern which is deposited in a collector.(217, 218) The filaments can have nanometer diameters and parameters such as viscosity, conductivity and material concentration deeply influence the final result.(219) Cell-electrospinning (C-ES) is a variation of this method where fibers with living cells embedded are fabricated maintaining high cellular viability.(218) However, when using C-ES it is challenging to control cell density and positioning due to the process of how the fibers are generated.(218)

dECM hydrogels have been used in conjunction with carrier polymers or on their own to produce bioactive scaffolds.(202, 220, 221) A mixture of porcine cardiac dECM hydrogel and polyethylene oxide (PEO) has been successfully used in electrospinning with hexafluoro-2-propanol (HFIP) as a solvent. After fabrication, the PEO was washed with aqueous medium leaving only the dECM hydrogel fibers.(201) These fibers when placed in contact with water showed swelling, and collagen self-assembly into native-like structures. These matrices proved to be cytocompatible since they allowed cell adhesion and proliferation during the 4 weeks of culture. Immunogenic assessment was also measured by implanting the dECM scaffold in C57 black mice. There was not a significant immunological response to the implantation when compared with the PLGA scaffold used as a control group.(201) Another group recently developed a technique to produce electrospun muscle ECM hydrogels without using a carrier polymer; they only used HFIP as a solvent.(222) The constructs permitted cell attachment, growth, differentiation, and guided the formation of myotubes in mouse myoblasts *in-vitro*.(202) In an animal study,

they observed cell infiltration, angiogenesis and myogenesis in groups where electrospun dECM hydrogel scaffolds were implanted.(221)

Electrospraying is a variation of electrospinning where the electric field applied to the nozzle containing the material forces its dispersion into droplets.(223) These can vary in range from hundreds of micrometers down to tens of nanometer.(223) This technique has been used with dECM hydrogels to create microcarriers of porcine dermis, myocardium and human adipose tissues to be used in dynamic culture conditions with spinner flasks.(224, 225) Electrospraying has also been used to fabricate nanometer sized particles from porcine lung dECM hydrogels that could be used to induce pro-regenerative cell response in lungs,(226) and to fabricate microparticles from cardiac dECM hydrogels to use for tissue regeneration post heart injury in mice.(194)

Table 2. Fabrication Techniques for dECM Hydrogels

Fabrication technique	Advantages	Disadvantages	Material requirements	References
Pipetting, injection and mold casting	▪ Simple setup and easy to implement ▪ No complex equipment is required.	▪ Lack of reproducibility between samples ▪ Cell positioning is not controlled	▪ Injectable or pourable material ▪ Stable in culture conditions after fabrication	(185)
Extrusion printing	▪ Automatization of fabrication ensures sample reproducibility ▪ Extrusion printing is compatible with high cell densities ▪ Heterogeneous multi-cellular and -material models can be achieved with multiple cartridges and simple coding. ▪ Bioprinting is a highly customisable technology. ▪ Plenty of literature on material reinforcements is available. ▪ Temperature controlled cartridges and stages are available for thermosensitive materials.	▪ Resolution is in the hundreds of micrometers ▪ Specialized personnel training ▪ Shear stress can reduce cell viability. ▪ Rheological characterization and tunability of flow properties is required ▪ Scalability and scaffold generation speed is dependent on setup	Compatible materials with extrusion printing must exhibit: ▪ Shear thinning behavior. ▪ Fast recovery after shear properties. ▪ Tuned gelation and bioprinting window. ▪ An ideal liquid phase for cell mixing.	(32, 42, 203-206, 227)
Digital Light Processing (DLP)	▪ High speed when compared to extrusion bioprinting. ▪ Mechanical properties can be controlled by modifying the light exposure time. ▪ Photopolymerizers and photoinitiators can be incorporated in dECM hydrogels	▪ Photopolymerizes are known to be cytotoxic. ▪ Long UV exposure times can compromise cell viability.	▪ Photopolymerizers are required to conduct DLP	(213-215)
Electrospinning	▪ Increased scalability ▪ Control of fiber alignment is possible ▪ Compatible with cell encapsulation ▪ Capable of controlling porosity	▪ Cell density and location is challenging to control when cells are encapsulated in the material ▪ Crosslinking after fabrication might be required to increase mechanical properties.	▪ Solvents such as HFIP are required to make dECM hydrogels compatible with this technique. ▪ dECM hydrogels may be mixed with other materials to create hybrid scaffolds and promote better mechanical characteristics for fabrication.	(217-219)

2.2.5. Instabilities of dECM hydrogels

Mechanical properties of dECM hydrogels are significantly different when compared to the tissue of origin. Features such as porosity, stiffness and fiber alignment of the ECM components are drastically changed by the decellularization and solubilization steps performed to fabricate these gels. The physical characteristics of dECM hydrogels and how different decellularization protocols affect the final dECM are discussed in detail in Section 2.1 of this review. This section covers the features that make dECM hydrogels unstable either *in-vitro* or *in-vivo* to later discuss in Section 6 how the scientific community has overcome these obstacles by modifying either the material or the fabrication technique of 3D the constructs.

Altered mechanics

The process of removing cells from tissue ECM inevitably results in physicochemical disruption of the original tissue. In general, decellularization processes are known to alter the mechanical properties of tissues often resulting in gels that are more viscous and have a lower yield strength than the expected value of the tissue ECM. For instance, decellularized lung tissues have been demonstrated to have a reduced elastic modulus correlated to the decrease in the elastin content that occurs when decellularizing the native tissue.(228) Moreover, it has been observed that decellularized porcine aortic valves (AV) possessed a greater extensibility (from 68.85% for the native AV to ~140% after decellularization), but in turn have a lower flexural modulus (from 156 ± 24.6 kPa for the native AV to ~ 23.5±5.8 kPa after decellularization).(229) Some reports have highlighted the loss of mechanical properties during whole tissue decellularization prior to solubilization.(230, 231) As significant processing steps are required to create dECM

hydrogels from decellularized tissues including enzymatic and acidic digestion, neutralization to a physiological pH, and reconstitution into hydrogels, it is challenging to retain structural and mechanical properties. Typical decellularization processes are optimized to preserve most of the relevant proteins from the tissue, but may affect the architectural and mechanical characteristics, thus requiring reinforcement strategies to circumvent the lack of stability and create complex tissue or organ models (see section 5.1).

Degradation

ECM-based implants are promising in the field of tissue regeneration. However, these are often mechanically unstable and experience fast degradation rates when implanted. All implanted materials summon inflammatory responses and trigger a cascade of immunological events known as the foreign body reaction (FBR).(232) For any type of implant to perform as intended, modulation of the FBR is required to increase the probability of implant assimilation by the host.(233) Upon material implantation, cells of the immune system become attracted to the foreign material and attempt to degrade it. Specifically, macrophages are known to challenge implant stability by fusing into foreign body giant cells (FBGCs) and secreting proteolytic enzymes to resolve the lesion either via foreign body encapsulation or degradation.(234-236) Furthermore, even though macrophages pose challenges for material implantation, these cells are crucial in shaping a favorable regenerative immune microenvironment around the implanted material.(236) dECM degradation byproducts trigger further immunological responses that activate macrophages towards a constructive and favorable phenotype (IL4-dependent-polarization). (237) For example, ECM-based implant coatings have been

demonstrated to aid synthetic implant integration by reducing macrophage accumulation and formation of FBGCs.(238)

Long term, non-degradable implants are also susceptible to unwanted immune attacks. However, ECM-based implantable materials such as dECM hydrogels take advantage of degradation events to become assimilated by the host and are known to exhibit favorable *in-vitro* and *in-vivo* degradation(239). Following a successful and sterile implantation, a delicate balance between degradation and regeneration is required to recover tissue function and induce appropriate healing. This balance can be achieved by tuning the implant's properties to meet the expected degradation rates. For instance, researchers have demonstrated that a dense dECM implant (8 mg/ml) can remain inside the brain of animal specimens 12 weeks post-implantation despite some biodegradation.(240) The same group continued the investigation and correlated the volume of ECM implant to the number of infiltrated cells at day 90 post-implantation. The authors found an inverse proportional relationship where lower dECM concentrations allowed for higher infiltrating cell densities within the implantation area.(239) Moreover, additional research has demonstrated that *in-vivo* and *in-vitro* dECM implant degradation rates can be modulated by chemical crosslinking.*(241, 242)* Some *in-vitro* ECM crosslinkers such as glutaraldehyde could be problematic in a clinical setting.(243) Careful selection of these molecules is recommended as they may alter cell behavior. Additionally, *in-vivo* implant degradation can be modulated by matrix metalloproteinase (MMP) inhibitors incorporated within the dECM implant.*(241)*

Furthermore, special attention to the presence of contaminants and unwanted material within dECM hydrogels must be given. Genomic residuals, detergents, proteases, and

other small molecules can influence implant assimilation.(244) Moreover, decellularization and solubilization processes used to produce dECM hydrogels are known to disrupt the structural integrity of tissue which further alters the mechanical behavior of the dECM. From the mechanical perspective, ECM implants are expected to exhibit decreased mechanical properties attributed to the onset of degradation and the absence of tissue regeneration.(245, 246) However, as new tissue is formed and integrates into the implant site, the mechanical properties increase and eventually can match the native tissue.(245) In the following sections, we will detail and exemplify the challenges with dECM-hydrogel mechanics and how these have been outmaneuvered using composite hydrogels, chemical modifications, support materials, and microstructural reorganization.

2.2.6. Mechanically Stable dECM hydrogels

To control the mechanical properties and ensure structural stability of dECM hydrogels, strategies have been developed employing the addition of rheological-modifying molecules, incorporating crosslinkers/additives, chemical modifications, and deposition of fibers into set geometries (247-249).

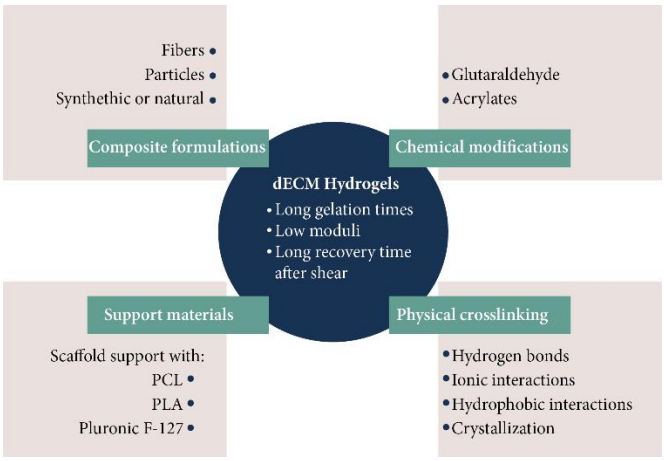

Fig. 6: Compensating Mechanics of dECM Hydrogels

dECM Hydrogels do not retain the mechanical properties of the native tissue. Different techniques have been used to compensate the lack of desired mechanical characteristics by creating dECM composite formulations, modifying the material physically or chemically or providing structural support with more stable materials.

Composite dECM hydrogels

A composite hydrogel consists of a combination of two or more macromolecular constituents designed to interact via inter- or intramolecular forces by controlled network formation, cross-linking, non-covalent interactions, external physical stimuli, or chemical properties of the microenvironment.(250) dECM material consists of the use of a dECM material as a base where additional elements can be added to improve matrix relevance or to provide specific functions; additional ECM-like elements to improve mechanical properties such as synthetic or natural hydrogels, biomolecules to enhance biological cues, or any of these combinations dECM hydrogels contain native ECM components that permit cell-ECM interactions which allow cellular growth and proliferation, but pure dECM hydrogels often form weak gels that require material reinforcements to achieve extrudable formats.(54) Apart from allowing cell encapsulation and development, these

materials must have suitable rheological properties to withstand commonly used fabrication techniques, preserve defined geometries, and have tunable physical characteristics that can match the tissue of interest.(32, 251) For that reason, fabrication of dECM-containing composites is an approach to improve its weak mechanical properties.

It has been shown that incorporating alginate and gelatin as supporting materials into a composite hydrogel containing dECM from porcine tongue results in a mechanically stable gel compatible with extrusion bioprinting.(32) The composite hydrogel demonstrated a tunable elastic modulus that was able to match that of tumor xenografts grown in mouse models. Other efforts have reported the use of milling dECM into particles and incorporation into inert synthetic or biological scaffolds to formulate composite dECM materials. (252, 253) The incorporation of dECM particles from porcine liver and chemically crosslinked with modified GAGs (chondroitin sulfate, hyaluronic acid), showed excellent gelation kinetics and mechanical properties, where gel stiffness increased and reached a steady state on the order of tens of minutes when tested in different ratios, and was able to sustain concentric geometries. (253) Enforcement of a gastric tissue derived decellularized bioink with cellulose nanoparticles (CN) demonstrated an increase of the mechanical strength of the dECM bioink as a more biophysical reliable gastric cancer environment; furthermore, cellulose nanoparticles increased the size of cell aggregates from 2178 ± 211 μm^2 in the pure dECM group, to 3564 ± 583 μm^2, and 5667 ± 1440 μm^2 in the 0.01% and 0.1% CN-g-dECM gels. (254)

Chemical modifications

Materials can require further chemical modifications to induce hydrogel formation and overcome other mechanical limitations, such as structure formation, gelation kinetics, mechanical strength, stability, and degradability.(255) The extent in which the mechanical properties of hydrogels are modified is driven by the degree and type of cross-linking and the concentration of the biopolymer. The structure and mechanics can be changed by chemically cross-linking with glutaraldehyde, genipin, oligourethanes, carbodiimides, acrylates, among others. (248) It is important to consider that features such as porosity can be heavily modified after the crosslinking process affecting cellular migration and the efficiency of nutrient-waste exchange.(256)

GelMA (257) is a photocrosslinkable gelatin-based hydrogel that is prepared using gelatin and methacrylic anhydride (MAA). GelMA is synthesized when the methacryloyl group from the MAA replaces the amino groups of the gelatin. (258) Cross-linking of the methacrylamide side groups with ultraviolet (UV) light results in an increase of stiffness that can be controlled by changing the concentration of the photo-initiator, the UV intensity and exposure time. (259) GelMA has been proven as a potential platform for 3D culture systems and different applications. (259) Decellularized human heart with GelMA was compared with GelMA-methacrylated hyaluronic acid (MelHA) by encapsulating human induced pluripotent stem cell derived cardiomyocytes (iCMs). The dECM-GelMA bioink demonstrated extrudability and improved elastic modulus when compared with the GelMA-HA, furthermore, the crosslinking method enabled the creation of tissue constructs with similar stiffness to native human heart tissue (~10 kPa). (260) Also, methacryloyl-functionalized decellularized liver ECM (dECM-MA) reinforced with PCL-

MA, has been used to bioprint tissue scaffolds, where the dECM scaffold served as a matrix mimicking environment for seeded cells. (261)

Other forms of chemical modification include cross-linking with glutaraldehyde (GA), where the ε-amine groups of collagen create an imine bond when interacting with GA molecules, improving mechanical characteristics and resistance to degradation. (262) While the use of GA as a cross-linking agent for the preparation of natural polymers has been widely reported (263-267), GA cross-linking often needs to be hydrolyzed to recover the starting material after GA fixation. (268) A decellularized skeletal muscle extracellular matrix crosslinked with GA vapor created a physicochemical-tunable system that enabled the control of mouse myoblast growth and myotube formation. (202) When evaluating properties such as fiber alignment, fiber swelling, bulk alignment and bulk swelling, the degree of alignment and cross-linking on the dECM scaffolds supported cell attachment, growth, and myogenic differentiation.

A chemically crosslinked decellularized composite hydrogel with modified glycosaminoglycans (GAGs) functionalized onto dECM particles with multiple tissues (bone, fat, cartilage, lung, liver, spleen, or brain) has been developed. (253) The chemical modification resulted in controllable and faster gelation kinetics, and the shear modulus (G') of the mixtures increased when the ratio of tissue particle to modified GAGs was equal to or greater than 50%, offering regenerative specificity in accordance with their tissue of origin. Furthermore, PEG-modified hydrogels have shown greater hydrolytic stability (269) and have also been explored for dECM formulations. A modified liver dECM with PEG-based crosslinkers with different functional groups and molecular weights incorporated into the dECM, yielded tunable bioinks with different shear stiffness

properties, where primary human liver spheroids were encapsulated to the formulations prior to printing to create *in-vitro* liver constructs with high cell viability and quantifiable albumin and urea production. (270)

The use of a two-step process comprised of vitamin B2-induced UVA crosslinking followed by thermal gelation has been proposed to mechanically enhance a decellularized heart tissue bioink for 3D bioprinting. (57) The formulation consisting of riboflavin added to heart dECM, offered control over the 3D printed filaments and ensured high fidelity for the printed living tissue. Cardiac progenitor cells (CPCs) were mixed with the bioink prior to bioprinting. After mechanical evaluation and cell viability tests, it was found that the two-step crosslinking resulted in a dECM gel 33-times stiffer than thermally crosslinked gels, obtaining mechanical properties similar to that of native cardiac tissue. Moreover, dECM gels supported active proliferation, high viability, and promoted cardiac differentiation of the seeded progenitor cells.

Cross-linking can also be accomplished through the physical interactions between biopolymer chains and the introduction of cross-linking groups. Different types of physical cross-linking mechanisms have been explored (271), including hydrogen bonding (272), such as PMAA and PEG association under acidic conditions to form hydrogen-bonded complexes; block polymers such as PLGA, PEG, and PBT (273-275); crystallization (276), when a polymer is cooled under specific conditions, such as Polyvinyl alcohol (PVA) hydrogels using freeze-thaw process; and ionic interactions (277), such as the type of alginate gel that is formed in the presence of divalent cations.

Incorporation of support materials

Support materials can be added to composite materials internally or externally to aid in the fabrication of precise (278) or complex (279) structures. Support materials allow the tailoring of mechanical and physical properties in the structure, such as density and porosity.(42) Sacrificial materials are incorporated separately or within the construct, however, after solidification of the non-supporting material to its final geometry, sacrificial materials are removed. Incorporating dECM hydrogels into specifically designed structures made up of supporting materials that do not necessarily interact chemically with the dECM hydrogel but provide a scaffold for dECM to be deposited on has been also explored. (279-281) The incorporation of polycaprolactone (PCL) as a supporting material into dECM hydrogels has been previously reported. (42, 278, 282) Although co-deposited PCL scaffolds can have a controlled shape, mesh structure, and stiffness, its deposition requires preheating the nozzle at temperatures above 60 °C, which can decrease cell viability in the final structure. (283) However, efforts for allowing high cell viability with high melting temperature thermoplastics such as a late deposition of cells once the temperature of the fibers has decreased, have been explored. (283)

A dECM hydrogel consisting of decellularized cartilage and adipose porcine heart tissues with encapsulated human adipose-derived stem cells (hASCs) proved the ability to print constructs with a controllable porosity, depending on the structure of PCL as the supporting material, for possible nutrient and oxygen supply; cell viability also proved to be sufficiently high (>95%) and was not affected by the incorporation of the supporting material. (42) In another report (282), *in-vivo* tissue response to the PCL-decellularized adipose tissue scaffolds was investigated by performing subcutaneous implantation into

mice to evaluate the efficacy for regenerating adipose tissue. The scaffolds did not induce chronic inflammation nor a cytotoxic response; the scaffolds were able to support tissue infiltration, remodeling, and adipose tissue formation.

Sacrificial materials such as Pluronic F-127, can also serve as support materials for dECM hydrogels. This material has been used in conjunction with liver dECM hydrogel to create specifically designed structures. (279) Biliary epithelial cells (cholangiocytes) were encapsulated in the dECM hydrogel and printed inside the Pluronic F-127 structure. The thermal transition from the sol-gel phase of Pluronic F-127 that occurs below 37° C was used to create models where the deposited Pluronic would dissolve into the solution phase when cultured. These types of sacrificial material can be included in defined positions in the model design providing opportunities to create 4D models. These types of 4D sacrificial materials can be used to create complex structures such as biliary trees, with minimal negative impact on cell viability and proliferation.

Linearization of fibers

Mechanical stability and enhanced mechanical properties can also be achieved through the precise deposition of fibers and fibrillar proteins, such as collagen (284). Collagen fiber orientation and alignment in hydrogels has been reported using several methods, including bioprinting. (285, 286) Mechanical stability and enhanced mechanical properties can also be achieved through the precise deposition of fibers and fibrillar proteins, such as collagen. (284) Collagen fiber orientation and alignment in hydrogels has been reported using several methods, including bioprinting. (285, 286) Kim et al. (287) reported the precise manipulation and structural organization of collagen fibrils through the control of the size of the printing nozzles in their 3D printing technique, in a

decellularized corneal ECM bioink. After the group calculated shear stress during 3D printing and quantified shear-induced arrangement of collagen fibrils that occurred during extrusion, they observed that the alignment provided a stroma-like environment, inducing remodeling of the collagenous matrix.

The development of dECM hydrogels has widely improved thanks to new tools and technology development in recent years, allowing their application in different fields. With the combination of all the previously described fabrication techniques and modifications, including overcoming dECM mechanical limitations, we can generate different constructs for tissue engineering applications and reproducing the microenvironment *in-vitro*.

2.2.7. Applications of dECM hydrogels

dECM hydrogels have been widely explored for two main applications: tissue engineering and modeling microenvironments of healthy or diseased tissues *in-vitro*. These materials are appealing due to their bioactive nature that promotes dynamic reciprocity between cells and the environment. They have the potential to be clinically used and the versatility to re-create environments *in-vitro* of healthy or diseased tissues. Tissue engineering is an area that has been traditionally studied since dECM-based materials have shown to promote regeneration and positive immune response. However, creating microenvironments *in-vitro* has become a popular avenue in the past years. Having a system *in-vitro* that could recapitulate important characteristics present *in-vivo* while having the advantage of monitoring and measuring the culture over time is appealing for its high-throughput potential. In this section, examples of dECM hydrogel applications are presented.

Tissue Engineering

dECM from various organ systems has been studied and tested as a therapeutic approach for regenerative medicine (Fig. 7). dECM closely mimics features of the *in-vivo* environment from which the decellularized tissue originated. dECM from several tissues, including skeletal and cardiac muscle, cartilage, brain, and skin have been explored for its modeling and therapeutic potential.

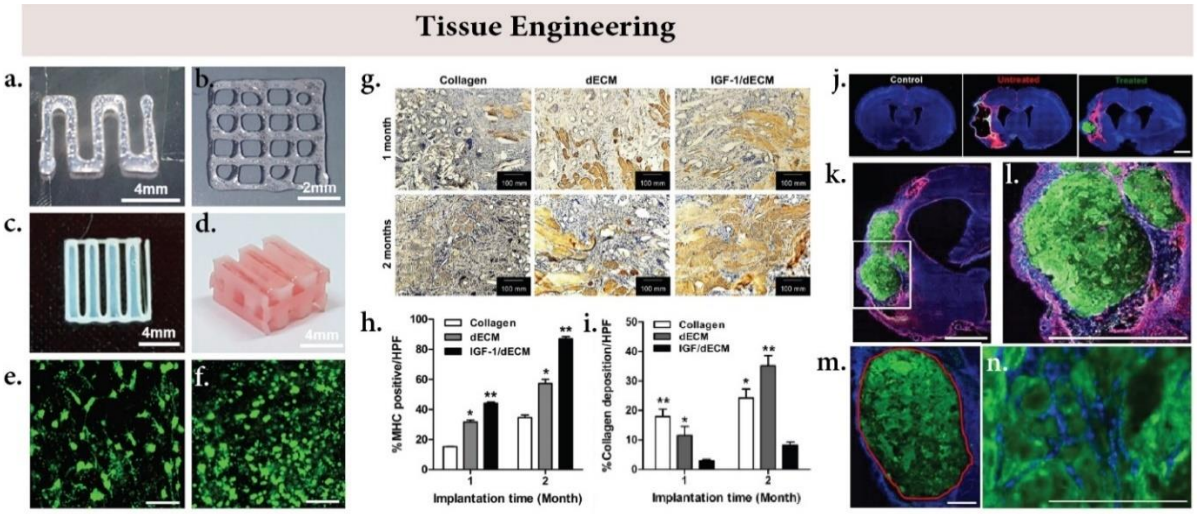

Fig. 7: Examples of Tissue Engineering Application of dECM hydrogels.

a.-f. Liver dECM hydrogel used to fabricate 2D constructs Reproduced from ref. (278) with permission from American Chemistry Society, Copyright 2017. (a.-b.) and 3D constructs with the addition of polycaprolactone (PCL) layers for reinforcement (c.-d.). (278) Cells encapsulated in the liver dECM hydrogel and fabricated into 3D constructs using PCL layers for support at day 7 of culture. e. Bone marrow hepatic cells and f. hepatic cancer cells. Live-dead assay stain. Scale bar for microscopy images: 200μm.(278) g. Immunohistochemistry of PLLA scaffolds containing either collagen, muscle dECM hydrogel or IGF-1/dECM hydrogel after 1-2 months of implantation in rabbit models.(288) Plots quantifying h. MHC and i. collagen deposition are presented for the three conditions.(288) g.-i. Reproduced from ref. (288) with permission from Elsevier, Copyright 2020. j. Comparison of three conditions for stroke animal models: control, untreated and treated with a dECM hydrogel derived from

porcine urinary bladder.(240) k.-l. dECM hydrogel retention after implantation.(240) Scale bar 2 mm m.-n. dECM hydrogel after 12 weeks of implantation.(240) n. Host cells invaded the dECM hydrogel.(240) Scale bar 100 µm Collagen I: green, DAPI: blue, Iba1: red GFAP: magenta. j.-n. Reproduced from ref. (240) with permission from Elsevier, Copyright 2017.

Skeletal Muscle

The development of therapies to promote skeletal muscle regeneration can aid patients that suffer from conditions such as volumetric muscle loss, trauma, muscle ablation, among others. Skeletal muscle-derived dECM hydrogels have been shown in multiple studies to induce greater proliferation and differentiation of myosatellite cells than conventional 3D cultures in materials such as collagen or PCL.(221, 288, 289) Implantation of dECM hydrogels can promote healing processes of various muscle injuries by enabling cell infiltration, angiogenesis and myogenesis as demonstrated in animal models.(221) Greater myotube formation and increased activity of anti-inflammatory M2 macrophages has been observed in animals to which dECM scaffold was implanted in regions with volumetric muscle loss.(221, 289) Skeletal muscle, being a structural and load bearing tissue, benefits from the addition of various modifiers that can stiffen their native dECM. For instance, the addition of PCL to muscle dECM can enhance the formation of MHC^+ myotubes which is mirrored in *in-vivo* measurements of muscle regeneration.(289) The addition of IGF-1 to muscle dECM has also been proven to further enhance the proliferation and differentiation of myosatellite cells and MHC^+ tissues after implantation.(288) *In-vivo* regeneration of muscle loss was also enhanced by the addition of IGF-1 into muscle dECM hydrogels (Fig. 7 g.-h.).(221, 288, 289) (288, 289)

Cardiac Tissue

dECM hydrogels derived from cardiac tissue used as cardiac patches have been proven to increase the cardiogenic expression of human cardiac progenitor cells when compared to the GelMA control group.(290) Also, neovascularization was observed after 14 days of implantation.(290) Injectable hydrogels have also been tested in small and large animal models after myocardial infarction (MI) and the material has shown to stop the progression of negative left ventricular remodelling including fibrosis and hyperthropy.(291) Both, bioprinted and injected constructs show vascularization after implantation.(290, 291) These examples show the potential benefits of products containing dECM hydrogels for cardiac regeneration. Although further testing and optimization are required, current studies using cardiac dECM show promising results in better mimicking native environments that are more biocompatible with cellular viability, phenotype, and regeneration. This promise has translated into several ongoing clinical trials. The first completed phase one study was conducted using a dECM harvested from porcine myocardium called VentriGel.(292) Patients who suffered from a myocardial infarction that caused a left-ventricular dysfunction were treated with an injection of VentriGel.(292) The material passed safety trials with two adverse cardiac effects that were deemed to be unrelated to the treatment.(292) Preliminary measurements of improvement showed an increase in the 6-minute walk test and a slight reduction in both left-ventricular and diastolic and systolic volumes.(292)

Neural Tissue

In-vivo dECM hydrogels have been shown to act as a bridge between nerves, allowing for recovery of spinal cord and brain injuries and can support axon growth and bridging

cavity spaces.(87) A reduction in inflammation along with recovery of locomotor functions were witnessed after injection of dECM hydrogels into spinal cord or brain lesions in mice.(87) Umbilical cord dECM hydrogels have also been proposed as a human origin alternative that allows neural tissue repair when injected in the lesion site with better prognosis when compared to other dECM hydrogel sources like porcine brain, spinal cord and urinary bladder.(87) dECM hydrogel injections have been shown to reduce the myelin disruption and lesion volume after weeks of implantation.(293) However, there were no significant improvements when the animals did the Morris water maze test when compared to the control group.(293) Overall, this technique suggests that using dECM hydrogels for neural regeneration is a promising area, but additional efforts are needed to fully understand the best approach for use in tissue regeneration and how physiological and motor function can be restored following implantation.

Cartilage Tissue

Cartilage-associated disease and trauma result in severe pain for patients and are very challenging to treat in orthopedic practice.(294) Hence, regenerative alternatives have been explored trying to find new ways to treat damaged tissue. Cartilage based dECM hydrogels have been tested for enhanced chondrocyte activity as demonstrated by an increase in ECM deposition.(295-298) Although dECM itself can have pro-regenerative and biomimicking capabilities, the addition of both biochemical and rheological supplements has been used to further enhance these properties. Cartilage is especially dependent on its rheological properties as it is the major load-bearing tissue between joints. The addition of stiffening components such as UV-crosslinked gelatin-methacrylate or chitosan in optimized concentrations to cartilaginous dECM can stiffen

the construct resulting in rheological properties closer to that of native cartilage.(295, 297) These stiffer constructs have been shown to enhance ECM deposition of encapsulated chondrocytes as well as delaying the progression of osteoarthritis in rat models.(295, 297) dECM hydrogels have also been proposed as an injectable material for drug delivery.(299)

Vascular Tissue

A vascular network is vital to maintaining adequate nutrient availability in *in-vitro* 3D constructs. Various methods to engineer an *in-vitro* vasculature have been implemented, ranging from 3D cultured endothelial cells,(300) fluidic devices,(301) and decellularized vascular grafts.(302) Capillaries are ubiquitous in all organ systems thus endothelial cells that form the capillary bed have an intrinsic adaptability to various environments.(303, 304) Considering materials with mechanical properties that encompass the physiological range, naturally derived hydrogels such as collagen, Matrigel, and dECM hydrogels can support the formation of a micro-vascular network.(305-310) dECM-based constructs containing endothelial cells benefit from the bioactivity that the dECM exhibits by retaining properties from the tissue of origin, and the intrinsic versatility of the vascular network can accommodate to the environmental needs of that organ system. Recent studies have demonstrated dECM hydrogels derived from porcine kidney,(310) bladder and small intestine,(311) as well as, mouse and human lungs,(312) were sufficient in inducing the formation of a capillary network. In cases where a dECM hydrogels failed to promote a vascular network, as is the case of decellularized adipose tissue, the dECM hydrogel can be supplemented with pro-angiogenic factors, such as VEGF.(313)

Other Tissues

Many other organ systems have been explored for the potential use of dECM hydrogels as modeling and therapeutic materials, such as heart,(292, 314), lung,(314), skin,(141) liver,(187, 278, 314) and colon (314). We invite the reader to further explore the following articles for a more extensive description.(19, 187, 227, 314-316)

Using dECM hydrogels for tissue engineering applications is promising due to their regenerative and cell differentiation capabilities with a positive inflammatory response when implanted. (221, 289) However, strict regulation agencies' protocols together with an inevitable variability and heterogeneity between tissue sources and processing makes the market approval a challenging task. However, human and animal-derived insolubilized dECM tissues are currently being used for therapeutic applications.(10, 19) Thus, successful clinical trials, product standardization and characterization could aid in accelerating the approval for use of these materials in the clinic.

Rebuilding 3D Microenvironments in-vitro

Miniaturized models of living tissue for experimental purposes opens new research avenues in clinical sciences. Specifically, *in-vitro* 3D tissue models have been proven to be accurate mimics for precision medicine, drug discovery, and overall translational research. (317-319) Generally, these 3D tissue analogs recreate native architectures and promote relevant cell behavior that would be otherwise difficult to elucidate when using traditional cell monolayers and animal models.(317) These advantages are particularly important when studying pathological conditions *in-vitro* such as cancer, where the microenvironment is a crucial element of the disease. Additionally, building microenvironments *in-vitro* is an attractive approach when the tissue or disease of interest does not have a robust animal model. In oncology research, even though

establishing tumor models through the transplantation of human cancer cells into the athymic nude mouse model has been the steppingstone for major preclinical studies and development of novel anticancer drugs, (320) these tumor models are subjected to stromal and selective pressures that could result in genetic drifting of the original tumor.(321, 322) Using dECM-hydrogels, several research groups have been able to demonstrate the importance of using tumor-derived dECM hydrogels to elucidate pathologically relevant cell behavior when compared dECM-hydrogels extracted from healthy tissues (323)

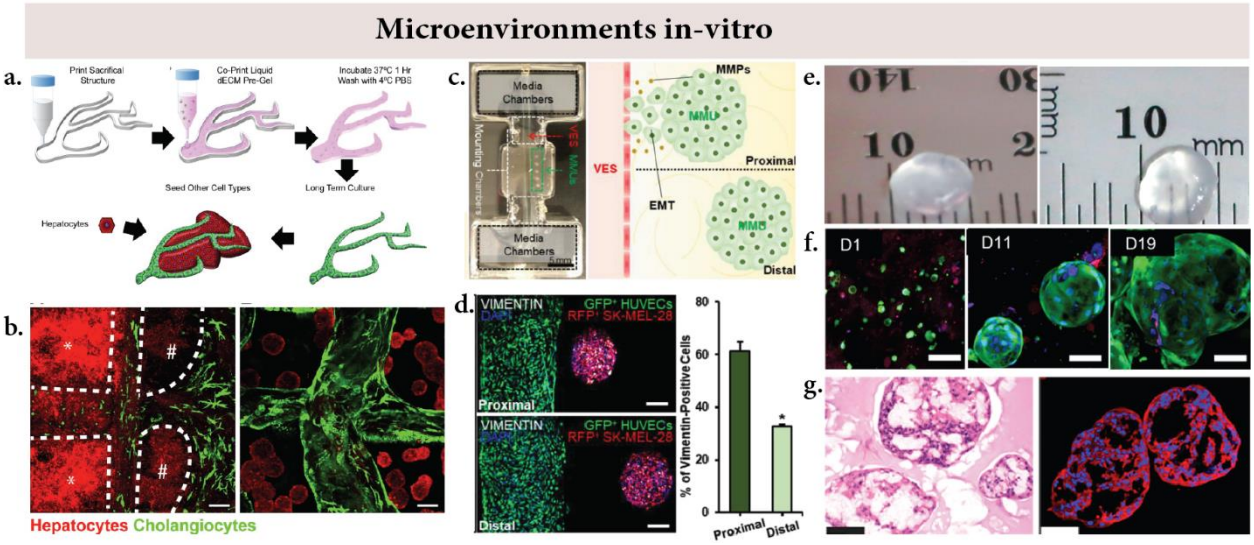

Fig. 8: Examples of Microenvironments in-vitro using dECM Hydrogels

a. Illustration of dual printing process to build co-culture models. Using this technique, a.- b. co-culture of hepatocytes and cholangiocytes was fabricated. Mature ducts structures are visible in green and human liver cell aggregates in red (right).(279) Scale bars: 250 µm. a.-b. *Reproduced from ref. (279) with permission from Elsevier, Copyright 2019. c. Fabricated platform containing a cancer-vascularized model to evaluate metastasis.(324) d. Immunofluorescence images that allow the quantification of EMT of melanoma metastatic units in relationship to the distance between the cancer and vascular regions of the platform. Vimentin expression is quantified for both scenarios.(324) Scale bars, 300 µm* c.-d.

Reproduced from ref. (324) with permissions from John Wiley and Sons, Copyright 2021. e. 3D printed tongue dECM containing bioink to fabricate a head and neck cancer model in-vitro.(32) f. Cellular aggregate formations over time.(32) Live-dead assay stain. Scale bar 100 μm g. H&E staining and immunofluorescence of cellular aggregates after 19 days of culture.(32) Scale bar 100 μm. e.-g.Reproduced from ref. (32) with permission from American Chemistry Society, Copyright 2021.

Furthermore, dECM hydrogels from different tissue sources have proven to be useful for promoting organoid formation. Liver dECM hydrogels promote hepatic function by allowing self-organization of liver cancer cells with human mesenchymal and endothelial cells while promoting hepatocyte specific transcripts.(325) Efforts have also been directed into mimicking liver function with liver dECM hydrogels and successfully fabricating biliary trees with epithelial cells which mature over time. (279) This technique is proposed to study duct formation and liver biology *in-vitro* (Fig. 8a.-b.).

dECM hydrogels have also been applied to *in-vitro* neural network models using a multi-electrode array to measure action potentials and neuronal connectivity.(326) Neurons cultured in dECM harvested from rat brains were able to facilitate a higher degree of connectivity between neural nodes suggesting that brain dECM can induce a more mature neural network.(326)

Photocrosslinkable dECM bioinks have been used to encapsulate human induced pluripotent stem cells (hiPSC) to later bioprint microscale tissue constructs.(325) The fabricated constructs contained the biochemical environment and mechanical properties to mature hiPSCs into hepatocytes or cardiomyocytes.(216) These models have been proposed as physiologically relevant tissue platforms to study disease, and to apply to personalized medicine or diagnostics.

A cancer-vascular model fabricated with a dECM hydrogel bioink has been used to demonstrate that it is possible to achieve hypoxic conditions and promote angiogenic signalling between the cancer and vascular unit *in-vitro*.(324) Changes in EMT were shown to be dependent on the architecture and proximity between the cancer and vascular unit.(324) This platform has the potential to mimic patient's metastatic progression *in-vitro* aiding personalized cancer treatments. (Fig. 8 c.-d.). Also, a head and neck cancer 3D printed model has been fabricated with a bioink formulated with alginate, gelatin, and porcine tongue-derived dECM hydrogel. The material allowed 3D cell aggregate formation and was used as a platform to test standard of care chemotherapeutic drugs in 3D *in-vitro* environments (Fig. 8 e.-f.).(32)

An infarct milieu *in-vitro* model has also been proposed to develop the infarct microenvironment *in-vitro* and predict the cell therapy outcomes.(163) Specifically, the regenerative potential and therapeutic efficacy of c-Kit+ cardiac progenitor cells (CPCs) which in this case were obtained from individual infarcted rat hearts. This model included hypoxic environment and soluble and inflammatory mediators and the dECM hydrogel group showed an increase of paracrine signaling which suggests these cells may function when implanted. Cell therapy has promising claims, but it is of high importance to be able to characterize the CPCs before implantation.

dECM hydrogels have been a strong candidate to build microenvironments *in-vitro* because they provide structural proteins and bioactive molecules present in the native source tissue.(319) These conditions are difficult to achieve using only synthetic materials, so sometimes combinations of multiple constituents are proposed as stable and bioactive materials for tissue fabrication. (54)

Overall, we see that dECM hydrogels have the potential to be used for multiple applications *in-vitro*. These can include mimicking healthy or diseased tissue to study its biology, creating personalized medicine platforms to better predict patient's outcome, or testing platforms for drug discovery. It is clear that the bioactive ability provided by dECM hydrogels has a positive impact in cell development *in-vitro* and it is aiding the scientific community in creating microtissues that mimic complex microenvironment cues that are difficult to replicate with other materials.

2.2.8. Clinical and commercial opportunities

dECM hydrogels can be candidates for tissue regeneration and implantation. The possibility of having commercially available dECM hydrogels is an appealing yet complicated task. There are opportunities to optimize, mass produce, and use dECM hydrogels *in-vivo* for minor and minimally invasive interventions to aid with immediate repairs. There is also potential to use these materials as an approach to induce tissue development and stem cell differentiation *in-vivo*. Nonetheless, to successfully produce clinically compatible dECM hydrogels the tissue provider must meet high quality standards that would satisfy regulatory agencies when used for implantation. This is a quickly changing area and regulations are evolving to accommodate new technologies.(327) However, allogenic and xenogeneic risks of using either human or animal tissues have to be considered.(54) Automated decellularization devices are available in the market, which is beneficial since it would promote a consistent protocol and outcome.(15) Furthermore, we believe the field will benefit from studying the effects of long-term preservation on tissue dECM and derived hydrogels. Shelf-life evaluations

such as structural integrity and bioactivity must be conducted to fully assess the feasibility of the dECM technology.

On the other hand, using dECM hydrogels as a 3D matrix for drug testing and drug discovery is an interesting avenue, especially in fields where there is a lack of a robust pre-clinical model like immunotherapy. However, one of the challenges to overcome is the protocol variability of dECM hydrogels. Physical properties of dECM can be often unassessed in peer-reviewed articles.(36) It is important to characterize the dECM end-product while providing guidelines for matrix characterization.(36) Good Manufacturing Practices (GMP) and Good Laboratory Practices (GLP) should be followed during the development and biomanufacturing of these materials to ensure research studies are correctly conducted and the final product has the desired quality and specifications.

2.2.9. Perspectives

From xenotransplantation of dECM into humans to the preparation of human tissue, decellularization has provided a unique way of manipulating and repurposing one of nature's most complex creations, the extracellular matrix. dECM hydrogels have been proven to be a valuable tool for numerous biomedical applications. Nonetheless, their weak biomechanics, variability, and material sourcing prove to be a challenge. This field is quickly evolving and plenty of material formulations and methodologies have been developed throughout the past years using these materials.

As technology moves forward, we envision the development of more sustainable ECM-containing materials made of recombinant proteins that provide the critical bioactive components while removing the less desirable traits that dECM hydrogels derived from tissue have such as immunogenicity, pathogens and remaining detergents or nucleic acids. For this to happen, significant improvements and scalability on recombinant protein production must happen to make their use a cost effective and desirable alternative to tissue-derived dECM products. This would enable controlled post-translational modifications and a decrease in product variability that is highly desired for tissue engineering applications and personalized medicine.

Nevertheless, these futuristic views may only become true in a distant future. For now, this review describes the field of dECM hydrogels up to-date. We described the general characteristics of dECM hydrogels, the importance of selecting an appropriate source and type of dECM, the modifications this material can be subjected to, its compatibility with fabrication techniques, and some of its applications. We hope this basic guide serves as a

starting point for anyone who may want to take on the challenge of leaping the field of dECM-based biomaterials.

2.2.10. Conclusions

Overall, there is potential to use dECM hydrogels for personalized and regenerative medicine, drug discovery and biological studies. However, limitations such as batch-to-batch variability, yield, and autologous reactions when implanted should be considered. After decellularization and solubilization, the final product has weaker mechanical characteristics and does not preserve the architecture of the source tissue. However, these materials contain a cocktail of native ECM structural and bioactive components that promote cell adhesion, differentiation, and proliferation. They have shown to promote a positive inflammatory response after implantation and proposed as a material to better mimic the tissue environment *in-vitro*. There is opportunity for dECM hydrogel containing blends to provide bioactive properties while being compatible with commonly used fabrication techniques. dECM hydrogels are complicated materials but they have given us the opportunity to create biomimetic tissue-like constructs.

Re-print acknowledgements

Figure 2 d. was reprinted from Preparation and rheological characterization of a gel form of the porcine urinary bladder matrix, Biomaterials, Volume 29, Donald O. Freytes, Jeffrey Martin, Sachin S. Velankar, Annie S. Lee, Stephen F. Badylak, with permission from Elsevier.

Figure 5 b. was reprinted from 3D cell printing of *in-vitro* stabilized skin model and *in-vivo* pre-vascularized skin patch using tissue-specific extracellular matrix bioink: A step towards advanced skin tissue engineering, Biomaterials, Volume 168, Byoung Soo Kim, Yang Woo Kwon, Jeong-Sik Kong, Gyu TaePark, Ge Gao, Wonil Han, Moon-Bum Kim, Hyungseok Lee, Jae HoKim, Dong-Woo Cho, with permission from Elsevier.

Figure 5 c. was reprinted from Fabrication of liver microtissue with liver decellularized extracellular matrix (dECM) bioink by digital light processing (DLP) bioprinting, Materials Science and Engineering: C, Volume 109, Qijiang Mao, Yifan Wang, Yang Li, Sarun Juengpanich, Wenhuan Li, Mingyu Chen, Jun Yin, Jianzhong Fu, Xiujun Cai with the permission from Elsevier.

Figure 5 d. was reprinted from Rapid 3D bioprinting of decellularized extracellular matrix with regionally varied mechanical properties and biomimetic microarchitecture, Biomaterials, Volume 185, Xuanyi Ma, Claire Yu, Pengrui Wang, Weizhe Xu, Xueyi Wan, Cheuk Sun Edwin Lai, Justin Liu, Anna Koroleva-Maharajh, Shaochen Chen with permission from Elsevier.

Figures 7 g.-i. were reprinted from A novel decellularized skeletal muscle-derived ECM scaffolding system for in situ muscle regeneration, Methods, Volume 171, Hyeongjin Lee,

Young Min Ju, Ickhee Kim, Ebrahim Elsangeedy, Joon Ho Lee, James J. Yoo, Anthony Atala, Sang Jin Lee with the permission from Elsevier.

Figures 7 j.-n. were reprinted from Long-term retention of ECM hydrogel after implantation into asub-acute stroke cavity reduces lesion volume, Acta Biomaterialia, Volume 63, Harmanvir Ghuman, Madeline Gerwig, Francesca J. Nicholls, Jessie R. Liu, Julia Donnelly, Stephen F. Badylak, Michel Modo with the permission from Elsevier.

Figures 8 a.-b. were reprinted from Directing the growth and alignment of biliary epithelium within extracellular matrix hydrogels, Acta Biomaterialia, Volume 85, Phillip L. Lewis, Ming Yan, Jimmy Su, Ramille N. Shah with the permission from Elsevier.

References

1. Hynes RO, Naba A. Overview of the Matrisome--An Inventory of Extracellular Matrix Constituents and Functions. Cold Spring Harbor Perspectives in Biology. 2012;4(1):a004903.

2. Hynes RO. The Extracellular Matrix: Not Just Pretty Fibrils. Science. 2009;326(5957):1216-9.

3. Huang G, Li F, Zhao X, Ma Y, Li Y, Lin M, et al. Functional and Biomimetic Materials for Engineering of the Three-Dimensional Cell Microenvironment. Chemical reviews. 2017;117(20):12764-850.

4. Bonnans C, Chou J, Werb Z. Remodelling the extracellular matrix in development and disease. Nature Reviews Molecular Cell Biology. 2014;15(12):786-801.

5. Walma DAC, Yamada KM. The extracellular matrix in development. Development. 2020;147(10):dev175596.

6. Miller AE, Hu P, Barker TH. Feeling Things Out: Bidirectional Signaling of the Cell-ECM Interface, Implications in the Mechanobiology of Cell Spreading, Migration, Proliferation, and Differentiation. Advanced healthcare materials. 2020;9(8):e1901445.

7. Saldin LT, Cramer MC, Velankar SS, White LJ, Badylak SF. Extracellular matrix hydrogels from decellularized tissues: Structure and function. Acta biomaterialia. 2017;49:1-15.

8. Fernandez-Perez J, Ahearne M. The impact of decellularization methods on extracellular matrix derived hydrogels. Sci Rep. 2019;9(1):14933.

9. Gilbert TW, Sellaro TL, Badylak SF. Decellularization of tissues and organs. Biomaterials. 2006;27(19):3675-83.

10. Crapo PM, Gilbert TW, Badylak SF. An overview of tissue and whole organ decellularization processes. Biomaterials. 2011;32(12):3233-43.

11. Zhang X, Chen X, Hong H, Hu R, Liu J, Liu C. Decellularized extracellular matrix scaffolds: Recent trends and emerging strategies in tissue engineering. Bioact Mater. 2022;10:15-31.

12. Swinehart IT, Badylak SF. Extracellular matrix bioscaffolds in tissue remodeling and morphogenesis. Developmental dynamics : an official publication of the American Association of Anatomists. 2016;245(3):351-60.

13. Moffat D, Ye K, Jin S. Decellularization for the retention of tissue niches. J Tissue Eng. 2022;13:20417314221101151.

14. Abaci A, Guvendiren M. Designing Decellularized Extracellular Matrix-Based Bioinks for 3D Bioprinting. Advanced healthcare materials. 2020;9(24):e2000734.

15. Choudhury D, Yee M, Sheng ZLJ, Amirul A, Naing MW. Decellularization systems and devices: State-of-the-art. Acta biomaterialia. 2020;115:51-9.

16. Voytik-Harbin SL, Brightman AO, Waisner BZ, Robinson JP, Lamar CH. Small Intestinal Submucosa: A Tissue-Derived Extracellular Matrix That Promotes Tissue-Specific Growth and Differentiation of Cells *in-vitro*. Tissue Engineering. 1998;4(2):157-74.

17. Uriel S, Huang J-J, Moya ML, Francis ME, Wang R, Chang S-Y, et al. The role of adipose protein derived hydrogels in adipogenesis. Biomaterials. 2008;29(27):3712-9.

18. Hussey GS, Nascari DG, Saldin LT, Kolich B, Lee YC, Crum RJ, et al. Ultrasonic cavitation to prepare ECM hydrogels. Acta biomaterialia. 2020;108:77-86.

19. Zhang W, Du A, Liu S, Lv M, Chen S. Research progress in decellularized extracellular matrix-derived hydrogels. Regen Ther. 2021;18:88-96.

20. Hulmes DJS. Collagen Diversity, Synthesis and Assembly. Collagen: Structure and Mechanics. Boston: Springer US; 2008. p. 15-47.

21. Brown BN, Badylak SF. Extracellular matrix as an inductive scaffold for functional tissue reconstruction. Translational research : the journal of laboratory and clinical medicine. 2014;163(4):268-85.

22. Mendibil U, Ruiz-Hernandez R, Retegi-Carrion S, Garcia-Urquia N, Olalde-Graells B, Abarrategi A. Tissue-Specific Decellularization Methods: Rationale and Strategies to Achieve Regenerative Compounds. International journal of molecular sciences. 2020;21(15):21155447.

23. Chun SY, Lee JN, Ha YS, Yoon BH, Lee EH, Kim BM, et al. Optimization of extracellular matrix extraction from human perirenal adipose tissue. J Biomater Appl. 2021;35(9):1180-91.

24. Chun SY, Ha YS, Yoon BH, Lee EH, Kim BM, Gil H, et al. Optimal delipidation solvent to secure extracellular matrix from human perirenal adipose tissue. Journal of biomedical materials research Part A. 2022;110(4):928-42.

25. Gardin C, Ricci S, Ferroni L, Guazzo R, Sbricoli L, De Benedictis G, et al. Decellularization and Delipidation Protocols of Bovine Bone and Pericardium for Bone Grafting and Guided Bone Regeneration Procedures. PLoS One. 2015;10(7):e0132344.

26. Sawkins MJ, Bowen W, Dhadda P, Markides H, Sidney LE, Taylor AJ, et al. Hydrogels derived from demineralized and decellularized bone extracellular matrix. Acta biomaterialia. 2013;9(8):7865-73.

27. Peterson B, Whang PG, Iglesias R, Wang JC, Lieberman JR. Osteoinductivity of commercially available demineralized bone matrix. Preparations in a spine fusion model. J Bone Joint Surg Am. 2004;86(10):2243-50.

28. Nagao RJ, Xu J, Luo P, Xue J, Wang Y, Kotha S, et al. Decellularized Human Kidney Cortex Hydrogels Enhance Kidney Microvascular Endothelial Cell Maturation and Quiescence. Tissue engineering Part A. 2016;22(19-20):1140-50.

29. Kc P, Hong Y, Zhang G. Cardiac tissue-derived extracellular matrix scaffolds for myocardial repair: advantages and challenges. Regen Biomater. 2019;6(4):185-99.

30. Amirazad H, Dadashpour M, Zarghami N. Application of decellularized bone matrix as a bioscaffold in bone tissue engineering. J Biol Eng. 2022;16(1):1.

31. Wolf MT, Daly KA, Brennan-Pierce EP, Johnson SA, Carruthers CA, D'Amore A, et al. A hydrogel derived from decellularized dermal extracellular matrix. Biomaterials. 2012;33(29):7028-38.

32. Kort-Mascort J, Bao G, Elkashty O, Flores-Torres S, Munguia-Lopez JG, Jiang T, et al. Decellularized Extracellular Matrix Composite Hydrogel Bioinks for the Development of 3D Bioprinted Head and Neck *in-vitro* Tumor Models. ACS Biomaterials Science & Engineering. 2021;7(11):5288-300.

33. Freytes DO, Martin J, Velankar SS, Lee AS, Badylak SF. Preparation and rheological characterization of a gel form of the porcine urinary bladder matrix. Biomaterials. 2008;29(11):1630-7.

34. Fitton JH, Dalton BA, Beumer G, Johnson G, Griesser HJ, Steele JG. Surface topography can interfere with epithelial tissue migration. J Biomed Mater Res. 1998;42(2):245-57.

35. Wolf K, te Lindert M, Krause M, Alexander S, te Riet J, Willis AL, et al. Physical limits of cell migration: Control by ECM space and nuclear deformation and tuning by proteolysis and traction force. Journal of Cell Biology. 2013;201(7):1069-84.

36. Behmer Hansen RA, Wang X, Kaw G, Pierre V, Senyo SE. Accounting for Material Changes in Decellularized Tissue with Underutilized Methodologies. Biomed Res Int. 2021;2021:6696295.

37. Chan BP, Leong KW. Scaffolding in tissue engineering: general approaches and tissue-specific considerations. Eur Spine J. 2008;17(Suppl 4):467-79.

38. Pouliot RA, Young BM, Link PA, Park HE, Kahn AR, Shankar K, et al. Porcine Lung-Derived Extracellular Matrix Hydrogel Properties Are Dependent on Pepsin Digestion Time. Tissue Eng Part C Methods. 2020;26(6):332-46.

39. Giobbe GG, Crowley C, Luni C, Campinoti S, Khedr M, Kretzschmar K, et al. Extracellular matrix hydrogel derived from decellularized tissues enables endodermal organoid culture. Nature communications. 2019;10(1):5658.

40. Zhu J, Kaufman J, Laura. Collagen I Self-Assembly: Revealing the Developing Structures that Generate Turbidity. Biophysical Journal. 2014;106(8):1822-31.

41. Wedgwood J, Freemont AJ, Tirelli N. Rheological and Turbidity Study of Fibrin Hydrogels. Macromolecular Symposia. 2013;334(1):117-25.

42. Pati F, Jang J, Ha DH, Won Kim S, Rhie JW, Shim JH, et al. Printing three-dimensional tissue analogues with decellularized extracellular matrix bioink. Nature communications. 2014;5:3935.

43. Kesti M, Fisch P, Pensalfini M, Mazza E, Zenobi-Wong M. Guidelines for standardization of bioprinting: a systematic study of process parameters and their effect on bioprinted structures. BioNanoMaterials. 2016;17(3-4):193-204.

44. Blaeser A, Duarte Campos DF, Puster U, Richtering W, Stevens MM, Fischer H. Controlling Shear Stress in 3D Bioprinting is a Key Factor to Balance Printing Resolution and Stem Cell Integrity. Advanced healthcare materials. 2016;5(3):326-33.

45. Kim MK, Jeong W, Lee SM, Kim JB, Jin S, Kang HW. Decellularized extracellular matrix-based bio-ink with enhanced 3D printability and mechanical properties. Biofabrication. 2020;12(2):025003.

46. Rathan S, Dejob L, Schipani R, Haffner B, Mobius ME, Kelly DJ. Fiber Reinforced Cartilage ECM Functionalized Bioinks for Functional Cartilage Tissue Engineering. Advanced healthcare materials. 2019;8(7):e1801501.

47. Ha D-H, Chae S, Lee JY, Kim JY, Yoon J, Sen T, et al. Therapeutic effect of decellularized extracellular matrix-based hydrogel for radiation esophagitis by 3D printed esophageal stent. Biomaterials. 2021;266:120477.

48. Mezger T. Rotational Tests. The Rheology Handbook: For users of rotational and oscillatory rheometers. 4 ed. Hanover: Vincentz Network; 2014. p. 38-44.

49. Zhang X, Liu Y, Luo C, Zhai C, Li Z, Zhang Y, et al. Crosslinker-free silk/decellularized extracellular matrix porous bioink for 3D bioprinting-based cartilage tissue engineering. Materials science & engineering C, Materials for biological applications. 2021;118:111388.

50. Li H, Tan YJ, Leong KF, Li L. 3D Bioprinting of Highly Thixotropic Alginate/Methylcellulose Hydrogel with Strong Interface Bonding. ACS applied materials & interfaces. 2017;9(23):20086-97.

51. Li H, Liu S, Lin L. Rheological study on 3D printability of alginate hydrogel and effect of graphene oxide. International Journal of Bioprinting; Vol 2, No 2 (2016). 2016;2(2):54-66.

52. Antich C, Jiménez G, de Vicente J, López-Ruiz E, Chocarro-Wrona C, Griñán-Lisón C, et al. Development of a Biomimetic Hydrogel Based on Predifferentiated Mesenchymal Stem-Cell-Derived ECM for Cartilage Tissue Engineering. Advanced healthcare materials. 2021;10(8):e2001847.

53. Tang M, Rich JN, Chen S. Biomaterials and 3D Bioprinting Strategies to Model Glioblastoma and the Blood-Brain Barrier. Advanced materials (Deerfield Beach, Fla). 2021;33(5):e2004776.

54. Choudhury D, Tun HW, Wang T, Naing MW. Organ-Derived Decellularized Extracellular Matrix: A Game Changer for Bioink Manufacturing? Trends Biotechnol. 2018;36(8):787-805.

55. Mousavi A, Mashayekhan S, Baheiraei N, Pourjavadi A. Biohybrid oxidized alginate/myocardial extracellular matrix injectable hydrogels with improved electromechanical properties for cardiac tissue engineering. Int J Biol Macromol. 2021;180:692-708.

56. Shin YJ, Shafranek RT, Tsui JH, Walcott J, Nelson A, Kim DH. 3D bioprinting of mechanically tuned bioinks derived from cardiac decellularized extracellular matrix. Acta biomaterialia. 2021;119:75-88.

57. Jang J, Kim TG, Kim BS, Kim S-W, Kwon S-M, Cho D-W. Tailoring mechanical properties of decellularized extracellular matrix bioink by vitamin B2-induced photo-crosslinking. Acta biomaterialia. 2016;33:88-95.

58. Ma X, Yu C, Wang P, Xu W, Wan X, Lai CSE, et al. Rapid 3D bioprinting of decellularized extracellular matrix with regionally varied mechanical properties and biomimetic microarchitecture. Biomaterials. 2018;185:310-21.

59. Wang X, Senapati S, Akinbote A, Gnanasambandam B, Park PSH, Senyo SE. Microenvironment stiffness requires decellularized cardiac extracellular matrix to promote heart regeneration in the neonatal mouse heart. Acta biomaterialia. 2020;113:380-92.

60. Mao Q, Wang Y, Li Y, Juengpanich S, Li W, Chen M, et al. Fabrication of liver microtissue with liver decellularized extracellular matrix (dECM) bioink by digital light processing (DLP) bioprinting. Materials Science and Engineering: C. 2020;109:110625.

61. Lee J, Hong J, Kim W, Kim GH. Bone-derived dECM/alginate bioink for fabricating a 3D cell-laden mesh structure for bone tissue engineering. Carbohydrate Polymers. 2020;250:116914.

62. Badylak SF, Freytes DO, Gilbert TW. Extracellular matrix as a biological scaffold material: Structure and function. Acta biomaterialia. 2009;5(1):1-13.

63. Costa A, Naranjo JD, Londono R, Badylak SF. Biologic Scaffolds. Cold Spring Harbor Perspectives in Medicine. 2017;7(9):a025676.

64. Rozario T, DeSimone DW. The extracellular matrix in development and morphogenesis: a dynamic view. Dev Biol. 2010;341(1):126-40.

65. Klecker C, Nair LS. Matrix Chemistry Controlling Stem Cell Behavior. In: Vishwakarma A, Karp JM, editors. Biology and Engineering of Stem Cell Niches. Boston: Academic Press; 2017. p. 195-213.

66. Ricard-Blum S. The Collagen Family. Cold Spring Harbor Perspectives in Biology. 2011;3(1):a004978-a.

67. Medberry CJ, Crapo PM, Siu BF, Carruthers CA, Wolf MT, Nagarkar SP, et al. Hydrogels derived from central nervous system extracellular matrix. Biomaterials. 2013;34(4):1033-40.

68. Mezzenga R, Mitsi M. The Molecular Dance of Fibronectin: Conformational Flexibility Leads to Functional Versatility. Biomacromolecules. 2019;20(1):55-72.

69. Yu Q, Xue Y, Liu J, Xi Z, Li Z, Liu Y. Fibronectin Promotes the Malignancy of Glioma Stem-Like Cells Via Modulation of Cell Adhesion, Differentiation, Proliferation and Chemoresistance. Front Mol Neurosci. 2018;11:130.

70. Yurchenco PD, Tsilibary EC, Charonis AS, Furthmayr H. Laminin polymerization *in-vitro*. Evidence for a two-step assembly with domain specificity. J Biol Chem. 1985;260(12):7636-44.

71. Yurchenco PD, Cheng Y-S. Self-assembly and calcium-binding sites in laminin. A three-arm interaction model. Journal of Biological Chemistry. 1993;268(23):17286-99.

72. Lin M, Ge J, Wang X, Dong Z, Xing M, Lu F, et al. Biochemical and biomechanical comparisions of decellularized scaffolds derived from porcine subcutaneous and visceral adipose tissue. J Tissue Eng. 2019;10:2041731419888168.

73. Faulk DM, Johnson SA, Zhang L, Badylak SF. Role of the extracellular matrix in whole organ engineering. Journal of cellular physiology. 2014;229(8):984-9.

74. Jackson RL, Busch SJ, Cardin AD. Glycosaminoglycans: molecular properties, protein interactions, and role in physiological processes. Physiol Rev. 1991;71(2):481-539.

75. Alberts B, Johnson A, Lewis J, Raff M, Roberts K, Walter P. Cell Junctions, Cell Adhesion, and the Extracellular Matrix. Molecular Biology of the Cell. 4 ed. New York: W.W. Norton & Company; 2015. p. 1058.

76. Frevert CW, Wight TN. Extracellular Matrix | Matrix Proteoglycans. In: Laurent GJ, Shapiro SD, editors. Encyclopedia of Respiratory Medicine. Oxford: Academic Press; 2006. p. 184-8.

77. Theocharis AD, Skandalis SS, Tzanakakis GN, Karamanos NK. Proteoglycans in health and disease: novel roles for proteoglycans in malignancy and their pharmacological targeting. FEBS J. 2010;277(19):3904-23.

78. Uhl FE, Zhang F, Pouliot RA, Uriarte JJ, Rolandsson Enes S, Han X, et al. Functional role of glycosaminoglycans in decellularized lung extracellular matrix. Acta biomaterialia. 2020;102:231-46.

79. Mendoza-Novelo B, Avila EE, Cauich-Rodriguez JV, Jorge-Herrero E, Rojo FJ, Guinea GV, et al. Decellularization of pericardial tissue and its impact on tensile viscoelasticity and glycosaminoglycan content. Acta biomaterialia. 2011;7(3):1241-8.

80. Booth AJ, Hadley R, Cornett AM, Dreffs AA, Matthes SA, Tsui JL, et al. Acellular normal and fibrotic human lung matrices as a culture system for *in-vitro* investigation. Am J Respir Crit Care Med. 2012;186(9):866-76.

81. Shen W, Berning K, Tang SW, Lam YW. Rapid and Detergent-Free Decellularization of Cartilage. Tissue Eng Part C Methods. 2020;26(4):201-6.

82. Jung SY, Tran AN, Kim HY, Choi E, Lee SJ, Kim HS. Development of Acellular Respiratory Mucosal Matrix Using Porcine Tracheal Mucosa. Tissue Eng Regen Med. 2020;17(4):433-43.

83. Norbertczak HT, Ingham E, Fermor HL, Wilcox RK. Decellularized Intervertebral Discs: A Potential Replacement for Degenerate Human Discs. Tissue Eng Part C Methods. 2020;26(11):565-76.

84. Mohiuddin OA, Campbell B, Poche JN, Thomas-Porch C, Hayes DA, Bunnell BA, et al. Decellularized Adipose Tissue: Biochemical Composition, *in-vivo* Analysis and Potential Clinical Applications. Adv Exp Med Biol. 2020;1212:57-70.

85. Nakamura S, Ijima H. Solubilized matrix derived from decellularized liver as a growth factor-immobilizable scaffold for hepatocyte culture. J Biosci Bioeng. 2013;116(6):746-53.

86. Viswanath A, Vanacker J, Germain L, Leprince JG, Diogenes A, Shakesheff KM, et al. Extracellular matrix-derived hydrogels for dental stem cell delivery. Journal of biomedical materials research Part A. 2017;105(1):319-28.

87. Koci Z, Vyborny K, Dubisova J, Vackova I, Jager A, Lunov O, et al. Extracellular Matrix Hydrogel Derived from Human Umbilical Cord as a Scaffold for Neural Tissue

Repair and Its Comparison with Extracellular Matrix from Porcine Tissues. Tissue Eng Part C Methods. 2017;23(6):333-45.

88. Hodde JP, Record RD, Liang HA, Badylak SF. Vascular endothelial growth factor in porcine-derived extracellular matrix. Endothelium. 2001;8(1):11-24.

89. Fercana GR, Yerneni S, Billaud M, Hill JC, VanRyzin P, Richards TD, et al. Perivascular extracellular matrix hydrogels mimic native matrix microarchitecture and promote angiogenesis via basic fibroblast growth factor. Biomaterials. 2017;123:142-54.

90. Bradshaw AD. Regulation of cell behavior by extracellular proteins. In: Lanza R, Langer R, Vacanti JP, Atala A, editors. Principles of Tissue Engineering. 5 ed. London: Academic Press; 2020. p. 205-15.

91. Choi JS, Kim BS, Kim JD, Choi YC, Lee HY, Cho YW. *In-vitro* cartilage tissue engineering using adipose-derived extracellular matrix scaffolds seeded with adipose-derived stem cells. Tissue engineering Part A. 2012;18(1-2):80-92.

92. Wuthrich T, Lese I, Haberthur D, Zubler C, Hlushchuk R, Hewer E, et al. Development of vascularized nerve scaffold using perfusion-decellularization and recellularization. Materials science & engineering C, Materials for biological applications. 2020;117:111311.

93. Huang YB, Mei J, Yu Y, Ding Y, Xia W, Yue T, et al. Comparative Decellularization and Recellularization of Normal Versus Streptozotocin-Induced Diabetes Mellitus Rat Pancreas. Artif Organs. 2019;43(4):399-412.

94. Ali M, Pr AK, Yoo JJ, Zahran F, Atala A, Lee SJ. A Photo-Crosslinkable Kidney ECM-Derived Bioink Accelerates Renal Tissue Formation. Advanced healthcare materials. 2019;8(7):e1800992.

95. Jiang Y, Sun SJ, Zhen Z, Wei R, Zhang N, Liao SY, et al. Myocardial repair of bioengineered cardiac patches with decellularized placental scaffold and human-induced pluripotent stem cells in a rat model of myocardial infarction. Stem Cell Res Ther. 2021;12(1):13.

96. Park K-M, Hussein KH, Hong S-H, Ahn C, Yang S-R, Park S-M, et al. Decellularized liver extracellular matrix as promising tools for transplantable bioengineered liver promotes hepatic lineage commitments of induced pluripotent stem cells. Tissue Engineering Part A. 2016;22(5-6):449-60.

97. van Dommelen SM, Vader P, Lakhal S, Kooijmans SA, van Solinge WW, Wood MJ, et al. Microvesicles and exosomes: opportunities for cell-derived membrane vesicles in drug delivery. J Control Release. 2012;161(2):635-44.

98. Akers JC, Gonda D, Kim R, Carter BS, Chen CC. Biogenesis of extracellular vesicles (EV): exosomes, microvesicles, retrovirus-like vesicles, and apoptotic bodies. J Neurooncol. 2013;113(1):1-11.

99. Nawaz M, Camussi G, Valadi H, Nazarenko I, Ekstrom K, Wang X, et al. The emerging role of extracellular vesicles as biomarkers for urogenital cancers. Nat Rev Urol. 2014;11(12):688-701.

100. Valadi H, Ekstrom K, Bossios A, Sjostrand M, Lee JJ, Lotvall JO. Exosome-mediated transfer of mRNAs and microRNAs is a novel mechanism of genetic exchange between cells. Nat Cell Biol. 2007;9(6):654-9.

101. Gangadaran P, Rajendran RL, Oh JM, Hong CM, Jeong SY, Lee S-W, et al. Extracellular vesicles derived from macrophage promote angiogenesis *In-vitro* and accelerate new vasculature formation *In-vivo*. Experimental Cell Research. 2020;394(2):112146.

102. Xu J-F, Yang G-H, Pan X-H, Zhang S-J, Zhao C, Qiu B-S, et al. Altered MicroRNA Expression Profile in Exosomes during Osteogenic Differentiation of Human Bone Marrow-Derived Mesenchymal Stem Cells. PLoS ONE. 2014;9(12):e114627.

103. Möller A, Lobb RJ. The evolving translational potential of small extracellular vesicles in cancer. Nature Reviews Cancer. 2020;20(12):697-709.

104. Xu R, Rai A, Chen M, Suwakulsiri W, Greening DW, Simpson RJ. Extracellular vesicles in cancer—implications for future improvements in cancer care. Nature reviews Clinical oncology. 2018;15(10):617-38.

105. Zhou X, Xie F, Wang L, Zhang L, Zhang S, Fang M, et al. The function and clinical application of extracellular vesicles in innate immune regulation. Cellular & Molecular Immunology. 2020;17(4):323-34.

106. Caruso S, Poon IKH. Apoptotic Cell-Derived Extracellular Vesicles: More Than Just Debris. Frontiers in Immunology. 2018;9.

107. Greening DW, Gopal SK, Mathias RA, Liu L, Sheng J, Zhu H-J, et al., editors. Emerging roles of exosomes during epithelial–mesenchymal transition and cancer progression. Seminars in cell & developmental biology; 2015: Elsevier.

108. Huleihel L, Hussey GS, Naranjo JD, Zhang L, Dziki JL, Turner NJ, et al. Matrix-bound nanovesicles within ECM bioscaffolds. Sci Adv. 2016;2(6):e1600502.

109. Arnaout MA, Mahalingam B, Xiong JP. Integrin structure, allostery, and bidirectional signaling. Annu Rev Cell Dev Biol. 2005;21:381-410.

110. Takada Y, Ye X, Simon S. The integrins. Genome Biol. 2007;8(5):215.

111. Thorne JT, Segal TR, Chang S, Jorge S, Segars JH, Leppert PC. Dynamic reciprocity between cells and their microenvironment in reproduction. Biol Reprod. 2015;92(1):25.

112. Gao M, Craig D, Lequin O, Campbell ID, Vogel V, Schulten K. Structure and functional significance of mechanically unfolded fibronectin type III1 intermediates. Proc Natl Acad Sci U S A. 2003;100(25):14784-9.

113. Klotzsch E, Smith ML, Kubow KE, Muntwyler S, Little WC, Beyeler F, et al. Fibronectin forms the most extensible biological fibers displaying switchable force-exposed cryptic binding sites. Proc Natl Acad Sci U S A. 2009;106(43):18267-72.

114. Lee GM, Loeser RF. Cell surface receptors transmit sufficient force to bend collagen fibrils. Exp Cell Res. 1999;248(1):294-305.

115. Uzawa K, Grzesik WJ, Nishiura T, Kuznetsov SA, Robey PG, Brenner DA, et al. Differential expression of human lysyl hydroxylase genes, lysine hydroxylation, and cross-linking of type I collagen during osteoblastic differentiation *in-vitro*. J Bone Miner Res. 1999;14(8):1272-80.

116. Chan CE, Odde DJ. Traction dynamics of filopodia on compliant substrates. Science. 2008;322(5908):1687-91.

117. Birkedal-Hansen H. Catabolism and turnover of collagens: collagenases. Methods Enzymol. 1987;144:140-71.

118. Cui N, Hu M, Khalil RA. Biochemical and Biological Attributes of Matrix Metalloproteinases. Prog Mol Biol Transl Sci. 2017;147:1-73.

119. Friedl P, Wolf K. Tube travel: the role of proteases in individual and collective cancer cell invasion. Cancer Res. 2008;68(18):7247-9.

120. Xu J, Rodriguez D, Petitclerc E, Kim JJ, Hangai M, Moon YS, et al. Proteolytic exposure of a cryptic site within collagen type IV is required for angiogenesis and tumor growth *in-vivo*. J Cell Biol. 2001;154(5):1069-79.

121. Calabro NE, Kristofik NJ, Kyriakides TR. Thrombospondin-2 and extracellular matrix assembly. Biochim Biophys Acta. 2014;1840(8):2396-402.

122. Mimeault M, Batra SK. Concise review: recent advances on the significance of stem cells in tissue regeneration and cancer therapies. Stem Cells. 2006;24(11):2319-45.

123. Zakrzewski W, Dobrzynski M, Szymonowicz M, Rybak Z. Stem cells: past, present, and future. Stem Cell Res Ther. 2019;10(1):68.

124. Dawson E, Mapili G, Erickson K, Taqvi S, Roy K. Biomaterials for stem cell differentiation. Advanced drug delivery reviews. 2008;60(2):215-28.

125. Xu Y, Zhou J, Liu C, Zhang S, Gao F, Guo W, et al. Understanding the role of tissue-specific decellularized spinal cord matrix hydrogel for neural stem/progenitor cell microenvironment reconstruction and spinal cord injury. Biomaterials. 2021;268:120596.

126. Peng Y, Huang D, Li J, Liu S, Qing X, Shao Z. Genipin-crosslinked decellularized annulus fibrosus hydrogels induces tissue-specific differentiation of bone mesenchymal stem cells and intervertebral disc regeneration. J Tissue Eng Regen Med. 2020;14(3):497-509.

127. Duan Y, Liu Z, O'Neill J, Wan LQ, Freytes DO, Vunjak-Novakovic G. Hybrid gel composed of native heart matrix and collagen induces cardiac differentiation of human embryonic stem cells without supplemental growth factors. J Cardiovasc Transl Res. 2011;4(5):605-15.

128. French KM, Boopathy AV, DeQuach JA, Chingozha L, Lu H, Christman KL, et al. A naturally derived cardiac extracellular matrix enhances cardiac progenitor cell behavior *in-vitro*. Acta biomaterialia. 2012;8(12):4357-64.

129. Milan PB, Lotfibakhshaiesh N, Joghataie MT, Ai J, Pazouki A, Kaplan DL, et al. Accelerated wound healing in a diabetic rat model using decellularized dermal matrix and human umbilical cord perivascular cells. Acta biomaterialia. 2016;45:234-46.

130. Belviso I, Romano V, Sacco AM, Ricci G, Massai D, Cammarota M, et al. Decellularized Human Dermal Matrix as a Biological Scaffold for Cardiac Repair and Regeneration. Front Bioeng Biotechnol. 2020;8:229.

131. Matoug-Elwerfelli M, Duggal MS, Nazzal H, Esteves F, Raif E. A biocompatible decellularized pulp scaffold for regenerative endodontics. Int Endod J. 2018;51(6):663-73.

132. Nichols JE, La Francesca S, Vega SP, Niles JA, Argueta LB, Riddle M, et al. Giving new life to old lungs: methods to produce and assess whole human paediatric bioengineered lungs. J Tissue Eng Regen Med. 2017;11(7):2136-52.

133. Zhang Z, Xu H, Mazza G, Zhang M, Frenguelli L, Liu Q, et al. Decellularized human liver scaffold-based three-dimensional culture system facilitate hepatitis B virus infection. Journal of biomedical materials research Part A. 2019;107(8):1744-53.

134. Mazza G, Al-Akkad W, Telese A, Longato L, Urbani L, Robinson B, et al. Rapid production of human liver scaffolds for functional tissue engineering by high shear stress oscillation-decellularization. Sci Rep. 2017;7(1):5534.

135. Peloso A, Petrosyan A, Da Sacco S, Booth C, Zambon JP, O'Brien T, et al. Renal Extracellular Matrix Scaffolds From Discarded Kidneys Maintain Glomerular

Morphometry and Vascular Resilience and Retains Critical Growth Factors. Transplantation. 2015;99(9):1807-16.

136. Guhathakurta S, Mathapati S, Bishi DK, Rallapalli S, Cherian KM. Nanofiber-reinforced myocardial tissue-construct as ventricular assist device. Asian Cardiovasc Thorac Ann. 2014;22(8):935-43.

137. Schneider C, Lehmann J, van Osch GJ, Hildner F, Teuschl A, Monforte X, et al. Systematic Comparison of Protocols for the Preparation of Human Articular Cartilage for Use as Scaffold Material in Cartilage Tissue Engineering. Tissue Eng Part C Methods. 2016;22(12):1095-107.

138. Hassanpour A, Talaei-Khozani T, Kargar-Abarghouei E, Razban V, Vojdani Z. Decellularized human ovarian scaffold based on a sodium lauryl ester sulfate (SLES)-treated protocol, as a natural three-dimensional scaffold for construction of bioengineered ovaries. Stem Cell Res Ther. 2018;9(1):252.

139. Porzionato A, Stocco E, Barbon S, Grandi F, Macchi V, De Caro R. Tissue-Engineered Grafts from Human Decellularized Extracellular Matrices: A Systematic Review and Future Perspectives. International journal of molecular sciences. 2018;19(12):19124117.

140. Dawson HD. A comparative assessment of the pig, mouse and human genomes. The Minipig in Biomedical Research. 1 ed. US: CRC Press; 2011. p. 323-42.

141. Kim BS, Kwon YW, Kong J-S, Park GT, Gao G, Han W, et al. 3D cell printing of *in-vitro* stabilized skin model and *in-vivo* pre-vascularized skin patch using tissue-specific extracellular matrix bioink: A step towards advanced skin tissue engineering. Biomaterials. 2018;168:38-53.

142. Kitahara H, Yagi H, Tajima K, Okamoto K, Yoshitake A, Aeba R, et al. Heterotopic transplantation of a decellularized and recellularized whole porcine heart. Interactive CardioVascular and Thoracic Surgery. 2016;22(5):571-9.

143. Baptista PM, Orlando G, Mirmalek-Sani SH, Siddiqui M, Atala A, Soker S. Whole organ decellularization - a tool for bioscaffold fabrication and organ bioengineering. Annu Int Conf IEEE Eng Med Biol Soc. 2009;2009:6526-9.

144. Goulle F. Use of porcine small intestinal submucosa for corneal reconstruction in dogs and cats: 106 cases. J Small Anim Pract. 2012;53(1):34-43.

145. Merguerian PA, Reddy PP, Barrieras DJ, Wilson GJ, Woodhouse K, Bagli DJ, et al. Acellular bladder matrix allografts in the regeneration of functional bladders: evaluation of large-segment (> 24 cm2) substitution in a porcine model. BJU International. 2001;85(7):894-8.

146. Denner J, Tönjes RR. Infection Barriers to Successful Xenotransplantation Focusing on Porcine Endogenous Retroviruses. Clinical Microbiology Reviews. 2012;25(2):318-43.

147. Toprakhisar B, Nadernezhad A, Bakirci E, Khani N, Skvortsov GA, Koc B. Development of bioink from decellularized tendon extracellular matrix for 3D bioprinting. Macromolecular bioscience. 2018;18(10):1800024.

148. Gupta SK, Dinda AK, Mishra NC. Antibacterial activity and composition of decellularized goat lung extracellular matrix for its tissue engineering applications. Biol Eng Med. 2017;2(1):1-7.

149. Johnson TD, Dequach JA, Gaetani R, Ungerleider J, Elhag D, Nigam V, et al. Human versus porcine tissue sourcing for an injectable myocardial matrix hydrogel. Biomater Sci. 2014;2(5):735-44.

150. Badylak SF, Gilbert TW. Immune response to biologic scaffold materials. Seminars in Immunology. 2008;20(2):109-16.

151. Dziki JL, Wang DS, Pineda C, Sicari BM, Rausch T, Badylak SF. Solubilized extracellular matrix bioscaffolds derived from diverse source tissues differentially influence macrophage phenotype. Journal of biomedical materials research Part A. 2017;105(1):138-47.

152. De Souza RR. Aging of myocardial collagen. Biogerontology. 2002;3(6):325-35.

153. Tottey S, Johnson SA, Crapo PM, Reing JE, Zhang L, Jiang H, et al. The effect of source animal age upon extracellular matrix scaffold properties. Biomaterials. 2011;32(1):128-36.

154. Nakayama KH, Batchelder CA, Lee CI, Tarantal AF. Renal Tissue Engineering with Decellularized Rhesus Monkey Kidneys: Age-Related Differences. Tissue Engineering Part A. 2011;17(23-24):2891-901.

155. Burgess ML, McCrea JC, Hedrick HL. Age-associated changes in cardiac matrix and integrins. Mech Ageing Dev. 2001;122(15):1739-56.

156. Gershlak JR, Resnikoff JI, Sullivan KE, Williams C, Wang RM, Black LD. Mesenchymal stem cells ability to generate traction stress in response to substrate stiffness is modulated by the changing extracellular matrix composition of the heart during development. Biochemical and Biophysical Research Communications. 2013;439(2):161-6.

157. Ayyildiz M, Aktas RG, Basdogan C. Effect of solution and post-mortem time on mechanical and histological properties of liver during cold preservation. Biorheology. 2014;51(1):47-70.

158. Lu P, Takai K, Weaver VM, Werb Z. Extracellular matrix degradation and remodeling in development and disease. Cold Spring Harb Perspect Biol. 2011;3(12):a005058.

159. Parker MW, Rossi D, Peterson M, Smith K, Sikstrom K, White ES, et al. Fibrotic extracellular matrix activates a profibrotic positive feedback loop. J Clin Invest. 2014;124(4):1622-35.

160. Gentilin E, D'Angelo E, Agostini M, Astolfi L. Decellularized normal and cancer tissues as tools for cancer research. Cancer Gene Therapy. 2021;29:979-888.

161. Wagner DE, Bonenfant NR, Parsons CS, Sokocevic D, Brooks EM, Borg ZD, et al. Comparative decellularization and recellularization of normal versus emphysematous human lungs. Biomaterials. 2014;35(10):3281-97.

162. Petrosyan A, Da Sacco S, Tripuraneni N, Kreuser U, Lavarreda-Pearce M, Tamburrini R, et al. A step towards clinical application of acellular matrix: A clue from macrophage polarization. Matrix Biology. 2017;57-58:334-46.

163. Sullivan KE, Burns LJ, Black LD. An *in-vitro* model for the assessment of stem cell fate following implantation within the infarct microenvironment identifies ISL-1 expression as the strongest predictor of c-Kit+ cardiac progenitor cells' therapeutic potential. Journal of Molecular and Cellular Cardiology. 2015;88:91-100.

164. Hoshiba T. Decellularized Extracellular Matrix for Cancer Research. Materials (Basel). 2019;12(8):12081311.

165. Jin Q, Liu G, Li S, Yuan H, Yun Z, Zhang W, et al. Decellularized breast matrix as bioactive microenvironment for *in-vitro* three-dimensional cancer culture. Journal of cellular physiology. 2019;234(4):3425-35.

166. Piccoli M, D'Angelo E, Crotti S, Sensi F, Urbani L, Maghin E, et al. Decellularized colorectal cancer matrix as bioactive microenvironment for *in-vitro* 3D cancer research. Journal of cellular physiology. 2018;233(8):5937-48.

167. Morse D, Rosas IO. Tobacco smoke-induced lung fibrosis and emphysema. Annu Rev Physiol. 2014;76:493-513.

168. Piasecki J, McPhee JS, Hannam K, Deere KC, Elhakeem A, Piasecki M, et al. Hip and spine bone mineral density are greater in master sprinters, but not endurance runners compared with non-athletic controls. Arch Osteoporos. 2018;13(1):72.

169. De Innocentiis C, Ricci F, Khanji MY, Aung N, Tana C, Verrengia E, et al. Athlete's Heart: Diagnostic Challenges and Future Perspectives. Sports Med. 2018;48(11):2463-77.

170. Quail DF, Dannenberg AJ. The obese adipose tissue microenvironment in cancer development and progression. Nat Rev Endocrinol. 2019;15(3):139-54.

171. Wishart AL, Conner SJ, Guarin JR, Fatherree JP, Peng Y, McGinn RA, et al. Decellularized extracellular matrix scaffolds identify full-length collagen VI as a driver of breast cancer cell invasion in obesity and metastasis. Sci Adv. 2020;6(43):eabc3175.

172. Timraz SBH, Rezgui R, Boularaoui SM, Teo JCM. Stiffness of Extracellular Matrix Components Modulates the Phenotype of Human Smooth Muscle Cells *in-vitro* and Allows for the Control of Properties of Engineered Tissues. Procedia Engineering. 2015;110:29-36.

173. Kim H, Kim MC, Asada HH. Extracellular matrix remodelling induced by alternating electrical and mechanical stimulations increases the contraction of engineered skeletal muscle tissues. Sci Rep. 2019;9(1):2732.

174. Frantz C, Stewart KM, Weaver VM. The extracellular matrix at a glance. J Cell Sci. 2010;123(24):4195-200.

175. Mao Y, Hoffman T, Wu A, Goyal R, Kohn J. Cell type–specific extracellular matrix guided the differentiation of human mesenchymal stem cells in 3D polymeric scaffolds. Journal of Materials Science: Materials in Medicine. 2017;28(7):100.

176. Statzer C, Ewald CY. The extracellular matrix phenome across species. Matrix Biology Plus. 2020;8:100039.

177. Balestrini JL, Gard AL, Gerhold KA, Wilcox EC, Liu A, Schwan J, et al. Comparative biology of decellularized lung matrix: Implications of species mismatch in regenerative medicine. Biomaterials. 2016;102:220-30.

178. Wong ML, Griffiths LG. Immunogenicity in xenogeneic scaffold generation: antigen removal vs. decellularization. Acta biomaterialia. 2014;10(5):1806-16.

179. Chakraborty J, Roy S, Ghosh S. Regulation of decellularized matrix mediated immune response. Biomaterials Science. 2020;8(5):1194-215.

180. Pagliarosi O, Picchio V, Chimenti I, Messina E, Gaetani R. Building an Artificial Cardiac Microenvironment: A Focus on the Extracellular Matrix. Frontiers in cell and developmental biology. 2020;8:559032-.

181. Ou DB, He Y, Chen R, Teng JW, Wang HT, Zeng D, et al. Three-dimensional co-culture facilitates the differentiation of embryonic stem cells into mature cardiomyocytes. J Cell Biochem. 2011;112(12):3555-62.

182. Beauchamp P, Jackson CB, Ozhathil LC, Agarkova I, Galindo CL, Sawyer DB, et al. 3D co-culture of hiPSC-derived cardiomyocytes with cardiac fibroblasts improves tissue-like features of cardiac spheroids. Frontiers in molecular biosciences. 2020;7:14.

183. Furtado MB, Nim HT, Boyd SE, Rosenthal NA. View from the heart: cardiac fibroblasts in development, scarring and regeneration. Development. 2016;143(3):387-97.

184. Mekhileri NV, Lim KS, Brown GCJ, Mutreja I, Schon BS, Hooper GJ, et al. Automated 3D bioassembly of micro-tissues for biofabrication of hybrid tissue engineered constructs. Biofabrication. 2018;10(2):024103.

185. Lehmanna R, Thurowa K, Stollb R, Weipperta M, editors. Human vs. Machine in Life Science Automation: Comparing Effectiveness of Manual and Automated 3-D Cell Culturing Processes. Advances in Ergonomics In Design, Usability & Special Populations: Part II; 2022: AHFE International.

186. Drewitz M, Helbling M, Fried N, Bieri M, Moritz W, Lichtenberg J, et al. Towards automated production and drug sensitivity testing using scaffold-free spherical tumor microtissues. Biotechnol J. 2011;6(12):1488-96.

187. Willemse J, van Tienderen G, van Hengel E, Schurink I, van der Ven D, Kan Y, et al. Hydrogels derived from decellularized liver tissue support the growth and differentiation of cholangiocyte organoids. Biomaterials. 2022;284:121473.

188. Zhang X, Xiao S, Liu B, Miao Y, Hu Z. Use of extracellular matrix hydrogel from human placenta to restore hair-inductive potential of dermal papilla cells. Regen Med. 2019;14(8):741-51.

189. Xing H, Zhang Z, Mao Q, Wang C, Zhou Y, Zhou X, et al. Injectable exosome-functionalized extracellular matrix hydrogel for metabolism balance and pyroptosis regulation in intervertebral disc degeneration. J Nanobiotechnology. 2021;19(1):264.

190. Massensini AR, Ghuman H, Saldin LT, Medberry CJ, Keane TJ, Nicholls FJ, et al. Concentration-dependent rheological properties of ECM hydrogel for intracerebral delivery to a stroke cavity. Acta biomaterialia. 2015;27:116-30.

191. Ghuman H, Massensini AR, Donnelly J, Kim S-M, Medberry CJ, Badylak SF, et al. ECM hydrogel for the treatment of stroke: Characterization of the host cell infiltrate. Biomaterials. 2016;91:166-81.

192. Ungerleider JL, Johnson TD, Hernandez MJ, Elhag DI, Braden RL, Dzieciatkowska M, et al. Extracellular Matrix Hydrogel Promotes Tissue Remodeling, Arteriogenesis, and Perfusion in a Rat Hindlimb Ischemia Model. JACC Basic Transl Sci. 2016;1(1-2):32-44.

193. Wu J, Ding Q, Dutta A, Wang Y, Huang YH, Weng H, et al. An injectable extracellular matrix derived hydrogel for meniscus repair and regeneration. Acta biomaterialia. 2015;16:49-59.

194. Wang X, Ansari A, Pierre V, Young K, Kothapalli CR, von Recum HA, et al. Injectable Extracellular Matrix Microparticles Promote Heart Regeneration in Mice with Post-ischemic Heart Injury. Advanced healthcare materials. 2022;11(8):e2102265.

195. Bejleri D, Davis ME. Decellularized Extracellular Matrix Materials for Cardiac Repair and Regeneration. Advanced healthcare materials. 2019;8(5):e1801217.

196. Liang J, Yi P, Wang X, Huang F, Luan X, Zhao Z, et al. Acellular matrix hydrogel for repair of the temporomandibular joint disc. Journal of biomedical materials research Part B, Applied biomaterials. 2020;108(7):2995-3007.

197. Lee JS, Shin J, Park HM, Kim YG, Kim BG, Oh JW, et al. Liver extracellular matrix providing dual functions of two-dimensional substrate coating and three-dimensional injectable hydrogel platform for liver tissue engineering. Biomacromolecules. 2014;15(1):206-18.

198. Schweinlin M, Wilhelm S, Schwedhelm I, Hansmann J, Rietscher R, Jurowich C, et al. Development of an Advanced Primary Human *In-vitro* Model of the Small Intestine. Tissue Eng Part C Methods. 2016;22(9):873-83.

199. Sellaro TL, Ranade A, Faulk DM, McCabe GP, Dorko K, Badylak SF, et al. Maintenance of human hepatocyte function *in-vitro* by liver-derived extracellular matrix gels. Tissue engineering Part A. 2010;16(3):1075-82.

200. Keane TJ, DeWard A, Londono R, Saldin LT, Castleton AA, Carey L, et al. Tissue-specific effects of esophageal extracellular matrix. Tissue Engineering Part A. 2015;21(17-18):2293-300.

201. Schoen B, Avrahami R, Baruch L, Efraim Y, Goldfracht I, Elul O, et al. Electrospun Extracellular Matrix: Paving the Way to Tailor-Made Natural Scaffolds for Cardiac Tissue Regeneration. Advanced Functional Materials. 2017;27(34):1700427.

202. Smoak MM, Hogan KJ, Grande-Allen KJ, Mikos AG. Bioinspired electrospun dECM scaffolds guide cell growth and control the formation of myotubes. Science Advances. 2021;7(20):eabg4123.

203. Jiang T, Munguia-Lopez JG, Flores-Torres S, Kort-Mascort J, Kinsella JM. Extrusion bioprinting of soft materials: An emerging technique for biological model fabrication. Applied Physics Reviews. 2019;6(1):011310.

204. Jiang T, Munguia-Lopez JG, Flores-Torres S, Grant J, Vijayakumar S, De Leon-Rodriguez A, et al. Directing the Self-assembly of Tumour Spheroids by Bioprinting Cellular Heterogeneous Models within Alginate/Gelatin Hydrogels. Scientific Reports. 2017;7(1):4575.

205. Nair K, Gandhi M, Khalil S, Yan KC, Marcolongo M, Barbee K, et al. Characterization of cell viability during bioprinting processes. Biotechnology Journal: Healthcare Nutrition Technology. 2009;4(8):1168-77.

206. Jungst T, Smolan W, Schacht K, Scheibel T, Groll J. Strategies and Molecular Design Criteria for 3D Printable Hydrogels. Chemical reviews. 2016;116(3):1496-539.

207. Murphy SV, Atala A. 3D bioprinting of tissues and organs. Nature biotechnology. 2014;32(8):773.

208. Kim H, Park MN, Kim J, Jang J, Kim HK, Cho DW. Characterization of cornea-specific bioink: high transparency, improved *in-vivo* safety. J Tissue Eng. 2019;10:2041731418823382.

209. Kim J, Shim IK, Hwang DG, Lee YN, Kim M, Kim H, et al. 3D cell printing of islet-laden pancreatic tissue-derived extracellular matrix bioink constructs for enhancing pancreatic functions. J Mater Chem B. 2019;7(10):1773-81.

210. Choi YJ, Kim TG, Jeong J, Yi HG, Park JW, Hwang W, et al. 3D Cell Printing of Functional Skeletal Muscle Constructs Using Skeletal Muscle-Derived Bioink. Advanced healthcare materials. 2016;5(20):2636-45.

211. Gao G, Lee JH, Jang J, Lee DH, Kong J-S, Kim BS, et al. Tissue Engineered Bio-Blood-Vessels Constructed Using a Tissue-Specific Bioink and 3D Coaxial Cell Printing Technique: A Novel Therapy for Ischemic Disease. Advanced Functional Materials. 2017;27(33):1700798.

212. Park JY, Ryu H, Lee B, Ha DH, Ahn M, Kim S, et al. Development of a functional airway-on-a-chip by 3D cell printing. Biofabrication. 2018;11(1):015002.

213. Davoudinejad A. Vat photopolymerization methods in additive manufacturing. Additive Manufacturing: Elsevier; 2021. p. 159-81.

214. Kim S, Bruyas A, Pan C-C, Stahl AM, Yang Y. Vascularized Tissue Regenerative Engineering Using 3D Bioprinting Technology. In: Narayan R, editor. Encyclopedia of Biomedical Engineering. Oxford: Elsevier; 2019. p. 696-706.

215. Mironi-Harpaz I, Wang DY, Venkatraman S, Seliktar D. Photopolymerization of cell-encapsulating hydrogels: crosslinking efficiency versus cytotoxicity. Acta biomaterialia. 2012;8(5):1838-48.

216. Yu C, Ma X, Zhu W, Wang P, Miller KL, Stupin J, et al. Scanningless and continuous 3D bioprinting of human tissues with decellularized extracellular matrix. Biomaterials. 2019;194:1-13.

217. Xue J, Wu T, Dai Y, Xia Y. Electrospinning and Electrospun Nanofibers: Methods, Materials, and Applications. Chemical reviews. 2019;119(8):5298-415.

218. Hong J, Yeo M, Yang GH, Kim G. Cell-Electrospinning and Its Application for Tissue Engineering. International journal of molecular sciences. 2019;20(24):20246208.

219. Dziemidowicz K, Sang Q, Wu J, Zhang Z, Zhou F, Lagaron JM, et al. Electrospinning for healthcare: recent advancements. J Mater Chem B. 2021;9(4):939-51.

220. Zhu Y, Wang D, Yao X, Wang M, Zhao Y, Lu Y, et al. Biomimetic hybrid scaffold of electrospun silk fibroin and pancreatic decellularized extracellular matrix for islet survival. J Biomater Sci Polym Ed. 2021;32(2):151-65.

221. Hogan KJ, Smoak MM, Koons GL, Perez MR, Bedell ML, Jiang EY, et al. Bioinspired electrospun decellularized extracellular matrix scaffolds promote muscle regeneration in a rat skeletal muscle defect model. Journal of Biomedical Materials Research Part A. 2022;110(5):1090-100.

222. Smoak MM, Han A, Watson E, Kishan A, Grande-Allen KJ, Cosgriff-Hernandez E, et al. Fabrication and Characterization of Electrospun Decellularized Muscle-Derived Scaffolds. Tissue Engineering Part C: Methods. 2019;25(5):276-87.

223. Jaworek A, Sobczyk AT. Electrospraying route to nanotechnology: An overview. Journal of Electrostatics. 2008;66(3):197-219.

224. Kornmuller A, Flynn LE. Development and characterization of matrix-derived microcarriers from decellularized tissues using electrospraying techniques. Journal of biomedical materials research Part A. 2022;110(3):559-75.

225. Yu C, Kornmuller A, Brown C, Hoare T, Flynn LE. Decellularized adipose tissue microcarriers as a dynamic culture platform for human adipose-derived stem/stromal cell expansion. Biomaterials. 2017;120:66-80.

226. Link PA, Ritchie AM, Cotman GM, Valentine MS, Dereski BS, Heise RL. Electrosprayed extracellular matrix nanoparticles induce a pro-regenerative cell response. Journal of Tissue Engineering and Regenerative Medicine. 2018;12(12):2331-6.

227. Kabirian F, Mozafari M. Decellularized ECM-derived bioinks: Prospects for the future. Methods (San Diego, Calif). 2020;171:108-18.

228. O'Neill JD, Anfang R, Anandappa A, Costa J, Javidfar J, Wobma HM, et al. Decellularization of human and porcine lung tissues for pulmonary tissue engineering. Ann Thorac Surg. 2013;96(3):1046-55; discussion 55-6.

229. Liao J, Joyce EM, Sacks MS. Effects of decellularization on the mechanical and structural properties of the porcine aortic valve leaflet. Biomaterials. 2008;29(8):1065-74.

230. Spina M, Ortolani F, El Messlemani A, Gandaglia A, Bujan J, Garcia-Honduvilla N, et al. Isolation of intact aortic valve scaffolds for heart-valve bioprostheses: extracellular matrix structure, prevention from calcification, and cell repopulation features. Journal of biomedical materials research Part A. 2003;67(4):1338-50.

231. Yang M, Chen CZ, Wang XN, Zhu YB, Gu YJ. Favorable effects of the detergent and enzyme extraction method for preparing decellularized bovine pericardium scaffold for tissue engineered heart valves. Journal of biomedical materials research Part B, Applied biomaterials. 2009;91(1):354-61.

232. Anderson JM, Rodriguez A, Chang DT. Foreign body reaction to biomaterials. Semin Immunol. 2008;20(2):86-100.

233. Chu C, Liu L, Rung S, Wang Y, Ma Y, Hu C, et al. Modulation of foreign body reaction and macrophage phenotypes concerning microenvironment. Journal of biomedical materials research Part A. 2020;108(1):127-35.

234. Sheikh Z, Brooks PJ, Barzilay O, Fine N, Glogauer M. Macrophages, Foreign Body Giant Cells and Their Response to Implantable Biomaterials. Materials (Basel). 2015;8(9):5671-701.

235. MacLauchlan S, Skokos EA, Meznarich N, Zhu DH, Raoof S, Shipley JM, et al. Macrophage fusion, giant cell formation, and the foreign body response require matrix metalloproteinase 9. J Leukoc Biol. 2009;85(4):617-26.

236. Kzhyshkowska J, Gudima A, Riabov V, Dollinger C, Lavalle P, Vrana NE. Macrophage responses to implants: prospects for personalized medicine. J Leukoc Biol. 2015;98(6):953-62.

237. Sicari BM, Dziki JL, Siu BF, Medberry CJ, Dearth CL, Badylak SF. The promotion of a constructive macrophage phenotype by solubilized extracellular matrix. Biomaterials. 2014;35(30):8605-12.

238. Wolf MT, Carruthers CA, Dearth CL, Crapo PM, Huber A, Burnsed OA, et al. Polypropylene surgical mesh coated with extracellular matrix mitigates the host foreign body response. Journal of biomedical materials research Part A. 2014;102(1):234-46.

239. Ghuman H, Mauney C, Donnelly J, Massensini AR, Badylak SF, Modo M. Biodegradation of ECM hydrogel promotes endogenous brain tissue restoration in a rat model of stroke. Acta biomaterialia. 2018;80:66-84.

240. Ghuman H, Gerwig M, Nicholls FJ, Liu JR, Donnelly J, Badylak SF, et al. Long-term retention of ECM hydrogel after implantation into a sub-acute stroke cavity reduces lesion volume. Acta biomaterialia. 2017;63:50-63.

241. Wassenaar JW, Braden RL, Osborn KG, Christman KL. Modulating *In-vivo* Degradation Rate of Injectable Extracellular Matrix Hydrogels. J Mater Chem B. 2016;4(16):2794-802.

242. Singelyn JM, Christman KL. Modulation of material properties of a decellularized myocardial matrix scaffold. Macromolecular bioscience. 2011;11(6):731-8.

243. van Wachem PB, van Luyn MJA, Damink LHHO, Dijkstra PJ, Feijen J, Nieuwenhuis P. Biocompatibility and tissue regenerating capacity of crosslinked dermal sheep collagen. Journal of Biomedical Materials Research. 1994;28(3):353-63.

244. Aamodt JM, Grainger DW. Extracellular matrix-based biomaterial scaffolds and the host response. Biomaterials. 2016;86:68-82.

245. Hiles MC, Badylak SF, Lantz GC, Kokini K, Geddes LA, Morff RJ. Mechanical properties of xenogeneic small-intestinal submucosa when used as an aortic graft in the dog. J Biomed Mater Res. 1995;29(7):883-91.

246. Badylak S, Kokini K, Tullius B, Whitson B. Strength over time of a resorbable bioscaffold for body wall repair in a dog model. The Journal of surgical research. 2001;99(2):282-7.

247. Park W, Gao G, Cho D-W. Tissue-Specific Decellularized Extracellular Matrix Bioinks for Musculoskeletal Tissue Regeneration and Modeling Using 3D Bioprinting Technology. International journal of molecular sciences. 2021;22(15):7837.

248. Claudio-Rizo JA, Delgado J, Quintero-Ortega IA, Mata-Mata JL, Mendoza-Novelo B. Decellularized ECM-Derived Hydrogels: Modification and Properties. Hydrogels. London: InTechOpen; 2018. p. 3-22.

249. Cui X, Li J, Hartanto Y, Durham M, Tang J, Zhang H, et al. Advances in Extrusion 3D Bioprinting: A Focus on Multicomponent Hydrogel-Based Bioinks. Advanced healthcare materials. 2020;9(15):1901648.

250. Zhao Z, Vizetto-Duarte C, Moay ZK, Setyawati MI, Rakshit M, Kathawala MH, et al. Composite Hydrogels in Three-Dimensional *in-vitro* Models. Front Bioeng Biotechnol. 2020;8:611.

251. Cho D-W, Kim BS, Jang J, Gao G, Han W, Singh NK. Decellularized Extracellular Matrix-Based Bioinks. 3D Bioprinting. 1 ed. Cham: Springer International Publishing; 2019. p. 41-51.

252. Chang C-H, Chen C-C, Liao C-H, Lin F-H, Hsu Y-M, Fang H-W. Human acellular cartilage matrix powders as a biological scaffold for cartilage tissue engineering with synovium-derived mesenchymal stem cells. Journal of Biomedical Materials Research Part A. 2014;102(7):2248-57.

253. Beachley V, Ma G, Papadimitriou C, Gibson M, Corvelli M, Elisseeff J. Extracellular matrix particle-glycosaminoglycan composite hydrogels for regenerative medicine applications. Journal of Biomedical Materials Research Part A. 2018;106(1):147-59.

254. Kim J, Jang J, Cho DW. Controlling Cancer Cell Behavior by Improving the Stiffness of Gastric Tissue-Decellularized ECM Bioink With Cellulose Nanoparticles. Front Bioeng Biotechnol. 2021;9:605819.

255. Muir VG, Burdick JA. Chemically Modified Biopolymers for the Formation of Biomedical Hydrogels. Chemical reviews. 2021;121(18):10908-49.

256. Heydarkhan-Hagvall S, Schenke-Layland K, Dhanasopon AP, Rofail F, Smith H, Wu BM, et al. Three-dimensional electrospun ECM-based hybrid scaffolds for cardiovascular tissue engineering. Biomaterials. 2008;29(19):2907-14.

257. Van Den Bulcke AI, Bogdanov B, De Rooze N, Schacht EH, Cornelissen M, Berghmans H. Structural and Rheological Properties of Methacrylamide Modified Gelatin Hydrogels. Biomacromolecules. 2000;1(1):31-8.

258. Zhu M, Wang Y, Ferracci G, Zheng J, Cho N-J, Lee BH. Gelatin methacryloyl and its hydrogels with an exceptional degree of controllability and batch-to-batch consistency. Scientific Reports. 2019;9(1):6863.

259. Kaemmerer E, Melchels FPW, Holzapfel BM, Meckel T, Hutmacher DW, Loessner D. Gelatine methacrylamide-based hydrogels: An alternative three-dimensional cancer cell culture system. Acta biomaterialia. 2014;10(6):2551-62.

260. Basara G, Ozcebe SG, Ellis BW, Zorlutuna P. Tunable Human Myocardium Derived Decellularized Extracellular Matrix for 3D Bioprinting and Cardiac Tissue Engineering. Gels. 2021;7(2):7020070.

261. Elomaa L, Keshi E, Sauer IM, Weinhart M. Development of GelMA/PCL and dECM/PCL resins for 3D printing of acellular *in-vitro* tissue scaffolds by stereolithography. Materials Science and Engineering: C. 2020;112:110958.

262. Wu X, Black L, Santacana-Laffitte G, Patrick, Charles W. Preparation and assessment of glutaraldehyde-crosslinked collagen–chitosan hydrogels for adipose tissue engineering. Journal of Biomedical Materials Research Part A. 2007;81A(1):59-65.

263. Monteiro OAC, Airoldi C. Some studies of crosslinking chitosan–glutaraldehyde interaction in a homogeneous system. International Journal of Biological Macromolecules. 1999;26(2-3):119-28.

264. Cunha PLR, Castro RR, Rocha FAC, De Paula RCM, Feitosa JPA. Low viscosity hydrogel of guar gum: Preparation and physicochemical characterization. International Journal of Biological Macromolecules. 2005;37(1-2):99-104.

265. Kulkarni AR, Soppimath KS, Aminabhavi TM. Controlled release of diclofenac sodium from sodium alginate beads crosslinked with glutaraldehyde. Pharmaceutica Acta Helvetiae. 1999;74(1):29-36.

266. Veríssimo DM, Leitão RFC, Ribeiro RA, Figueiró SD, Sombra ASB, Góes JC, et al. Polyanionic collagen membranes for guided tissue regeneration: Effect of progressive glutaraldehyde cross-linking on biocompatibility and degradation. Acta biomaterialia. 2010;6(10):4011-8.

267. George M, Abraham TE. pH sensitive alginate–guar gum hydrogel for the controlled delivery of protein drugs. International Journal of Pharmaceutics. 2007;335(1-2):123-9.

268. Khunmanee S, Jeong Y, Park H. Crosslinking method of hyaluronic-based hydrogel for biomedical applications. Journal of Tissue Engineering. 2017;8:204173141772646.

269. Singh RK, Seliktar D, Putnam AJ. Capillary morphogenesis in PEG-collagen hydrogels. Biomaterials. 2013;34(37):9331-40.

270. Skardal A, Devarasetty M, Kang H-W, Mead I, Bishop C, Shupe T, et al. A hydrogel bioink toolkit for mimicking native tissue biochemical and mechanical properties in bioprinted tissue constructs. Acta biomaterialia. 2015;25:24-34.

271. Madduma-Bandarage USK, Madihally SV. Synthetic hydrogels: Synthesis, novel trends, and applications. Journal of Applied Polymer Science. 2021;138(19):50376.

272. Mathur AM, Hammonds KF, Klier J, Scranton AB. Equilibrium swelling of poly(methacrylic acid-g-ethylene glycol) hydrogels. Journal of Controlled Release. 1998;54(2):177-84.

273. Bezemer JM, Grijpma DW, Dijkstra PJ, Van Blitterswijk CA, Feijen J. A controlled release system for proteins based on poly(ether ester) block-copolymers: polymer network characterization. Journal of Controlled Release. 1999;62(3):393-405.

274. Kurian P, Zschoche S, Kennedy JP. Synthesis and characterization of novel amphiphilic block copolymers di-, tri-, multi-, and star blocks of PEG and PIB. Journal of Polymer Science Part A: Polymer Chemistry. 2000;38(17):3200-9.

275. Lin H-H, Cheng Y-L. In-Situ Thermoreversible Gelation of Block and Star Copolymers of Poly(ethylene glycol) and Poly(N-isopropylacrylamide) of Varying Architectures. Macromolecules. 2001;34(11):3710-5.

276. Freyman TM, Yannas IV, Gibson LJ. Cellular materials as porous scaffolds for tissue engineering. Progress in Materials Science. 2001;46(3-4):273-82.

277. Gacesa P. Enzymic degradation of alginates. International Journal of Biochemistry. 1992;24(4):545-52.

278. Lee H, Han W, Kim H, Ha DH, Jang J, Kim BS, et al. Development of Liver Decellularized Extracellular Matrix Bioink for Three-Dimensional Cell Printing-Based Liver Tissue Engineering. Biomacromolecules. 2017;18(4):1229-37.

279. Lewis PL, Yan M, Su J, Shah RN. Directing the growth and alignment of biliary epithelium within extracellular matrix hydrogels. Acta biomaterialia. 2019;85:84-93.

280. Zare P, Pezeshki-Modaress M, Davachi SM, Chahsetareh H, Simorgh S, Asgari N, et al. An additive manufacturing-based-3D printed poly ε-caprolactone/alginate sulfate/extracellular matrix construct for nasal cartilage regeneration. Journal of Biomedical Materials Research Part A. 2022;110(6):1199- 209.

281. Savitri C, Ha SS, Liao E, Du P, Park K. Extracellular matrices derived from different cell sources and their effect on macrophage behavior and wound healing. Journal of Materials Chemistry B. 2020;8(42):9744-55.

282. Pati F, Ha D-H, Jang J, Han HH, Rhie J-W, Cho D-W. Biomimetic 3D tissue printing for soft tissue regeneration. Biomaterials. 2015;62:164-75.

283. Baena J, Jiménez G, López-Ruiz E, Antich C, Griñán-Lisón C, Perán M, et al. Volume-by-volume bioprinting of chondrocytes-alginate bioinks in high temperature thermoplastic scaffolds for cartilage regeneration. Experimental Biology and Medicine. 2019;244(1):13-21.

284. Sarrigiannidis SO, Rey JM, Dobre O, González-García C, Dalby MJ, Salmeron-Sanchez M. A tough act to follow: collagen hydrogel modifications to improve mechanical and growth factor loading capabilities. Materials Today Bio. 2021;10:100098.

285. Moncal KK, Ozbolat V, Datta P, Heo DN, Ozbolat IT. Thermally-controlled extrusion-based bioprinting of collagen. Journal of Materials Science: Materials in Medicine. 2019;30(5):55.

286. Marelli B, Ghezzi CE, James-Bhasin M, Nazhat SN. Fabrication of injectable, cellular, anisotropic collagen tissue equivalents with modular fibrillar densities. Biomaterials. 2015;37:183-93.

287. Kim H, Jang J, Park J, Lee KP, Lee S, Lee DM, et al. Shear-induced alignment of collagen fibrils using 3D cell printing for corneal stroma tissue engineering. Biofabrication. 2019;11(3):035017.

288. Lee H, Ju YM, Kim I, Elsangeedy E, Lee JH, Yoo JJ, et al. A novel decellularized skeletal muscle-derived ECM scaffolding system for in situ muscle regeneration. Methods (San Diego, Calif). 2020;171:77-85.

289. Patel KH, Talovic M, Dunn AJ, Patel A, Vendrell S, Schwartz M, et al. Aligned nanofibers of decellularized muscle extracellular matrix for volumetric muscle loss.

Journal of biomedical materials research Part B, Applied biomaterials. 2020;108(6):2528-37.

290. Bejleri D, Streeter BW, Nachlas ALY, Brown ME, Gaetani R, Christman KL, et al. A Bioprinted Cardiac Patch Composed of Cardiac-Specific Extracellular Matrix and Progenitor Cells for Heart Repair. Advanced healthcare materials. 2018;7(23):1800672.

291. Wassenaar JW, Gaetani R, Garcia JJ, Braden RL, Luo CG, Huang D, et al. Evidence for Mechanisms Underlying the Functional Benefits of a Myocardial Matrix Hydrogel for Post-MI Treatment. J Am Coll Cardiol. 2016;67(9):1074-86.

292. Traverse JH, Henry TD, Dib N, Patel AN, Pepine C, Schaer GL, et al. First-in-Man Study of a Cardiac Extracellular Matrix Hydrogel in Early and Late Myocardial Infarction Patients. JACC: Basic to Translational Science. 2019;4(6):659-69.

293. Zhang L, Zhang F, Weng Z, Brown BN, Yan H, Ma XM, et al. Effect of an inductive hydrogel composed of urinary bladder matrix upon functional recovery following traumatic brain injury. Tissue engineering Part A. 2013;19(17-18):1909-18.

294. Cancedda R, Dozin B, Giannoni P, Quarto R. Tissue engineering and cell therapy of cartilage and bone. Matrix Biol. 2003;22(1):81-91.

295. Chen D, Zhang Y, Lin Q, Chen D, Li X, Dai J, et al. The effect of cartilage decellularized extracellular matrix-chitosan compound on treating knee osteoarthritis in rats. PeerJ. 2021;9:e12188.

296. Yang Y, Lin H, Shen H, Wang B, Lei G, Tuan RS. Mesenchymal stem cell-derived extracellular matrix enhances chondrogenic phenotype of and cartilage formation by encapsulated chondrocytes *in-vitro* and *in-vivo*. Acta biomaterialia. 2018;69:71-82.

297. Beck EC, Barragan M, Tadros MH, Gehrke SH, Detamore MS. Approaching the compressive modulus of articular cartilage with a decellularized cartilage-based hydrogel. Acta biomaterialia. 2016;38:94-105.

298. Bordbar S, Lotfi Bakhshaiesh N, Khanmohammadi M, Sayahpour FA, Alini M, Baghaban Eslaminejad M. Production and evaluation of decellularized extracellular matrix hydrogel for cartilage regeneration derived from knee cartilage. Journal of biomedical materials research Part A. 2020;108(4):938-46.

299. Kwon JS, Yoon SM, Shim SW, Park JH, Min KJ, Oh HJ, et al. Injectable extracellular matrix hydrogel developed using porcine articular cartilage. Int J Pharm. 2013;454(1):183-91.

300. Wimmer RA, Leopoldi A, Aichinger M, Wick N, Hantusch B, Novatchkova M, et al. Human blood vessel organoids as a model of diabetic vasculopathy. Nature. 2019;565(7740):505-10.

301. Song J, Choi H, Koh SK, Park D, Yu J, Kang H, et al. High-Throughput 3D *In-vitro* Tumor Vasculature Model for Real-Time Monitoring of Immune Cell Infiltration and Cytotoxicity. Front Immunol. 2021;12:733317.

302. Quint C, Kondo Y, Manson RJ, Lawson JH, Dardik A, Niklason LE. Decellularized tissue-engineered blood vessel as an arterial conduit. Proc Natl Acad Sci U S A. 2011;108(22):9214-9.

303. Rafii S, Butler JM, Ding BS. Angiocrine functions of organ-specific endothelial cells. Nature. 2016;529(7586):316-25.

304. Augustin HG, Koh GY. Organotypic vasculature: From descriptive heterogeneity to functional pathophysiology. Science. 2017;357(6353):eaal2379.

305. Vailhe B, Ronot X, Tracqui P, Usson Y, Tranqui L. *In-vitro* angiogenesis is modulated by the mechanical properties of fibrin gels and is related to alpha(v)beta3 integrin localization. *In-vitro* Cell Dev Biol Anim. 1997;33(10):763-73.

306. Sieminski AL, Was AS, Kim G, Gong H, Kamm RD. The stiffness of three-dimensional ionic self-assembling peptide gels affects the extent of capillary-like network formation. Cell Biochem Biophys. 2007;49(2):73-83.

307. Byfield FJ, Reen RK, Shentu TP, Levitan I, Gooch KJ. Endothelial actin and cell stiffness is modulated by substrate stiffness in 2D and 3D. J Biomech. 2009;42(8):1114-9.

308. Mason BN, Starchenko A, Williams RM, Bonassar LJ, Reinhart-King CA. Tuning three-dimensional collagen matrix stiffness independently of collagen concentration modulates endothelial cell behavior. Acta biomaterialia. 2013;9(1):4635-44.

309. Benning L, Gutzweiler L, Trondle K, Riba J, Zengerle R, Koltay P, et al. Assessment of hydrogels for bioprinting of endothelial cells. Journal of biomedical materials research Part A. 2018;106(4):935-47.

310. Su J, Satchell SC, Shah RN, Wertheim JA. Kidney decellularized extracellular matrix hydrogels: Rheological characterization and human glomerular endothelial cell response to encapsulation. Journal of biomedical materials research Part A. 2018;106(9):2448-62.

311. Kobayashi M, Kadota J, Hashimoto Y, Fujisato T, Nakamura N, Kimura T, et al. Elastic Modulus of ECM Hydrogels Derived from Decellularized Tissue Affects Capillary Network Formation in Endothelial Cells. International journal of molecular sciences. 2020;21(17):21176304.

312. De Santis MM, Alsafadi HN, Tas S, Bolukbas DA, Prithiviraj S, Da Silva IAN, et al. Extracellular-Matrix-Reinforced Bioinks for 3D Bioprinting Human Tissue. Advanced materials (Deerfield Beach, Fla). 2021;33(3):e2005476.

313. Song M, Zhou Y, Liu Y. VEGF heparinized-decellularized adipose tissue scaffolds enhance tissue engineering vascularization *in-vitro*. RSC Adv. 2018;8(59):33614-24.

314. Kang B, Park Y, Hwang DG, Kim D, Yong U, Lim KS, et al. Facile Bioprinting Process for Fabricating Size-Controllable Functional Microtissues Using Light-Activated Decellularized Extracellular Matrix-Based Bioinks. Advanced Materials Technologies. 2022;7(1):2100947.

315. Spang MT, Christman KL. Extracellular matrix hydrogel therapies: *In-vivo* applications and development. Acta biomaterialia. 2018;68:1-14.

316. Chae S, Cho D-W. Three-dimensional bioprinting with decellularized extracellular matrix-based bioinks in translational regenerative medicine. MRS Bulletin. 2022;47(1):70-9.

317. Tan ML, Ling L, Fischbach C. Engineering strategies to capture the biological and biophysical tumor microenvironment *in-vitro*. Advanced drug delivery reviews. 2021;176:113852.

318. Pamies D, Hartung T. 21st Century Cell Culture for 21st Century Toxicology. Chem Res Toxicol. 2017;30(1):43-52.

319. Moroni L, Burdick JA, Highley C, Lee SJ, Morimoto Y, Takeuchi S, et al. Biofabrication strategies for 3D *in-vitro* models and regenerative medicine. Nature Reviews Materials. 2018;3(5):21-37.

320. Jin K, Teng L, Shen Y, He K, Xu Z, Li G. Patient-derived human tumour tissue xenografts in immunodeficient mice: a systematic review. Clin Transl Oncol. 2010;12(7):473-80.

321. Hylander BL, Punt N, Tang H, Hillman J, Vaughan M, Bshara W, et al. Origin of the vasculature supporting growth of primary patient tumor xenografts. J Transl Med. 2013;11:110.

322. Reyal F, Guyader C, Decraene C, Lucchesi C, Auger N, Assayag F, et al. Molecular profiling of patient-derived breast cancer xenografts. Breast Cancer Res. 2012;14(1):R11.

323. Aguado BA, Caffe JR, Nanavati D, Rao SS, Bushnell GG, Azarin SM, et al. Extracellular matrix mediators of metastatic cell colonization characterized using scaffold mimics of the pre-metastatic niche. Acta biomaterialia. 2016;33:13-24.

324. Kim BS, Cho WW, Gao G, Ahn M, Kim J, Cho DW. Construction of Tissue-Level Cancer-Vascular Model with High-Precision Position Control via In Situ 3D Cell Printing. Small Methods. 2021;5(7):e2100072.

325. Saheli M, Sepantafar M, Pournasr B, Farzaneh Z, Vosough M, Piryaei A, et al. Three-dimensional liver-derived extracellular matrix hydrogel promotes liver organoids function. J Cell Biochem. 2018;119(6):4320-33.

326. Lam D, Enright HA, Cadena J, Peters SKG, Sales AP, Osburn JJ, et al. Tissue-specific extracellular matrix accelerates the formation of neural networks and communities in a neuron-glia co-culture on a multi-electrode array. Scientific Reports. 2019;9(1):4159.

327. Hourd P, Medcalf N, Segal J, Williams DJ. A 3D bioprinting exemplar of the consequences of the regulatory requirements on customized processes. Regenerative Medicine. 2015;10(7):863-83.

Preface to Chapter 3

After reviewing relevant literature for this project, the upcoming chapter includes the experiments to complete aims 1 and 2.

- **Aim 1:** Develop and characterize an extrudable physiologically-relevant cell-laden hydrogel bioink.
- **Aim 2:** Fabricate and validate a three-dimensional printed (3DP) monoculture *in-vitro* model of HNSCC and evaluate tumor response to chemotherapeutic treatment.

The article covers the decellularization process for my tissue of choice: dECM from porcine tongue and its solubilization into a dECM hydrogel. I also incorporate alginate and gelatin as rheological modifiers to make the bioink compatible with extrusion bioprinting and with relevant mechanical properties, similar to HNSCC tumors found *in-vivo*. The dECM hydrogel was thoroughly characterized mechanically and biochemically.

In this composite, the dECM provides the bioactive element to the blend, the gelatin facilitates the fabrication process by stabilizing the ink at room temperature and the alginate, which is ionically crosslinked after the models are fabricated, ensures the geometric fidelity throughout the several weeks of culture. I quantified the rheological characteristics of the material and compared it with pure dECM and HNSCC tumors.

To prove the material allowed the development of cells I encapsulated HNSCC cells and cultured them in standard conditions. Cells were able to attach to the matrix and proliferate under standard culturing conditions with high cell viability.

I also wanted to ensure that the material permitted variable quantifications with functional assays since the main goal of this project is to create a platform for drug discovery or disease modeling *in-vitro*. The models were compatible with cell proliferation assays and allowed the dose testing for two chemotherapeutic drugs: cisplatin and 5-fluorouracil.

With the correct decellularization and solubilization process for the tissue, a bioink blend that is well characterized, allows cell development, and permits variable quantification with commonly used assays I have the tools to continue with my third aim which has the objective of creating a heterogenous model. The final model has multiple variables hence the importance of taking the time to develop and characterize each of them at a time.

This article was published in ACS Biomaterials Science & Engineering the 18th of October 2021.

3. Decellularized extracellular matrix composite hydrogel bioinks for the development of 3D bioprinted head and neck in-vitro tumor models

This manuscript was published in ACS Biomaterials Science & Engineering the 18th of October 2021. DOI: **https://doi.org/10.1021/acsbiomaterials.1c00812**

Authors: Jacqueline Kort-Mascort[a], Guangyu Bao[b], Osama Elkashty[c,d], Salvador Flores-Torres[a], Jose G. Munguia-Lopez[a, c], Tao Jiang[e], Allen J. Ehrlicher[a,b], Luc Mongeau[b], Simon D. Tran[c], Joseph M. Kinsella[a,*]

joseph.kinsella@mcgill.ca

[a] Department of Bioengineering, McGill University, Montreal, Quebec, Canada.

[b] Department of Mechanical Engineering, McGill University, Montreal, Quebec, Canada.

[c] Faculty of Dentistry, McGill University, Montreal, Quebec, Canada.

[d] Oral Pathology Department, Faculty of Dentistry, Mansoura University, Mansoura, Egypt.

[e] Department of Intelligent Machinery and Instrument, College of Intelligence Science and Technology, National University of Defense Technology Changsha, Hunan, China.

3.1. Abstract

Reinforced extracellular matrix (ECM)-based hydrogels recapitulate several mechanical and biochemical features found in the tumor microenvironment (TME) *in-vivo*. While these gels retain several critical structural and bioactive molecules that promote cell-matrix interactivity their mechanical properties tend toward the viscous regime limiting their ability to retain ordered structural characteristics when considered as architectured scaffolds. To overcome this limitation of pure ECM hydrogels we present a composite material containing alginate, a seaweed derived polysaccharide, and gelatin, denatured collagen, as rheological modifiers which impart mechanical integrity to the biologically active dECM. After an optimization process the reinforced gel proposed is mechanically stable, bioprintable, and has a stiffness within the expected physiological values. Our hydrogel's elastic modulus has no significant difference when compared to tumors induced in preclinical xenograft head and neck squamous cell carcinoma (HNSCC) mouse models. The bioprinted cell-laden model is highly reproducible and allows proliferation and reorganization of HNSCC cells while maintaining cell viability above 90% for periods of nearly three weeks. Cells encapsulated in our bioink produce spheroids of at least 3000μm^2 of cross-sectional area by day 15 of culture and are positive for cyto-keratin in immunofluorescence quantification, a common marker of HNSCC model validation in 2D and 3D models. We use this *in-vitro* model system to evaluate the standard-of-care small molecule therapeutics used to treat HNSCC clinically and report a 4-fold increase in the IC_{50} of cisplatin and an 80-fold increase for 5-fluorouracil compared to monolayer cultures. Our work suggests that fabricating *in-vitro* models using reinforced dECM provides a physiologically relevant system to evaluate malignant neoplastic phenomena

in-vitro due to the physical and biological features replicated from the source tissue microenvironment.

Graphical Abstract

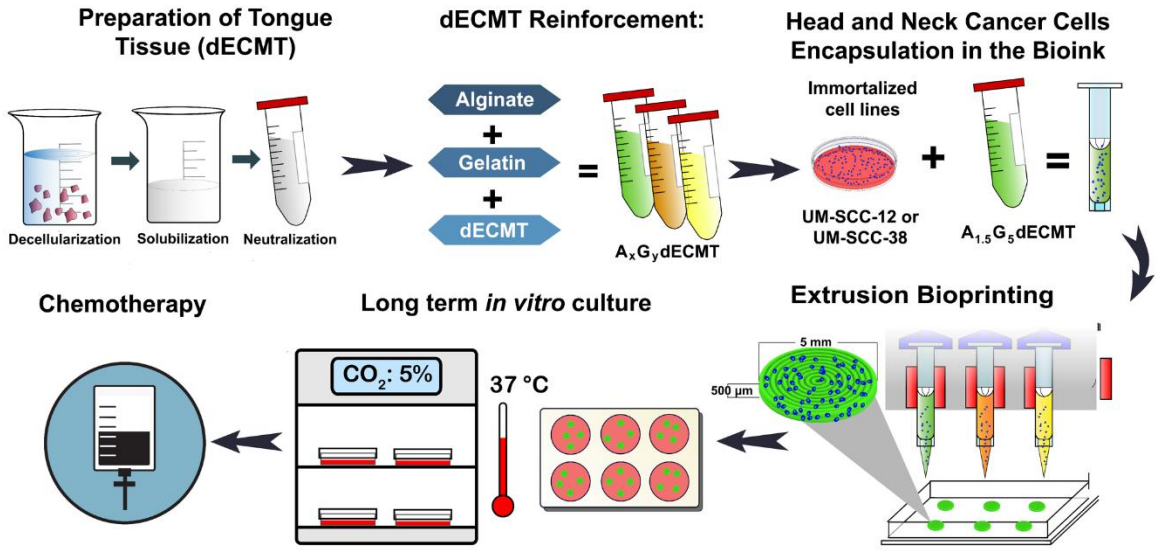

Scheme 1. Illustration depicting the development of a bioprinted platform using extracellular matrix bioinks for toxicology testing. Porcine tongue tissue is decellularized, solubilized, and neutralized to form a hydrogel (dECMT). The dECMT material is subsequently reinforced with alginate and gelatin to improve its mechanical properties. Then, the bioink is used to encapsulate HNSCC immortalized human cell lines to later bioprint 3D cell-laden structures capable of withstanding long-term culture. After development, these structures can be used to perform *in-vitro* screening of chemotherapeutic drugs for HNSCC treatment.

KEYWORDS. Bioprinting, Decellularized Extracellular Matrix, Tissue Engineering, Biofabrication, *In-vitro* Disease Models, Tumor Microenvironment.

3.2. Introduction

To mechanistically understand cancer biology and advance new therapeutic strategies, conventional models such as *in-vitro* monolayer cell culture systems, and preclinical *in-vivo* small animal models are commonly used.[1] Even though landmark discoveries have been made using these tools, cell culture models and tumor xenografts are either deficient, or introduce biological cues, that are not present in native human tumors.[2-4] These models also lack the natural interactivity that occurs between the tumor epithelium, tumor-associated stromal cells, and the tumor microenvironment (TME) in human tumors.[5-6] Primary tumors are known to be heterogeneous. They are comprised of a core of cancer cells surrounded by stromal cells, which are in continuous interaction with the extracellular matrix (ECM).[7] Altogether, cells and ECM form the TME, and they orchestrate functions that can promote tumor metastasis and result in poor prognosis.[7]

Alternatives to preclinical and monolayer cell culture models such as tissue-engineered *in-vitro* tumor models[8] have been introduced; including 3D hydrogel culture systems,[6, 9-10] spheroids,[11] organoid cultures,[12-13] and organ-on-a-chip[8, 12, 14] platforms. Among the fabrication tools, extrusion bioprinting offers the potential to create culture systems with user-defined settings to control the geometry of the construct, placement of cell types, cell density, and scaffold materials or bioinks.[15-16] Several bioinks have been developed for this technique using synthetic hydrogels, which have excellent mechanical properties and have been proven to be reliable, consistent, and with reproducible mechanical characteristics.[17-18] Nevertheless, these materials often fail to recapitulate the biochemical and biomechanical complexity found in native ECM, resulting in the absence of intrinsic physiological function and aberrant cell behavior.[19] Hence, tissue-derived biomaterials

have been used to formulate bioinks with their intrinsic bioactive properties.[15] Solubilized decellularized ECM (dECM) is a tissue-derived material that has unsuitable stiffness, viscosity, yield point, and mechanical properties[20] when compared to synthetic hydrogels.[15] However, it possesses exceptional bioactive and inductive properties,[19] including the promotion of cell proliferation and differentiation,[21] as well as cell-ECM,[22] and cell-cell interactions.[23] The combination of these properties and interactions can be influential in regulating cell and tissue behavior and remodelling;[24] thus, the use of tissue-derived materials provide a more physiologically relevant environment.[25] It has been reported that tissue-specific ECMs are beneficial for cell expansion and function in primary cultures since cultivated cells have shown *in-vivo*-like phenotypes.[26] dECM has frequently been proposed as one of the most promising bioprinting and tissue engineering materials for its ability to mimic the complex conditions and provide a macromolecular microenvironment conducive to growth factors from the native tissue.[27]

For instance, a bioprintable dECM hydrogel derived from bovine tendon was used to successfully encapsulate NIH 3T3 fibroblasts which showed show lineage-specific morphology at the third day of the culture.[28] Also, cell-laden dECM has been bioprinted by incorporating a polycaprolactone (PCL) scaffold as a secondary structural framework.[19] PCL scaffolded dECM bioprinting technique has been used to demonstrate that dECM isolated from adipose, cartilage, and heart tissues has the potential to be used as bioinks in extrusion bioprinting.[19] It has also been reported that the incorporation of crosslinkers to the dECM hydrogel can improve the mechanical properties, including shear stiffness[23] and viscosity[29]. In one study, the composite dECM material consisted of a combination of PEG-based additives allowing a 2-step crosslinking process, prior- and

post-printing.[23] Additionally, a bioink containing methacrylated dECM derived from bone after crosslinking allowed osteogenic differentiation of human adipose stem cells.[30]

We have previously demonstrated that composite materials constituted of alginate, a seaweed-derived polysaccharide, and gelatin, a bovine or porcine-derived denatured collagen, can be tuned to recapitulate the mechanical properties of soft tissues[31] while keeping their biocompatibility and printability.[32-33] In the present study, we make use of our previous findings to create a mechanically tunable biomaterial that includes alginate, gelatin, and dECM in its formulation. We propose this bioink for its bioprintable and bioactive properties, and its ability to be mechanically tuned for this or future applications. For the dECM source, we chose to use porcine tissue since the porcine genome bears more resemblance to the human genome than other animal models such as rodents.[34] Furthermore, the base and lateral borders of the tongue are the most prevalent sites of HNSCC development. Hence, we use the most common primary site for intraoral dECM of this tissue to reproduce the HNSCC, the border of the tongue environment.[35]

Herein, we report a bioink prepared by decellularizing porcine tissue and incorporating sodium alginate and gelatin at controlled weight percentages as rheological modifiers to reinforce and positively impact the mechanical integrity of the composite material. Each of the bioink components was chosen to support the fabrication, and culture of the hydrogel constructs. dECM contains structural proteins,[36-38] glycosaminoglycans,[36-38] and growth factors[37, 39] preserved from the tissue of origin. Gelatin provides mechanical stability during the printing process. Our group has previously determined that formulations between 5-7% of gelatin result in printable materials that allow construct

fabrication while keeping the extrusion pressure and shear low enough resulting in cell viabilities of more than 90% in different types of cancer epithelial cells.[32-33] Crosslinked alginate chains in low concentration maintain sample integrity in long-term cell culture conditions. We have previously reported that stiff gel formulations containing 5% (A_5G_y), or greater, alginate did not allow cellular proliferation and cells remained as single cells even after 28 days in culture.[32]

We characterize the mechanical and biochemical properties of the composite materials, use them to encapsulate human HNSCC cells (UM-SCC-12 and UM-SCC-38) and bioprint 3D structures that are stable in traditional culture conditions for at least 19 days. We make use of rheological measurements to understand the intrinsic mechanical characteristics of our bioinks and their behaviour when exposed to temperature changes relevant to the bioprinting process and physiological conditions needed for the cells to develop. Utilizing extrusion bioprinting as our fabrication tool we control model geometry and cell density which enables sample-to-sample biological reproducibility and assay addressable models. Our findings indicate that our composite material promotes cell proliferation with high viability. It also allows the formation of tumor-like spheroids that display phenotypes previously reported in UM-SCC-12 tumors created in xenograft mouse models.[40] Additionally, our drug testing experiments demonstrate the ability to use this platform for several applications including but not limited to drug screening and personalized medicine.

3.3. Materials and methods

3.3.1. Decellularization and solubilization of tissue

Tongue decellularization and solubilization of the tissue were inspired by these protocols.[19, 41] The porcine tongue tissue was obtained from a local market. The tissue was cut into pieces of approximately 0.5 cm. Then, it was ground into smaller pieces using a food processor until the tissue was homogeneously minced. The agitation of all the following solutions was performed at 350 rpm. The tissue was immersed and agitated in a solution of 0.1% sodium dodecyl sulfate (SDS) (Bioshop®) and 1% penicillin-streptomycin (Wisent Bio Products®) in PBS-1X (Wisent Bio Products®) for 4 days. During those 4 days, the solution was changed every 24 h. The tissue was then stirred for 24 h in PBS-1X, and 24h in 1% Triton X-100 (Bioshop®). Then, the tissue was washed with PBS-1X for at least 5 days changing the solution daily. After, the tissue was transferred to a solution of DNAse (50 U/mL) and RNAse (1 U/mL) (Sigma-Aldrich®) and stirred at 37°C for 4 h. The sample was strained and incubated at 4°C in pure acetone (Sigma-Aldrich®) overnight. The following day, the ECM was divided into 50 mL centrifuge tubes and agitated with pure ice-cold acetone for 10 min to later centrifuge at 5,000 g for 10 min at 4°C, the supernatant was discarded from the tube. The last two steps were repeated five times. After the final centrifugation, the samples were air-dried at room temperature. The dECMT was sterilized by stirring it into an aqueous solution of 0.1% peracetic acid (Sigma-Aldrich®) and 4% ethanol (Sigma-Aldrich®) for 24 h. All the following manipulations were performed under a biological safety cabinet to keep the dECMT sterile. The peracetic solution was strained and washed with PBS-1X for 24 h, and homogenized (Ultra Turrax TP-18 from IKA®) in PBS-1X with an S25KG homogenizing

probe. Lastly, the sample was centrifuged at 5,000 g for 10 min and the supernatant removed. Samples were frozen at -80°C, lyophilized, and stored at -20°C before using.

To solubilize the tissue, the Freytes[41] method was used with some modifications. For every 1 g of lyophilized dECM, 250,000 units of pepsin from porcine gastric mucosa (Sigma-Aldrich®) were added to 100 mL of 0.5 M acetic acid (Sigma-Aldrich®), sterilized using a 0.22 μm filter, and stirred with the tissue at 350 rpm until no pieces of dECMT were visible (≈96 h). Neutralization was completed while keeping the dECMT on ice and adding 10 mL of a sterile solution of 0.1 N NaOH (Sigma-Aldrich®) and 11 mL of sterile PBS-10X (Wisent Bio Products®) for every gram of lyophilized tissue. The pH was adjusted to 7.4 using concentrated NaOH. Keeping the solubilized dECMT at 4°C, it was filtered through a 100 μm cell sieve centrifuging the sample at 5,000 g for 5 min at 4°C. The solubilized dECMT was stored at -20°C.

3.3.2. Total protein quantification

To quantify total protein content, a Bradford Assay (Biorad®) was performed following the protocol provided by the manufacturer using bovine serum albumin (BSA) for the control curve. Briefly, one part of the concentrated dye reagent was diluted with four parts of distilled deionized water and filtered through a Whatman #1 filter. BSA standards were prepared from 0-300 μg/mL. Ten μL of the standards dilutions and dECMT were added to a 96-microtiter plate. Then, 100 μL of the diluted Bradford reagent was added using a multichannel pipette and incubated at room temperature for 10 min. Absorbance was measured at 595 nm using a Nanodrop® 2000 (Thermo Fisher Scientific®).

3.3.3. Sulfated glycosaminoglycan (sGAG) quantification

Dimethyl methylene blue (DMMB) assay was used to quantify the sGAG present in the sample. Prior to quantification, we extracted the sGAG of the dECM using papain digestion. To prepare the DMMB reagent, we used 16 mg of DMMB in 1 L of water containing 1.6 g of NaCl (Alfa Aesar®), 3.04 g of glycine (Sigma-Aldrich®), and 95 mL of 0.1 M acetic acid (Sigma-Aldrich®). We used bovine chondroitin 4-sulfate (Sigma-Aldrich®) to prepare a standard curve from 0-10 µg/mL. In a 96-well plate, we added 20 µL of standard or sample to each well and 200 µL of the DMMB reagent to later measure the absorbance at 525 nm.

3.3.4. Liquid chromatography-tandem mass spectrometry (LC/MS/MS)

LC/MS/MS was used to determine the different proteins present in the dECMT. One µL of dECMT was diluted with 50 mM ammonium bicarbonate into a final volume of 10 µL. Then 1 µL of proteomics grade Trypsin (Promega®) was added to a concentration of 12 ng/µL. One µL of this digest was injected onto a C18 trapping column (Acclaim PepMap 100, Thermo Scientific®) and subjected to reverse-phase LC-MS-MS, using a nanoflow Easy-nLC 1000 UHPLC and a Q-Exactive HF Orbitrap mass spectrometer (Thermo Scientific®): LC: Digested peptides were resolved on a 25 cm nano-Reverse Phase C18 UHPLC analytical column (Acclaim PepMap RSLC, Thermo Scientific®), running a water/acetonitrile (ACN) gradient from 3-20% ACN during the initial 20 min and a subsequent 20-35% ACN solvent during the next 10 min (30 min in total) at a flow rate of 350 nL/ min. MS: Eluting peptides were recorded by the Orbitrap mass spectrometer at a resolution of 120,000 (FWHM) and at a trap ion load of $3x10^6$. The top 25 most abundant ions at any given time point were subjected to isolation (isolation width: 2 m/z)

and HCD fragmentation. MS/MS spectra were recorded at a resolution of 15,000. Data analysis: Acquired spectra (MS and MS/MS) were extracted with Mascot Distiller (Matrix Sciences Ltd.®) and searched against a relevant proteome database (Sus scrofa (Pig) - UniProt) using the 'Mascot' proteomics search engine (Matrix Sciences Ltd.®). The searches were performed with the following settings: MS mass tolerance: 5 ppm. MS/MS mass tolerance: 50 mDa. Digestion enzyme: Trypsin. Missed cleavages: 2 Variable modifications: Methionine (oxidized). Mascot search results were validated using the software analyses platform 'Scaffold' (Proteome Software Inc.®), and identified proteins were visualized as total redundant spectral counts.

3.3.5. Composite bioink preparation

To prepare the A_xG_5dECMT composites we prepared a 9% (w/v) solution of sodium alginate (Protanal LF 10/60 FT, FMC biopolymer®) in DPBS-1X (Wisent Bio Products®). This solution was mixed with the neutralized dECMT to obtain the desired concentration of alginate (1% or 1.5%) and stirred overnight at room temperature at 350 rpm. The next day we prepared a 5% (w/v) solution of type B gelatin from bovine skin (Sigma®) in the alginate-dECMT material and stirred it at 37°C until the gelatin was fully dissolved.

The alginate crosslinking solution was prepared by dissolving calcium chloride in sterile ultrapure water at a final concentration of 100 mM.

3.3.6. Rheology

To characterize the mechanical properties of dECMT and the reinforced bioink, an oscillation rheometer MCR 302 (Anton Paar®) was utilized with a ø25 mm conical plate (Part No. 79038). Mineral oil was used to cover the edge of the plate to avoid evaporation.

To determine the linear viscoelastic region (LVR) of the pure dECMT and the composite bioink, we performed amplitude sweep tests with a shear strain (γ) from 0.01% to 1000% at a frequency of 0.1 Hz and a temperature of 24°C for $A_{1.5}G_5$, A_xG_5dECMT and 37°C for pure dECMT. We also conducted a flow curve test with a logarithmic ramp at a variable shear rate from 0.001 s^{-1} to 1000 s^{-1} and a temperature of 24°C. The following experiments were set at a 0.1% strain, which is 1/10 of the ultimate linear strain obtained in the amplitude sweeps. This strain ensures the material's response is within its linear elastic regime. To determine the change of mechanical characteristics with changing temperature, we simulated our bioprinting protocol conditions in a gelation kinetics test. The $A_{1.5}G_5$ and A_xG_5dECMT samples were incubated at 37°C for 60 min; then, the temperature was changed to 24°C and incubated for 90 min. The dECMT sample was incubated at 4°C for 60 min and at 37°C for 90 min. For the gelation tests, a strain of 1 Hz was applied. The exponential model used to fit the gelation kinetics is: $Y=Y_0+(Plateau-Y_0)*(1-e^{(-K*x)})$

3.3.7. In-vivo tumor formation

The animal experiments were approved by the University Animal Care Committee at McGill University (Protocol #5330, www.animalcare.mcgill.ca). The protocol was previously reported by Elkashty et.al.[40] Briefly, NU/NU Nude (Crl:NU-Foxn1nu) mice (Charles River®). Mice were anesthetized with isoflurane (Isoba VetTM, Schering Plough®) (4% induction and 2% maintenance). Six to ten-week-old male mice were injected with unsorted UM-SCC-12 cells suspended in 30 µl of normal saline, into the side of the tongue, using a 1-ml tuberculin syringe with a 30-gauge hypodermic needle. The mice were examined for tumor formation on the tongue each week, measured

bidirectionally using a caliber under gas anesthesia. Animals were sacrificed after 32 days, and tumors were isolated and stored at -20°C until ready to use for nanoindentation. For histological analysis, tissue was fixed in 10 % neutral buffered formalin and embedded in paraffin.

3.3.8. Nanoindentation

An atomic force microscope (JPK® NanoWizard@3) was used to conduct nanoindentation tests to measure the Young's modulus of the structure surface. Samples were cut into 200 μm slices with a cryotome (Leica®) and fixed onto a Petri dish with a biocompatible green glue (JPK®) before being immersed in PBS. Silicon cantilevers with 25 μm diameter spherical beads attached as probes were used (Novascan®). Cantilevers with a nominal spring constant of 0.35 and 0.6 N/m were used for testing the samples. The spring constants of the cantilevers were determined with a thermal noise method before the experiments. Indentations were conducted on at least 15 different locations for each sample. All the calibrations and measurements were performed while samples were immersed in PBS. The Hertzian contact model was used to calculate the Young's moduli.

3.3.9. Bioprinting and culturing of 3D structures

For all cell viability assays, two immortalized human squamous cell carcinoma cell lines were used: UM-SCC-12,[42-44] a moderately differentiated carcinoma derived from the larynx of a male patient and UM-SCC-38,[43-44] a moderately differentiated carcinoma derived from the tonsillar pillar of a male patient. Both cell lines were purchased from the University of Michigan. Short Tandem Repeat (STR) analysis was performed in both cell lines (Table S4).

To grow cells in 2D prior 3D culture, cells were cultured with DMEM supplemented with 10% Fetal Bovine Serum and 1% penicillin-streptomycin in T-flasks with traditional incubation parameters (5% CO_2, 95% humidity, 37°C). To passage the cells, trypsin-EDTA was used to disrupt cell attachments. All cell culture reagents were purchased from Wisent Bio Products®.

Before printing, we placed the desired A_xG_5dECMT bioink in a 37°C water bath for 30 min to liquify the gelatin component of the material. We cultured the cells in 2D until 80% confluence, trypsinized, counted, and resuspended in media, accounting for less than 1% of the total volume when encapsulated in the bioink. To embed the cells in the bioink, we removed the bioink from the water bath, loaded it into a cartridge, and incorporated the cells by mechanically mixing them at a concentration of 1 million cells/mL. We centrifuged the cartridge at 200 g for 2 min to remove any bubbles and incubated the cartridge for 15 min at room temperature to ensure proper gelation before bioprinting.

The bioprinting of A_xG_5dECMT was performed using a Bioscaffolder 3.1 (GeSiM®). We used a 3-cc cartridge with a 22 G conical tip (Nordson®) to fabricate a disc with a 5 mm diameter and 500 μm height. Pressure requirements for extrusion varied between 45±10 kPa depending on the time of extrusion, temperature parameters were set at room temperature (24°C), and the printing speed to 10±2 mm/s.

Later, samples were crosslinked using an aqueous solution of calcium chloride (100 mM) for 3 min. Samples were rinsed twice with PBS-1X, placed onto agarose-coated dishes, and developed in a tissue culture incubator. Cell media was replaced every 3 days. Agarose-coated plates were replaced weekly.

3.3.10. Histology and immunofluorescence

We performed histological analysis using Hematoxylin and Eosin (H&E) staining to observe cell morphology, and cell arrangement present within the discs. The same samples used for confocal microscopy were fixed with ice-cold 4% paraformaldehyde overnight and followed by 10 min serial immersions in 20%, 50%, and 70% ethanol. Samples were later subjected to 1-hour serial immersions in ethanol at 70%, 95%, and 100% to ensure full dehydration of the samples. Washes using absolute ethanol were repeated three times, followed by another three 1 h washes in neat xylene. Finally, samples were immersed in two wax baths of paraffin (1 h per bath). Five mm sectioning and H&E staining (Leica® ST Infinity H&E Stain) was performed using the Leica® TS5025 specimen stainer. Light microscopy images of these samples were acquired for pathological analysis by an oral pathologist. For these tests, one disc per cell line per day was sliced four times with a thickness of 5 μm and a step size of 20 μm between each slice. For immunofluorescent staining, 5 μm thick sections were cut on coated slides from formalin-fixed paraffin-embedded tissue sample blocks. Slides were dewaxed with CitriSolv and rehydrated through serial immersions in graded alcohol solutions. For antigen retrieval, slides were immersed in a 10% citrate buffer and treated in a water bath at 98°C for 15 min. The slides were then blocked with Power Block Universal Blocking Reagent (Biogenex) for 10 min, followed by 5% goat and donkey serum for 1 h to inhibit any potential nonspecific binding. The slides were reacted with polyclonal anti-wide spectrum cytokeratin antibody (AB9377) overnight at 4°C in a humid chamber. After three washes in PBS, slides were incubated with secondary antibodies (1:100) in the dark for 1 h at room temperature. We used Rhodamine Red™-X (RRX) (Jackson

ImmunoReserach). Finally, 4,6-diamidino-2-phenylindole, dihydrochloride (DAPI, Invitrogen) was added for 3 min to label cell nuclei.

3.3.11. Mold casted 3D cultures

For the pure dECMT 3D cultures, cells were cultured in 2D until 80% confluence, trypsinized, and counted. Cells were centrifuged, resuspended in media, accounting for less than 1% of the total volume when encapsulated in the dECMT. Cells were embedded at a concentration of 1 million cells/mL while keeping the dECMT between 4°C-10°C. 200 µL of cell-laden dECMT was added to a 48-well plate and placed in the incubator to allow dECMT gelation for at least 1 h. Culture media was added on top of the dECMT after gelation. Discs were transferred to an agarose-coated dish for long-term culture after 24 h.

3.3.12. Cell viability assay

3D cultured cell-laden dECMT were incubated in a triple staining solution of Calcein-AM (Invitrogen®)/ Ethidium Homodimer-I (Invitrogen®)/ Hoechst 33342 (TOCRIS Bioscience®) to stain live, dead cells, and DNA respectively. To prepare the staining solution for 1 mL of DPBS-1X, 0.5 µL of Calcein-AM (4 mM), 2 µL of Ethidium Homodimer-I (2 mM), and 2.3 µL of Hoechst 33342 (18 mM) were added. The tube was vortexed, and dECMT discs were incubated in the solution at 37°C for 30 min covered from light. Before confocal imaging, discs were washed from the staining solution using PBS-1X. Images were acquired using a Nikon A1+ confocal microscope capturing the Z-stack (5 µM step size) of the entire bioprinted disc. Growth rates and cell viability were quantified over time in ImageJ®[45] software using 4 discs per timepoint (n=4).

3.3.13. Dose testing

We conducted drug response curves to calculate the half-maximal inhibitory concentration (IC_{50}) of cisplatin and 5-fluorouracil (independently) in UM-SCC-12 and -38 when cultured in 2D and 3D environments. Cisplatin (Cayman Chemical®) was dissolved to the desired concentration in a 0.9% NaCl solution (Sigma-Aldrich®). 5-fluorouracil was dissolved in dimethyl sulfoxide (Sigma-Aldrich®). Further dilutions were done using DMEM. For the 2D cultures, we seeded 5,000 cells/well in a 96-well plate and performed serum starvation overnight. The next day, cells were treated for 7 days with different doses of cisplatin or 5-fluorouracil. We washed the cells with PBS-and performed the WST-1 Cell Proliferation Reagent (Roche®) according to the manufacturer's directions. Absorbance was read after a 2 h incubation time.

For the 3D bioprinted cultures, we cultured the samples for 7 days in an agarose-coated 96-well plate. As the 2D experiment, cells were serum-starved for 24 h before treatment. 3D cultures were exposed 7 days to different concentrations of cisplatin or 5-fluoruracil. Then, we performed the WST-1 proliferation assay by adding the following reagents to each well: 50 µL of trisodium citrate in ultrapure water (55 µM) to decrosslink the alginate in the bioink, 50 µL of DMEM and 10 µL of WST-1 reagent. The absorbance was measured at 450 nm after 2 h incubation time protected from light.

3.3.14. Statistical analysis

Data are presented as the mean ± standard deviation (SD). Data analysis was conducted using GraphPad Prism 7 software (Graphpad Software®). Image analysis was performed using ImageJ®.[45] For the growth rates, geometric means were presented due to data skewness. The logistic model was used to fit the growth rates data. One-way analysis of variance (ANOVA) was applied to the drug testing data followed by post hoc Tukey's test

to determine differences in the dose-response between 2D and 3D environments. Statistical significance of data was calculated at 99% ($P < 0.01$) confidence intervals.

3.4. Results

3.4.1. Decellularization and solubilization of tissue

To develop a bioink with tissue-derived constituents, ECM was extracted from porcine tongue, and proteins were solubilized to create a tissue-derived hydrogel (Figure 1. a-b). We chose to use porcine tongue since the porcine genome bears more resemblance to the human genome than other animal models such as rodents[34] and the base of the tongue the base and lateral borders of the tongue are the most prevalent sites of cancer development.[35] The tongues composition consists primarily of skeletal muscle,[46] which provides sufficient concentration of structural ECM proteins. The decellularized tissue results in a soft material that while retaining the relevant physiological and biochemical components required for tissue function, still requires reinforcement to be optimally used in extrusion bioprinting techniques.

To decellularize the ECM, we performed a series of washes with nucleases, and mechanical mixing to remove residual cellular components present in the tissue. The tissue was later sterilized, lyophilized, solubilized, and neutralized to a pH of 7.2. For every 100 g of wet tissue, a yield of 4±0.4 g of ECM was obtained after the decellularization process. Mass spectrometry was used to characterize the biochemical composition of the decellularized ECM from porcine tongue (dECMT). Measured ECM proteins are presented as a percentage of spectral counts (Table 1, Table S1). The ECM proteins found include different types of collagens, laminin, and glycosaminoglycans. Collagens are the most abundant structural protein in dECMT, accounting for more than

90% of the total ECM protein occurrences in the LC-MS-MS assay. Collagens, which are insoluble at physiological pH,[47] were solubilized using enzyme digestion and neutralized. Before use, the dECMT was brought to a concentration of 180±80 μg/mL of total protein content to use in bioink preparation, which resulted in a sulfated glycosaminoglycan content of 0.28 μg/mL.

The solubilized dECMT is a hydrogel with thermally dependent mechanical properties, mainly attributed to the presence of collagen. A vial inversion test revealed that the dECMT flows at 4°C and 24°C immediately after the vials were inverted. However, at 37°C, the material is substantially gelled and does not flow under inversion (Figure 1. c). A rheological characterization of dECMTs shows shear-thinning behavior corroborated by the negative slope of the flow curve (Figure 2. b).

The amplitude sweep (Figure 2. c) reveals that the dECMT yield point at 37°C is 14.8 Pa. The gelation kinetics analysis (Figure 2. e) indicates that dECMT behaves as a soft gel at 4°C that reaches its maximum storage modulus at 37°C (10.03±1.34 Pa) and a tan(δ)= 0.2. Previous work done by Pati et al. (2014), has characterized decellularized heart, cartilage, and adipose tissue gels.[19] Their rheological analysis shows a similar shear-thinning behavior and an increase in moduli when the dECM was kept at 37°C.[19]

The fabrication of 3D printed structures using only dECMT is challenging due to its mechanical properties. Similar to collagen, dECM is characterized with low stiffness values and long crosslinking times, which make the fabrication of structures difficult to achieve.[48] These characteristics hamper the use of pure dECMT for extrusion bioprinting. Hence, the incorporation of rheological modifiers was considered.

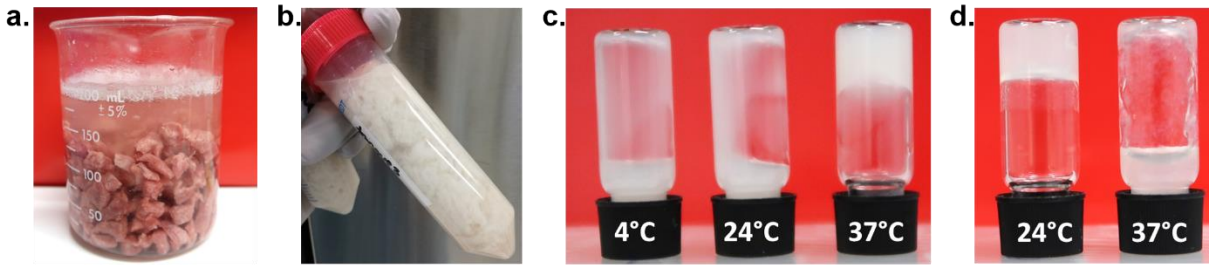

Figure 1. Decellularization and solubilization of tissue. a.-b. Representative images of the decellularization process a. Tissue immersed in a solution of 0.1% sodium dodecyl sulfate. b. Tongue tissue after the decellularization process. Inversion tests after incubation at different temperatures for 24h: c. dECMT, and d. A1.5G5dECMT after solubilization and neutralization.

Table 3. Liquid chromatography-mass spectrometry results of extracellular matrix proteins present in the dECMT. Shown in descending order according to the peptide occurrences. The percentage of spectral counts from the total ECM proteins found in the dECMT is presented. Additional information available in Table S1.

Structural ECM Proteins	Spectral Counts of Structural ECM Proteins (%)	
	Mean (%)	SD (%)
Collagen I	64.65	5.38
Collagen IV	16.06	6.77
Collagen III	6.76	1.99
Collagen V	4.08	1.00
Laminin	2.68	0.60
Collagen VI	1.41	1.99
Keratin	0.99	1.39
Decorin	0.99	1.00
Nidogen	0.85	1.20
Collagen XXI	0.70	0.60
Fibrilin	0.42	0.60
Heparan Sulfate	0.42	0.60

3.4.2. A_xG_5dECMT formulation and characterization

The solubilized dECMT was used to prepare a composite bioink containing gelatin and alginate as rheological modifiers. In this study, we will refer to the composite bioink using

the following format: A_xG_ydECMT, where "x" corresponds to the w/v percentage of alginate, "y" corresponds to the w/v percentage of gelatin, and the dECMT is used in a concentration of 180±80 μg/mL of total protein content.

We previously characterized alginate-gelatin bioinks[32] and had determined that softer gels (A_1G_5, A_1G_7, A_1G_9) allow the proliferation and spheroid formation of immortalized breast cancer cells (MDA-MB-231). Sample handling with softer gel formulations can be challenging, resulting in potential sample breakage, deformation, and difficulties reproducibly performing experimental protocols that require relocation or shearing forces such as histology. Additionally, we performed another study with a consisting of controlled fractions of alginate, gelatin and Matrigel that supported the growth and development of patient-derived epithelial cancer cells. The bioink used for this set of experiments was A_1G_7 and a 5% concentration of Matrigel.[33]

With all the knowledge previously stated, we opted for A_1G_5dECMT as our starting point during the bioink development process. We later increased the alginate concentration 0.5% to give the bioink more stability ($A_{1.5}G_5$dECMT). Both formulations are bioprintable, compatible with cell culture and with a Young's moduli comparable to tumors induced in xenograft mouse models[40], but we used $A_{1.5}G_5$dECMT as the proposed bioink for our model. Results of $A_{1.5}G_5$dECMT samples are presented here. The data obtained for A_1G_5dECMT can be found in the supporting information.

For $A_{1.5}G_5$dECMT, the dECMT total protein content is 160μg/mL. The inversion tests show opposing gelation behavior of the bioink in comparison to pure dECMT. $A_{1.5}G_5$dECMT does not collapse at 24°C yet flows at 37°C (Figure 1. d). These results show

the predominance of gelatin's mechanical properties over those of the dECMT, which ensures bioink stability at room temperature during the extrusion printing process.

$A_{1.5}G_5$dECMT showed a shear-thinning behavior and temperature sensitivity in the rheological tests (Figure 2. b, d). Shear-thinning is essential for materials used in extrusion bioprinting.[49] The results of the amplitude sweep test show that the apparent yield stress of $A_{1.5}G_5$dECMT is 18 Pa higher than that of pure dECMT. Additionally, the $A_{1.5}G_5$dECMT composite storage modulus is over 50 times larger, and its loss modulus 20 times higher than those of pure dECMT, revealing a stiffer and more solid-like composite material. A table with exact values for G', G" and yield point is presented in (Table S2).

The settings for the gelation kinetics (Figure 2. d-e) were chosen to mimic the temperature conditions that the bioink would experience during the bioprinting process. Due to the difference in gelation properties of these materials, dECMT would ideally be printed at 37°C and $A_{1.5}G_5$dECMT at room temperature (24°C). Hence, the difference in testing conditions between the two gelation tests.

In Figure 2. e, the storage modulus of pure dECMT reaches a maximum value at 37°C (10.03±1.34 Pa), which decreases by 2.57±0.22 Pa when the temperature is reduced to 4°C.

In contrast, $A_{1.5}G_5$dECMT's storage modulus is 7.77±0.17Pa at 37°C and increases to 172.7±7.38 Pa when the temperature is decreased to 24°C. After the immediate change in temperature from 37°C to 24°C, the storage and loss moduli increase to reach a plateau within 30 min. Subsequently, the increase in moduli remains less than 2 Pa/min. In Figure 2. d, the moduli of $A_{1.5}G_5$dECMT were observed to decay exponentially with time

constants of τ=28.96±0.09 min and 26.28±0.90 min for G' and G", respectively. $A_{1.5}G_5$dECMT is viscoelastic, with a predominant solid-like behavior since G' remains over G" through the range of temperatures tested. During bioink development, experiments with A_1G_5dECMT and $A_{1.5}G_5$ rheological tests were also performed (Figure S1-S2, Table S2).

Experimentally, we found that it is possible to embed cells in $A_{1.5}G_5$dECMT within the first 10 min of the material being exposed to room temperature (24°C). The bioink is ready for the bioprinting process after 30 min of incubation at room temperature. Later, the 3D structures can be stabilized for long term culture by ionically crosslinking the alginate with calcium ions.

The Young's modulus of ionically crosslinked A_xG_5dECMT was measured using nanoindentation (Figure 2.a, Figure S1). The results were compared with a xenograft tumor formed by injecting human UM-SCC-12 cells into the tongue of an immunocompromised mouse and the surrounding healthy muscle tissue.[40] This measurement allowed us to tune our bioink to have a comparable Young's modulus to the tumor induced in a xenograft mouse model.[40] We did not find a significant difference between the Young's modulus of both A_xG_5dECMT formulations when compared to the mouse tumor. However, there was a significant difference ($p<0.01$), in that of the surrounding healthy muscle tissue (Figure 2. a). We consider $A_{1.5}G_5$dECMT to be the best candidate out of both A_xG_5dECMT bioinks because it is bioprintable, it holds its shape after construct fabrication, sample handling is achieved successfully, its Young's modulus is comparable to the xenograft tumor, and it can form consistent lattices and structures of at least 5 mm height without collapsing (Figure 3. a-b).

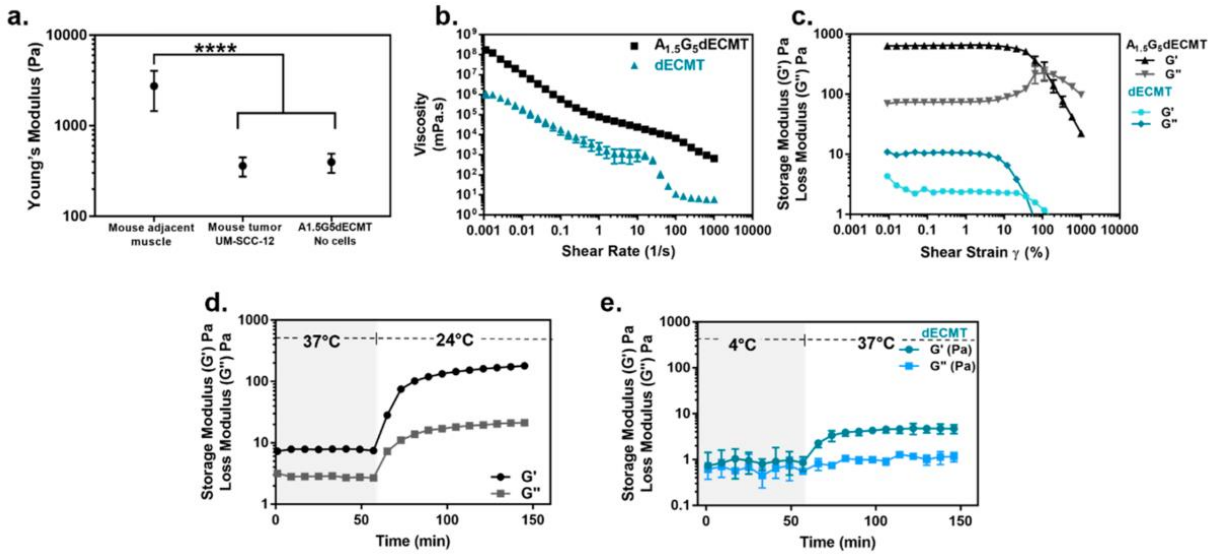

Figure 2. Mechanical characterization of dECMT and $A_{1.5}G_5$dECMT. a. Nanoindentation test of ionically crosslinked $A_{1.5}G_5$dECMT compared with a tumor formed in a mouse tongue after UM-SCC-12 implantation. Surrounding tongue muscle non-tumor tissue is also presented for comparison (n=15, $p<0.0001$). b.-e. Rheological characterization of the dECMT and the reinforced $A_{1.5}G_5$dECMT bioink (n=3). b. Flow curve performed at 24°C of dECMT and $A_{1.5}G_5$dECMT . c. Amplitude sweep presenting the storage (G') and loss (G") modulus. Gelation kinetics: simulation of temperature conditions needed for 3D printing of d. $A_{1.5}G_5$dECMT. and e. dECMT. Mechanical characterization of A_1G_5dECMT and $A_{1.5}G_5$ is presented in the supplementary information (Figure S1-S2).

3.4.3. 3D printing of cell-laden structures with A_xG_5dECMT

UM-SCC-12 and UM-SCC-38 cells independently encapsulated in $A_{1.5}G_5$dECMT or $A_{1.5}G_5$dECMT were bioprinted into disc models with 5 mm in diameter and a thickness of 500 µm. We were able to bioprint up to 50 discs per hour. Post-printing, the alginate component was ionically crosslinked using calcium chloride, and the models were successfully cultured for up to 19 days using standard cell culture conditions. Sample handling difficulties occurred when manipulating A_1G_5dECMT after crosslinking, but

crosslinked $A_{1.5}G_5$dECMT resulted in a material that was stable enough for us to handle without breaking the samples. (Figure 3.)

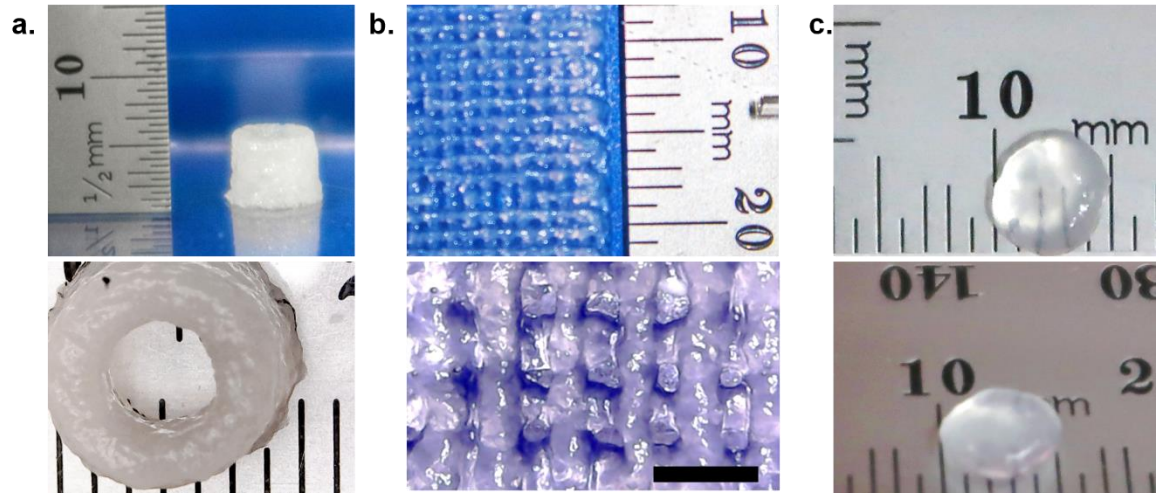

Figure 3. Extrusion printing using $A_{1.5}G_5$dECMT bioink with a 22G conical tip. a.-c. Examples of 3D printed structures. c. $A_{1.5}G_5$dECMT discs after being ionically crosslinked with $CaCl_2$. Scale bar: 2mm.

3.4.4. Cell viability tests and immunofluorescence

A live-dead analysis of the bioprinted structures was conducted using confocal microscopy. Data shows that both A_xG_5dECMT formulations allow cell proliferation and development without compromising cell viability (Figures 4, 5, S3-S5). In $A_{1.5}G_5$dECMT Tumor spheroids start to occur by day 11 for UM-SCC-12 (Figure 4. a, Figure S4) and by day 8 for UM-SCC-38 (Figure 4. b, Figure S4). The growth of the spheroids formed within $A_{1.5}G_5$dECMT models was measured over time using confocal microscopy (Figure S4, S5). For 19 days, the viability of the cultures remained above 95% in both bioinks for both cell lines tested (Figure 5. a). Analysis of growth rates shows an increasing trend in spheroid size for both UM-SCC-12 and UM-SCC-38 cell lines (Figure 5. b). Both UM-SCC-12 and UM-SCC-38 growth rates fit a logistic growth model with an R^2=0.99 and reaching a

plateau in the area at 3339 μm² and 4238 μm², respectively. The spheroidal morphology within the $A_{1.5}G_5$dECMT models differs from that of structures observed when these cells are cultured in pure dECMT (Figure S4). Cells cultured in pure dECMT exhibit a planar arrangement in contrast to the spheroid development shown in our reinforced bioink. We also cultured the cells in $A_{1.5}G_5$ and A_1G_5dECMT. Cells encapsulated in $A_{1.5}G_5$ dropped their viability over time reaching less than 20% by day 19 for both cell lines (Figures S7-S9, Table S3). For cells encapsulated in A_1G_5dECMT, spheroid formation and cell viability were observed, but we decided to use $A_{1.5}G_5$dECMT for future experiments to avoid sample handling issues and sample breakage (Figure S3).

Histological evaluation of the UM-SCC-12 and UM-SCC-38 spheroids using H&E staining showed cellular distribution comparable to cell nests seen in xenograft transplantation of human HNSCC cell lines.[40] Squamous cells form a stratified peripheral layer (Figure 5. left column). Immunofluorescence staining with pan-cytokeratin showed similar keratin expression in the bioprinted spheroid models (Figure 5. right column) and the xenograft mouse model previously reported.[40]

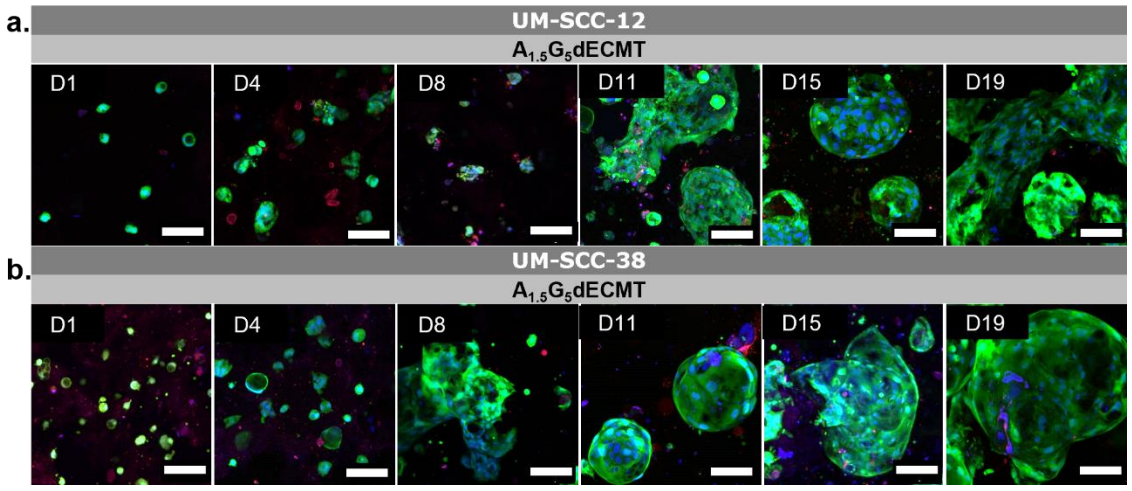

Figure 4. Confocal microscopy of bioprinted HNSCC cells encapsulated in $A_{1.5}G_5$dECMT. a. UM-SCC-12, and b. UM-SCC-38 over time in $A_{1.5}G_5$dECMT. Live-dead stains: Calcein-AM: live (green), Ethidium Homodimer-I: dead (red), and Hoechst 33342: DNA (blue). Scale bar: 100µm

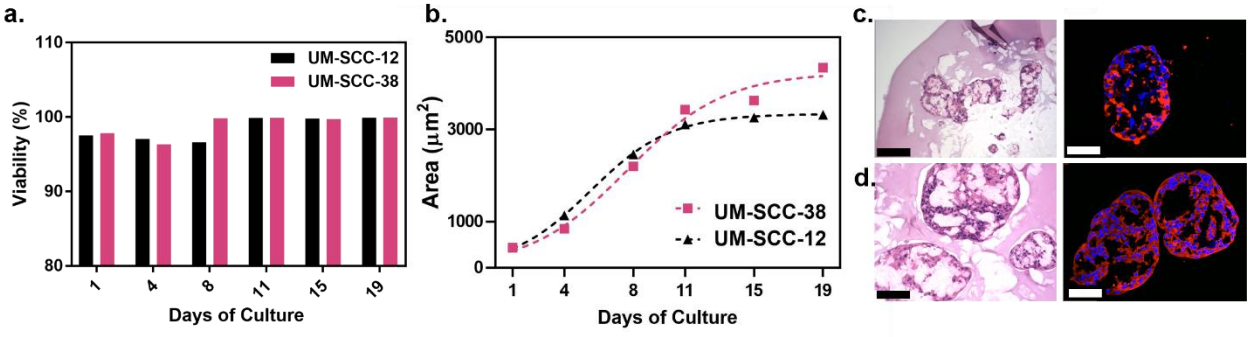

Figure 5. Quantitative analysis of live-dead assay and histological data of 3D printed HNSCC cells encapsulated in $A_{1.5}G_5$dECMT. a. Cell viability over time (n=4 $p<0.0001$). The difference in viability within the same cell line over time did not exhibit statistical significance. Additional data in Table S3. b. Growth rate of spheroids area over time (n=500, R^2 =0.99). c-d. Hematoxylin and eosin stain in the left column and immunofluorescence stain of polyclonal keratin (red) and DAPI (blue) in the right column. c. UM-SCC-12, and d. UM-SCC-38 cells encapsulated in the bioink blend and bioprinted at 19 days of culture. Scale bar: 100µm

3.4.5. Drug testing assays and microscopy of treated samples

The half-maximal inhibitory concentrations (IC_{50}) of cisplatin and 5-fluorouracil for both HNSCC cells were computed using monolayer cultures and the 3D bioprinted culture formats (Figure 6. a-d).

After 7 days of treatment with cisplatin, the IC_{50} values obtained for UM-SCC-12 and UM-SCC-38 monolayers were 2.38±0.43 µM and 1.18±1.36 µM, respectively (Figure 6. a, b). These concentrations were considered as a baseline and control for subsequent 3D experiments. Cell-laden $A_{1.5}G_5$dECMT gels were developed for 7 days and followed by a 7-

day incubation period with cisplatin. The IC_{50} values for these samples were 10.89±2.66 μM for UM-SCC-12, and 7.6±0.19 μM for UM-SCC-38. When comparing 2D and 3D cisplatin IC_{50} values, we observe a 4.6-fold increase for UM-SCC-12 and a 6.4-fold increase for UM-SCC-38. For both cell lines, there we observe a significant difference in the cisplatin IC_{50} values between the 2D environment and the 3D printed samples ($p<0.01$).

Drug testing with 5-fluoruracil was performed under the same time conditions as cisplatin experiments. The IC_{50} values obtained for UM-SCC-12 and UM-SCC-38 monolayers were 1.38±0.18 μM and 0.09±0.02 μM, respectively (Figure 6. c, d). The IC_{50} values for the cell-laden bioprinted samples were 111.10±20.08 μM for UM-SCC-12, and 121.40±16.63 μM for UM-SCC-38. With 5-fluorouracil, we also found a significant difference in response between the 2D environment, and the 3D printed samples ($p<0.01$). When comparing 2D and 3D 5-fluorouracil IC_{50} values, we observe more than an 80-fold increase for UM-SCC-12 and a 1,340 -fold increase for UM-SCC-38.

Morphology of the cancer spheroids in 3D cultures was observed following chemotherapy treatment. Cells were treated with either a lethal concentration, the IC_{50} value established for the 3D model, or without the drug as control, and monitored using confocal microscopy. Figure 6. f-g shows the maximum intensity projection image of spheroids for each dosage. The microscopy images confirm the data in Figure 6. a-e. Most of the cell population was affected upon exposure to the maximum dose. 3D cultures of UM-SCC-12 and -38 exposed to the maximum concentration of cisplatin present a cell viability lower than 5%. 5-flurouracil maximum exposure resulted in less than 15% viability for both cell lines. Spheroid disruption is observed when the IC_{50} dose was

applied. Untreated positive control models show no signs of nuclei disturbance and high cell viability. The qualitative data follows the behavior observed in the drug response curves (Figure 6. a-e).

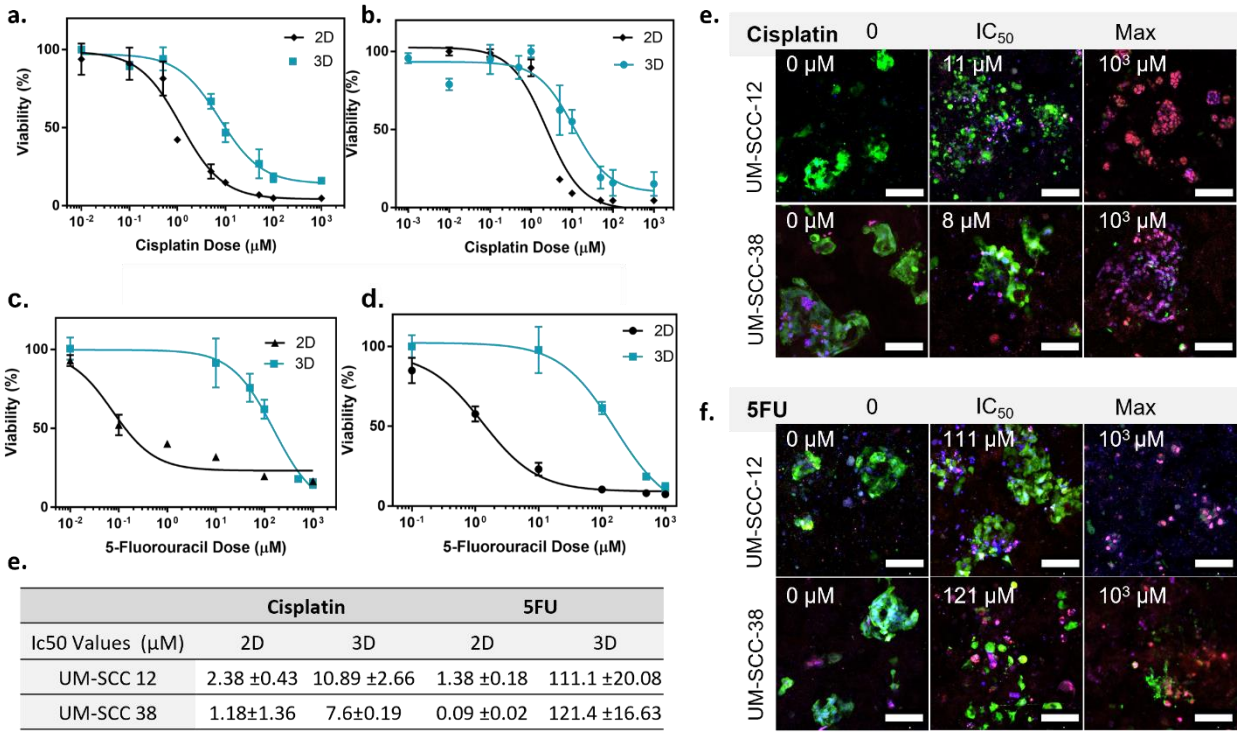

e.

	Cisplatin		5FU	
Ic50 Values (μM)	2D	3D	2D	3D
UM-SCC 12	2.38 ±0.43	10.89 ±2.66	1.38 ±0.18	111.1 ±20.08
UM-SCC 38	1.18±1.36	7.6±0.19	0.09 ±0.02	121.4 ±16.63

Figure 6. Drug response curves of HNSCC cells exposed to cisplatin and 5-fluorouracil in 2D and 3D environments. a.-d. 2D and 3D dose response curves of HNSCC cells following exposure to cisplatin (a.-b.), and 5-fluorouracil (c.-d.) over a 7-day treatment course (n=3, $p<0.01$). a.,c. UM-SCC-38, b.,d. UM-SCC-12. All 3D cultures correspond to the $A_{1.5}G_5$dECMT cell-laden bioprinted structures. e. IC_{50} values for reported from data presented in plots a.-d. f.,g. Maximum intensity projection of bioprinted 14-day old spheroids following to a 7-day exposure to varying drug doses (0, IC_{50}, 10 mM) stained with Calcein-AM: live (green), Ethidium Homodimer-I: dead (red) and Hoechst 33342: DNA (blue). Scale bar: 100μm

3.5. Discussion

Three-dimensional (3D) models have gained interest in the scientific community for their capacity to mimic cell-cell and cell-matrix interactions. Moving away from 2D models to

engineered 3D cancer systems can give further insights on druggable targets, opening avenues for translational research. A challenge for such applications is the selection of a matrix that can promote biomolecular interactions between both the cells and simulated ECM. Naturally derived dECM materials have been proven useful as they provide the required biochemical and biophysical characteristics for tissue development.[27] Aberrant cell behavior can occur when utilizing inappropriate 3D environments for cell and tissue culture.[50] Multiple studies have shown the advantages of using tissue-derived dECM in biomedical applications.[19, 51] To the best of our knowledge, there have been no studies exploring the use of a 3D printable material blend containing dECMT for head and neck cancer capable of simulating *in-vivo* mechanical and biochemical features.

In this study, we proposed the use of porcine tissue since the porcine genome bears more resemblance to the human genome than other animal models such as rodents.[34] Furthermore, the base and lateral borders of the tongue are the most prevalent sites of cancer development. Hence, we use the most common primary site for intraoral dECM of this tissue to reproduce the HNSCC, the border of the tongue environment.[35] Our decellularization process yields a collagen-rich soft gel with temperature-dependent mechanical properties. Reinforcing dECMT gels allows us to use extrusion bioprinting to create 3D environments. As revealed by our rheological studies, the dECMT itself is a weak gel that, once reinforced, has a 50-fold increase in storage modulus (650.5Pa).

The mechanically enhanced dECMT maintained its intrinsic shear-thinning behavior, a characteristic that is beneficial for extrudable bioinks to avoid excessive shear on cell membranes.[49] Material nanoindentation revealed that our dECMT blend possesses a Young's modulus comparable to a human HNSCC xenograft in an immunocompromised

mouse. It has been previously shown that matrix stiffness plays a role in regulating cell behavior, and it is a crucial aspect of tumorigenic progression.[52] Thus, encapsulating the cells within a matrix which does not resemble the mechanics of the tumor *in-vivo* can lead to ambiguous conclusions. In this study, we show that after testing different alginate-gelatin-dECMT formulations, $A_{1.5}G_5$dECMT is an adequate bioprintable material for encapsulating HNSCC cells for its printability, capacity to sustain cell proliferation, spheroid formation, and its resemblance to the Young's modulus obtained from a xenograft-derived HNSCC tumor.

Additionally, our bioprinted cell-laden environments allowed squamous cell carcinoma cells (UM-SCC-12 and -38) to develop into tumor spheroids over 19 days while maintaining high cell viability and supporting proliferation. Spheroid formation did not happen when cells were cultured in either dECMT or $A_{1.5}G_5$. We attribute the difference in cellular morphology between the $A_{1.5}G_5$dECMT and pure dECMT cultures to the enhanced mechanics of the alginate-gelatin based ink. For the $A_{1.5}G_5$ cultures, the absence of spheroid formation may be attributed to the lack of bioactive molecules and binding sites when compared to $A_{1.5}G_5$dECMT. Mechanical characteristics of the matrix have been shown to determine cell differentiation[53] and tumor progression.[52] Moreover, native dECM has exhibited degradation *in-vitro*, producing molecules that promote chemotactic and mitogenic processes.[54] In our growth rates curves, both cell lines show a behavior that fits the logistic growth model suggesting that availability of space may be a limited after day 11, where the curve starts leveling to reach a plateau. Reducing cell density or printing models with greater volumetric space for spheroids to expand may mitigate the crowding and subsequent retardation of spheroid proliferation. It has been previously reported that

cells drive epigenetic alterations that change the characteristics of their environment over time by crosslinking or degrading proteins, especially during disease progression.[55-56] These changes may lead to a difference in mechanical properties of our bioprinted models over time which should be furtherly explored. However, challenges arise when searching for a non-invasive method that can quantify the modulus of the samples over time while maintaining sterility and cell culture conditions to ensure cell viability is not affected.

Histological examination with H&E staining of the UM-SCC-12 and UM-SCC-38 spheres formed in our 3D model showed stratified cellular distribution at the sphere's periphery, resembling a tumor induced in a xenograft mouse model.[40] Other studies using suspension culture in ultra-low attachment plates reported a similar stratified appearance.[57-58] This data is evidence that a more complex representation of the native *in-vivo* physiological characteristics of HNSCC is possible using 3D culture techniques. Also, our spheroids show keratin expression after 19 days of culture comparable to the xenograft mouse model[40] suggesting that the cellular function of the moderately differentiated squamous cell carcinoma cell lines was maintained. Keratin expression has been used as a method for HNSCC model validation both in 2D and 3D culture models.[59-61]

Furthermore, we tested UM-SCC-12 and -38 cells both as monolayer and 3D formats with two clinically used chemotherapeutic agents for HNSCC treatment: cisplatin and 5-fluorouracil. Our results indicate that the IC_{50} values for the 2D and 3D groups are statistically different. When treated with 5-fluorouracil bioprinted samples had an 80-fold increase in the IC_{50} value relative to monolayer cultured UM-SCC-12, while UM-SCC-38 had a 1340-fold increase. In the case of cisplatin an increase in the IC_{50} values of 4.6-

fold increase in UM-SCC-12 and 6.4 for UM-SCC-38. In the microscopy images acquired after drug treatment, we corroborate the behavior quantified by the IC_{50} curves. The decrease in sensitivity observed in 3D cultures has been previously reported and can be attributed to the non-physiological conditions 2D cultures offers.[62] In 3D cultures, cell-ECM interactions can lead to heterogeneous drug response with matrix-attached cells being more resistant than the matrix-free cells found in inner regions of the spheroids.[63] The 3D environment also allows cell-cell interactions and the formation of concentration gradients of oxygen,[64] nutrients, waste and drugs which are present in the clinical environment. These gradients can create proliferative and quiescent cell regions that decrease cell-doubling rates promoting different behaviors to antineoplastic treatments[65] since various therapeutic treatments' form of action relies on cell replication.

Overall, this platform can be tailored into a more complex environment by incorporating different cell types in specific regions, and by modifying the positioning of cells into pertinent positions to emulate the *in-vivo* organization in an *in-vitro* model. It is also possible to perform drug testing experiments, including but not limited to cisplatin and 5-flurouracil. Additionally, the use of patient-derived tumor cells is an avenue that can be further studied for personalized medicine applications. This tool has the versatility to be used for different neoplastic tissues by changing the tissue source for the dECM and tailoring the alginate and gelatin concentration to simulate the mechanical characteristic of the bioink with the tissue of interest.[32]

3.6. Conclusions

In conclusion, we fabricated an *in-vitro* model of HNSCC based on a bioprintable hydrogel comprised of alginate, gelatin, and decellularized extracellular matrix derived

from tongue tissue (dECMT). We selected specific ratios of the constituents to match the elastic modulus of oral tumors induced in mice (xenografts). Mass spectrometry revealed the presence of important ECM biomolecules that cells use as anchoring sites, confirming that important biochemical structures were preserved after decellularization. However, bioprinting with pure, uncrosslinked, and unmodified dECM is a challenging procedure as a result of the solubilization step. We take advantage of the naturally derived microenvironment factors intrinsically present in decellularized tissue that permit spheroid development over time and use them to create a stable composite by adding rheological modifiers. Gelatin was added to reinforce the material during extrusion bioprinting and alginate to crosslink and maintain structural integrity during cell culture conditions. Moreover, the bioprinted environment promoted high HNSCC cell viability and division up to 19 days. Dose-response experiments revealed increased IC_{50} values for both cisplatin and 5-fluorouracil, for both cell lines cultured in 3D models when compared to 2D conditions. Overall, our model has the potential to be mechanically and biologically tuned for other tissue engineering applications involving either diseased or healthy tissue.

Associated content

Supporting Information. The following files are available free of charge. Supporting Information (file type, PDF). **Appendix 1**

Mechanical comparison of dECMT, $A_{1.5}G_{5,}$ A_1G_5dECMT and $A_{1.5}G_5$dECMT; Confocal microscopy of bioprinted HNSCC cells encapsulated in, $A_{1.5}G_{5.,}$ dECM, A_1G_5dECMT, $A_{1.5}G_5$dECMT; Quantitative analysis of live-dead assay of 3D printed HNSCC cells encapsulated in $A_{1.5}G_{5.}$, $A_{1.5}G_5$dECMT, Viability data of UM-SCC-12 and UM-SCC-38;

Structural proteins identified in dECMT using LC/MS/MS; STR analysis of UM-SCC-12 and UM-SCC-38.

AUTHOR INFORMATION

Corresponding Author

Joseph M. Kinsella – *Bioengineering Department, McGill University, Montreal, Quebec, Canada, H3A 0E9;* Email: joseph.kinsella@mcgill.ca; orcid.org/0000-0002-3052-0782

Authors

Jacqueline Kort-Mascort – Bioengineering Department, McGill University, *Montreal, Quebec, Canada, H3A 0E9;* orcid.org/0000-0003-0650-3162

Guangyu Bao – Mechanical Engineering Department, McGill University, *Montreal, Quebec, Canada, H3A 0C3;* orcid.org/0000-0001-5794-9020

Osama Elkashty – Oral Pathology Department, Faculty of Dentistry, Mansoura University, Mansoura, Egypt; orcid.org/0000-0002-4875-7534

Salvador Flores-Torres – Bioengineering Department, McGill University, *Montreal, Quebec, Canada, H3A 0E9;* orcid.org/0000-0002-2947-9786

Jose Gil Munguia-Lopez – Bioengineering Department, McGill University, *Montreal, Quebec, Canada, H3A 0E9;* Faculty of Dentistry, McGill University, *Montreal, Quebec, Canada, H3A 0C7;* orcid.org/0000-0002-5173-6494

Tao Jiang – Department of Intelligent Machinery and Instrument, College of Intelligence Science and Technology, National University of Defense Technology, Changsha, Hunan, China, 410073; orcid.org/0000-0002-9406-5061

Allen Ehrlicher – Bioengineering Department, McGill University, *Montreal, Quebec, Canada, H3A 0E9;* Mechanical Engineering Department, McGill University, *Montreal, Quebec, Canada, H3A 0C3;* orcid.org/0000-0003-3030-979X

Luc Mongeau – Mechanical Engineering Department, McGill University, *Montreal, Quebec, Canada, H3A 0C3;* orcid.org/0000-0003-0344-227X

Simon D. Tran – Faculty of Dentistry, McGill University, *Montreal, Quebec, Canada, H3A 0C7;* orcid.org/0000-0001-5594-359X

Author Contributions

JKM designed, planned, and executed the decellularization and solubilization of the tissue. **JKM** also performed rheological experiments, bioprinting, imaging, cell culture, functional assays, drug testing experiments, and processed the data. **GB** acquired and processed the nanoindentation results performing statistical analysis. **OE** examined the histopathological slides, stained and analyzed immunostaining for cytokeratin. **SFT, JGML,** and **TJ** contributed to experimental planning, image analysis, and statistical data results. **AJE** and **LM** contributed experimental resources and data for the biomechanical evaluation and manuscript editing. **ST** co-supervised this work, contributed to the experimental design and planned experimental methods. **JMK** supervised the research, designed, and planned experimental methods. **JKM, GB, OE, SFT, JGML, TJ, ST**, and **JMK** each contributed to writing the article.

Acknowledgments

JMK thanks the National Science and Engineering Research Council (NSERC RGPIN-06671-14), the Canadian Foundation for Innovation, the Townshend-Lamarre Family Foundation, and McGill University for funding. JKM thanks CONACYT-I2T2 for scholarship funding (751540), McGill Engineering Doctoral Award (90025) and the FRQNT (288490) for the scholarship. OE thanks the Ministry of Higher Education in Egypt for scholarship funding (MOHE post-graduate studies funding). ST thanks the Canadian Institutes of Health Research (CIHR grant 119585), Natural Sciences and Engineering Research Council of Canada (NSERC grant 05247), MJW Kim research fund. SFT thanks CONACYT-I2T2 (754427), McGill Engineering Doctoral Award (90025) and the FRQNT (291010) for the scholarship. JGML thanks CONACYT for scholarship funding (291168 and 291258) and FRQNT (258421). TJ thanks the China Scholarship Council (201403170354), McGill Engineering Doctoral Award (90025) for the scholarship, and the Research Project Funding of National University of Defense Technology (ZK19-33). G. B. and LM thank the National Institutes of Health (NIH) for their support under awards number R01 DC 018577-01, and DC 005788-15 (Mongeau, PI).

Please note that the views expressed in the present paper are the authors' own and not necessarily those of the NIH.AJE thanks the Natural Sciences and Engineering Research Council of Canada (NSERC) (RGPIN/05843-2014, EQPEQ/472339-2015).

Abbreviations

2D, two dimensional; 3D, three dimensional; ACN, acetonitrile; ANOVA, analysis of variance; BSA, bovine serum albumin; DAPI, 4′,6-diamidino-2-phenylindole; dECM, decellularized extracellular matrix; dECMT, decellularized extracellular matrix from tongue; DMEM, Dulbecco's modified Eagle medium; DMMB, dimethylmethylene blue; DNAse, deoxyribonuclease; DPBS, Dulbecco′s phosphate buffered saline; ECM, extracellular matrix; FWHM, full width at half maximum; H&E, hematoxylin and eosin; HCD, higher-energy C-trap dissociation; HNSCC, head and neck squamous cell carcinomas; IC_{50}, half-maximal inhibitory concentration; LC/MS/MS, liquid Chromatography with tandem mass spectrometry; LVR, linear viscoelastic region; MS/MS, tandem mass spectrometry; PBS, phosphate buffered saline; PCL, polycaprolactone; PEG, polyethylene glycol; RNAse, ribonuclease; RRX, rhodamine red-X; SDS, Sodium dodecyl sulfate; sGAG, sulfated glycosaminoglycans; STR, short tandem repeat; TME, tumor microenvironment; UHPLC, ultra-high-performance liquid chromatography; WST, water soluble tetrazolium salts.

References

1. Gengenbacher, N.; Singhal, M.; Augustin, H. G., Preclinical mouse solid tumour models: status quo, challenges and perspectives. *Nature Reviews Cancer* **2017,** *17* (12), 751. DOI: 10.1158/0008-5472.CAN-08-3030.

2. Cekanova, M.; Rathore, K., Animal models and therapeutic molecular targets of cancer: utility and limitations. *Drug design, development and therapy* **2014,** *8*, 1911-21. DOI: 10.2147/dddt.s49584.

3. McGonigle, P.; Ruggeri, B., Animal models of human disease: challenges in enabling translation. *Biochemical pharmacology* **2014,** *87* (1), 162-71. DOI: 10.1016/j.bcp.2013.08.006.

4. Ruggeri, B. A.; Camp, F.; Miknyoczki, S., Animal models of disease: pre-clinical animal models of cancer and their applications and utility in drug discovery. *Biochemical pharmacology* **2014,** *87* (1), 150-61. DOI: 10.1016/j.bcp.2013.06.020.

5. Imamura, Y.; Mukohara, T.; Shimono, Y.; Funakoshi, Y.; Chayahara, N.; Toyoda, M.; Kiyota, N.; Takao, S.; Kono, S.; Nakatsura, T., Comparison of 2D-and 3D-culture models as drug-testing platforms in breast cancer. *Oncology reports* **2015,** *33* (4), 1837-1843. DOI: 10.3892/or.2015.3767.

6. Loessner, D.; Stok, K. S.; Lutolf, M. P.; Hutmacher, D. W.; Clements, J. A.; Rizzi, S. C., Bioengineered 3D platform to explore cell–ECM interactions and drug resistance of epithelial ovarian cancer cells. *Biomaterials* **2010,** *31* (32), 8494-8506. DOI: 10.1016/j.biomaterials.2010.07.064.

7. Balkwill, F. R.; Capasso, M.; Hagemann, T., The tumor microenvironment at a glance. *Journal of Cell Science* **2012,** *125* (23), 5591-5596. DOI: 10.1242/jcs.116392.

8. Young, E. W., Cells, tissues, and organs on chips: challenges and opportunities for the cancer tumor microenvironment. *Integrative Biology* **2013,** *5* (9), 1096-1109. DOI: 10.1039/c3ib40076j.

9. Jiang, T.; Munguia-Lopez, J. G.; Flores-Torres, S.; Grant, J.; Vijayakumar, S.; De Leon-Rodriguez, A.; Kinsella, J. M., Directing the Self-assembly of Tumour Spheroids by Bioprinting Cellular Heterogeneous Models within Alginate/Gelatin Hydrogels. *Scientific Reports* **2017,** *7* (1), 4575. DOI: 10.1038/s41598-017-04691-9.

10. Tibbitt, M. W.; Anseth, K. S., Hydrogels as extracellular matrix mimics for 3D cell culture. *Biotechnology and bioengineering* **2009,** *103* (4), 655-663. DOI: 10.1002/bit.22361.

11. Sant, S.; Johnston, P. A., The production of 3D tumor spheroids for cancer drug discovery. *Drug Discovery Today: Technologies* **2017,** *23*, 27-36. DOI: 10.1016/j.ddtec.2017.03.002.

12. Skardal, A.; Shupe, T.; Atala, A., Organoid-on-a-chip and body-on-a-chip systems for drug screening and disease modeling. *Drug Discovery Today* **2016,** *21* (9), 1399-1411. DOI: 10.1016/j.drudis.2016.07.003.

13. Driehuis, E.; Kolders, S.; Spelier, S.; Lõhmussaar, K.; Willems, S. M.; Devriese, L. A.; De Bree, R.; De Ruiter, E. J.; Korving, J.; Begthel, H.; Van Es, J. H.; Geurts, V.; He, G.-W.; Van Jaarsveld, R. H.; Oka, R.; Muraro, M. J.; Vivié, J.; Zandvliet, M. M. J. M.; Hendrickx, A. P. A.; Iakobachvili, N.; Sridevi, P.; Kranenburg, O.; Van Boxtel, R.; Kops, G. J. P. L.; Tuveson, D. A.; Peters, P. J.; Van Oudenaarden, A.; Clevers, H., Oral Mucosal Organoids as a Potential Platform for Personalized Cancer Therapy. *Cancer Discovery* **2019,** *9* (7), 852-871. DOI: 10.1158/2159-8290.cd-18-1522.

14. Huh, D.; Hamilton, G. A.; Ingber, D. E., From 3D cell culture to organs-on-chips. *Trends in Cell Biology 21* (12), 745-754. DOI: 10.1016/j.tcb.2011.09.005.

15. Ozbolat, I. T.; Hospodiuk, M., Current advances and future perspectives in extrusion-based bioprinting. *Biomaterials* **2016,** *76*, 321-43. DOI: 10.1016/j.biomaterials.2015.10.076.

16. Murphy, S. V.; Atala, A., 3D bioprinting of tissues and organs. *Nature biotechnology* **2014,** *32* (8), 773. DOI: 10.1038/nbt.2958.

17. Jia, J.; Richards, D. J.; Pollard, S.; Tan, Y.; Rodriguez, J.; Visconti, R. P.; Trusk, T. C.; Yost, M. J.; Yao, H.; Markwald, R. R., Engineering alginate as bioink for bioprinting. *Acta biomaterialia* **2014,** *10* (10), 4323-4331. DOI: 10.1016/j.actbio.2014.06.034.

18. Stanton, M.; Samitier, J.; Sanchez, S., Bioprinting of 3D hydrogels. *Lab on a Chip* **2015,** *15* (15), 3111-3115. DOI: 10.1039/c5lc90069g.

19. Pati, F.; Jang, J.; Ha, D. H.; Won Kim, S.; Rhie, J. W.; Shim, J. H.; Kim, D. H.; Cho, D. W., Printing three-dimensional tissue analogues with decellularized extracellular matrix bioink. *Nature communications* **2014,** *5*, 3935. DOI: 10.1038/ncomms4935.

20. Badylak, S. F.; Freytes, D. O.; Gilbert, T. W., Reprint of: Extracellular matrix as a biological scaffold material: Structure and function. *Acta biomaterialia* **2015,** *23 Suppl*, S17-26. DOI: 10.1016/j.actbio.2015.07.016.

21. Das, S.; Pati, F.; Choi, Y.-J.; Rijal, G.; Shim, J.-H.; Kim, S. W.; Ray, A. R.; Cho, D.-W.; Ghosh, S., Bioprintable, cell-laden silk fibroin–gelatin hydrogel supporting multilineage differentiation of stem cells for fabrication of three-dimensional tissue constructs. *Acta biomaterialia* **2015,** *11*, 233-246. DOI: 10.1016/j.actbio.2014.09.023.

22. Pizzo, A. M.; Kokini, K.; Vaughn, L. C.; Waisner, B. Z.; Voytik-Harbin, S. L., Extracellular matrix (ECM) microstructural composition regulates local cell-ECM biomechanics and fundamental fibroblast behavior: a multidimensional perspective. *Journal of applied physiology* **2005,** *98* (5), 1909-1921. DOI: 10.1152/japplphysiol.01137.2004.

23. Skardal, A.; Devarasetty, M.; Kang, H.-W.; Mead, I.; Bishop, C.; Shupe, T.; Lee, S. J.; Jackson, J.; Yoo, J.; Soker, S., A hydrogel bioink toolkit for mimicking native tissue biochemical and mechanical properties in bioprinted tissue constructs. *Acta biomaterialia* **2015,** *25*, 24-34. DOI: 10.1016/j.actbio.2015.07.030.

24. Badylak, S. F., The extracellular matrix as a biologic scaffold material. *Biomaterials* **2007,** *28* (25), 3587-3593. DOI: 10.1016/j.biomaterials.2007.04.043.

25. DeQuach, J. A.; Yuan, S. H.; Goldstein, L. S.; Christman, K. L., Decellularized porcine brain matrix for cell culture and tissue engineering scaffolds. *Tissue engineering. Part A* **2011,** *17* (21-22), 2583-92. DOI: 10.1089/ten.TEA.2010.0724.

26. Zhang, Y.; He, Y.; Bharadwaj, S.; Hammam, N.; Carnagey, K.; Myers, R.; Atala, A.; Van Dyke, M., Tissue-specific extracellular matrix coatings for the promotion of cell proliferation and maintenance of cell phenotype. *Biomaterials* **2009,** *30* (23-24), 4021-4028. DOI: 10.1016/j.biomaterials.2009.04.005.

27. Heinrich, M. A.; Liu, W.; Jimenez, A.; Yang, J.; Akpek, A.; Liu, X.; Pi, Q.; Mu, X.; Hu, N.; Schiffelers, R. M.; Prakash, J.; Xie, J.; Zhang, Y. S., 3D Bioprinting: from Benches to Translational Applications. *Small* **2019,** *15* (23), 1805510. DOI: 10.1002/smll.201805510.

28. Toprakhisar, B.; Nadernezhad, A.; Bakirci, E.; Khani, N.; Skvortsov, G. A.; Koc, B., Development of bioink from decellularized tendon extracellular matrix for 3D bioprinting. *Macromolecular bioscience* **2018,** *18* (10), 1800024. DOI: 10.1002/mabi.201800024.

29. Jang, J.; Kim, T. G.; Kim, B. S.; Kim, S.-W.; Kwon, S.-M.; Cho, D.-W., Tailoring mechanical properties of decellularized extracellular matrix bioink by vitamin B2-induced photo-crosslinking. *Acta biomaterialia* **2016,** *33*, 88-95. DOI: 10.1016/j.actbio.2016.01.013.

30. Lee, J.; Hong, J.; Kim, W.; Kim, G. H., Bone-derived dECM/alginate bioink for fabricating a 3D cell-laden mesh structure for bone tissue engineering. *Carbohydrate Polymers* **2020,** *250*, 116914. DOI: 10.1016/j.carbpol.2020.116914.

31. Khavari, A.; Nydén, M.; Weitz, D. A.; Ehrlicher, A. J., Composite alginate gels for tunable cellular microenvironment mechanics. *Scientific reports* **2016,** *6*, 30854. DOI: 10.1038/srep30854.

32. Jiang, T.; Mungia-Lopez, J.; Gu, K.; Bavoux, M.; Flores-Torres, S.; Kort-Mascort, J.; Grant, J.; Vijayakumar, S.; De Leon Rodriguez, A.; Ehrlicher, A.; Kinsella, J. M., Engineering bioprintable alginate/gelatin composite hydrogels with tunable mechanical and cell adhesive properties to modulate tumor spheroid growth kinetics. *Biofabrication* **2019**. DOI: 10.1088/1758-5090/ab3a5c.

33. Flores-Torres, S.; Chavez, O. P.; Kuasne, H.; Munguia-Lopez, J. G.; Kort-Mascort, J.; Ferri, L.; Jiang, T.; Rajadurai, C. V.; Park, M.; Sangwan, V., Alginate-gelatin-Matrigel hydrogels enable the development and multigenerational passaging of patient-derived 3D bioprinted cancer spheroid models. *Biofabrication* **2021**. DOI: 10.1088/1758-5090/abdb87.

34. Dawson, H. D., A comparative assessment of the pig, mouse and human genomes. In *The Minipig in Biomedical Research*, 1 ed.; CRC Press: US, 2011; pp 323-42.

35. Pires, F. R.; Ramos, A. B.; Oliveira, J. B. C. d.; Tavares, A. S.; Luz, P. S. R. d.; Santos, T. C. R. B. d., Oral squamous cell carcinoma: clinicopathological features from 346 cases from a single oral pathology service during an 8-year period. *Journal of Applied Oral Science* **2013,** *21* (5), 460-467. DOI: 10.1590/1679-775720130317.

36. Pouliot, R. A.; Link, P. A.; Mikhaiel, N. S.; Schneck, M. B.; Valentine, M. S.; Kamga Gninzeko, F. J.; Herbert, J. A.; Sakagami, M.; Heise, R. L., Development and characterization of a naturally derived lung extracellular matrix hydrogel. *Journal of Biomedical Materials Research Part A* **2016,** *104* (8), 1922-1935. DOI: 10.1002/jbm.a.35726.

37. Kim, E. J.; Choi, J. S.; Kim, J. S.; Choi, Y. C.; Cho, Y. W., Injectable and thermosensitive soluble extracellular matrix and methylcellulose hydrogels for stem cell delivery in skin wounds. *Biomacromolecules* **2015,** *17* (1), 4-11. DOI: 10.1021/acs.biomac.5b01566.

38. Park, K.-M.; Hussein, K. H.; Hong, S.-H.; Ahn, C.; Yang, S.-R.; Park, S.-M.; Kweon, O.-K.; Kim, B.-M.; Woo, H.-M., Decellularized liver extracellular matrix as promising tools for transplantable bioengineered liver promotes hepatic lineage commitments of induced pluripotent stem cells. *Tissue Engineering Part A* **2016,** *22* (5-6), 449-460. DOI: 10.1089/ten.tea.2015.0313.

39. Liang, R.; Yang, G.; Kim, K. E.; D'Amore, A.; Pickering, A. N.; Zhang, C.; Woo, S. L., Positive effects of an extracellular matrix hydrogel on rat anterior cruciate ligament fibroblast proliferation and collagen mRNA expression. *Journal of orthopaedic translation* **2015,** *3* (3), 114-122. DOI: 10.1016/j.jot.2015.05.001.

40. Elkashty, O. A.; Abu Elghanam, G.; Su, X.; Liu, Y.; Chauvin, P. J.; Tran, S. D., Cancer stem cells enrichment with surface markers CD271 and CD44 in human head and neck squamous cell carcinomas. *Carcinogenesis* **2019**. DOI: 10.1093/carcin/bgz182.

41. Freytes, D. O.; Martin, J.; Velankar, S. S.; Lee, A. S.; Badylak, S. F., Preparation and rheological characterization of a gel form of the porcine urinary bladder matrix. *Biomaterials* **2008,** *29* (11), 1630-7. DOI: 10.1016/j.biomaterials.2007.12.014.

42. Krause, C. J.; Carey, T. E.; Ott, R. W.; Hurbis, C.; McClatchey, K. D.; Regezi, J. A., Human Squamous Cell Carcinoma: Establishment and Characterization of New Permanent Cell Lines. *Archives of Otolaryngology* **1981,** *107* (11), 703-710. DOI: 10.1001/archotol.1981.00790470051012.

43. Grénman, R.; Carey, T. E.; McClatchey, K. D.; Wagner, J. G.; Pekkola-Heino, K.; Schwartz, D. R.; Wolf, G. T.; Lacivita, L. P.; Ho, L.; Baker, S. R., *In-vitro* radiation resistance among cell lines established from patients with squamous cell carcinoma of the head and neck. *Cancer* **1991,** *67* (11), 2741-2747. DOI: 10.1002/1097-0142(19910601)67:11<2741::AID-CNCR2820671105>3.0.CO;2-S.

44. Brenner, J. C.; Graham, M. P.; Kumar, B.; Saunders, L. M.; Kupfer, R.; Lyons, R. H.; Bradford, C. R.; Carey, T. E., Genotyping of 73 UM-SCC head and neck squamous cell carcinoma cell lines. *Head & neck* **2010,** *32* (4), 417-26. DOI: 10.1002/hed.21198.

45. Schindelin, J.; Arganda-Carreras, I.; Frise, E.; Kaynig, V.; Longair, M.; Pietzsch, T.; Preibisch, S.; Rueden, C.; Saalfeld, S.; Schmid, B., Fiji: an open-source platform for biological-image analysis. *Nature methods* **2012,** *9* (7), 676-682. DOI: 10.1038/nmeth.2019.

46. McLoon, L. K.; Andrade, F., Craniofacial Muscles: A New Framework for Understanding the Effector Side of Craniofacial Muscle Control. Springer New York: 2012.

47. Fujii, K.; Yamagishi, T.; Nagafuchi, T.; Tsuji, M.; Kuboki, Y., Biochemical properties of collagen from ligaments and periarticular tendons of the human knee. *Knee Surgery, Sports Traumatology, Arthroscopy* **1994,** *2* (4), 229-233. DOI: 10.1007/BF01845593.

48. Cho, D.-W.; Kim, B. S.; Jang, J.; Gao, G.; Han, W.; Singh, N. K., Decellularized Extracellular Matrix-Based Bioinks. In *3D Bioprinting*, Springer: 2019; pp 41-51. DOI: 10.1007/978-3-030-32222-9_6.

49. Liu, W.; Heinrich, M. A.; Zhou, Y.; Akpek, A.; Hu, N.; Liu, X.; Guan, X.; Zhong, Z.; Jin, X.; Khademhosseini, A., Bioprinting: Extrusion Bioprinting of Shear-Thinning Gelatin Methacryloyl Bioinks *Advanced healthcare materials* **2017,** *6* (12). DOI: 10.1002/adhm.201601451.

50. Kapałczyńska, M.; Kolenda, T.; Przybyła, W.; Zajączkowska, M.; Teresiak, A.; Filas, V.; Ibbs, M.; Bliźniak, R.; Łuczewski, Ł.; Lamperska, K., 2D and 3D cell cultures–a comparison of different types of cancer cell cultures. *Archives of medical science: AMS* **2018,** *14* (4), 910. DOI: 10.5114/aoms.2016.63743.

51. Jin, Y.; Lee, J. S.; Kim, J.; Min, S.; Wi, S.; Yu, J. H.; Chang, G.-E.; Cho, A.-N.; Choi, Y.; Ahn, D.-H., Three-dimensional brain-like microenvironments facilitate the direct reprogramming of fibroblasts into therapeutic neurons. *Nature biomedical engineering* **2018,** *2* (7), 522-539. DOI: 10.1038/s41551-018-0260-8.

52. Cukierman, E.; Bassi, D. E., Physico-mechanical aspects of extracellular matrix influences on tumorigenic behaviors. *Seminars in Cancer Biology* **2010,** *20* (3), 139-145. DOI: 10.1016/j.semcancer.2010.04.004.

53. McBeath, R.; Pirone, D. M.; Nelson, C. M.; Bhadriraju, K.; Chen, C. S., Cell shape, cytoskeletal tension, and RhoA regulate stem cell lineage commitment. *Developmental cell* **2004,** *6* (4), 483-495. DOI: 10.1016/S1534-5807(04)00075-9.

54. Reing, J. E.; Zhang, L.; Myers-Irvin, J.; Cordero, K. E.; Freytes, D. O.; Heber-Katz, E.; Bedelbaeva, K.; McIntosh, D.; Dewilde, A.; Braunhut, S. J., Degradation products of extracellular matrix affect cell migration and proliferation. *Tissue Engineering Part A* **2009,** *15* (3), 605-614. DOI: 10.1089/ten.tea.2007.0425.

55. Theocharis, A. D.; Manou, D.; Karamanos, N. K., The extracellular matrix as a multitasking player in disease. *The FEBS Journal* **2019,** *286* (15), 2830-2869. DOI: 10.1111/febs.14818.

56. Manou, D.; Caon, I.; Bouris, P.; Triantaphyllidou, I.-E.; Giaroni, C.; Passi, A.; Karamanos, N. K.; Vigetti, D.; Theocharis, A. D., The Complex Interplay Between Extracellular Matrix and Cells in Tissues. In *The Extracellular Matrix*, Springer New York: 2019; pp 1-20. DOI: 10.1007/978-1-4939-9133-4_1.

57. Kochanek, S. J.; Close, D. A.; Johnston, P. A., High Content Screening Characterization of Head and Neck Squamous Cell Carcinoma Multicellular Tumor

Spheroid Cultures Generated in 384-Well Ultra-Low Attachment Plates to Screen for Better Cancer Drug Leads. *Assay and drug development technologies* **2019,** *17* (1), 17-36. DOI: 10.1089/adt.2018.896.

58. Kijima, T.; Nakagawa, H.; Shimonosono, M.; Chandramouleeswaran, P. M.; Hara, T.; Sahu, V.; Kasagi, Y.; Kikuchi, O.; Tanaka, K.; Giroux, V., Three-dimensional organoids reveal therapy resistance of esophageal and oropharyngeal squamous cell carcinoma cells. *Cellular and molecular gastroenterology and hepatology* **2019,** *7* (1), 73-91. DOI: 10.1016/

j.jcmgh.2018.09.003.

59. Brauchle, E.; Johannsen, H.; Nolan, S.; Thude, S.; Schenke-Layland, K., Design and analysis of a squamous cell carcinoma *in-vitro* model system. *Biomaterials* **2013,** *34* (30), 7401-7407. DOI: 10.1016/j.biomaterials.2013.06.016.

60. Yanagi, T.; Watanabe, M.; Hata, H.; Kitamura, S.; Imafuku, K.; Yanagi, H.; Homma, A.; Wang, L.; Takahashi, H.; Shimizu, H., Loss of TRIM29 alters keratin distribution to promote cell invasion in squamous cell carcinoma. *Cancer research* **2018,** *78* (24), 6795-6806. DOI: 10.1158/0008-5472.CAN-18-1495.

61. Gawas, N. P.; Navarange, S. S.; Chovatiya, G. L.; Chaturvedi, P.; Waghmare, S. K., Establishment and characterization of novel human oral squamous cell carcinoma cell lines from advanced-stage tumors of buccal mucosa. *Oncology reports* **2019,** *41* (4), 2289-2298. DOI: 10.3892/or.2019.7003.

62. Langhans, S. A., Three-dimensional *in-vitro* cell culture models in drug discovery and drug repositioning. *Frontiers in pharmacology* **2018,** *9*, 6. DOI: 10.3389/fphar.2018.00006.

63. Muranen, T.; Selfors, L. M.; Worster, D. T.; Iwanicki, M. P.; Song, L.; Morales, F. C.; Gao, S.; Mills, G. B.; Brugge, J. S., Inhibition of PI3K/mTOR leads to adaptive resistance in matrix-attached cancer cells. *Cancer cell* **2012,** *21* (2), 227-239. DOI: 10.1016/j.ccr.2011.12.024.

64. Carrera, S.; de Verdier, P. J.; Khan, Z.; Zhao, B.; Mahale, A.; Bowman, K. J.; Zainol, M.; Jones, G. D.; Lee, S. W.; Aaronson, S. A., Protection of cells in physiological oxygen tensions against DNA damage-induced apoptosis. *Journal of Biological Chemistry* **2010,** *285* (18), 13658-13665. DOI: 10.1074/jbc.M109.062562.

65. Stock, K.; Estrada, M. F.; Vidic, S.; Gjerde, K.; Rudisch, A.; Santo, V. E.; Barbier, M.; Blom, S.; Arundkar, S. C.; Selvam, I., Capturing tumor complexity *in-vitro*: Comparative analysis of 2D and 3D tumor models for drug discovery. *Scientific reports* **2016,** *6* (1), 1-15. DOI: 10.1038/srep28951.

Preface to Chapter 4

The intent of the previous article was to develop and characterize the individual components needed for the fabrication of a heterogenous HNSCC model. The upcoming chapter includes a second research article which focuses on the completion of aim 3:

- **Aim 3:** Fabricate and validate a three-dimensional (3D) bioprinted co-culture *in-vitro* model of HNSCC.

It will help me validate my hypothesis, which states that a co-culture model including epithelial and stromal cells encapsulated in a dECM-containing bioink will provide an environment with crucial characteristics found *in-vivo*.

In this article, I quantify the topographical characteristics of the pure dECM hydrogel and the composite material. HNSCC cells and vocal fold fibroblasts are encapsulated in the bioink and cultivated in standard conditions. Morphological changes that resemble the tumor microenvironment *in-vivo* are observed in my cultures. Additionally, changes in matrix metalloproteinases and soluble collagen are observed. All the results observed in the co-culture are compared with the monoculture control groups.

The result of this article is a well-characterized platform that has the potential to be used in drug discovery. It can be fabricated consistently due to the use of extrusion bioprinting. I also wanted to highlight the importance of correctly understanding the tool before using it as a preclinical model. We constantly see in the literature impressive models with multiple components. However, the more variables we want to replicate *in-vitro*, the more complex the model becomes. This can be a positive aspect since we can reproduce tissues more accurately. Still, it comes with the disadvantage of not knowing if the

response obtained is due to the molecule or drug of study or the model itself. Characterization is a crucial step that should not be overlooked when developing *in-vitro* models.

This manuscript in the following chapter was submitted for publication. Approval is pending.

4. Bioprinted cancer-stromal *in-vitro* models in a decellularized ECM-based bioink exhibit progressive remodeling and maturation

Authors: Jacqueline Kort-Mascort[a], Molly L. Shen [b, c], Emma Martin [a], Salvador Flores-Torres [a], Lucas Antonio Pardo [a], Peter M. Siegel [c,d], Simon D. Tran[e], Joseph Kinsella [a].

joseph.kinsella@mcgill.ca

[a] Department of Bioengineering, McGill University, Montreal, Quebec, Canada.

[b] Department of Biomedical Engineering, McGill University, Montreal, Quebec, Canada.

[c] Goodman Cancer Institute, McGill University, Montreal, Quebec, Canada.

[d] Department of Medicine, Division of Experimental Medicine, McGill University, Montreal, Quebec, Canada.

[e] Faculty of Dental Medicine and Oral Health Sciences, McGill University, Montreal, Quebec, Canada.

4.1. Abstract

Constant matrix remodeling and cellular heterogeneity in cancer are key contributors to its development and can profoundly alter treatment efficacy. Developing *in-vitro* models containing relevant features that can recapitulate these aspects of the tumor microenvironment (TME) and that are well characterized can circumvent the limitations of conventional 2D cultures and animal models. Automated fabrication methods combined with biomimetic biomaterials have provided the opportunity to create platforms that can potentially incorporate a heterogenous population of cells in a 3D environment that allows cell-cell and cell-ECM interactions with reproducibility.

This study used 3D extrusion bioprinting and a composite bioink containing a reinforced decellularized extracellular matrix hydrogel to fabricate a head and neck cancer *in-vitro* model. The constituents of this model included fibroblasts and active extracellular matrix proteins to represent the stroma, along with HNSCC cells to represent the tumor component. The topographical characterization of the bioink showed a fibrous network with nanometer-sized pores. After cell encapsulation and model fabrication, we observed spheroid development and growth over time with cancer cells in the core and fibroblasts in the periphery. Our model is compatible with MMP quantification techniques and showed significant differences in the presence of MMP-9 and MMP-10 compared to the control groups. This characterized model is proposed as a tool for further translational and drug discovery applications since it provides a biomimetic scenario that allows the study of the tumor microenvironment *in-vitro* using non-destructive longitudinal monitoring over time.

4.2. Introduction

During tumorigenesis, neoplastic cells in solid tumors interact with cellular and non-cellular components present in the stroma, forming the tumor microenvironment (TME).[1,2] The TME is an environment comprised of a heterogenous population of cancer cells and the stroma, a collection of cell types recruited by the cancer cells and non-cellular components that aid in tumor development.[1,3] The TME works in synergy through two-way communication to promote cancer progression by providing nutrients and constantly remodeling the extracellular matrix (ECM) physically and biochemically through tumor-stromal interactions.[4,5] Endothelial cells, fibroblasts, and immune cells, among other cell types, are generally present in the stroma interacting with a dysregulated extracellular matrix.[3,6,7] Fibroblasts represent an abundant cell population in the TME and are known to be the main contributors to ECM changes over time.[8] They can be transformed into cancer-associated fibroblasts (CAFs), which behave in an abnormal manner.[1,8,9] Fibroblasts are known to synthesize structural proteins such as collagens and fibronectin, which modify the mechanical properties of the environment.[8] Also, fibroblasts can secrete non-structural proteins like cytokines, growth factors, and matrix metalloproteinases (MMPs) that can degrade or break mature regions of the ECM to favor cancer metastasis.[8,9] In healthy tissues, MMPs are tightly regulated with tissue inhibitor of metalloproteinases (TIMPs), and increased expression of TIMPs has also been linked to cancer progression, in particular TIMP-1 which has been proposed as a possible marker for cancer treatment.[10-12] The extracellular matrix is an essential actuator in tumorigenesis[6], and it has been shown to affect the sensitivity of drug treatments since it

acts as a physical barrier and can sequester drugs due to affinity making it more difficult to penetrate the tumor region.[13,14]

3D in-vitro culture models have become popular as an alternative to traditional animal preclinical models to test and better understand disease.[5,15-17] These models intend to recapitulate, in a controlled manner, variables that mimic the conditions found *in-vitro*.[5,16] The ideal 3D *in-vitro* model must include a 3D environment with relevant architecture and dimensions, a matrix resembling the extracellular matrix of the tissue in question, and relevant cell populations for the disease studied.[17] Several biomaterials have been proposed to mimic the ECM *in-vitro*.[18] Specifically, decellularized ECM (dECM) hydrogels are of great interest for their bioactive capabilities.[19] dECM hydrogels are thermally dependent tissue-derived biomaterials produced through a decellularization and solubilization process.[20] Collagens, glycosaminoglycans, laminins, cytokines, growth factors, and vesicles have been detected in dECM matrices.[21-25] These bioactive components allow cellular adhesion, development, and differentiation.[20,21] Mechanical properties of dECM tissues, such as stiffness, decrease after decellularization.[26] Then, the solubilization process uses enzymes to structurally break the tissue and form dECM hydrogels.[27] These processing steps significantly change the structure of the final product, making it challenging to use in conjunction with automated fabrication techniques such as extrusion bioprinting. dECM-containing blends have been proposed to keep the bioactive benefits provided by the ECM while adding reinforcements to create a material that has mechanical properties similar to the tissue of study and compatible with *in-vitro* culture fabrication.[28-30]

Here, we use a bioink blend containing alginate, gelatin, and dECM derived from porcine tongue that has been previously characterized and which promoted tumor formation of encapsulated cancer cells.[28] Spheroid formation was not observed in the pure dECM.[28] We used this composite hydrogel in conjunction with head and neck cancer (HNSCC) cells and fibroblasts to fabricate and characterize a bioprinted heterogenous *in-vitro* HNSCC model that is consistent and scalable. This was achieved using extrusion bioprinting since it allows the fabrication of reproducible, high-fidelity constructs with comparable cell densities in an automated and serial manner.[31,32]

These models develop over more than 20 days showing cell reorganization, spheroid formation, and matrix remodeling through time. They allow their non-destructive study and quantification of collagen and small molecules such as MMPs through time. They are proposed as an *in-vitro* alternative to study cancer-fibroblast interactions through time. We propose this platform not only to study HNSCC but as a model that can be tailored to different neoplastic diseases.

4.3. Methods

4.3.1. Bioink fabrication

We used $A_{1.5}G_5$dECMT, a combination of alginate, gelatin, and decellularized extracellular matrix derived from porcine tongue (dECMT), as the bioink for cell encapsulation. Detailed formulation methods and characterization of this blend have been previously published.[28]

Briefly, porcine tongue tissue was decellularized using mechanical agitation with several solutions, including 0.1% sodium dodecyl sulfate (SDS) (Bioshop) and 1% penicillin–streptomycin, PBS1-x, 1% Triton X100 (Bioshop), DNase (50 U/mL), RNase (1 U/mL) (Sigma-Aldrich) and acetone washes. The dECMT was sterilized using an ethanol-peracetic acid solution, homogenized, and solubilized with pepsin from porcine gastric mucosa (Sigma-Aldrich) in acidic conditions. The decellularized hydrogel was finally neutralized to physiological pH and stored at -20°C prior to use.

Our composite bioink nomenclature follows the format: A_xG_ydECMT, where "x" corresponds to the w/v percentage of alginate, and "y" corresponds to the w/v percentage of gelatin. To prepare $A_{1.5}G_5$dECMT, a 9% (w/v) solution of sodium alginate (FMC biopolymer) in DPBS-1X (Wisent Bio Products) was mixed overnight at RT with the neutralized dECMT to obtain a final concentration of 1.5% alginate. Next, type B gelatin from bovine skin (gel strength: 300, G2500, Sigma-Aldrich) was added to the alginate-dECMT solution at a 5% (w/v) final concentration. The neutralized dECMT has a protein concentration of f 180 ± 80 μg/mL.[28] The final dECMT protein concentration in the $A_{1.5}G_5$dECMT is 160 μg/mL.[28] $A_{1.5}G_5$dECMT was kept at -20°C for long-term storage or at 4°C if used within 4 weeks.

4.3.2. Scanning electron microscopy

Both pure dECMT and $A_{1.5}G_5$dECMT were mold-casted without encapsulating cells in them. $A_{1.5}G_5$dECMT was crosslinked with CaCl2 (100mM, Sigma-Aldrich) for 3 minutes before immersing the samples in supplemented media for 24h at physiological conditions.

After culture, 3D printed discs were fixed with 4% PFA for 30 minutes, washed with PBS-1x, and gradually dehydrated up to 100% ethanol. Samples were placed in a critical point dryer (EM CPD030, Leica), and 20x1 minute cycles of CO2 exchange were performed. Discs were attached to SEM specimen studs using carbon tape and sputter coated with an 8nm layer of platinum (EM ACE600, Leica). Samples were stored in a desiccator at room temperature prior to SEM acquisition.

SEM images were acquired using an Environmental Scanning Electron Microscope (Quanta 450, FEI).

4.3.3. Pore size fiber alignment and diameter

Sample porosity was quantified using ImageJ. A threshold was applied to a ROI (region of interest), and images were binarized before analyzing the particle size. Four samples were imaged per experimental group. At least four ROIs were selected per group yielding more than 400 pores measured per experimental group.

The diameter of the fibers was measured by selecting a ROI with a single fiber from the SEM images. The ROI was pre-processed using an image-processing algorithm developed by D.A. Antonia et al. [33] with MATLAB (The MathWorks). Briefly, the algorithm increases the contrast using image equalization, reduces the noise while preserving structure edges using three by three median filtering, and separates the outer fiber network from the

background with a global histogram threshold using Otsu's method.[34] The pre-processed images were then analyzed using Image J by overlaying the original region of interest of the SEM image with the pre-processed image obtained in MATLAB to verify the accuracy of the fiber edges after binarization and were adjusted manually if necessary. The overlay was then removed. Finally, after proper calibration of the scale, the fiber diameter was measured by drawing a line across the fiber using the plot profile command. More than 40 fibers were measured per experimental group.

Fiber orientation and alignment were quantified by vectorizing the SEM images using Inkscape. The vectorized and original images were overlapped in Image J to verify the accuracy of the fiber edges. The images were then cropped in 2x2, 3x3, and 4x4, depending on the resolution, and the final images were analyzed using the Orientation J plugin. The dominant direction command in Orientation J returns the dominant fiber orientation and the alignment as a coherency value. The prevailing direction is in degrees (°) with values between -90° to 90°.[35] The coherency is a value between 0 and 1 measuring the anisotropic properties of the region of interest. A coherency of 1 indicates that the structure has a dominant direction and a coherency of 0 indicates that the network is isotropic with no preferred direction of alignment.[35] Four samples were imaged per experimental group. From the data obtained more than 20 ROI were measured for each group.

4.3.4. 2D cell culture and lentiviral transduction

An immortalized human head and neck cancer cell line derived from the base of the tongue (UM-SCC-38)[36] and immortalized human vocal fold fibroblasts (A8-HVFFs)[37] were used for this study. Stably transduced RFP-expressing UM-SCC-38 (RFP-UM-SCC-38) was generated to enable long-term, non-invasive cell tracking in the 3D bioprinted cultures. Membrane-targeting monomeric RFP (Addgene plasmid # 32604) was cloned into a pHIV-blasticidin lentiviral vector. pCAG:myr-mRFP1 was a gift from Anna-Katerina Hadjantonakis of the Memorial Sloan Kettering Cancer Center.[38] Engineered lentivirus bearing the above-mentioned vector was packaged in 293T cells and used to generate a UM-SCC-38 cell line that expresses RFP. Cells were infected with the engineered lentivirus in media supplemented with polybrene (8 μg/mL) for 24h. Cells with stable RFP expression were selected via media supplementation of selection antibiotic blasticidin (Invitrogen) at 6 μg/mL for two weeks. Desired RFP expression level in the final RFP-UM-SCC-38 cell line was selected via fluorescence-activated cell sorting (FACS) and validated via fluorescence.

Non-transduced cells were cultured in DMEM with 10% fetal bovine serum, 1% Penicillin -Streptomycin, and 1% non-essential amino acids. Media and supplements were purchased from Wisent Bio Products. RFP-UM-SCC-38 used the same media formulation with the addition of blasticidin to maintain homogeneity and persistence of RFP transgene expression. Cells were cultured in traditional 2D conditions (37°C and 5% Co_2) until they reached 85% confluency and passaged using trypsin-EDTA (Wisent Bio Products) to disrupt cell attachments.

4.3.5. Fabrication and culture of 3D bioprinted models

Cells were encapsulated in $A_{1.5}G_5$dECMT at a final concentration of 10 million cells per ml. For the co-culture experiments, a 2:1 ratio of HVFFs:UM-SCC38 was used. Before encapsulation, a syringe with $A_{1.5}G_5$dECMT was placed in a 37°C water bath for at least 30 minutes to liquefy the gelatin in the composite bioink. Cells cultured in 2D conditions were detached using trypsin-EDTA (Wisent Bio Products), counted, and centrifuged. The cell pellet was resuspended in media accounting for less than 1% of the total volume, and the warm bioink was loaded into a 3cc 3D printer-compatible cartridge. The cells were pipetted into the warm bioink and mechanically mixed until evenly distributed. The cartridge was centrifuged at 200g for 2 minutes to remove air bubbles and later incubated for 15 minutes at room temperature to allow the gelation of the gelatin in the bioink to occur. Discs of 5mm diameter and 500µm height were bioprinted using a Bioscaffolder 3.1 (GeSiM). A 22 G conical tip (Nordson) was used to fabricate the discs at room temperature (24°C) with a pressure of 45 ± 10 kPa and a printing speed of 10 ± 2 mm/s. After printing, samples were crosslinked with a 100 mM aqueous solution of calcium chloride for 3 minutes. Samples were rinsed with PBS-1X, placed in culture dishes, and immersed in DMEM with 10% fetal bovine serum, 1% Penicillin -Streptomycin, and 1% non-essential amino acids. Cell media was changed every 3-4 days depending on the experiment. Cell-free $A_{1.5}G_5$dECMT discs were printed as controls.

4.3.6. Confocal microscopy

RFP-transduced UM-SCC-38 and non-fluorescent HVFFs were used to observe cell development over time. Experimental groups included monocultures of HVFFs, UM-SCC-38, and the co-culture 2:1, HVFF: UM-SCC-38. Prior imaging samples were

immersed in Calcein-AM (Invitrogen) and Hoechst 33342 (Invitrogen) in DPBS-1X at a final concentration of 2µM and 18 mM respectively and incubated at 37°C for 30 minutes, covered from the light. Samples were washed with DPBS-1X and imaged while encapsulated in a humidity chamber set to 37°C and 5% CO_2. Microscopy was acquired with a Nikon A1+ confocal microscope capturing the Z-stack (5µm step size). During analysis, cells with double positive signal were considered cancer cells, and cells only positive with Calcein-AM were considered fibroblasts. All image analysis was performed in ImageJ[39] using three discs per time point and per experimental group (n = 3).

4.3.7. Collagen quantification

Sircol collagen assay (S1000, Biocolor) was used to quantify collagen over time. 3D printed models were harvested every three days and frozen at -80°C until ready to use. We used the manufacturer's protocol with some modifications. We followed the acid-pepsin protocol provided by the company to extract the soluble collagen from the samples. Due to the nature of our samples, we added 100 µl of a 55 mM trisodium citrate to decrosslink the alginate in the models, increasing the surface area for collagen extraction. Then, we performed the suggested collagen concentration protocol and the Sircol Assay. Samples were plated in a 96-well plate, and absorbance was measured at 555 nm. Experimental groups included HVFFs, UM-SCC-38, and the co-culture 2:1, HVFF: UM-SCC-38 at a final concentration of 10 million cells per ml and cell-free $A_{1.5}G_5$dECMT. Data were plotted using JMP Pro 16 (JMP), and the cubic spline method was used for smoothing the data with a λ of 0.033.

4.3.8. Matrix metalloproteinases (MMPs) quantification

Samples were bioprinted, ionically crosslinked, and cultured under standard conditions (37°C, 5% CO_2) for the duration of the experiment. Media was changed every 3 days. Three-day old media was harvested, centrifuged at 400g for 15 minutes to remove cellular debris and supernatant was frozen at -80°C until ready to use. The multiplexing analysis was performed using the Luminex™ 200 system (Luminex) by Eve Technologies Corp. (Calgary, Alberta). Thirteen markers were simultaneously measured in the samples using Eve Technologies' Human MMP/TIMP 13-Plex Discovery Assay®, which consists of two separate kits; one 9 plex and one 4 plex (R&D Systems, Inc.) according to the manufacturer's protocol. The 9-plex consisted of MMP-1, MMP-2, MMP-3, MMP-7, MMP-8, MMP-9, MMP-10, MMP-12 and MMP-13. The 4-Plex consisted of TIMP-1, TIMP-2, TIMP-3, and TIMP-4. Assay sensitivities of these markers range from 0.28 – 253 pg/mL for the 13-plex. Individual analyte sensitivity values are available in the product datasheet for the 4-Plex and by building the panel on the R&D Systems Magnetic Luminex Performance product page for the 9-Plex. At least six samples per experimental group were measured.

4.3.9. Statistical analysis

Data are presented as the mean ± standard deviation (SD). Data analysis was conducted using GraphPad Prism 8 software (GraphPad Software), Matlab, and JMP Pro 16 (JMP). Image analysis was performed using ImageJ (Fiji),[39], and Matlab. A two-tailed t-test ($P<0.05$) was used to compare the two experimental groups for pore size, fiber orientation, and diameter. One-way analysis of variance (ANOVA) was performed on the spheroid diameter, MMPs, and collagen quantification data, followed by post hoc Tukey's

test to determine differences between groups. The statistical significance of data was calculated at 95% ($P < 0.05$) confidence intervals. GP: 0.1234(ns), 0.0332(*), 0.0021(**), 0.0002(***), <0.0001(****)

4.4. Results

4.4.1. Hydrogel topography and characterization

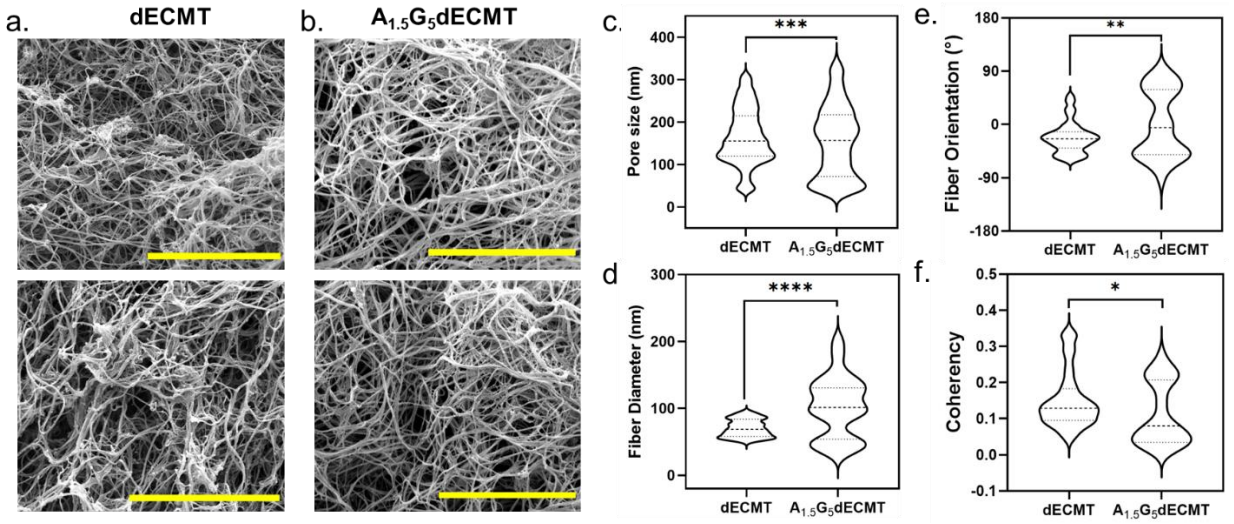

Fig. 1: Topological Characterization of dECMT and $A_{1.5}G_5$dECMT. *Scanning electron microscopy images of Pt coated column a. dECMT and column b. $A_{1.5}G_5$dECMT. Quantification of c. pore size, d. fiber diameter, e. fiber orientation, and e. coherency. Scale bar: 5μm.*

We previously developed and characterized a composite bioink ($A_{1.5}G_5$dECMT) composed of alginate, gelatin, and dECM derived from porcine tongue.[28] This blend has a comparable Young's modulus to a HNSCC tumor xenograft.[28] Here, we further characterize this material by looking into the topography using scanning electron microscopy and comparing it with the pure dECMT hydrogel (Fig. 1). We are interested in determining the topographical differences between these two materials. Scanning

electron microscopy (SEM) enabled the visualization of randomly interwoven fibers that have been previously observed in other dECM hydrogels and characterized as a self-assembled network of mainly collagen fibrils (Fig.1a).[23,27] There is a significant difference in pore size, fiber diameter, coherence, and fiber orientation when comparing the pure dECMT hydrogel and $A_{1.5}G_5$dECMT (Fig. 1c-f). The reinforcements used to enhance the dECMT hydrogel changed the topography of the constructs making them more heterogenous.

Pore size mean values have been shown to decrease when the concentration of dECM is increased in the sample.[40] For dECMT and $A_{1.5}G_5$dECMT the average pore size is 165.9±65.7nm and 153.3±84.3nm, respectively (Fig. 1c). Both experimental groups are skewed to the right 0.25 and 0.28, respectively. The geometric means of dECMT and $A_{1.5}G_5$dECMT are 151.2nm and 126.9nm, respectively. Examples of mean pore size for dECM hydrogels are 112nm for small intestinal submucosa (SIS) gels [23] and 152-670 nm for brain, depending on the dECM concentration,[40] etc.[41] By looking at the frequency distribution; we can determine that 48% of the pores in the dECM sample are between 100-160nm. For $A_{1.5}G_5$dECMT, there are two regions to highlight. 31.2% of the pores are between 1-80nm, and 38% are between 140-220nm. We can attribute the differences in porosity to the presence of additional components in the bioink blend group. Alginate and gelatin occupy space within the dECM fiber network, causing a decrease in pore size.

Fiber diameter quantification shows a significant difference between samples (Fig. 1d). dECMT and $A_{1.5}G_5$dECMT have mean values of 70.3±13nm and 102.6±44.9nm, respectively. They present a right skewness of 0.28 and 0.2, respectively. The geometric means of dECMT and $A_{1.5}G_5$dECMT are 69.1nm and 91.9nm. For the dECMT group, 100%

of the measurements are between 50-100nm. For $A_{1.5}G_5$dECMT, we observe two regions in the frequency distribution. 28.6% of the measurements are between 30-50nm, and 59.2% of the measurements are between 90-140nm. Our dECM data resemble to measurements previously reported.[42,43] The mean diameter of collagen fibrils can range between 40-80nm in mammals, but they can measure up to 500nm.[42,43] Specifically for dECM hydrogels, an average fiber diameter of 92-112nm for myocardial matrices,[44] 74nm for sub intestinal submucosa matrices,[23] 130-140nm for brain matrices[40] has been measured.

Fiber orientation is shown in a -90° to +90°range (Fig 1e). For dECMT, the mean value is -22.1±26.4° with 80% of the measurements showing a preferential orientation between -10° to -60°. For $A_{1.5}G_5$dECMT, 44% of the measurements show an orientation between -30° and -60°. However, 36% of the population shows the opposite orientation preference, between 50° and 80°. These results show that dECMT has a more consistent alignment across different samples and regions when compared to $A_{1.5}G_5$dECMT. The bioink shows two groups with opposite orientations, suggesting that this material has a more heterogenous alignment.

The coherence values are a representation of the isotropy of the samples. If the values are close to 1, the region of interest has a dominant orientation. However, if the values tend to 0, the image is isotropic. Coherence values are 0.15±0.1 for dECMT and 0.11±0.1 for $A_{1.5}G_5$dECMT, indicate the bioink samples are more isotropic (Fig. 1f). The fiber orientation data paired with the coherency values show a higher organization in dECMT samples characterized by consistent fiber alignment and higher coherency values. Overall, both matrices have a high degree of isotropy, which has also been observed in other

tissues.[45] However, when comparing both samples, the decrease in organization observed in $A_{1.5}G_5$dECMT can be mainly attributed to the incorporation of reinforcement materials. Alginate and gelatin chains are in contact with the dECMT. Changes in fiber network formation are expected when additional materials are incorporated. However, all measurements are in the same order of magnitude, demonstrating that abrupt topographical changes in the matrix did not occur when providing mechanical stability to the dECMT.

4.4.2. 3D Co-culture fabrication and spheroid development

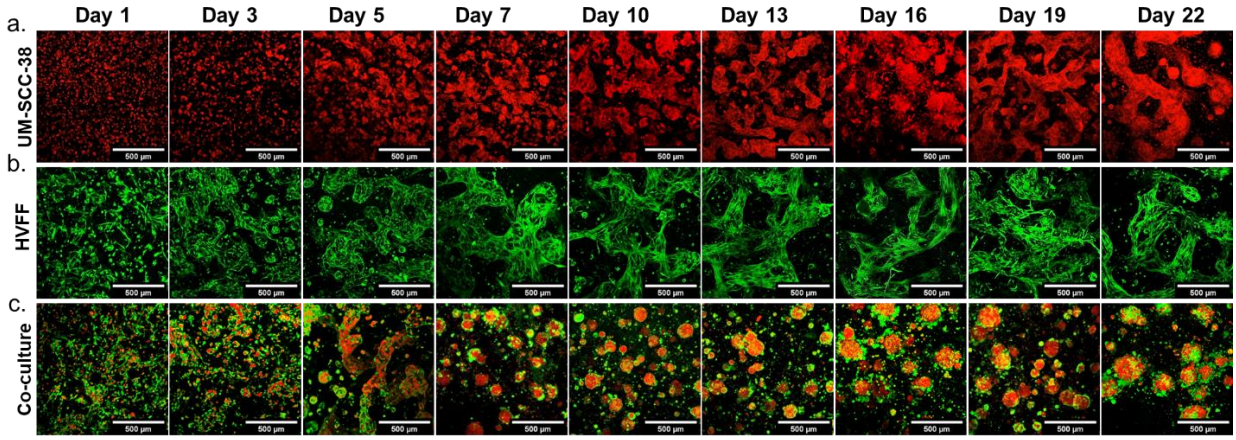

Fig. 2: 3D bioprinted cultures of cells encapsulated in $A_{1.5}G_5$dECMT. *Cells were encapsulated in $A_{1.5}G_5$dECMT and bioprinted into discs with 5mm diameter and 500µm height. a. Transduced RFP-UM-SCC-38. b. HVFFs stained with Calcein-AM c. 2:1 Co-culture of HVFF: RFP-UM-SCC-38. Red: UM-SCC-38, Green: HVFF. Scalebar 500µm. Z-stack maximum intensity projection.*

3D printed constructs, after crosslinked, were immersed in cell media, and cultured for 22 days. Sample immersion allows nutrient-waste exchange to happen around the entire disc. This behavior is challenging to replicate with 3D cultures in traditional well plates since the media is in contact with the sample only from the top. Monocultures of UM-SCC-38 or HVFF encapsulated at a final concentration of 10 million cells/ml were

fabricated as controls to observe cell development over time. UM-SCC-38 culture is characterized by forming spheroids that grow up to Day 22 (Fig. 2a). This behavior has been previously reported.[28] HVFF culture shows a spindle morphology which has been previously reported[37] (Fig. 2b).

Co-cultures constituted by a 2:1 ratio of HVFF: UM-SCC-38 with a final concentration of 10 million cells/ml were fabricated with the same dimensions as the monocultures. Co-cultures start as single cells, but the formation of spheroids is observed by day 7. UM-SCC-38s aggregate in the center while HVFFs wrap the cancer cells (Fig. 2c). Representative high-magnification images are presented in Fig. 3a-b. This cellular arrangement corresponds to what is observed in the tumor microenvironment *in-vivo*. Neoplastic cells are surrounded by stromal cells that promote cancer development, progression, and metastasis.[3] Qualitative SEM images of these experimental groups are presented in Fig S1. the co-culture group, fibroblasts present both, round and spindle-like morphologies which have been previously reported in cancer-fibroblast co-cultures encapsulated in collagen matrices.[46]

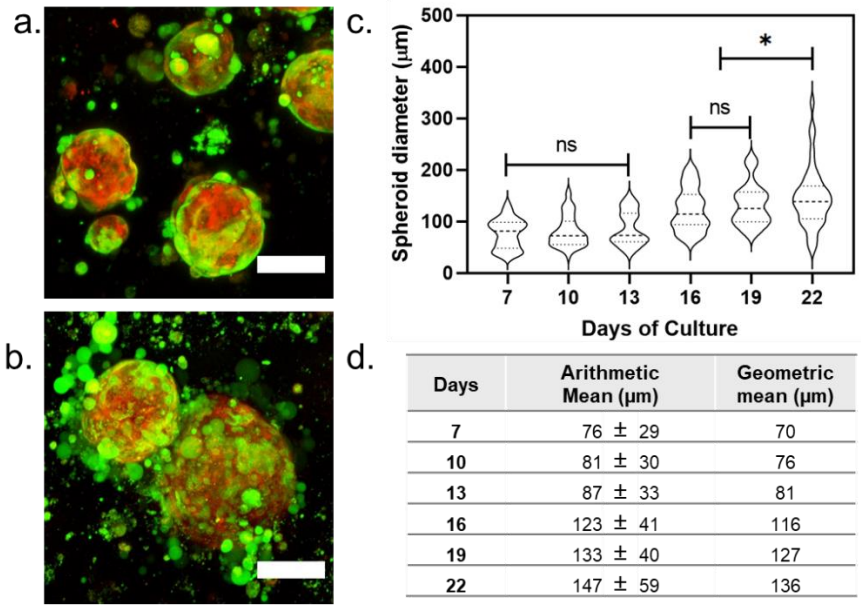

Days	Arithmetic Mean (µm)	Geometric mean (µm)
7	76 ± 29	70
10	81 ± 30	76
13	87 ± 33	81
16	123 ± 41	116
19	133 ± 40	127
22	147 ± 59	136

Fig. 3: Spheroid morphology and diameter quantification through time. *Representative images of spheroids formed in heterogenous models at a. day 13 and b. day 16 of culture. UM-SCC-38: Red, HVFF: Green. Scalebar 100µm Z-stack maximum intensity projection. c. Spheroid diameter from day 7 to day 22 of culture n=35. d. Spheroid diameter arithmetic and geometric means. Cross section images can be found in Fig. S2*

Spheroid organization is consistently observed for up to 22 days. Since the observation of spheroid formation (day 7). Diameter quantification is shown in Fig. 3c. Figure 3d shows the arithmetic and geometric means. There is no significant difference in spheroid size between days 7, 10, and 13. However, spheroids significantly increase in size by day 16 and maintain a similar diameter on day 19. The diameter continues to grow by day 22. The co-culture results show a consistent organizational development through time that is not observed in the monoculture group

4.4.3. Matrix metalloproteinases (MMPs) analysis

Changes in the presence of relevant MMPs and TIMPs are observed over time in all experimental groups (Fig. S3). HVFF monocultures show higher levels of MMP-1, MMP-2, MMP-3, MMP-12, and TIMP-2 compared to the co-culture and UM-SCC-38 monoculture at day 4. In Figure 4a, the protein profile for both HVFF and co-culture on day 4 is highlighted with a dashed yellow outline. Similarities in expression levels of MMP-1, MMP-2, MMP-3, MMP-12, MMP-13, and TIMP-2, TIMP4 are observed. Both experimental groups were fabricated with a final concentration of 10 million cells per ml. However, lower fibroblast related MMPs are expected in the co-culture group since, at day 0, the fibroblasts corresponded to 2/3 of the total population and cancer cells to 1/3. Over time, the co-culture profile diverges from the HVFF monoculture and presents MMP levels similar to the ones observed in the UM-SCC-38 monoculture. We attribute the lower MMP levels to the presence of fibroblasts and UM-SCC-38 in this group. TIMP-1, a glycoprotein that has been associated with poor prognosis in cancer,[11] presents increased levels between day 4 and day 10 in the HVFF monoculture and co-culture groups.

MMP-9 and MMP-10 are highlighted in this study since these molecules have been linked with the progression and invasiveness of HNSCC. [47,48] MMP-9 levels are the highest in UM-SCC-38 across all timepoints. These results are expected since these cancer cells are cataloged as moderately well-differentiated squamous cell carcinoma.[49]

A significant increase of MMP-9 and MMP-10 levels are observed in both UM-SCC-38 and UM-SCC-38 /HVFF co-culture groups between day 4 and day 10 (Fig. S3-S4). These timescales, when compared with the confocal images presented in Figure 2, coincide with the transition from individual cells to spheroids in the co-culture group. The co-culture

group has no significant changes in MMP-9 starting day 10. However, both monocultures continue changing their MMP-9 levels throughout the 22 days of culture (Fig. S4). MMP-10 levels remain stable for all groups from day 16 onwards (Fig. S4).

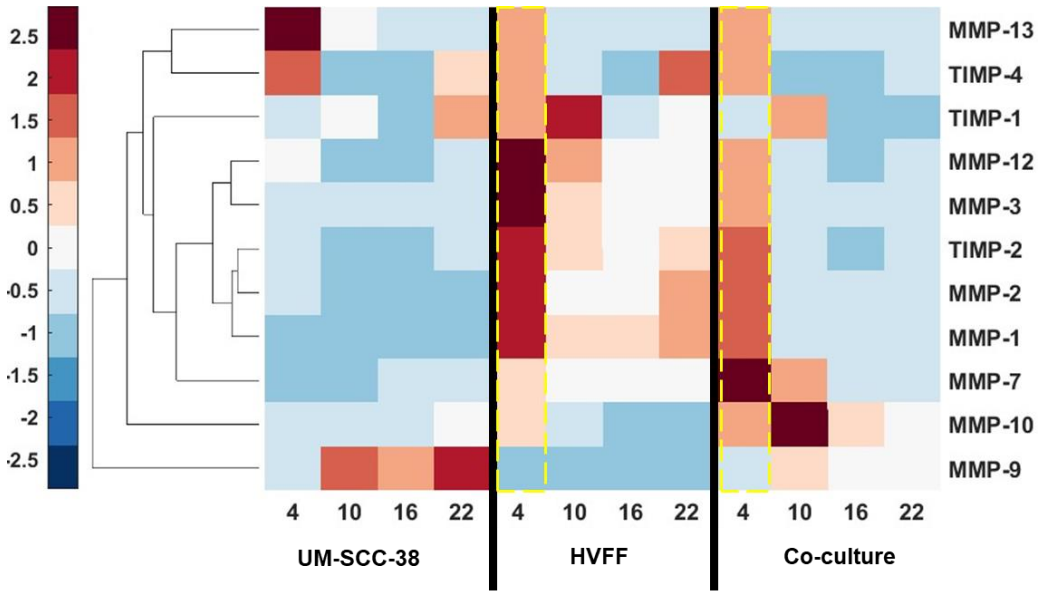

Fig 4. Matrix metalloproteinases (MMPs) and tissue inhibitors of metalloproteinases (TIMPs) quantification through time. *a. Heatmap showing z-score values of MMPs and TIMPs present in cell media through time for UM-SCC-38 and HVFF monocultures and a co-culture of 2:1 HVFF: UM-SCC38.*

Figure 5 compares the MMP levels of all experimental groups by day. No significant difference in MMP-9 levels is observed at day 4 between the co-culture and the UM-SCC-38 monoculture. However, for the following time points, the UM-SCC-38 group consistently presented the highest levels of MMP-9, followed by the co-culture. The lowest levels of MMP-9 were always quantified in the HVFF group. There is a significant difference in MMP-9 for all groups starting day 10.

No significant difference in MMP-10 is observed at day 4 between the co-culture and the HVFF group. However, a decrease in MMP-10 occurs as the HVFF monoculture develops. MMP-10 is significantly higher across all time points in the co-culture group compared to the monocultures. This can indicate that the heterogenous culture promotes the production of MMP-10. On day 10, the co-culture MMP-10 levels are five times higher than the monocultures. Overall, these results show significant differences in the co-culture showing the importance of recapitulating the heterogeneity in *in-vitro* models for a more biomimetic scenario.

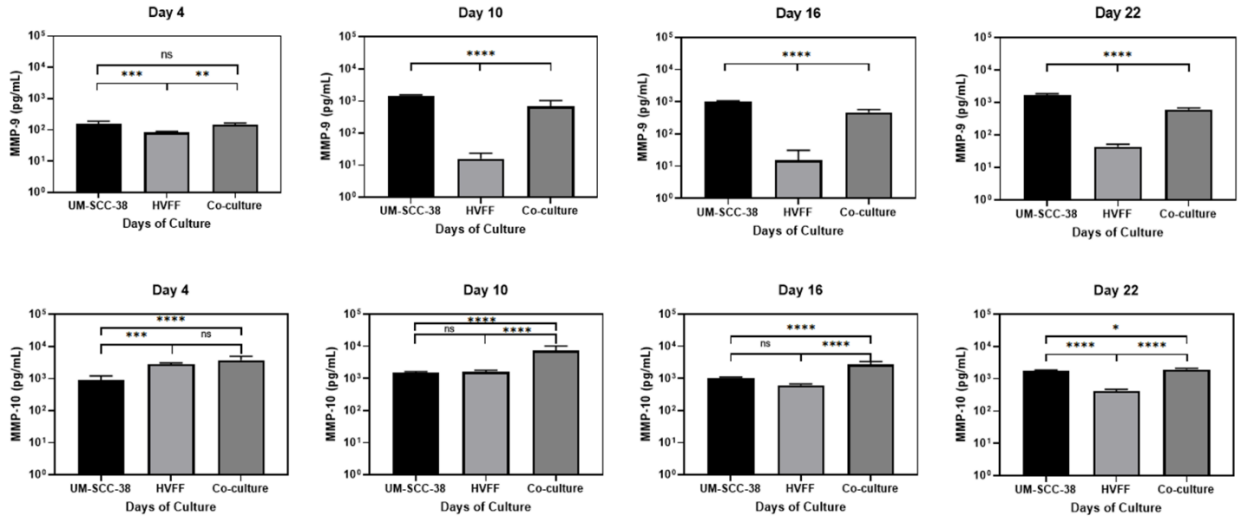

Fig. 5: Matrix Metalloproteinases 9 and 10 levels through time

a. MMP-9 and b. MMP-10 levels of HVFF and UM-SCC-38 monocultures, and co-culture models at days 4, 10, 16, and 22. Logarithmic y scale n=3. One-way ANOVA followed by post hoc Tukey's test ($P < 0.05$).

4.4.4. Collagen quantification in 3D models over time

Sircol soluble collagen assay was performed for all groups, including the bioink in culture without cells (Fig. 6). We chose this assay to demonstrate the compatibility of our models

with traditionally used ECM quantification techniques. Statistical analysis shows no significant difference between experimental groups on days 1, 4, and 7. However, minor differences between the UM-SCC-38 group and the acellular bioink have been observed since day 10. The co-culture group becomes significantly different from the bioink group starting on day 16 (Fig. S5). Soluble collagen levels are maintained throughout the 22 days of culture in the HVFF and bioink groups. Significant changes are observed over time in the co-culture and UM-SCC-38 groups. All groups show comparable soluble collagen levels from day 1 and 7. However, a significant increase in soluble collagen is present in the UM-SCC-38 culture at days 10 and 13 compared to the other experimental groups. From day 16 onwards, the co-culture levels remain significantly higher than the cell-free bioink group (Fig.6, Fig S5).

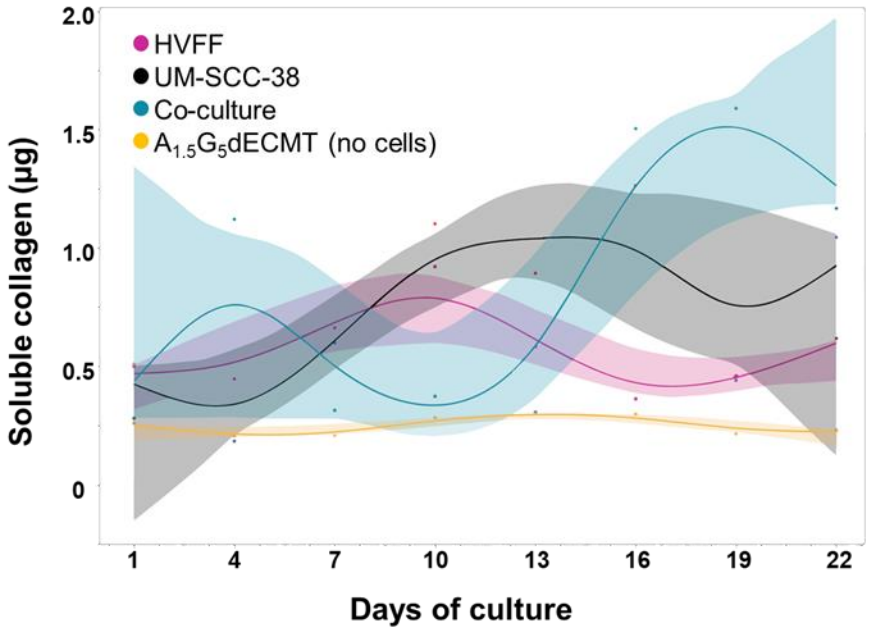

Fig. 6: Soluble collagen in 3D cultures over time. *Cubic spline smoothing (continuous lines) and 95% confidence intervals (shading).*

4.5. Discussion

In cancer, stromal components, cell-cell interactions, and cell-ECM interactions play a pivotal role in tumor development and progression.[50] For this reason, there is a pressing need for clinically relevant 3D *in-vitro* models. We need models that can recapitulate the physical and biochemical characteristics which drive and control cancer progression.[5] These bioengineering models provide a new window to understand molecular mechanisms and find and test effective therapies. The ECM is one of the primary actuators in the stroma.[5] Hence, using ECM-containing materials to create *in-vitro* models is appealing for their biomimetic nature. dECM hydrogels have been successfully used in tissue engineering applications and to re-create healthy and diseased tissues *in-vitro*.[21]

Here, we used a bioink composite containing a dECM hydrogel derived from porcine tongue (dECMT) reinforced with alginate and gelatin to fabricate a heterogenous HNSCC model that contains stromal and cancer cells. This blend has comparable mechanical properties to *in-vivo* tumors and has been previously used to manufacture monocultures of HNSCC cells with high viability.[28] Additionally, this bioink blend promotes spheroid formation in HNSCC cancer cells.[28] Behavior that is not observed in pure dECMT.[28]

In the topographical characterization of the pure dECMT and $A_{1.5}G_5$dECMT, we observed fibers previously reported as a self-assembled collagen network.[27] The dECM architecture has been reported as significant since it can allow cell-matrix interactions via integrins that are key for cell proliferation and migration.[44] Differences in pore size between our samples show that the reinforcements in $A_{1.5}G_5$dECMT occupy space in the matrix, making the pore size of the composite smaller. However, measurements for both groups

are in the same order of magnitude and within the ranges reported for dECM hydrogels from other tissues. [23,40,41] The mean fiber diameter in dECMT is within what other studies have reported. [23,42-44] However, the composite bioink has a higher mean fiber diameter suggesting that the incorporation of the rheological reinforcements is the reason for the difference. Since cells can interact with the dECMT, we expect to see changes over time as they remodel their environment. The significant changes in fiber alignment and decrease in coherency observed in $A_{1.5}G_5$dECMT when compared to pure dECMT demonstrate that the presence of alginate and gelatin influence the orientation and organization of the dECMT network. However, both samples can be considered isotropic which could be beneficial to replicate the ECM heterogeneity observed in tumors. Additionally, electrostatic charges are known to be present in all constituents and can heavily influence their arrangement in a composite blend.[51-53]

In-vivo, tumor-associated collagen signatures (TACS) have been categorized from highly isotropic (TACS-1) to highly aligned collagen fibers (TACS-3).[54] TACs-3 has been correlated with progression and metastasis.[54] Our materials resemble to TACS-1 since the coherency values are close to zero (dECMT: 0.15±0.1 $A_{1.5}G_5$dECMT : 0.11±0.1). We hypothesize that if an increase in alignment is present in our material during cell culture it could further indicate matrix remodelling increasing the TACS category to a more developed cancer model.

The stromal content in tumours has been shown to be a good predictor of patient prognosis in solid tumors.[55] Hence, tumor-stroma ratio has been proposed as a valuable feature to predict patient outcome in head and neck cancer.[56,57] Patients with stroma-rich (>50%) tumors had worse disease-free survival and higher mortality when compared to

patients with stroma-poor (<50%) tumors.[58] In this study, we used a 2:1 ratio of stomal cells (HVFFs):HNSCC cancer cells (UM-SCC-38) to mimic the in-vivo proportions of a stromal-rich tumor. We encapsulated UM-SCC-38 and HVFF cells in the bioink and 3D-printed monocultures or co-cultures. Cell attachment and proliferation are observed in all groups. However, architecturally relevant organoid regeneration is heavily promoted in the co-culture. It has been shown that fibroblast-cancer cell cultures have interactions that promote reciprocal activation in growth rate, ECM expression, etc.[59] Tumor spheres surrounded by fibroblasts are observed since day 7 of culture and continue to grow, reaching a mature and stable state by day 22. This organizational development can be attributed to the crosstalk between the two cell types, which is non-existent in the monoculture groups.[60] This architecture commonly observed in cancer *in-vivo* indicates that this heterogenous model has biomimetic characteristics and can provide more accurate results than traditional 2D monocultures. Studies done in fibroblasts cultured in 3D collagen matrices show diverse morphologies from highly "activated" to "quiescent" phenotypes.[61] Fibroblast spindle morphology in collagen co-cultures has been linked to higher invasion trajectories which indicate cell motility.[46] While round morphology, present in fibroblasts at rest, has been linked to low proliferation, low motility, and low ECM deposition.[61,62] We observed both, spindle and round morphologies in fibroblasts co-cultured with cancer cells. These behaviors have been previously reported in 3D in vitro co-cultures of HNSCC and fibroblasts.[46] Understanding of fibroblast morphology in 3D environments in-vitro and their behavior during neoplasia is still in development.[61,63] We foresee our model as a tool that could be used to study the synergies between fibroblasts and the tumor milieu in a three-dimensional and biologically relevant setting.

MMP and TIMP analysis for all experimental groups shows similar MMP and TIMP signatures observed at the beginning of the culture between the co-culture and the HVFF monoculture, indicating HVFF secretions dominate the co-culture behavior at early stages. However, at the endpoint (day 22), the co-culture signature resembles the UM-SCC-38 monoculture indicating that the cancer cells dominate the co-culture towards the end. This staged cell domination can be attributed to an environment adaptation at early points of the culture to allow tumor spheroid formation to dominate after. In the early stages of cancer, fibroblasts promote tissue repair, leading to TME remodeling.[64] As cancer cells develop, cancer-associated fibroblasts (CAFs) later switch to tumor promoters since CAF-secreted growth factors are used by cancer cells in their survival and proliferation.[64] A specific tipping point where the shift happens is challenging to identify, but a gradual pro-tumorigenic behavior may be observed.[64]

MMP-9 and MMP-10 are highlighted in this study since they are both remodeling indicators. They have been deemed responsible for promoting the invasion and metastasis of cancer cells in HNSCC.[47,48] MMP-9 and -10 levels increase by day 10 coinciding with spheroid formation observed in the confocal microscopy assay. At day 10, the MMP-10 levels in the co-culture were five times higher than in the monocultures. This behavior shows that an increase in MMP-10 can be attributed to the presence of both cells in the same culture and highlights the importance of including the stromal component in *in-vitro* cancer models. TIMP-1 levels also show an increase at day 10 in the fibroblast monoculture and co-culture groups. TIMP-1 has been proposed as a prognostic biomarker for multiple cancers and it is known to be highly expressed in HNSCC.[11] This molecule is expressed by fibroblasts and tumours cells and has been shown

to inhibit apoptosis and promote metastatic behaviour.[65] TIMP-1 and MMPs as targets for cancer treatment is an avenue that is still in development, but further testing is required to assess their effectiveness. The morphological changes in MMP levels in the medium suggest that matrix remodeling events are taking place in the co-culture model.[66,67] The presence of metalloproteinases during cancer progression is a well-stablished phenomenon that is closely associated with ECM remodeling.[66] Therefore, the observed differences in the co-culture model against the monoculture controls could be an indicative of matrix modifications driven by cancer cells and fibroblasts, which may have important implications for understanding cancer development and identifying therapeutic targets. Nevertheless, future research is necessary to investigate this hypothesis and determine the significance of these events for clinical or drug development applications. This experiment shows the capability of measuring secretomic analytes longitudinally allowing the monitoring of the samples in a non-destructive manner which is challenging to achieve with *in-vivo* models.

Tumor- and stroma-derived ECM components are present in the TME.[68] Soluble collagen can be secreted by cancer cells.[68] However, HVFFs have also been reported to be capable of secreting collagen.[37] After day 16, the co-culture model shows soluble collagen levels significantly different from the cell-free bioink. An increase in collagen levels can indicate matrix remodeling and tumor progression.[69] Increase levels of collagen are associated with higher migration, invasion, and poor prognosis in oral squamous cell carcinomas.[70] Soluble collagen can also be derived from the matrix. MMP-9 can cleave mature collagen into soluble collagen as part of their ECM remodelling mechanisms.[71,72] This study highlights the compatibility of our constructs with assays such as Sircol Assay which can

reveal collagen contents through time. Additional techniques such as second harmonic generation could further support ECM colorimetric assays.[73]

Our model has been proven to create a scenario that shows different behavior to the monoculture groups in cellular morphology, 3D organization, MMP expression, and collagen levels through time. This platform can be used to provide a more realistic representation of the complexity of cancer *in-vitro* and can be complemented further by including other components of the TME, such as immune or endothelial components. Using 3D bioprinting allows the fabrication of consistent models in a semi-high-throughput matter which can be used to test multiple conditions and scenarios in parallel. This technique has micron level resolution, and it removes the user error ensuring models are comparable in dimensions and cell density which is particularly challenging to achieve with manual fabrication techniques.[32] This is of high importance when using the same model for different conditions to ensure the fabrication method is not the reason for changes in sample development and results obtained. 3D bioprinting is also capable of extruding a broad range of viscosities (30 mPa s^{-1} to >6 × 10^7 mPa s^{-1}) which is challenging for other extrusion techniques such as liquid handlers.[31] It also allows the fabrication of constructs with high cell densities (<10^6 cells/ml) which can bring us closer to cell densities found in tissues.[31,74] Here, we show it is possible to non-destructively monitor these models through time. To evaluate how the same model is changing depending on stimuli or conditions without sacrificing the model is valuable contribution since it provides a new window of opportunities to study potential targets for the disease of study. Applications for *in-vitro* models include the identification of relevant cancer biomarkers and testing the efficacy of new treatments. Here, we used HNSCC as the

disease of study, but these constructs can be tailored to represent other neoplastic diseases. It would be interesting to create stage-related tumors with patient-derived cells to closely match more biological features and potentially use this technique for personalized medicine. Overall, using 3D *in-vitro* models can help us understand cancer, reduce reliance on traditional animal models and hopefully incorporate them as a standard of validation for new treatments because they recapitulate important variables to study and treat cancer.

4.6. Conclusions

We demonstrated that $A_{1.5}G_5$dECMT is a suitable bioink to fabricate heterogenous HNSCC models since it allows the development of several cell types over more than two weeks of culture. We observed significant changes in morphology, MMP expression, suggesting matrix remodelling and crosstalk between the stromal and cancer cells. This *in-vitro* model can be helpful for studying HNSCC's biology or new treatments due to the biomimetic components that permit the replication of crucial variables *in-vivo*. Furthermore, this platform has the potential to be tailored to study other applications and diseases.

Supporting information

Supporting information is included as an appendix.

Acknowledgements

JMK thanks the Natural Science and Engineering Research Council (RGPIN-2020-05692) for funding. JKM thanks FRQNT (288490) for the scholarship. SFT thanks the FRQNT (291010) for the scholarship. ST thanks the Canadian Institutes of Health Research (CIHR grant 119585), Natural Sciences and Engineering Research Council of Canada (NSERC grant 03615), MJW Kim research fund. The authors sincerely thank Susan Thibeault from the University of Wisconsin, Madison for providing the A8 human vocal fold fibroblast cells that were originally isolated, purfied, and characterized by her lab. MLS thanks E. Solymoss, M. Annis, and S. Tabariès for their expertise and assistance in cloning and lentiviral transduction.

Conflicts of interest

There are no conflicts of interest.

References

1 Quail, D. F. & Joyce, J. A. Microenvironmental regulation of tumor progression and metastasis. *Nat Med* **19**, 1423-1437, doi:10.1038/nm.3394 (2013).

2 Joyce, J. A. & Pollard, J. W. Microenvironmental regulation of metastasis. *Nat Rev Cancer* **9**, 239-252, doi:10.1038/nrc2618 (2009).

3 Balkwill, F. R., Capasso, M. & Hagemann, T. The tumor microenvironment at a glance. *Journal of Cell Science* **125**, 5591-5596, doi:10.1242/jcs.116392 (2012).

4 Naba, A. *et al*. The matrisome: in silico definition and in vivo characterization by proteomics of normal and tumor extracellular matrices. *Mol Cell Proteomics* **11**, M111 014647, doi:10.1074/mcp.M111.014647 (2012).

5 Rodrigues, J., Heinrich, M. A., Teixeira, L. M. & Prakash, J. 3D In Vitro Model (R)evolution: Unveiling Tumor-Stroma Interactions. *Trends Cancer* **7**, 249-264, doi:10.1016/j.trecan.2020.10.009 (2021).

6 Eble, J. A. & Niland, S. The extracellular matrix in tumor progression and metastasis. *Clin Exp Metastasis* **36**, 171-198, doi:10.1007/s10585-019-09966-1 (2019).

7 Mohan, V., Das, A. & Sagi, I. Emerging roles of ECM remodeling processes in cancer. *Semin Cancer Biol* **62**, 192-200, doi:10.1016/j.semcancer.2019.09.004 (2020).

8 Ohlund, D., Elyada, E. & Tuveson, D. Fibroblast heterogeneity in the cancer wound. *J Exp Med* **211**, 1503-1523, doi:10.1084/jem.20140692 (2014).

9 Kalluri, R. The biology and function of fibroblasts in cancer. *Nat Rev Cancer* **16**, 582-598, doi:10.1038/nrc.2016.73 (2016).

10 Arpino, V., Brock, M. & Gill, S. E. The role of TIMPs in regulation of extracellular matrix proteolysis. *Matrix Biol* **44-46**, 247-254, doi:10.1016/j.matbio.2015.03.005 (2015).

11 Ma, J. *et al*. Upregulated TIMP-1 correlates with poor prognosis of laryngeal squamous cell carcinoma. *Int J Clin Exp Pathol* **7**, 246-254 (2014).

12 Jiang, Y., Goldberg, I. D. & Shi, Y. E. Complex roles of tissue inhibitors of metalloproteinases in cancer. *Oncogene* **21**, 2245-2252, doi:10.1038/sj.onc.1205291 (2002).

13 Wu, T. & Dai, Y. Tumor microenvironment and therapeutic response. *Cancer Lett* **387**, 61-68, doi:10.1016/j.canlet.2016.01.043 (2017).

14 Grantab, R., Sivananthan, S. & Tannock, I. F. The penetration of anticancer drugs through tumor tissue as a function of cellular adhesion and packing density of tumor cells. *Cancer Res* **66**, 1033-1039, doi:10.1158/0008-5472.CAN-05-3077 (2006).

15 Breslin, S. & O'Driscoll, L. Three-dimensional cell culture: the missing link in drug discovery. *Drug Discov Today* **18**, 240-249, doi:10.1016/j.drudis.2012.10.003 (2013).

16 Liu, X. *et al.* Tumor-on-a-chip: from bioinspired design to biomedical application. *Microsyst Nanoeng* **7**, 50, doi:10.1038/s41378-021-00277-8 (2021).

17 Flores-Torres, S. *et al.* Constructing 3D In Vitro Models of Heterocellular Solid Tumors and Stromal Tissues Using Extrusion-Based Bioprinting. *ACS Biomaterials Science & Engineering*, doi:10.1021/acsbiomaterials.2c00998 (2023).

18 Shimpi, A. A. & Fischbach, C. Engineered ECM models: Opportunities to advance understanding of tumor heterogeneity. *Curr Opin Cell Biol* **72**, 1-9, doi:10.1016/j.ceb.2021.04.001 (2021).

19 Zhang, W., Du, A., Liu, S., Lv, M. & Chen, S. Research progress in decellularized extracellular matrix-derived hydrogels. *Regen Ther* **18**, 88-96, doi:10.1016/j.reth.2021.04.002 (2021).

20 Saldin, L. T., Cramer, M. C., Velankar, S. S., White, L. J. & Badylak, S. F. Extracellular matrix hydrogels from decellularized tissues: Structure and function. *Acta biomaterialia* **49**, 1-15, doi:10.1016/j.actbio.2016.11.068 (2017).

21 Kort-Mascort, J. *et al.* Decellularized ECM hydrogels: prior use considerations, applications, and opportunities in tissue engineering and biofabrication. *Biomater Sci*, doi:10.1039/d2bm01273a (2022).

22 Lin, M. *et al.* Biochemical and biomechanical comparisions of decellularized scaffolds derived from porcine subcutaneous and visceral adipose tissue. *Journal of Tissue Engineering* **10**, 2041731419888168, doi:10.1177/2041731419888168 (2019).

23 Wolf, M. T. *et al.* A hydrogel derived from decellularized dermal extracellular matrix. *Biomaterials* **33**, 7028-7038, doi:10.1016/j.biomaterials.2012.06.051 (2012).

24 Fercana, G. R. *et al.* Perivascular extracellular matrix hydrogels mimic native matrix microarchitecture and promote angiogenesis via basic fibroblast growth factor. *Biomaterials* **123**, 142-154, doi:10.1016/j.biomaterials.2017.01.037 (2017).

25 Huleihel, L. *et al.* Matrix-bound nanovesicles within ECM bioscaffolds. *Sci Adv* **2**, e1600502, doi:10.1126/sciadv.1600502 (2016).

26 O'Neill, J. D. *et al.* Decellularization of human and porcine lung tissues for pulmonary tissue engineering. *Ann Thorac Surg* **96**, 1046-1055; discussion 1055-1046, doi:10.1016/j.athoracsur.2013.04.022 (2013).

27 Freytes, D. O., Martin, J., Velankar, S. S., Lee, A. S. & Badylak, S. F. Preparation and rheological characterization of a gel form of the porcine urinary bladder matrix. *Biomaterials* **29**, 1630-1637, doi:10.1016/j.biomaterials.2007.12.014 (2008).

28 Kort-Mascort, J. *et al.* Decellularized Extracellular Matrix Composite Hydrogel Bioinks for the Development of 3D Bioprinted Head and Neck in Vitro Tumor Models. *ACS Biomaterials Science & Engineering* **7**, 5288-5300, doi:10.1021/acsbiomaterials.1c00812 (2021).

29 Kim, J., Jang, J. & Cho, D. W. Controlling Cancer Cell Behavior by Improving the Stiffness of Gastric Tissue-Decellularized ECM Bioink With Cellulose Nanoparticles. *Front Bioeng Biotechnol* **9**, 605819, doi:10.3389/fbioe.2021.605819 (2021).

30 Beachley, V. *et al.* Extracellular matrix particle-glycosaminoglycan composite hydrogels for regenerative medicine applications. *Journal of Biomedical Materials Research Part A* **106**, 147-159, doi:10.1002/jbm.a.36218 (2018).

31 Murphy, S. V. & Atala, A. 3D bioprinting of tissues and organs. *Nature biotechnology* **32**, 773, doi:10.1038/nbt.2958 (2014).

32 Cui, X. *et al.* Advances in Extrusion 3D Bioprinting: A Focus on Multicomponent Hydrogel-Based Bioinks. *Advanced healthcare materials* **9**, e1901648, doi:10.1002/adhm.201901648 (2020).

33 D'Amore, A., Stella, J. A., Wagner, W. R. & Sacks, M. S. Characterization of the complete fiber network topology of planar fibrous tissues and scaffolds. *Biomaterials* **31**, 5345-5354, doi:https://doi.org/10.1016/j.biomaterials.2010.03.052 (2010).

34 Otsu, N. A Threshold Selection Method from Gray-Level Histograms. *IEEE Transactions on Systems, Man, and Cybernetics* **9**, 62-66, doi:10.1109/TSMC.1979.4310076 (1979).

35 Rezakhaniha, R. *et al.* Experimental investigation of collagen waviness and orientation in the arterial adventitia using confocal laser scanning microscopy. *Biomechanics and Modeling in Mechanobiology* **11**, 461-473, doi:10.1007/s10237-011-0325-z (2012).

36 Brenner, J. C. *et al.* Genotyping of 73 UM-SCC head and neck squamous cell carcinoma cell lines. *Head & neck* **32**, 417-426, doi:10.1002/hed.21198 (2010).

37 Chen, X. & Thibeault, S. L. Novel isolation and biochemical characterization of immortalized fibroblasts for tissue engineering vocal fold lamina propria. *Tissue Eng Part C Methods* **15**, 201-212, doi:10.1089/ten.tec.2008.0390 (2009).

38 Nowotschin, S. & Hadjantonakis, A. K. Use of KikGR a photoconvertible green-to-red fluorescent protein for cell labeling and lineage analysis in ES cells and mouse embryos. *BMC Dev Biol* **9**, 49, doi:10.1186/1471-213X-9-49 (2009).

39 Schindelin, J. *et al.* Fiji: an open-source platform for biological-image analysis. *Nature methods* **9**, 676-682, doi:10.1038/nmeth.2019 (2012).

40 Hong, J. Y. *et al.* Decellularized brain matrix enhances macrophage polarization and functional improvements in rat spinal cord injury. *Acta biomaterialia* **101**, 357-371, doi:10.1016/j.actbio.2019.11.012 (2020).

41 Loneker, A. E., Faulk, D. M., Hussey, G. S., D'Amore, A. & Badylak, S. F. Solubilized liver extracellular matrix maintains primary rat hepatocyte phenotype in-vitro. *Journal of biomedical materials research. Part A* **104**, 957-965, doi:10.1002/jbm.a.35636 (2016).

42 Ushiki, T. Collagen fibers, reticular fibers and elastic fibers. A comprehensive understanding from a morphological viewpoint. *Arch Histol Cytol* **65**, 109-126, doi:10.1679/aohc.65.109 (2002).

43 Parry, D. A. D. & Craig, A. S. in *Ultrastructure of the Connective Tissue Matrix* (eds A. Ruggeri & P. M. Motta) 34-64 (Springer US, 1984).

44 Johnson, T. D., Lin, S. Y. & Christman, K. L. Tailoring material properties of a nanofibrous extracellular matrix derived hydrogel. *Nanotechnology* **22**, 494015, doi:10.1088/0957-4484/22/49/494015 (2011).

45 Zvarova, B. *et al.* Residual Detergent Detection Method for Nondestructive Cytocompatibility Evaluation of Decellularized Whole Lung Scaffolds. *Tissue Engineering. Part C, Methods* **22**, 418-428, doi:10.1089/ten.tec.2015.0439 (2016).

46 Chen, Y. Q. *et al.* Fibroblast Promotes Head and Neck Squamous Cell Carcinoma Cell Invasion through Mechanical Barriers in 3D Collagen Microenvironments. *ACS Appl Bio Mater* **3**, 6419-6429, doi:10.1021/acsabm.0c00603 (2020).

47 Yin, P. *et al.* MMP-9 Knockdown Inhibits Oral Squamous Cell Carcinoma Lymph Node Metastasis in the Nude Mouse Tongue-Xenografted Model through the RhoC/Src Pathway. *Anal Cell Pathol (Amst)* **2021**, 6683391, doi:10.1155/2021/6683391 (2021).

48 Deraz, E. M. *et al.* MMP-10/stromelysin-2 promotes invasion of head and neck cancer. *PLoS One* **6**, e25438, doi:10.1371/journal.pone.0025438 (2011).

49 Grénman, R. *et al.* In vitro radiation resistance among cell lines established from patients with squamous cell carcinoma of the head and neck. *Cancer* **67**, 2741-2747, doi:10.1002/1097-0142(19910601)67:11<2741::AID-CNCR2820671105>3.0.CO;2-S (1991).

50 Baghban, R. *et al.* Tumor microenvironment complexity and therapeutic implications at a glance. *Cell Commun Signal* **18**, 59, doi:10.1186/s12964-020-0530-4 (2020).

51 Rehm, B. H. A. *Alginates: Biology and Applications*. (Springer Berlin Heidelberg, 2009).

52 Gresham, R. C. H., Bahney, C. S. & Leach, J. K. Growth factor delivery using extracellular matrix-mimicking substrates for musculoskeletal tissue engineering and repair. *Bioact Mater* **6**, 1945-1956, doi:10.1016/j.bioactmat.2020.12.012 (2021).

53 Deshmukh, K. *et al.* in *Biopolymer Composites in Electronics* (eds K. K. Sadasivuni *et al.*) 27-128 (Elsevier, 2017).

54 Provenzano, P. P. *et al.* Collagen reorganization at the tumor-stromal interface facilitates local invasion. *BMC Med* **4**, 38, doi:10.1186/1741-7015-4-38 (2006).

55 Wu, J., Liang, C., Chen, M. & Su, W. Association between tumor-stroma ratio and prognosis in solid tumor patients: a systematic review and meta-analysis. *Oncotarget* **7**, 68954-68965, doi:10.18632/oncotarget.12135 (2016).

56 Mascitti, M. *et al.* Addition of the tumour-stroma ratio to the 8th edition American Joint Committee on Cancer staging system improves survival prediction for patients with oral tongue squamous cell carcinoma. *Histopathology* **77**, 810-822, doi:10.1111/his.14202 (2020).

57 Almangush, A. *et al.* Clinical significance of tumor-stroma ratio in head and neck cancer: a systematic review and meta-analysis. *BMC Cancer* **21**, 480, doi:10.1186/s12885-021-08222-8 (2021).

58 Almangush, A. *et al.* Prognostic impact of tumour-stroma ratio in early-stage oral tongue cancers. *Histopathology* **72**, 1128-1135, doi:10.1111/his.13481 (2018).

59 Jeong, S. Y., Lee, J. H., Shin, Y., Chung, S. & Kuh, H. J. Co-Culture of Tumor Spheroids and Fibroblasts in a Collagen Matrix-Incorporated Microfluidic Chip Mimics Reciprocal Activation in Solid Tumor Microenvironment. *PLoS One* **11**, e0159013, doi:10.1371/journal.pone.0159013 (2016).

60 Kim, S. A., Lee, E. K. & Kuh, H. J. Co-culture of 3D tumor spheroids with fibroblasts as a model for epithelial-mesenchymal transition in vitro. *Exp Cell Res* **335**, 187-196, doi:10.1016/j.yexcr.2015.05.016 (2015).

61 Woodley, J. P., Lambert, D. W. & Asencio, I. O. Understanding Fibroblast Behavior in 3D Biomaterials. *Tissue engineering. Part B, Reviews* **28**, 569-578, doi:10.1089/ten.TEB.2021.0010 (2022).

62 Grinnell, F. Fibroblasts, myofibroblasts, and wound contraction. *J Cell Biol* **124**, 401-404, doi:10.1083/jcb.124.4.401 (1994).

63 Derynck, R. & Weinberg, R. A. EMT and Cancer: More Than Meets the Eye. *Dev Cell* **49**, 313-316, doi:10.1016/j.devcel.2019.04.026 (2019).

64 LeBleu, V. S. & Kalluri, R. A peek into cancer-associated fibroblasts: origins, functions and translational impact. *Dis Model Mech* **11**, doi:10.1242/dmm.029447 (2018).

65 Lambert, E., Dasse, E., Haye, B. & Petitfrere, E. TIMPs as multifacial proteins. *Crit Rev Oncol Hematol* **49**, 187-198, doi:10.1016/j.critrevonc.2003.09.008 (2004).

66 Winkler, J., Abisoye-Ogunniyan, A., Metcalf, K. J. & Werb, Z. Concepts of extracellular matrix remodelling in tumour progression and metastasis. *Nature communications* **11**, 5120, doi:10.1038/s41467-020-18794-x (2020).

67 Kaushik, N., Kim, S., Suh, Y. & Lee, S. J. Proinvasive extracellular matrix remodeling for tumor progression. *Arch Pharm Res* **42**, 40-47, doi:10.1007/s12272-018-1097-0 (2019).

68 Naba, A., Clauser, K. R., Lamar, J. M., Carr, S. A. & Hynes, R. O. Extracellular matrix signatures of human mammary carcinoma identify novel metastasis promoters. *Elife* **3**, e01308, doi:10.7554/eLife.01308 (2014).

69 Dolor, A. & Szoka, F. C., Jr. Digesting a Path Forward: The Utility of Collagenase Tumor Treatment for Improved Drug Delivery. *Mol Pharm* **15**, 2069-2083, doi:10.1021/acs.molpharmaceut.8b00319 (2018).

70 Li, H. X. *et al.* Expression of alphavbeta6 integrin and collagen fibre in oral squamous cell carcinoma: association with clinical outcomes and prognostic implications. *J Oral Pathol Med* **42**, 547-556, doi:10.1111/jop.12044 (2013).

71 Van den Steen, P. E. *et al.* Biochemistry and molecular biology of gelatinase B or matrix metalloproteinase-9 (MMP-9). *Crit Rev Biochem Mol Biol* **37**, 375-536, doi:10.1080/10409230290771546 (2002).

72 Bigg, H. F., Rowan, A. D., Barker, M. D. & Cawston, T. E. Activity of matrix metalloproteinase-9 against native collagen types I and III. *FEBS J* **274**, 1246-1255, doi:10.1111/j.1742-4658.2007.05669.x (2007).

73 de Andrade Natal, R., Adur, J., Cesar, C. L. & Vassallo, J. Tumor extracellular matrix: lessons from the second-harmonic generation microscopy. *Surgical and Experimental Pathology* **4**, 7, doi:10.1186/s42047-021-00089-0 (2021).

74 McClelland, R. E. *et al.* in *Introduction to Biomedical Engineering (Third Edition)* (eds John D. Enderle & Joseph D. Bronzino) 273-357 (Academic Press, 2012).

5. Discussion

Cancer is a leading cause of death worldwide, and the current lack of effective and targeted treatments remains a major challenge towards reducing mortality and disease management. Head and neck cancer (HNSCC) is a group of cancers in the head and neck region.[34] It is a malignancy associated with human papillomavirus (HPV) type 16,[40] which has an increasing incidence in patients in Europe and North America. [34] In Canada, HNSCC is three times more frequent in men than women.[35] Despite the recent approval of targeted therapies,[44,45] there is a need for practical, reliable, and curative treatments, but limited preclinical models prove their development challenging.

The conventional preclinical models of HNSCC include 2D epithelial cell culture and small animal orthotopic, xenograft, gene-edited models, etc. Critical discoveries into fundamental cellular mechanisms and the development of our current standard-of-care have occurred using these models. Still, the lack of physical and biochemical co-factors originating from cell-cell or cell-matrix interactions in tumor tissue and healthy adjacent tissues limits their capabilities. Here we've developed a model capable of investigating and understanding the role of the tumor microenvironment (TME) capable of untangling the interactions among the diverse populations of cells and the environmentally responsive tumor extracellular matrix. There is a pressing need for biomimetic models that can accurately mimic the TME, specifically by developing patient-representative *in-vitro* models. Non-animal, physiologically representative models are now recognized as alternatives to small animal models by regulators, including the Food and Drug Administration (FDA), which in 2022, passed the FDA Modernization Act 2.0, allowing alternative pre-clinical models to prove drug effectiveness. This act opens the opportunity

for novel technologies, such as extrusion-based bioprinting (EBB), to be used as a drug testing platform.

EBB offers the capability of depositing material onto a surface in a controlled manner and allows the design of multi-material or multi-cellular architectures.[15,16] EBB can fabricate models with high fidelity in a semi-high-throughput way. It has become an important tool in bioengineering since it allows the creation of 3D customized tissue constructs. To best replicate tissues *in-vitro*, cells are cultured using materials that are selected to accurately mimic specific or selected functions of the extracellular matrix (ECM). As cancer progresses, the remodeled ECM plays a crucial role in the stroma.[48] In cancer, ECM stiffness in conjunction with poor vascularization can lead to hypoxic conditions in epithelial cells, causing an increase in hypoxia-inducible factors (HIFs), which promote angiogenesis and ECM remodeling through fibroblast recruitment.[49] It would be valuable to perform studies using our co-culture models in hypoxic conditions to determine differences in spheroid growth and secrotomic data due to the lack of oxygen in their culturing conditions. Deregulated ECM presents relevant issues during treatment. The overproduction of ECM molecules leads to decreased permeability, causing issues with delivering antineoplastic drugs.[50,51] Hence, using ECM materials to create *in-vitro* models is appealing for their capability to better biomimic the tissue conditions than synthetic materials. ECM components have been shown to influence differentiation, cell-cell, and cell-ECM interactions *in-vitro*.[20,21] Specifically, decellularized ECM materials are known to retain biomimetic characteristics of the original tissue and have shown advantages in biomedical applications.[19-21,52]

This thesis develops new methods to generate mechanically-controlled dECM hydrogels and EBB processes to fabricate a cellular heterogenous HNSCC model. The results in the previous section support my hypothesis, which claims that an EBB model incorporating epithelial and stromal cells in co-culture will remodel the microenvironment using mechanisms that occur *in-vivo*. The features in the EBB co-culture model include culture in a 3D architecture, a biomimetic ECM with comparable mechanical properties to HNSCC *in-vivo*, cell-cell and cell-ECM interactions, cancer-stromal cross-talk, and TME architectural arrangement where the stroma surrounds cancer cells.

In HNSCC, the border of the tongue is the most common site for cancer development.[53] The homology of the ECM between porcine and human, and their genome resemblance guided the selection of porcine tongue as the source of decellularized ECM.[54] Acellular ECM derived from porcine has been an FDA-approved material for several implantable products. as porcine liver, dermis, small intestine, and urinary bladder.[55] Additionally, enzymatic and chemical decellularization processes typically yield limited amounts of tissue following isolation, purification, and sterilization, limiting organs or tissues from smaller mammals.

The tissue was processed and cleaned with detergents and nucleases, sterilized with peracetic acid, and solubilized via enzymatic digestion using pepsin. After tissue decellularization and solubilization, the final product (dECMT) is a thermosensitive, highly collagenous gel. Following solubilization, the mechanical properties significantly decreased compared to the tissue before processing due to fragmentation of structural proteins or denaturation during detergent washes and enzymatic treatments. dECM hydrogels contain partially fragmented ECM components cleaved at non-specific sites,

resulting in a weak viscous but highly bioactive gel. For this reason, secondary materials to reinforce the dECM are required to increase the elastic moduli of the material to generate formulations compatible with EBB. Gelatin was added as a stabilizer to native porcine tongue dECM under controlled mole fractions before adding cells. At room temperature, gelatin undergoes a phase change to transition from sol to gel providing the required support to maintain the shape fidelity during extrusion. While these materials can print short-term support of cell culture at 37C the gelatin undergoes dissolution into the media and ultimately weakens the remaining cell-laden gel, limiting its lifecycle to days. To develop a gel that would persist for extended culture periods in the deposited geometry, a tertiary component, alginate, was incorporated into the bioink. Alginate did not affect the mechanical properties abruptly during the 3D structure fabrication. After fabrication, the alginate in the bioink was ionically crosslinked with calcium chloride making it stable for long-term culture under physiological conditions.

Rheological tests show that both the pure dECM hydrogel and the reinforced bioink ($A_{1.5}G_5$dECMT) have shear-thinning properties, which are ideal for EBB since they allow the fabrication of cell-laden structures without excessive shear on cell membranes which would compromise cell viability.[56]

Matrix mechanical properties such as stiffness can change cell physiology, a crucial aspect of tumor progression and cell differentiation.[57,58] Encapsulating cells in an environment with mechanical properties that are not in the same range as the physiological conditions of the tissue of interest can lead to undesired results in cell behavior.[59] For this reason, I tuned the ratio of the bioink constituents by benchmarking it against a HNSCC tumor tissue. The final formulation consisted of a 1.5%w/v of alginate, 5%w/v of gelatin, and

solubilized dECMT at a final protein concentration of 160μg/mL. Indentation tests confirmed that $A_{1.5}G_5$dECMT has a Young's modulus of 397.6±95.86Pa, which is not significantly different from a human HNSCC xenograft in an immunocompromised mouse (361.9±86.51Pa).[60] Rheological quantification showed a 50-fold increase in storage modulus (650.5Pa) in $A_{1.5}G_5$dECMT compared to pure dECMT. These changes in moduli make the bioink compatible with extrusion-based bioprinting while providing a mechanically-relevant matrix to the encapsulated HNSCC cells.

This bioink was used to fabricate cell-laden monocultures of HNSCC models that, over 19 days of culture, exhibited high cell viability and the formation of spheroids. Cell morphology in 3D cultures suggests cell-matrix interactions occurred and can be attributed to the presence of dECMT. HNSCC cell growth can be fitted into a logistic model, which models the cell growth with consideration to carrying capacity and better approximates cell proliferation in complex systems relative to an arithmetic-generated mean value.[61] The population reaches a maximum spheroid area of 3339 μm^2 and 4238 μm^2 for UM-SCC-12 and UM-SCC-38 respectively, and plateaus after day 11. This behavior may occur due to the lack of space within the 3D matrix as proliferating cells and spheroid development occupy an increasing volume in the model. Lowering the initial cell seeding density overcomes this limitation, but sparse cell populations delay the formation of 3D structures. Spheroids maintain keratin expression after 19 days of culture, demonstrating that the moderately differentiated characteristics of the cell lines are maintained. Keratin expression is a standard method for clinically validating and diagnosing stage status in HNSCC samples. [62-64] Although other methods such as hanging

drop have been used to create spheroids *in-vitro*, we consider the presence of an ECM-like material in the system as a crucial component to mimic cancer.

The monoculture HNSCC *in-vitro* models were challenged using two standard-of-care chemotherapeutic agents: cisplatin (cis-Pt) and 5-fluorouracil (5-FU). The IC_{50} (the inhibitory level where 50% of cells show a positive effect) between 3D cultures and 2D controls treated with 5-fluorouracil resulted in an 80-fold difference. With cisplatin, a difference of at least 4-fold was observed between experimental groups. Cell-ECM interactions in 3D cultures can enable heterogeneous drug responses. Matrix-attached cells are more resistant to drugs than matrix-free cells.[65] Gradients of oxygen, nutrients, and drugs can also contribute to a higher IC_{50} in 3D cultures. These gradients can promote the formation of proliferative and quiescent cell regions that display different doubling rates and metabolic behavior, affecting the response to both treatments, which rely mechanistically on cell replication processes.[50,66,67] Knowing the importance of the ECM in cancer progression, it is currently considered a potential target.[68] Inhibiting and degrading collagens, integrins, fibronectin, and capillaries are a few strategies proposed to hinder cancer progression.[68] Therapies targeting stromal ECM could benefit from having an accurate representation of ECM *in-vitro* that can provide significant insights into the treatment effectiveness.

This monoculture platform has shown significant advantages to 2D cultures and animal models. It allows non-destructive monitoring and sampling and permits iterative dosing opportunities, which could provide additional insights into small animal models. However, monoculture models would greatly benefit from a crucial part of the tumor microenvironment, tumor stromal cells. Therefore, I incorporated fibroblasts to

recapitulate the cellular heterogeneity observed in cancer. Fibroblasts are the most abundant cell in the TME since they are recruited by cancer cells to promote their progression. Fibroblasts are known to aid in wound repair in healthy tissue. However, once they shift to cancer-associated fibroblasts (CAFs), they exhibit a myofibroblastic phenotype, increased levels of α-SMA, and pro-tumorigenic behavior by producing above-average levels of ECM components such as collagens which result in drug resistance during treatment and recruiting immunosuppressive cells.[69,70] Additionally, It has been shown that CAFs promote angiogenesis and can provide nutrients for cancer cells through oxidative stress.[71,72]

I analyzed the topographical properties of the bioink ($A_{1.5}G_5$dECMT) and observed randomly interwoven self-assembled collagen fibers also present in the pure dECMT and reported in other dECM hydrogel studies.[73] This architecture is crucial since it allows cell-matrix interactions through integrins allowing cell proliferation and migration. Pore size measurements show significant differences between $A_{1.5}G_5$dECMT and dECMT, which can be attributed to the presence of additional constituents in the hydrogel blend. However, these measurements are in the same order of magnitude as dECM hydrogels derived from other tissue sources. [74-76] Fiber diameter is also significantly bigger in $A_{1.5}G_5$dECMT. This difference can be attributed to the addition of alginate and gelatin. Both matrices are isotropic, but changes in matrix alignment can be expected as the model develops and cells promote matrix remodeling.

Fabrication of the co-culture model consisted in encapsulating both HNSCC cancer cells and human vocal fold fibroblasts (HVFFs) into $A_{1.5}G_5$dECMT. Bioprinted structures showed cell attachment and proliferation throughout the three weeks of culture. It has

been observed that fibroblast-cancer cell cultures interact to induce bidirectional activation in growth rate, ECM production, etc.[77] Tumor spheroids surrounded by fibroblasts are evident on day 7 of culture and continue to develop until they reach a relative equilibrium on day 22. The interaction between both cell types, which is absent in the monoculture groups, can be the reason for this organizational development.[78] This architecture, in which cancer cells remain in the center, is typically seen in cancer *in-vivo*. Our model indicates that the biomimetic properties may yield more accurate findings than standard 2D monocultures.

To further understand and characterize the potential to study ECM remodeling using this model, matrix metalloproteinases (MMPs) and tissue inhibitors of matrix metalloproteinases (TIMPs) were quantified several times during culture using a Luminex assay. MMPs are proteolytic enzymes that are known to cleave ECM components.[79] During remodeling and matrix deposition, the regulation of MMPs provides a feedback loop that, when MMPs are upregulated, affects the cells' active migration modes.[80] TIMPs are inhibitors and, conversely, form a feedback loop that inhibits MMP activity. In healthy tissue, there is a delicate balance between MMPs and TIMPs. In cancer, higher levels of MMP are associated with a poor prognosis due to metastasis and their role in the EMT process, allowing invasive cancer cells to move outside of the primary tumor and into secondary tissues.[81] Results from the co-culture model indicate a series of staged developmental processes in which fibroblasts dominate at the beginning and slowly transition to a signature resembling the HNSCC monoculture. This tiered cell predominance can be linked to an early environmental adaption in the culture that allows a subsequent increase in the rate and frequency of developing cancer

spheroids. In the early stages of cancer, fibroblasts promote tissue healing, which results in TME remodeling.[70] CAFs later switch to tumor promoters when cancer cells grow and develop as CAF-secreted growth factors are required by cancer cells in their survival and proliferation.[70] A precise tipping moment at which the phenotypical transition from a stromal fibroblast to a cancer-associated fibroblast occurs is difficult to pinpoint. [70] However, gradual pro-tumorigenic activity may be identified by quantifying the regulation of MMPs, TIMPs, and fibroblast using non-destructive sampling of conditioned media.

Increased expression of MMP-9 and MMP-10 are linked to cancer invasiveness and metastasis due to their role in remodeling in HNSCC.[82,83] Our co-culture model showed an increase in MMP-9 and MMP-10 occurring in Luminex measurements taken from conditioned media at day 10, which correlates to the time spheroid formation is observed. MMP-10 levels in the co-culture samples were five times higher than in the monocultures on day 10. An increase in MMP-10 in the co-culture, but not in the monoculture models, suggests regulation mechanisms that require both cell types. We see an equilibrium in spheroid size and MMP levels towards the end of the third week of culture.

Another characteristic I was interested in observing was the presence of soluble collagen through time in the 3D co-cultures. In this experimental group, the HNSCC cells are observed to be the main soluble collagen contributors despite the known collagen-secreting activity of HVFFs.[84] After 16 days, the co-culture model had significantly higher soluble collagen levels than control cell-free hydrogel models cultured for an equal time. Elevated collagen levels are an indicator of matrix remodeling and can be used to predict

tumor growth.[85] Increased collagen levels are linked to increased migration, invasion, and a poor prognosis in oral squamous cell carcinomas.[86]

Overall, the model has been proven to be a well-characterized tool that recapitulates vital extracellular and cellular components of the TME. It can be used as a biomimetic environment for drug discovery, specifically for HNSCC. However, it can be modified and tuned to study other malignancies. There is a potential to continue improving the model or using it as a testing platform. The TME is a complex and constantly changing environment that can be better represented by adding more elements to the existing model. Exploring the possibility of adding an immune component or endothelial cells, which are known to be present in the stroma, would be a sensible way of complementing and upgrading the system. Also, developing stage-relevant cancer models could provide more information on how the TME evolves as the disease progresses.

Applying complementary mechanical and structural characterization techniques such as passive microrheology, second harmonic generation microscopy, and magnetic cytometry may be used during the development of this model, providing mechanistic insight into the matrix remodeling over time. Including cells obtained from patient-derived biopsies or tissue resections would provide optimal interventional strategies personalized for the patient and can within a timescale for actionable clinical decisions to be informed.

Decellularization and solubilization have given us a unique approach to reusing tissue, an intricate creation of nature. There is significant potential in using dECM hydrogels for various biomedical applications since they can successfully recapitulate the tissue-specific niches found in the native ECM in an accessible *in-vitro* model. Even though their mechanical properties are weaker than the original tissue, they may present batch-to-

batch variability, and sourcing it from relevant species can be challenging; they are a promising naturally derived ECM alternative. dECM hydrogels can be formulated with materials that provide specific, reproducible, and mechanically defined properties.

dECM hydrogels offer biomimetic characteristics that are challenging to replicate with synthetic materials and can be used with automated fabrication techniques. They provide anchorage points for encapsulated cells promoting natural cell-ECM interactions and increased cell differentiation. Proper regulations with Good Manufacturing Practices (GMP) and Good Laboratory Practices (GLP) should be followed by adequate characterization to ensure the quality of the final product, which is especially important for tissue engineering applications where implantation is needed. Also, researching the impacts of long-term storage on tissue dECM and generated hydrogels will improve the field and promote commercialization opportunities. To properly examine the practicality of the dECM technology, shelf-life studies such as mechanical stability and bioactivity must be performed.

For building microenvironments *in-vitro*, such as disease models, dECM hydrogels have the potential to become critical factors for accurate ECM representation. As technology advances, we anticipate the development of more sustainable ECM-containing materials made of recombinant proteins that provide essential bioactive constituents while separating the less desirable characteristics of dECM hydrogels derived from tissue, such as immunogenicity, pathogens, and residual detergents or nucleic acids. This would enable controlled post-translational modifications and a decrease in product variability, which is highly desired for tissue engineering applications and personalized medicine.

Pre-clinical assessment is quickly evolving, and technologies only envisioned and tested in academic settings have higher opportunities to be commercially and clinically used. However, correct and rigorous evaluation of these tools must be conducted before their use. This can mean that initial *in-vitro* models will be a simplified version of the tissue of study. Still, it will avoid generating aberrant results due to a lack of knowledge of how the model behaves. Traditional models for cancer were developed out of necessity when therapies did not target specific malignancy components; however, as the treatments become more sophisticated and precise, we require elegantly created models to study their effectiveness.

5.1. Conclusion and summary

In conclusion, I fulfilled the main objective of my project and completed the three aims presented at the beginning of this thesis. I developed a protocol to prepare dECM hydrogels derived from porcine tongue tissue. This material was later used to prepare a composite bioink formulation containing alginate and gelatin as rheological modifiers. This biomaterial was able to recapitulate the mechanical characteristics of HNSCC *in-vitro*. I chose specific ratios of each constituent to match the elastic modulus of HNSCC tumors grown in mouse xenografts. However, if desired, the formulation can be tuned to present different properties that can benefit other malignancies or stages of HNSCC. This formulation enabled the fabrication of a heterogenous co-culture model using extrusion bioprinting and generated stable constructs. This co-culture model contained encapsulated HNSCC cells and fibroblasts, which developed into spheroids for up to three weeks. Spheroids presented a TME-like architecture by arranging cancer cells in the

center surrounded by fibroblasts. Characterization shows changes in spheroid morphology, MMP and TIMP expression, and matrix remodeling in the co-cultures, comparing them to the monoculture controls, indicating stromal-cancer interaction. This platform proves that with proper materials and fabrication techniques, it is possible to accurately recapitulate variables such as 3D architecture, cell-cell, and cell-ECM interactions, cancer-stromal cross-talk, and biochemical changes into a single *in-vitro* model. These models can be used to make observations that have proven challenging to acquire using traditional preclinical models, especially for targeted new which aim to target stromal cells or the ECM.

6. References

1 Spence, T., Bruce, J., Yip, K. W. & Liu, F.-F. HPV Associated Head and Neck Cancer. *Cancers* **8**, 75, doi:10.3390/cancers8080075 (2016).

2 Marur, S., D'Souza, G., Westra, W. H. & Forastiere, A. A. HPV-associated head and neck cancer: a virus-related cancer epidemic. *The lancet oncology* **11**, 781-789 (2010).

3 Suh, Y., Amelio, I., Guerrero Urbano, T. & Tavassoli, M. Clinical update on cancer: molecular oncology of head and neck cancer. *Cell Death &Amp; Disease* **5**, e1018, doi:10.1038/cddis.2013.548 (2014).

4 Imamura, Y. *et al.* Comparison of 2D-and 3D-culture models as drug-testing platforms in breast cancer. *Oncology reports* **33**, 1837-1843, doi:10.3892/or.2015.3767 (2015).

5 Loessner, D. *et al.* Bioengineered 3D platform to explore cell–ECM interactions and drug resistance of epithelial ovarian cancer cells. *Biomaterials* **31**, 8494-8506, doi:10.1016/j.biomaterials.2010.07.064 (2010).

6 Biotechnology Innovation Organization (BIO), B., Amplion,. Clinical Development Success Rates 2006-2015. 28 (2016).

7 Cekanova, M. & Rathore, K. Animal models and therapeutic molecular targets of cancer: utility and limitations. *Drug design, development and therapy* **8**, 1911-1921, doi:10.2147/dddt.s49584 (2014).

8 McGonigle, P. & Ruggeri, B. Animal models of human disease: challenges in enabling translation. *Biochemical pharmacology* **87**, 162-171, doi:10.1016/j.bcp.2013.08.006 (2014).

9 Ruggeri, B. A., Camp, F. & Miknyoczki, S. Animal models of disease: pre-clinical animal models of cancer and their applications and utility in drug discovery. *Biochemical pharmacology* **87**, 150-161, doi:10.1016/j.bcp.2013.06.020 (2014).

10 Young, E. W. Cells, tissues, and organs on chips: challenges and opportunities for the cancer tumor microenvironment. *Integrative Biology* **5**, 1096-1109, doi:10.1039/c3ib40076j (2013).

11 Jiang, T. *et al.* Directing the Self-assembly of Tumour Spheroids by Bioprinting Cellular Heterogeneous Models within Alginate/Gelatin Hydrogels. *Scientific Reports* **7**, 4575, doi:10.1038/s41598-017-04691-9 (2017).

12 Tibbitt, M. W. & Anseth, K. S. Hydrogels as extracellular matrix mimics for 3D cell culture. *Biotechnology and bioengineering* **103**, 655-663, doi:10.1002/bit.22361 (2009).

13 Skardal, A., Shupe, T. & Atala, A. Organoid-on-a-chip and body-on-a-chip systems for drug screening and disease modeling. *Drug Discovery Today* **21**, 1399-1411, doi:10.1016/j.drudis.2016.07.003 (2016).

14 Huh, D., Hamilton, G. A. & Ingber, D. E. From 3D cell culture to organs-on-chips. *Trends in Cell Biology* **21**, 745-754, doi:10.1016/j.tcb.2011.09.005.

15 Ozbolat, I. T. & Hospodiuk, M. Current advances and future perspectives in extrusion-based bioprinting. *Biomaterials* **76**, 321-343, doi:10.1016/j.biomaterials.2015.10.076 (2016).

16 Murphy, S. V. & Atala, A. 3D bioprinting of tissues and organs. *Nature biotechnology* **32**, 773, doi:10.1038/nbt.2958 (2014).

17 Jia, J. *et al.* Engineering alginate as bioink for bioprinting. *Acta biomaterialia* **10**, 4323-4331, doi:10.1016/j.actbio.2014.06.034 (2014).

18 Stanton, M., Samitier, J. & Sanchez, S. Bioprinting of 3D hydrogels. *Lab on a Chip* **15**, 3111-3115, doi:10.1039/c5lc90069g (2015).

19 Pati, F. *et al.* Printing three-dimensional tissue analogues with decellularized extracellular matrix bioink. *Nature communications* **5**, 3935, doi:10.1038/ncomms4935 (2014).

20 Das, S. *et al.* Bioprintable, cell-laden silk fibroin–gelatin hydrogel supporting multilineage differentiation of stem cells for fabrication of three-dimensional tissue constructs. *Acta biomaterialia* **11**, 233-246, doi:10.1016/j.actbio.2014.09.023 (2015).

21 Pizzo, A. M., Kokini, K., Vaughn, L. C., Waisner, B. Z. & Voytik-Harbin, S. L. Extracellular matrix (ECM) microstructural composition regulates local cell-ECM biomechanics and fundamental fibroblast behavior: a multidimensional perspective. *Journal of applied physiology* **98**, 1909-1921, doi:10.1152/japplphysiol.01137.2004 (2005).

22 Jungst, T., Smolan, W., Schacht, K., Scheibel, T. & Groll, J. Strategies and Molecular Design Criteria for 3D Printable Hydrogels. *Chemical reviews* **116**, 1496-1539, doi:10.1021/acs.chemrev.5b00303 (2016).

23 Kabirian, F. & Mozafari, M. Decellularized ECM-derived bioinks: Prospects for the future. *Methods (San Diego, Calif.)* **171**, 108-118, doi:10.1016/j.ymeth.2019.04.019 (2020).

24 Kim, H. *et al.* Characterization of cornea-specific bioink: high transparency, improved in vivo safety. *J Tissue Eng* **10**, 2041731418823382, doi:10.1177/2041731418823382 (2019).

25 Kim, J. *et al.* 3D cell printing of islet-laden pancreatic tissue-derived extracellular matrix bioink constructs for enhancing pancreatic functions. *J Mater Chem B* **7**, 1773-1781, doi:10.1039/c8tb02787k (2019).

26 Kim, B. S. *et al.* 3D cell printing of in vitro stabilized skin model and in vivo pre-vascularized skin patch using tissue-specific extracellular matrix bioink: A step towards advanced skin tissue engineering. *Biomaterials* **168**, 38-53, doi:10.1016/j.biomaterials.2018.03.040 (2018).

27 Choi, Y. J. *et al.* 3D Cell Printing of Functional Skeletal Muscle Constructs Using Skeletal Muscle-Derived Bioink. *Advanced healthcare materials* **5**, 2636-2645, doi:10.1002/adhm.201600483 (2016).

28 Kort-Mascort, J. *et al.* Decellularized Extracellular Matrix Composite Hydrogel Bioinks for the Development of 3D Bioprinted Head and Neck in Vitro Tumor Models. *ACS Biomaterials Science & Engineering* **7**, 5288-5300, doi:10.1021/acsbiomaterials.1c00812 (2021).

29 Gao, G. *et al.* Tissue Engineered Bio-Blood-Vessels Constructed Using a Tissue-Specific Bioink and 3D Coaxial Cell Printing Technique: A Novel Therapy for Ischemic Disease. *Advanced Functional Materials* **27**, 1700798, doi:https://doi.org/10.1002/adfm.201700798 (2017).

30 Park, J. Y. *et al.* Development of a functional airway-on-a-chip by 3D cell printing. *Biofabrication* **11**, 015002, doi:10.1088/1758-5090/aae545 (2018).

31 Park, W., Gao, G. & Cho, D.-W. Tissue-Specific Decellularized Extracellular Matrix Bioinks for Musculoskeletal Tissue Regeneration and Modeling Using 3D Bioprinting Technology. *International journal of molecular sciences* **22**, 7837, doi:10.3390/ijms22157837 (2021).

32 Claudio-Rizo, J. A., Delgado, J., Quintero-Ortega, I. A., Mata-Mata, J. L. & Mendoza-Novelo, B. in *Hydrogels* 3-22 (InTechOpen, 2018).

33 Cui, X. *et al.* Advances in Extrusion 3D Bioprinting: A Focus on Multicomponent Hydrogel-Based Bioinks. *Advanced healthcare materials* **9**, 1901648, doi:10.1002/adhm.201901648 (2020).

34 Chow, L. Q. M. Head and Neck Cancer. *New England Journal of Medicine* **382**, 60-72, doi:10.1056/NEJMra1715715 (2020).

35 Canadian Cancer Statistics Advisory, the Canadian Cancer Society, Statistics Canada & Public Health Agency of Canada. *Canadian Cancer Statistics: A 2022 special report on cancer prevalence*, < cancer.ca/Canadian-Cancer-Statistics-2022-EN> (2022).

36 Sung, H. *et al.* Global Cancer Statistics 2020: GLOBOCAN Estimates of Incidence and Mortality Worldwide for 36 Cancers in 185 Countries. *CA Cancer J Clin* **71**, 209-249, doi:10.3322/caac.21660 (2021).

37 Wyss, A. *et al.* Cigarette, cigar, and pipe smoking and the risk of head and neck cancers: pooled analysis in the International Head and Neck Cancer Epidemiology Consortium. *Am J Epidemiol* **178**, 679-690, doi:10.1093/aje/kwt029 (2013).

38 Hashibe, M. *et al.* Interaction between tobacco and alcohol use and the risk of head and neck cancer: pooled analysis in the International Head and Neck Cancer Epidemiology Consortium. *Cancer Epidemiol Biomarkers Prev* **18**, 541-550, doi:10.1158/1055-9965.EPI-08-0347 (2009).

39 Menezes, F. D. S., Fernandes, G. A., Antunes, J. L. F., Villa, L. L. & Toporcov, T. N. Global incidence trends in head and neck cancer for HPV-related and -unrelated subsites: A systematic review of population-based studies. *Oral Oncol* **115**, 105177, doi:10.1016/j.oraloncology.2020.105177 (2021).

40 Gillison, M. L., Chaturvedi, A. K., Anderson, W. F. & Fakhry, C. Epidemiology of Human Papillomavirus-Positive Head and Neck Squamous Cell Carcinoma. *J Clin Oncol* **33**, 3235-3242, doi:10.1200/JCO.2015.61.6995 (2015).

41 Johnson, D. E. *et al.* Head and neck squamous cell carcinoma. *Nat Rev Dis Primers* **6**, 92, doi:10.1038/s41572-020-00224-3 (2020).

42 Pignon, J. P., le Maitre, A., Maillard, E., Bourhis, J. & Group, M.-N. C. Meta-analysis of chemotherapy in head and neck cancer (MACH-NC): an update on 93 randomised trials and 17,346 patients. *Radiother Oncol* **92**, 4-14, doi:10.1016/j.radonc.2009.04.014 (2009).

43 Mody, M. D., Rocco, J. W., Yom, S. S., Haddad, R. I. & Saba, N. F. Head and neck cancer. *Lancet* **398**, 2289-2299, doi:10.1016/S0140-6736(21)01550-6 (2021).

44 Ferris, R. L. *et al.* Nivolumab vs investigator's choice in recurrent or metastatic squamous cell carcinoma of the head and neck: 2-year long-term survival update of CheckMate 141 with analyses by tumor PD-L1 expression. *Oral Oncol* **81**, 45-51, doi:10.1016/j.oraloncology.2018.04.008 (2018).

45 Burtness, B. *et al.* Pembrolizumab alone or with chemotherapy versus cetuximab with chemotherapy for recurrent or metastatic squamous cell carcinoma of the head and neck (KEYNOTE-048): a randomised, open-label, phase 3 study. *Lancet* **394**, 1915-1928, doi:10.1016/S0140-6736(19)32591-7 (2019).

46 Vokes, E. E., Weichselbaum, R. R., Lippman, S. M. & Hong, W. K. Head and Neck Cancer. *New England Journal of Medicine* **328**, 184-194, doi:10.1056/nejm199301213280306 (1993).

47 Darrow, J. J., Avorn, J. & Kesselheim, A. S. FDA Approval and Regulation of Pharmaceuticals, 1983-2018. *JAMA* **323**, 164-176, doi:10.1001/jama.2019.20288 (2020).

48 Rodrigues, J., Heinrich, M. A., Teixeira, L. M. & Prakash, J. 3D In Vitro Model (R)evolution: Unveiling Tumor-Stroma Interactions. *Trends Cancer* **7**, 249-264, doi:10.1016/j.trecan.2020.10.009 (2021).

49 Emon, B., Bauer, J., Jain, Y., Jung, B. & Saif, T. Biophysics of Tumor Microenvironment and Cancer Metastasis - A Mini Review. *Comput Struct Biotechnol J* **16**, 279-287, doi:10.1016/j.csbj.2018.07.003 (2018).

50 Zanoni, M. *et al.* 3D tumor spheroid models for in vitro therapeutic screening: a systematic approach to enhance the biological relevance of data obtained. *Sci Rep* **6**, 19103, doi:10.1038/srep19103 (2016).

51 Trédan, O., Galmarini, C. M., Patel, K. & Tannock, I. F. Drug Resistance and the Solid Tumor Microenvironment. *JNCI: Journal of the National Cancer Institute* **99**, 1441-1454, doi:10.1093/jnci/djm135 (2007).

52 Jin, Y. *et al.* Three-dimensional brain-like microenvironments facilitate the direct reprogramming of fibroblasts into therapeutic neurons. *Nature biomedical engineering* **2**, 522-539, doi:10.1038/s41551-018-0260-8 (2018).

53 Pires, F. R. *et al.* Oral squamous cell carcinoma: clinicopathological features from 346 cases from a single oral pathology service during an 8-year period. *Journal of Applied Oral Science* **21**, 460-467, doi:10.1590/1679-775720130317 (2013).

54 Dawson, H. D. in *The Minipig in Biomedical Research* Ch. 22, 323-342 (CRC Press, 2011).

55 Costa, A., Naranjo, J. D., Londono, R. & Badylak, S. F. Biologic Scaffolds. *Cold Spring Harbor Perspectives in Medicine* **7**, a025676, doi:10.1101/cshperspect.a025676 (2017).

56 Liu, W. *et al.* Bioprinting: Extrusion Bioprinting of Shear-Thinning Gelatin Methacryloyl Bioinks *Advanced healthcare materials* **6**, doi:10.1002/adhm.201601451 (2017).

57 McBeath, R., Pirone, D. M., Nelson, C. M., Bhadriraju, K. & Chen, C. S. Cell shape, cytoskeletal tension, and RhoA regulate stem cell lineage commitment. *Developmental cell* **6**, 483-495, doi:10.1016/S1534-5807(04)00075-9 (2004).

58 Cukierman, E. & Bassi, D. E. Physico-mechanical aspects of extracellular matrix influences on tumorigenic behaviors. *Seminars in Cancer Biology* **20**, 139-145, doi:10.1016/j.semcancer.2010.04.004 (2010).

59 Jiang, T. *et al.* Engineering bioprintable alginate/gelatin composite hydrogels with tunable mechanical and cell adhesive properties to modulate tumor spheroid growth kinetics. *Biofabrication*, doi:10.1088/1758-5090/ab3a5c (2019).

60 Elkashty, O. A. *et al.* Cancer stem cells enrichment with surface markers CD271 and CD44 in human head and neck squamous cell carcinomas. *Carcinogenesis*, doi:10.1093/carcin/bgz182 (2019).

61 Charlebois, D. A. & Balazsi, G. Modeling cell population dynamics. *In Silico Biol* **13**, 21-39, doi:10.3233/ISB-180470 (2019).

62 Brauchle, E., Johannsen, H., Nolan, S., Thude, S. & Schenke-Layland, K. Design and analysis of a squamous cell carcinoma in vitro model system. *Biomaterials* **34**, 7401-7407, doi:10.1016/j.biomaterials.2013.06.016 (2013).

63 Yanagi, T. *et al.* Loss of TRIM29 alters keratin distribution to promote cell invasion in squamous cell carcinoma. *Cancer research* **78**, 6795-6806, doi:10.1158/0008-5472.CAN-18-1495 (2018).

64 Gawas, N. P., Navarange, S. S., Chovatiya, G. L., Chaturvedi, P. & Waghmare, S. K. Establishment and characterization of novel human oral squamous cell carcinoma cell lines from advanced-stage tumors of buccal mucosa. *Oncology reports* **41**, 2289-2298, doi:10.3892/or.2019.7003 (2019).

65 Muranen, T. *et al.* Inhibition of PI3K/mTOR leads to adaptive resistance in matrix-attached cancer cells. *Cancer cell* **21**, 227-239, doi:10.1016/j.ccr.2011.12.024. (2012).

66 Stock, K. *et al.* Capturing tumor complexity in vitro: Comparative analysis of 2D and 3D tumor models for drug discovery. *Scientific reports* **6**, 1-15, doi:10.1038/srep28951 (2016).

67 Mehta, G., Hsiao, A. Y., Ingram, M., Luker, G. D. & Takayama, S. Opportunities and challenges for use of tumor spheroids as models to test drug delivery and efficacy. *J Control Release* **164**, 192-204, doi:10.1016/j.jconrel.2012.04.045 (2012).

68 Huang, J. *et al.* Extracellular matrix and its therapeutic potential for cancer treatment. *Signal Transduct Target Ther* **6**, 153, doi:10.1038/s41392-021-00544-0 (2021).

69 Monteran, L. & Erez, N. The Dark Side of Fibroblasts: Cancer-Associated Fibroblasts as Mediators of Immunosuppression in the Tumor Microenvironment. *Front Immunol* **10**, 1835, doi:10.3389/fimmu.2019.01835 (2019).

70 LeBleu, V. S. & Kalluri, R. A peek into cancer-associated fibroblasts: origins, functions and translational impact. *Dis Model Mech* **11**, doi:10.1242/dmm.029447 (2018).

71 Tang, D. *et al.* Cancer-associated fibroblasts promote angiogenesis in gastric cancer through galectin-1 expression. *Tumour Biol* **37**, 1889-1899, doi:10.1007/s13277-015-3942-9 (2016).

72 Lisanti, M. P. *et al.* Understanding the "lethal" drivers of tumor-stroma co-evolution. *Cancer Biology & Therapy* **10**, 537-542, doi:10.4161/cbt.10.6.13370 (2010).

73 Freytes, D. O., Martin, J., Velankar, S. S., Lee, A. S. & Badylak, S. F. Preparation and rheological characterization of a gel form of the porcine urinary bladder matrix. *Biomaterials* **29**, 1630-1637, doi:10.1016/j.biomaterials.2007.12.014 (2008).

74 Wolf, M. T. *et al.* A hydrogel derived from decellularized dermal extracellular matrix. *Biomaterials* **33**, 7028-7038, doi:10.1016/j.biomaterials.2012.06.051 (2012).

75 Hong, J. Y. *et al.* Decellularized brain matrix enhances macrophage polarization and functional improvements in rat spinal cord injury. *Acta biomaterialia* **101**, 357-371, doi:10.1016/j.actbio.2019.11.012 (2020).

76 Loneker, A. E., Faulk, D. M., Hussey, G. S., D'Amore, A. & Badylak, S. F. Solubilized liver extracellular matrix maintains primary rat hepatocyte phenotype in-vitro. *Journal of biomedical materials research. Part A* **104**, 957-965, doi:10.1002/jbm.a.35636 (2016).

77 Jeong, S. Y., Lee, J. H., Shin, Y., Chung, S. & Kuh, H. J. Co-Culture of Tumor Spheroids and Fibroblasts in a Collagen Matrix-Incorporated Microfluidic Chip Mimics Reciprocal Activation in Solid Tumor Microenvironment. *PLoS One* **11**, e0159013, doi:10.1371/journal.pone.0159013 (2016).

78 Kim, S. A., Lee, E. K. & Kuh, H. J. Co-culture of 3D tumor spheroids with fibroblasts as a model for epithelial-mesenchymal transition in vitro. *Exp Cell Res* **335**, 187-196, doi:10.1016/j.yexcr.2015.05.016 (2015).

79 Nagase, H. & Woessner, J. F., Jr. Matrix Metalloproteinases. *Journal of Biological Chemistry* **274**, 21491-21494, doi:10.1074/jbc.274.31.21491 (1999).

80 Page-McCaw, A., Ewald, A. J. & Werb, Z. Matrix metalloproteinases and the regulation of tissue remodelling. *Nat Rev Mol Cell Biol* **8**, 221-233, doi:10.1038/nrm2125 (2007).

81 Egeblad, M. & Werb, Z. New functions for the matrix metalloproteinases in cancer progression. *Nat Rev Cancer* **2**, 161-174, doi:10.1038/nrc745 (2002).

82 Yin, P. *et al.* MMP-9 Knockdown Inhibits Oral Squamous Cell Carcinoma Lymph Node Metastasis in the Nude Mouse Tongue-Xenografted Model through the

RhoC/Src Pathway. *Anal Cell Pathol (Amst)* **2021**, 6683391, doi:10.1155/2021/6683391 (2021).

83 Deraz, E. M. *et al.* MMP-10/stromelysin-2 promotes invasion of head and neck cancer. *PLoS One* **6**, e25438, doi:10.1371/journal.pone.0025438 (2011).

84 Chen, X. & Thibeault, S. L. Novel isolation and biochemical characterization of immortalized fibroblasts for tissue engineering vocal fold lamina propria. *Tissue Eng Part C Methods* **15**, 201-212, doi:10.1089/ten.tec.2008.0390 (2009).

85 Dolor, A. & Szoka, F. C., Jr. Digesting a Path Forward: The Utility of Collagenase Tumor Treatment for Improved Drug Delivery. *Mol Pharm* **15**, 2069-2083, doi:10.1021/acs.molpharmaceut.8b00319 (2018).

86 Li, H. X. *et al.* Expression of alphavbeta6 integrin and collagen fibre in oral squamous cell carcinoma: association with clinical outcomes and prognostic implications. *J Oral Pathol Med* **42**, 547-556, doi:10.1111/jop.12044 (2013).

Appendix 1

Supplementary information for Chapter 3

Decellularized extracellular matrix composite hydrogel bioinks for the development of 3D bioprinted head and neck *in-vitro* tumor models

Jacqueline Kort-Mascort[a], Guangyu Bao[b], Osama Elkashty[c,d], Salvador Flores-Torres[a], Jose G. Munguia-Lopez[a, c], Tao Jiang[e], Allen J. Ehrlicher[a,b], Luc Mongeau[b], Simon D. Tran[c], Joseph M. Kinsella[a,*]

[a] *Department of Bioengineering, McGill University, Montreal, Quebec, Canada.*

[b] *Department of Mechanical Engineering, McGill University, Montreal, Quebec, Canada.*

[c] *Faculty of Dentistry, McGill University, Montreal, Quebec, Canada.*

[d] *Oral Pathology Department, Faculty of Dentistry, Mansoura University, Mansoura, Egypt.*

[e] *Department of Intelligent Machinery and Instrument, College of Intelligence Science and Technology, National University of Defense Technology Changsha, Hunan, China*

**Corresponding author: E-mail:* joseph.kinsella@mcgill.ca

List of supporting figures

List of supporting tables

Table S1: Structural proteins identified in dECMT using LC/MS/MS.

Table S2: Mean values of rheological parameters. Storage modulus, loss modulus and yield point of $A_{1.5}G_5$dECMT and dECMT.

Table S3: Viability of encapsulated UM-SCC-12 and UM-SCC-38 cancer cells in $A_{1.5}G_5$dECMT and $A_{1.5}G_5$.

Table S4: Short Tandem Repeat (STR) analysis of UM-SCC-12 and UM-SCC-38 immortalized cell lines.

Supporting Figures

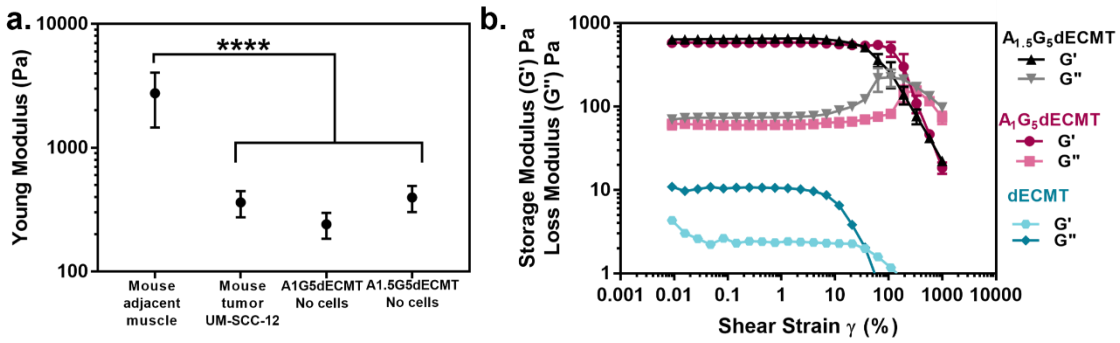

Figure S1: Mechanical comparison of A_1G_5dECMT and $A_{1.5}G_5$dECMT. *a. Nanoindentation test of ionically crosslinked* A_1G_5dECMT and $A_{1.5}G_5$dECMT *compared with a tumor formed in a mouse xenograft after 35 days of implanting UM-SCC-12 cells. b. Amplitude sweep presenting the storage (G') and loss (G") modulus (uncrosslinked alginate) at 24°C.*

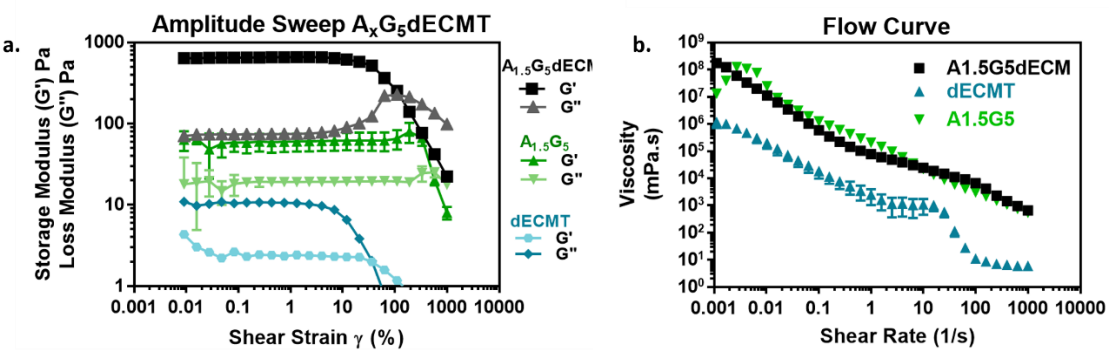

Figure S2: Rheological characterization of dECMT, $A_{1.5}G_5$, and the reinforced $A_{1.5}G_5$dECMT bioink. *a. Amplitude sweep presenting the storage (G') and loss (G") modulus. b. Flow curve performed at 24°C of dECMT,* $A_{1.5}G_5$, *and* $A_{1.5}G_5$dECMT.

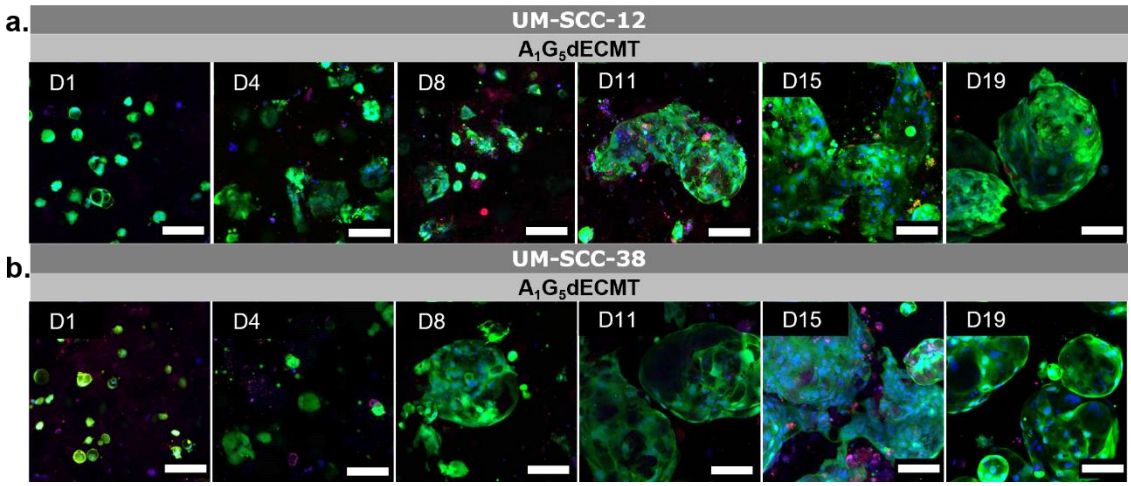

Figure S3: Confocal microscopy of bioprinted HNSCC cells encapsulated in A_1G_5dECMT. a. UM-SCC-12, and b. UM-SCC-38 over time in A_1G_5dECMT. Live-dead stains: Calcein-AM: live (green), Ethidium Homodimer-I: dead (red), and Hoechst 33342: DNA (blue). Scalebar 100μM.

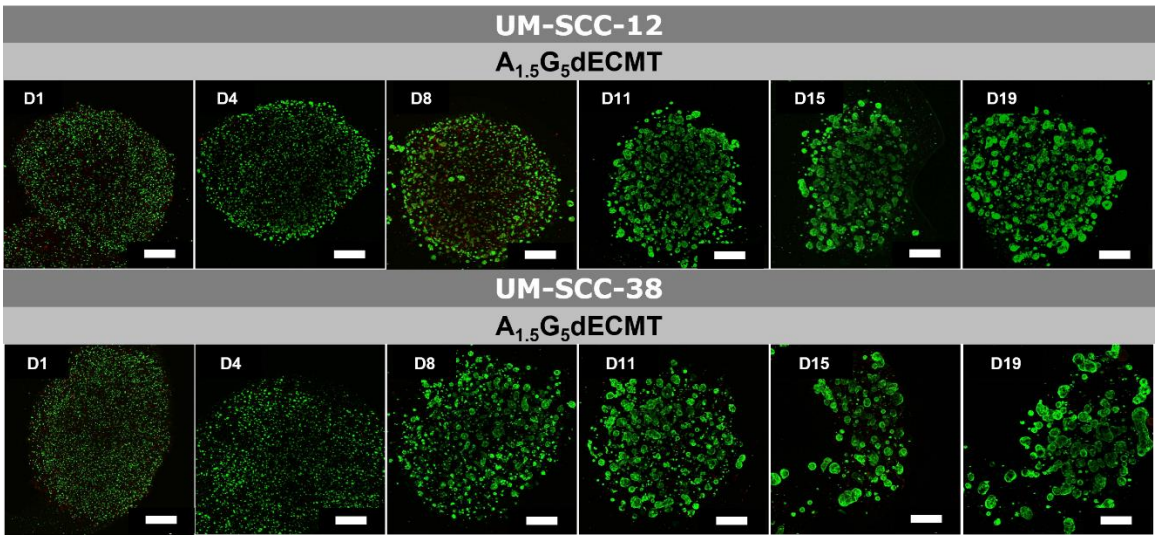

Figure S4: Morphological variation of a. UM-SCC-12 and b. UM-SCC-38 over time encapsulated in $A_{1.5}G_5$dECMT. Calcein-AM: live (green), Ethidium Homodimer-I: dead (red). Scalebar 1000μM.

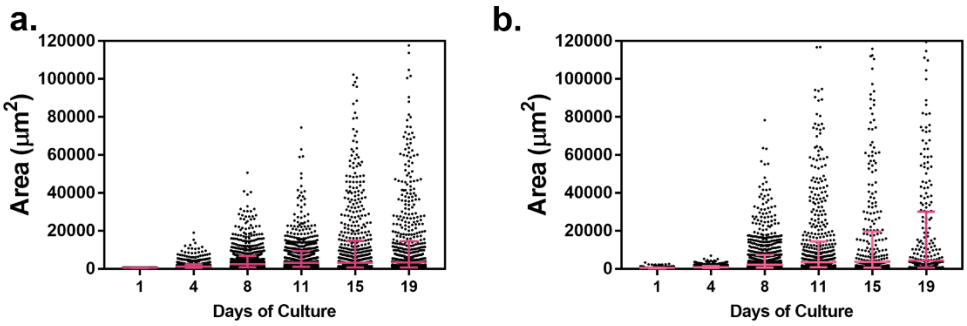

Figure S5: Quantitative analysis of cancer cells encapsulated in $A_{1.5}G_5$dECMT. Spheroid size distribution over time after segmentation analysis of a. UM-SCC-12, and b.UM-SCC-38 microscopy data (Figure S4).

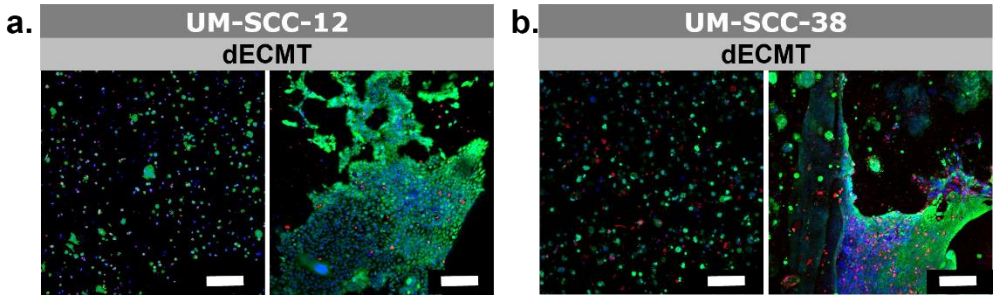

Figure S6: Fluorescence microscopy of pure dECM mold-casted 3D cultures. Maximum intensity projections showing control groups of a. UM-SCC-12 and b. UM-SCC-38 cells encapsulated in pure dECMT and mold-casted on an agarose-coated plate. Figure shows days 1 and 16 of culture under standard conditions. Scalebar 200μM.

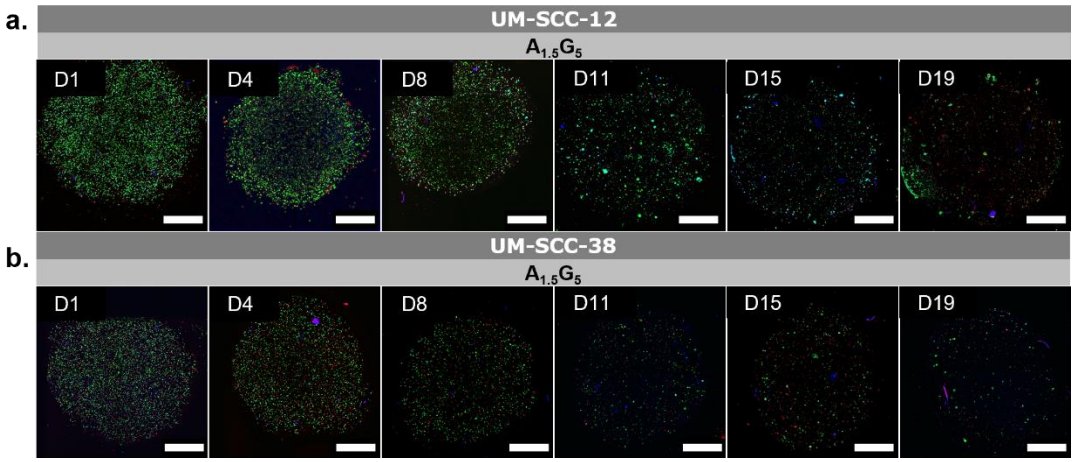

Figure S7:Morphological variation of **a.** UM-SCC-12 and **b.** UM-SCC-38 over time encapsulated in $A_{1.5}G_5$. Calcein-AM: live (green), Ethidium Homodimer-I: dead (red). Scalebar 1000µM.

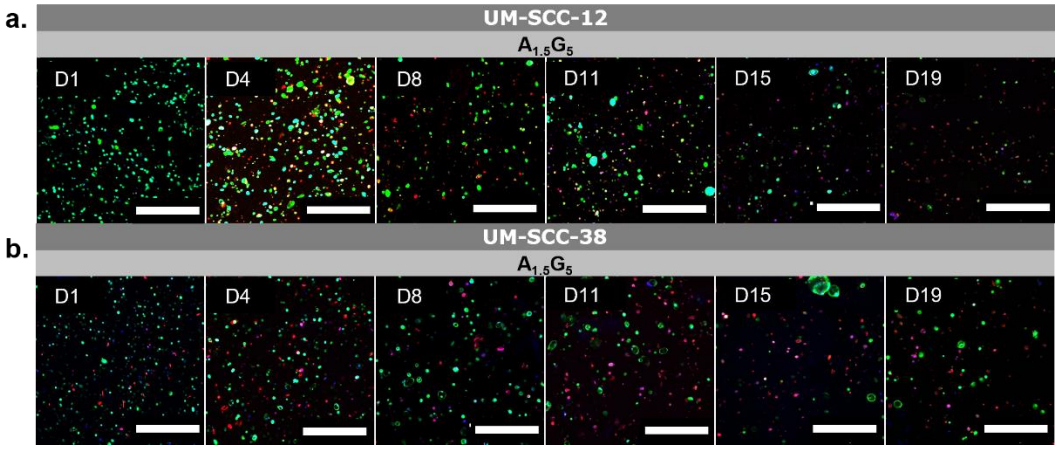

Figure S8: Confocal microscopy of bioprinted HNSCC cells encapsulated in $A_{1.5}G_5$. a. UM-SCC-12, and b. UM-SCC-38 over time in $A_{1.5}G_5$. Live-dead stains: Calcein-AM: live (green), Ethidium Homodimer-I: dead (red), and Hoechst 33342: DNA (blue). Scalebar 500µM.

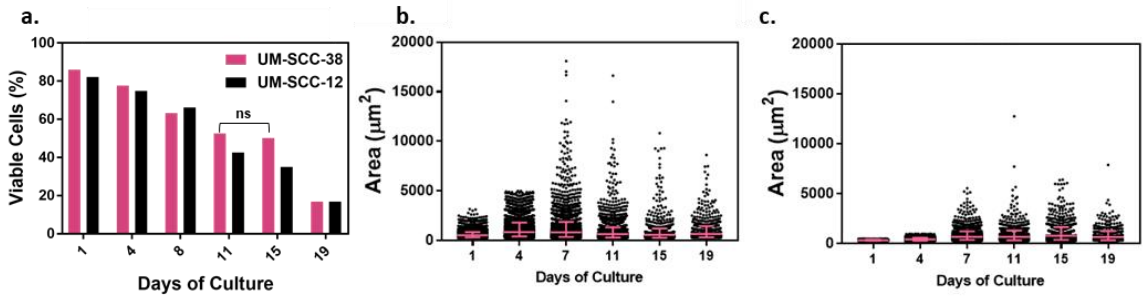

Figure S9: Quantitative analysis of live-dead assay of 3D printed HNSCC cells encapsulated in $A_{1.5}G_{5}$. **a.** Cell viability over time (n=4, p<0.0001). The difference in viability within the same cell line is statistically different unless stated in the plot. Spheroid size distribution over time after segmentation analysis of **b.** UM-SCC-12, and **c.**UM-SCC-38 microscopy data (Figure S7).

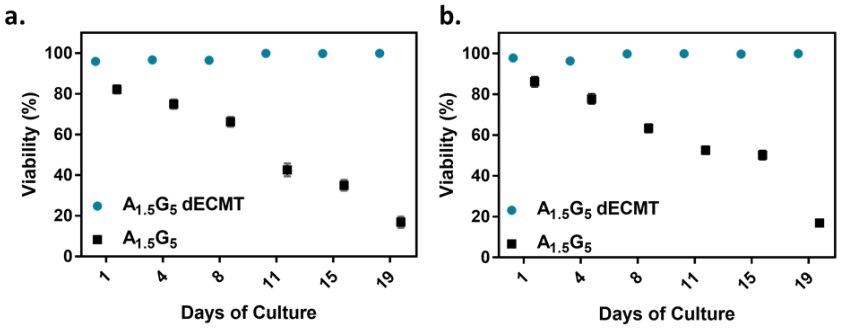

Figure S10: Viability data presented by cell line. a. UM-SCC-12 b. UM-SCC-38 encapsulated independently in either in $A_{1.5}G_{5}$ or $A_{1.5}G_{5}$dECMT from Figure S4 and Figure S7 (Data presented in Table S3)

Supporting Tables

Table S1:Structural proteins identified in dECMT using LC/MS/MS (n=2). Acquired spectra extracted with Mascot Distiller and searched against a relevant proteome database (Sus scrofa (Pig) - UniProt) using the 'Mascot' proteomics search engine

Identified Proteins	Accession Number	Molecular Weight	Sample 1	Sample 2	Mean
Uncharacterized protein OS=Sus scrofa OX=9823 GN=COL1A2 PE=1 SV=2	I3L781_PIG	129 kDa	164	151	157.5
Collagen type I alpha 1 chain OS=Sus scrofa OX=9823 GN=COL1A1 PE=1 SV=1	A0A287A1S6_PIG (+1)	139 kDa	79	65	72
Cluster of Collagen type VI alpha 3 chain OS=Sus scrofa OX=9823 GN=COL6A3 PE=1 SV=1 (A0A286ZMC0_PIG)	A0A286ZMC0_PIG [5]	209 kDa	18	46	32
Collagen type VI alpha 2 chain OS=Sus scrofa OX=9823 GN=COL6A2 PE=1 SV=2	I3LQ84_PIG	103 kDa	22	20	21
Cluster of Uncharacterized protein OS=Sus scrofa OX=9823 GN=COL5A1 PE=1 SV=3 (F1S021_PIG)	F1S021_PIG [2]	184 kDa	8	8	8
Uncharacterized protein OS=Sus scrofa OX=9823 GN=COL3A1 PE=1 SV=1	A0A286ZQ85_PIG	114 kDa	29	19	24
Collagen type IV alpha 2 chain OS=Sus scrofa OX=9823 GN=COL4A2 PE=1 SV=3	F1RLL9_PIG	167 kDa	0	8	4
Uncharacterized protein OS=Sus scrofa OX=9823 GN=LAMC1 PE=1 SV=2	F1S663_PIG	163 kDa	7	6	6.5
Uncharacterized protein OS=Sus scrofa OX=9823 GN=COL5A3 PE=4 SV=3	F1S3G7_PIG (+1)	172 kDa	7	3	5
Laminin subunit beta 2 OS=Sus scrofa OX=9823 GN=LAMB2 PE=1 SV=1	A0A287AJ64_PIG (+2)	197 kDa	1	5	3
Keratin 84 OS=Sus scrofa OX=9823 GN=KRT84 PE=1 SV=3	F1SGI2_PIG	64 kDa	7	0	3.5
Collagen type VI alpha 6 chain OS=Sus scrofa OX=9823 GN=COL6A6 PE=1 SV=1	A0A287A0A6_PIG	229 kDa	0	10	5
Fibrillin-1 OS=Sus scrofa OX=9823 GN=FBN1 PE=1 SV=3	F1SN67_PIG (+1)	312 kDa	0	3	1.5
Decorin OS=Sus scrofa OX=9823 GN=DCN PE=3 SV=2	F1SQ10_PIG (+1)	40 kDa	1	6	3.5
Nidogen 1 OS=Sus scrofa OX=9823 GN=NID1 PE=1 SV=1	A0A286ZL08_PIG (+2)	127 kDa	0	6	3
Uncharacterized protein OS=Sus scrofa OX=9823 GN=COL5A2 PE=1 SV=1	A0A287BPM1_PIG	140 kDa	2	1	1.5
Collagen type XXI alpha 1 (Fragment) OS=Sus scrofa OX=9823 GN=COL21A1 PE=4 SV=1	D5KRL1_PIG	93 kDa	4	1	2.5
Heparan sulfate proteoglycan 2 OS=Sus scrofa OX=9823 GN=HSPG2 PE=1 SV=1	A0A286ZHV7_PIG (+3)	451 kDa	0	3	1.5

Table S2: Mean values of rheological parameters. Storage modulus, loss modulus and yield point of $A_{1.5}G_5$dECMT and dECMT.

	$A_{1.5}G_5$dECMT		dECMT	
	Mean	**SD**	**Mean**	**SD**
Storage Modulus (Pa)	650.5	64.6	10.7	1.8
Loss Modulus (Pa)	73.7	2.5	2.3	0.8
Yield stress (Pa)	32.9		14.8	

Table S3**:** Viability of encapsulated *UM-SCC-12 and UM-SCC-38* cancer cells in $A_{1.5}G_5$dECMT and $A_{1.5}G_5$. Data analyzed from Figure S4 and Figure S7 (n=4).

		$A_{1.5}G_5$dECMT		$A_{1.5}G_5$	
UM-SCC-38	Days of Culture	Average (%)	SD (%)	Average (%)	SD (%)
	1	97.8	0.1	86.1	2.6
	4	96.3	0.3	77.7	2.6
	8	99.8	0.0	63.3	2.2
	11	99.9	0.0	52.6	2.1
	15	99.7	0.0	50.2	2.4
	19	99.9	0.0	16.9	1.4

		$A_{1.5}G_5$dECMT		$A_{1.5}G_5$	
UM-SCC-12	**Days of Culture**	**Average (%)**	**SD (%)**	**Average (%)**	**SD (%)**
	1	95.9	0.1	82.2	2.0
	4	96.7	0.5	74.9	2.3
	8	96.5	0.7	66.2	2.4
	11	99.9	0.0	42.6	3.1
	15	99.8	0.1	35.0	2.6
	19	99.9	0.0	16.9	2.7

Table S4: Short Tandem Repeat (STR) analysis of UM-SCC-12 and UM-SCC-38 immortalized cell lines.

CELL LINE	UM-SCC-12	UM-SCC-38
Gender	Male	Male
Specimen Site	Larynx	Tonsillar pillar
AMEL	X	X Y
vWA	16	17, 18
D21S11	29	27,29
D5S818	12	12
D7S820	10,11	10
CSF1PO	8	8
D16S539	12	10
TH01	7	8,9
TPOX	9,10	8,11

Supplementary information for Chapter 4

Bioprinted cancer-stromal *in-vitro* models in a decellularized ECM-based bioink exhibit progressive remodelling and maturation

Authors: Jacqueline Kort-Mascort[a], Molly L. Shen [b, c], Emma Martin [a], Salvador Flores-Torres [a], Lucas Antonio Pardo [a], Peter M. Siegel [c,d], Susan L Thibeault[e], Simon D. Tran[f], Joseph Kinsella [a].

joseph.kinsella@mcgill.ca

[a] Department of Bioengineering, McGill University, Montreal, Quebec, Canada.

[b] Department of Biomedical Engineering, McGill University, Montreal, Quebec, Canada.

[c] Goodman Cancer Institute, McGill University, Montreal, Quebec, Canada.

[d] Department of Medicine, Division of Experimental Medicine, McGill University, Montreal, Quebec, Canada.

[e] Department of Surgery, University of Wisconsin, Madison, Wisconsin, USA.

[f] Faculty of Dental Medicine and Oral Health Sciences, McGill University, Montreal, Quebec, Canada.

List of supporting figures

Fig. S1: Scanning electron microscopy images

Fig. S2: Matrix metalloproteinases (MMPs) tissue inhibitors of metalloproteinases (TIMPs) quantification through time.

Fig. S3: MMP-9 and MMP-10 levels through time grouped by experimental group.

Fig. S4: Soluble collagen quantification of monocultures (HVFF and UM-SCC-38), co-culture (2:1 HVFF:UM-SCC-38), and cell-free bioink through time.

Supporting Figures

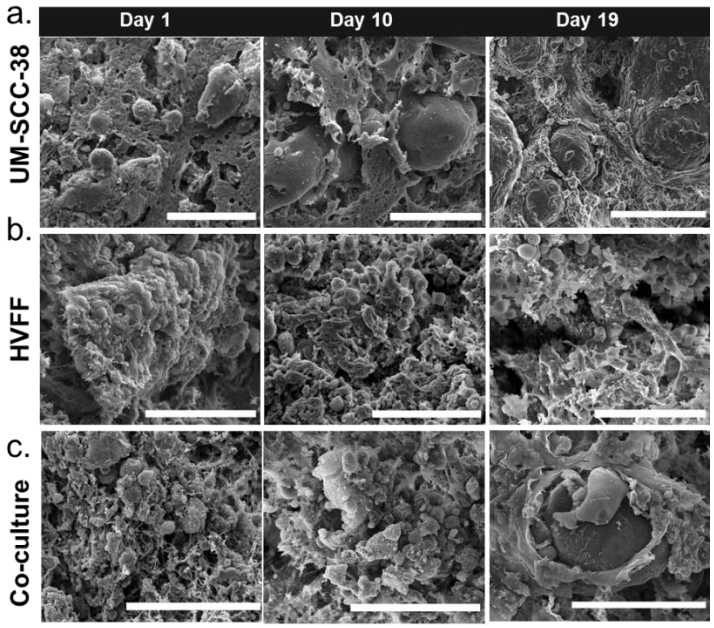

Fig. S1: Scanning electron microscopy images of Pt coated $A_{1.5}G_5$dECMT samples with encapsulated cells. a. UM-SCC-38, b. HVFF, c. co-culture-2:1 ration of HVFF:UM-SCC-38. Scale bar: 100μm

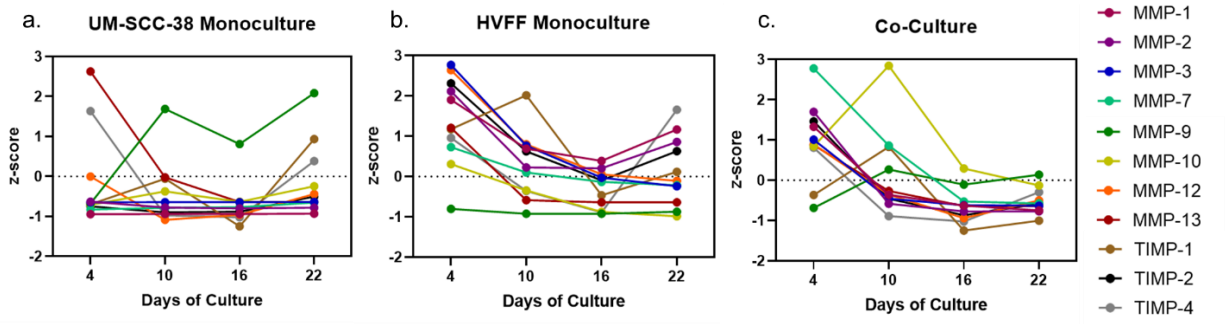

Fig. S2: Matrix metalloproteinases (MMPs) tissue inhibitors of metalloproteinases (TIMPs) quantification through time. Results shown in z-scores and grouped by experimental group.

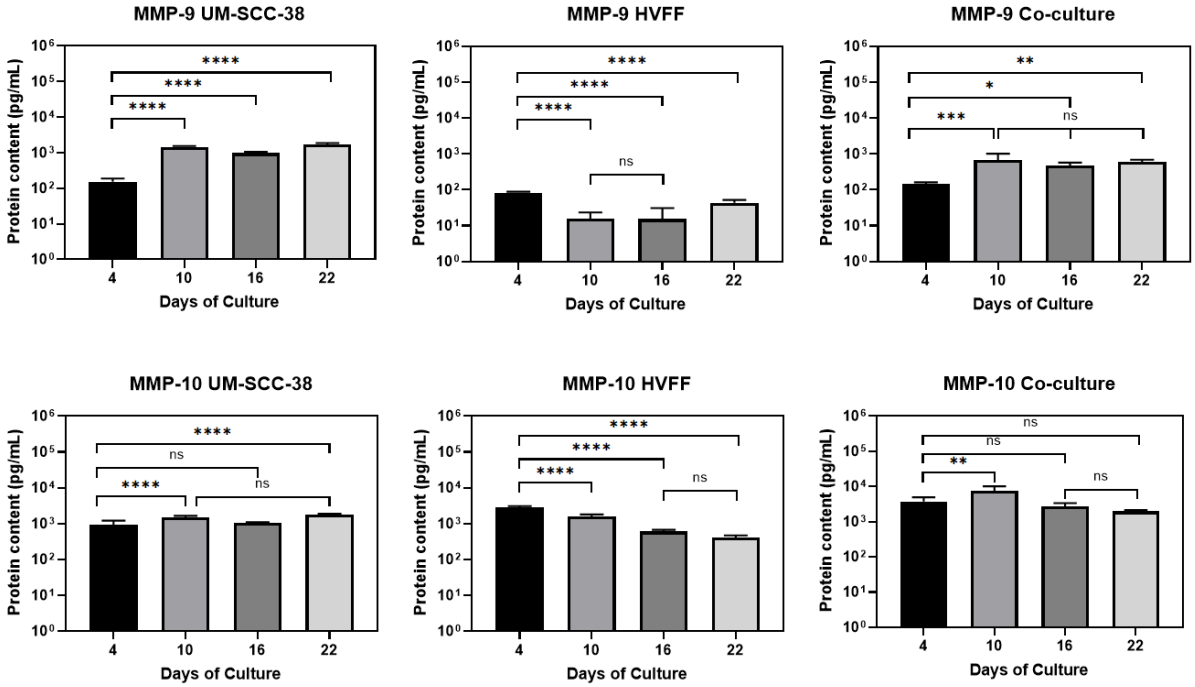

Fig. S3: MMP-9 and MMP-10 levels through time grouped by experimental group. Logarithmic y scale. One-way ANOVA followed by post hoc Tukey's test (P < 0.05).

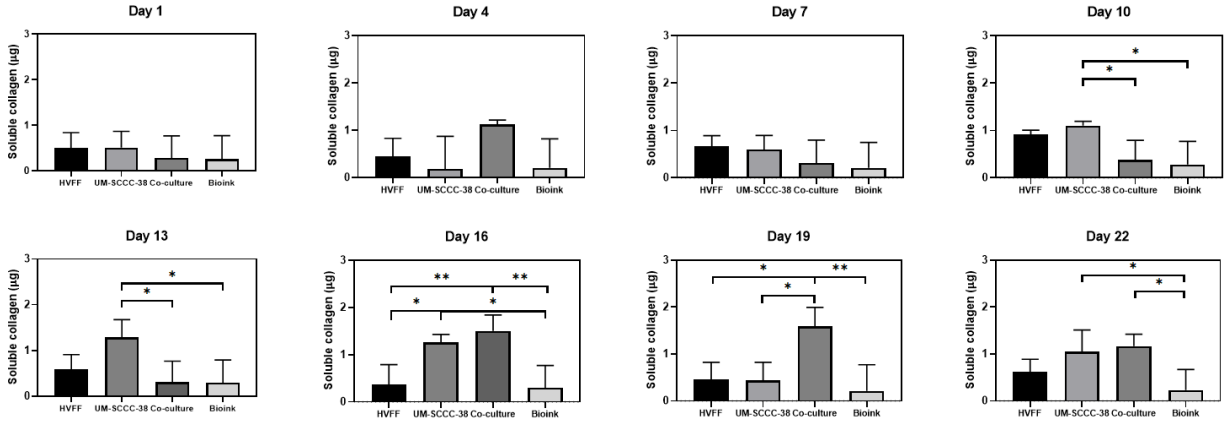

Fig. S4: Soluble collagen quantification of monocultures (HVFF and UM-SCC-38), co-culture (2:1 HVFF:UM-SCC-38), and cell-free bioink through time. One-way ANOVA followed by post hoc Tukey's test (P < 0.05), n=3.

Reprint permissions

Permission to reprint review article (Section 2.2)

Decellularized ECM hydrogels: prior use considerations, applications, and opportunities in tissue engineering and biofabrication

J. Kort-Mascort, S. Flores-Torres, O. Peza-Chavez, J. H. Jang, L. A. Pardo, S. D. Tran and J. Kinsella, *Biomater. Sci.*, 2023, **11**, 400 **DOI:** 10.1039/D2BM01273A

To request permission to reproduce material from this article, please go to the Copyright Clearance Center request page.

If you are **an author contributing to an RSC publication, you do not need to request permission** provided correct acknowledgement is given.

If you are **the author of this article, you do not need to request permission to reproduce figures and diagrams** provided correct acknowledgement is given. If you want to reproduce the whole article in a third-party publication (excluding your thesis/dissertation for which permission is not required) please go to the Copyright Clearance Center request page.

Read more about how to correctly acknowledge RSC content.

Reprint permissions of images used in the review article

Figure 2 a-b

SPRINGER NATURE

The impact of decellularization methods on extracellular matrix derived hydrogels

Author: Julia Fernández-Pérez et al
Publication: Scientific Reports
Publisher: Springer Nature
Date: Oct 17, 2019

Figure 2 c

ACS Publications
Most Trusted. Most Cited. Most Read.

Decellularized Extracellular Matrix Composite Hydrogel Bioinks for the Development of 3D Bioprinted Head and Neck in Vitro Tumor Models

Author: Jacqueline Kort-Mascort, Guangyu Bao, Osama Elkashty, et al
Publication: ACS Biomaterials Science & Engineering
Publisher: American Chemical Society
Date: Nov 1, 2021

Figure 2 d

License Number	5479051050592
License date	Jan 30, 2023
Licensed Content Publisher	Elsevier
Licensed Content Publication	Biomaterials
Licensed Content Title	Preparation and rheological characterization of a gel form of the porcine urinary bladder matrix
Licensed Content Author	Donald O. Freytes,Jeffrey Martin,Sachin S. Velankar,Annie S. Lee,Stephen F. Badylak
Licensed Content Date	Apr 1, 2008
Licensed Content Volume	29
Licensed Content Issue	11
Licensed Content Pages	8
Type of Use	reuse in a thesis/dissertation
Portion	figures/tables/illustrations
Number of figures/tables/illustrations	1
Format	both print and electronic
Are you the author of this Elsevier article?	No
Will you be translating?	No
Title	Development and Characterization of a Co-culture Model of Head and Neck Cancer Using Bioprintable Decellularized Extracellular Matrix Bioinks
Institution name	McGill University
Expected presentation date	Jan 2023
Portions	Figure 6
Requestor Location	McGill University McConnell Engineering Building 3480 University Room 350 Montreal, QC H3A 0E9 Canada Attn: McGill University
Publisher Tax ID	GB 494 6272 12
Total	**0.00 CAD**

Figure 5 a

SPRINGER NATURE

Printing three-dimensional tissue analogues with decellularized extracellular matrix bioink

Author: Falguni Pati et al

Publication: Nature Communications

Publisher: Springer Nature

Date: Jun 2, 2014

Creative Commons

BACK CLOSE WINDOW

Figure 5 b

License Number	5479051386455
License date	Jan 30, 2023
Licensed Content Publisher	Elsevier
Licensed Content Publication	Biomaterials
Licensed Content Title	3D cell printing of in vitro stabilized skin model and in vivo pre-vascularized skin patch using tissue-specific extracellular matrix bioink: A step towards advanced skin tissue engineering
Licensed Content Author	Byoung Soo Kim,Yang Woo Kwon,Jeong-Sik Kong,Gyu Tae Park,Ge Gao,Wonil Han,Moon-Bum Kim,Hyungseok Lee,Jae Ho Kim,Dong-Woo Cho
Licensed Content Date	Jun 1, 2018
Licensed Content Volume	168
Licensed Content Issue	n/a
Licensed Content Pages	16
Type of Use	reuse in a thesis/dissertation
Portion	figures/tables/illustrations
Number of figures/tables/illustrations	1
Format	both print and electronic
Are you the author of this Elsevier article?	No
Will you be translating?	No
Title	Development and Characterization of a Co-culture Model of Head and Neck Cancer Using Bioprintable Decellularized Extracellular Matrix Bioinks
Institution name	McGill University
Expected presentation date	Jan 2023
Portions	Figure 2
Requestor Location	McGill University McConnell Engineering Building 3480 University Room 350 Montreal, QC H3A 0E9 Canada Attn: McGill University
Publisher Tax ID	GB 494 6272 12
Total	**0.00 USD**

Figure 5 c

License Number	5479060071154
License date	Jan 30, 2023
Licensed Content Publisher	Elsevier
Licensed Content Publication	Materials Science and Engineering: C
Licensed Content Title	Fabrication of liver microtissue with liver decellularized extracellular matrix (dECM) bioink by digital light processing (DLP) bioprinting
Licensed Content Author	Qijiang Mao,Yifan Wang,Yang Li,Sarun Juengpanich,Wenhuan Li,Mingyu Chen,Jun Yin,Jianzhong Fu,Xiujun Cai
Licensed Content Date	Apr 1, 2020
Licensed Content Volume	109
Licensed Content Issue	n/a
Licensed Content Pages	1
Type of Use	reuse in a thesis/dissertation
Portion	figures/tables/illustrations
Number of figures/tables/illustrations	1
Format	both print and electronic
Are you the author of this Elsevier article?	No
Will you be translating?	No
Title	Development and Characterization of a Co-culture Model of Head and Neck Cancer Using Bioprintable Decellularized Extracellular Matrix Bioinks
Institution name	McGill University
Expected presentation date	Jan 2023
Portions	Figure 5
Requestor Location	McGill University McConnell Engineering Building 3480 University Room 350 Montreal, QC H3A 0E9 Canada Attn: McGill University
Publisher Tax ID	GB 494 6272 12
Total	**0.00 USD**

Figure 5 d

License Number	5479070088117
License date	Jan 30, 2023
Licensed Content Publisher	Elsevier
Licensed Content Publication	Biomaterials
Licensed Content Title	Rapid 3D bioprinting of decellularized extracellular matrix with regionally varied mechanical properties and biomimetic microarchitecture
Licensed Content Author	Xuanyi Ma,Claire Yu,Pengrui Wang,Weizhe Xu,Xueyi Wan,Cheuk Sun Edwin Lai,Justin Liu,Anna Koroleva-Maharajh,Shaochen Chen
Licensed Content Date	Dec 1, 2018
Licensed Content Volume	185
Licensed Content Issue	n/a
Licensed Content Pages	12
Type of Use	reuse in a thesis/dissertation
Portion	figures/tables/illustrations
Number of figures/tables/illustrations	1
Format	both print and electronic
Are you the author of this Elsevier article?	No
Will you be translating?	No
Title	Development and Characterization of a Co-culture Model of Head and Neck Cancer Using Bioprintable Decellularized Extracellular Matrix Bioinks
Institution name	McGill University
Expected presentation date	Jan 2023
Portions	Figure 5
Requestor Location	McGill University McConnell Engineering Building 3480 University Room 350 Montreal, QC H3A 0E9 Canada Attn: McGill University
Publisher Tax ID	GB 494 6272 12
Total	**0.00 USD**

Figure 5 e-g

License Number	5479070343004
License date	Jan 30, 2023
Licensed Content Publisher	John Wiley and Sons
Licensed Content Publication	Advanced Functional Materials
Licensed Content Title	Electrospun Extracellular Matrix: Paving the Way to Tailor-Made Natural Scaffolds for Cardiac Tissue Regeneration
Licensed Content Author	Beth Schoen, Ron Avrahami, Limor Baruch, et al
Licensed Content Date	Jul 18, 2017
Licensed Content Volume	27
Licensed Content Issue	34
Licensed Content Pages	9
Type of Use	Dissertation/Thesis
Requestor type	University/Academic
Format	Print and electronic
Portion	Figure/table
Number of figures/tables	1
Will you be translating?	No
Title	Development and Characterization of a Co-culture Model of Head and Neck Cancer Using Bioprintable Decellularized Extracellular Matrix Bioinks
Institution name	McGill University
Expected presentation date	Jan 2023
Portions	Figure 1
Requestor Location	McGill University McConnell Engineering Building 3480 University Room 350 Montreal, QC H3A 0E9 Canada Attn: McGill University
Publisher Tax ID	EU826007151
Total	**0.00 USD**

Figure 5 h-i

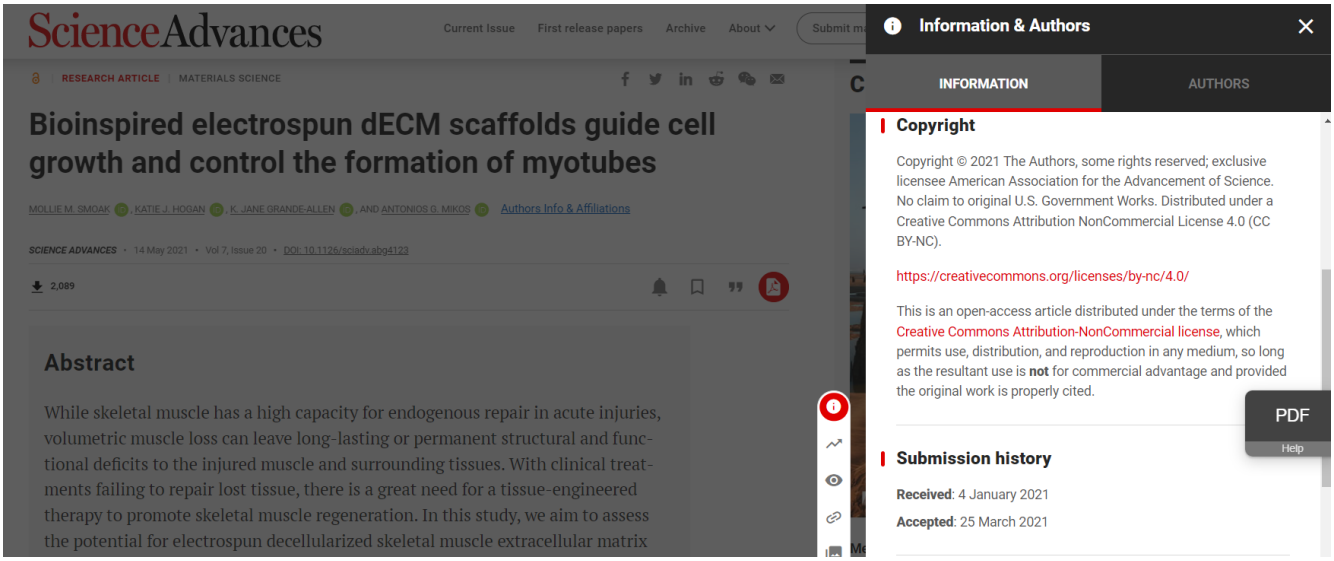

Figure 7 a-f

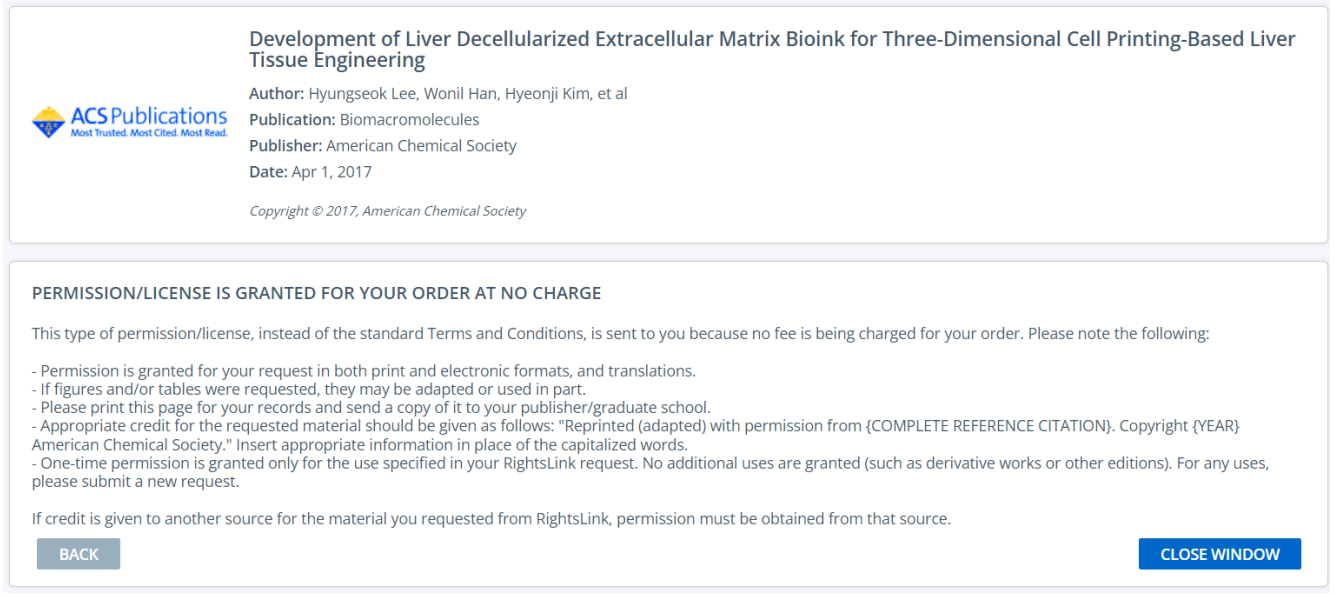

Figure 7 g-i

License Number	5479070977129
License date	Jan 30, 2023
Licensed Content Publisher	Elsevier
Licensed Content Publication	Methods
Licensed Content Title	A novel decellularized skeletal muscle-derived ECM scaffolding system for in situ muscle regeneration
Licensed Content Author	Hyeongjin Lee,Young Min Ju,Ickhee Kim,Ebrahim Elsangeedy,Joon Ho Lee,James J. Yoo,Anthony Atala,Sang Jin Lee
Licensed Content Date	Jan 15, 2020
Licensed Content Volume	171
Licensed Content Issue	n/a
Licensed Content Pages	9
Type of Use	reuse in a thesis/dissertation
Portion	figures/tables/illustrations
Number of figures/tables/illustrations	2
Format	both print and electronic
Are you the author of this Elsevier article?	No
Will you be translating?	No
Title	Development and Characterization of a Co-culture Model of Head and Neck Cancer Using Bioprintable Decellularized Extracellular Matrix Bioinks
Institution name	McGill University
Expected presentation date	Jan 2023
Portions	Figure 6 and Figure 7
Requestor Location	McGill University McConnell Engineering Building 3480 University Room 350 Montreal, QC H3A 0E9 Canada Attn: McGill University
Publisher Tax ID	GB 494 6272 12
Total	**0.00 USD**

Figure 7 j-n

License Number	5479071127076
License date	Jan 30, 2023
Licensed Content Publisher	Elsevier
Licensed Content Publication	Acta Biomaterialia
Licensed Content Title	Long-term retention of ECM hydrogel after implantation into a sub-acute stroke cavity reduces lesion volume
Licensed Content Author	Harmanvir Ghuman,Madeline Gerwig,Francesca J. Nicholls,Jessie R. Liu,Julia Donnelly,Stephen F. Badylak,Michel Modo
Licensed Content Date	Nov 1, 2017
Licensed Content Volume	63
Licensed Content Issue	n/a
Licensed Content Pages	14
Type of Use	reuse in a thesis/dissertation
Portion	figures/tables/illustrations
Number of figures/tables/illustrations	2
Format	both print and electronic
Are you the author of this Elsevier article?	No
Will you be translating?	No
Title	Development and Characterization of a Co-culture Model of Head and Neck Cancer Using Bioprintable Decellularized Extracellular Matrix Bioinks
Institution name	McGill University
Expected presentation date	Jan 2023
Portions	Figure 4 and Figure 5
Requestor Location	McGill University McConnell Engineering Building 3480 University Room 350 Montreal, QC H3A 0E9 Canada Attn: McGill University
Publisher Tax ID	GB 494 6272 12
Total	**0.00 USD**

Figure 8 a-b

License Number	5479071281014
License date	Jan 30, 2023
Licensed Content Publisher	Elsevier
Licensed Content Publication	Acta Biomaterialia
Licensed Content Title	Directing the growth and alignment of biliary epithelium within extracellular matrix hydrogels
Licensed Content Author	Phillip L. Lewis,Ming Yan,Jimmy Su,Ramille N. Shah
Licensed Content Date	Feb 1, 2019
Licensed Content Volume	85
Licensed Content Issue	n/a
Licensed Content Pages	10
Type of Use	reuse in a thesis/dissertation
Portion	figures/tables/illustrations
Number of figures/tables/illustrations	2
Format	both print and electronic
Are you the author of this Elsevier article?	No
Will you be translating?	No
Title	Development and Characterization of a Co-culture Model of Head and Neck Cancer Using Bioprintable Decellularized Extracellular Matrix Bioinks
Institution name	McGill University
Expected presentation date	Jan 2023
Portions	Figure 1 and figure 6
Requestor Location	McGill University McConnell Engineering Building 3480 University Room 350 Montreal, QC H3A 0E9 Canada Attn: McGill University
Publisher Tax ID	GB 494 6272 12
Total	**0.00 USD**

Figure 8 c-d

License Number	5479071405293
License date	Jan 30, 2023
Licensed Content Publisher	John Wiley and Sons
Licensed Content Publication	Small Methods
Licensed Content Title	Construction of Tissue-Level Cancer-Vascular Model with High-Precision Position Control via In Situ 3D Cell Printing
Licensed Content Author	Byoung Soo Kim, Won-Woo Cho, Ge Gao, et al
Licensed Content Date	Apr 28, 2021
Licensed Content Volume	5
Licensed Content Issue	7
Licensed Content Pages	12
Type of Use	Dissertation/Thesis
Requestor type	University/Academic
Format	Print and electronic
Portion	Figure/table
Number of figures/tables	1
Will you be translating?	No
Title	Development and Characterization of a Co-culture Model of Head and Neck Cancer Using Bioprintable Decellularized Extracellular Matrix Bioinks
Institution name	McGill University
Expected presentation date	Jan 2023
Portions	Figure 4
Requestor Location	McGill University McConnell Engineering Building 3480 University Room 350 Montreal, QC H3A 0E9 Canada Attn: McGill University
Publisher Tax ID	EU826007151
Total	**0.00 USD**

Figure 8 e-g

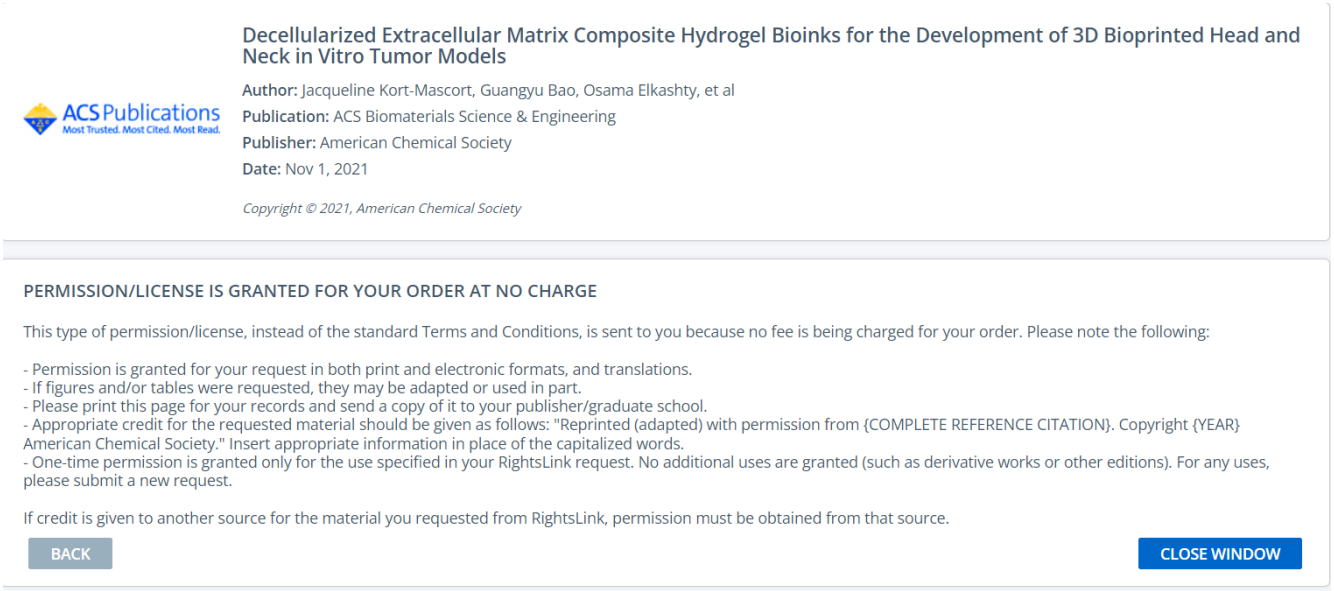

Decellularized Extracellular Matrix Composite Hydrogel Bioinks for the Development of 3D Bioprinted Head and Neck in Vitro Tumor Models

Author: Jacqueline Kort-Mascort, Guangyu Bao, Osama Elkashty, et al
Publication: ACS Biomaterials Science & Engineering
Publisher: American Chemical Society
Date: Nov 1, 2021

Copyright © 2021, American Chemical Society

PERMISSION/LICENSE IS GRANTED FOR YOUR ORDER AT NO CHARGE

This type of permission/license, instead of the standard Terms and Conditions, is sent to you because no fee is being charged for your order. Please note the following:

- Permission is granted for your request in both print and electronic formats, and translations.
- If figures and/or tables were requested, they may be adapted or used in part.
- Please print this page for your records and send a copy of it to your publisher/graduate school.
- Appropriate credit for the requested material should be given as follows: "Reprinted (adapted) with permission from {COMPLETE REFERENCE CITATION}. Copyright {YEAR} American Chemical Society." Insert appropriate information in place of the capitalized words.
- One-time permission is granted only for the use specified in your RightsLink request. No additional uses are granted (such as derivative works or other editions). For any uses, please submit a new request.

If credit is given to another source for the material you requested from RightsLink, permission must be obtained from that source.

BACK CLOSE WINDOW

Permissions to reprint research article (Chapter 3)

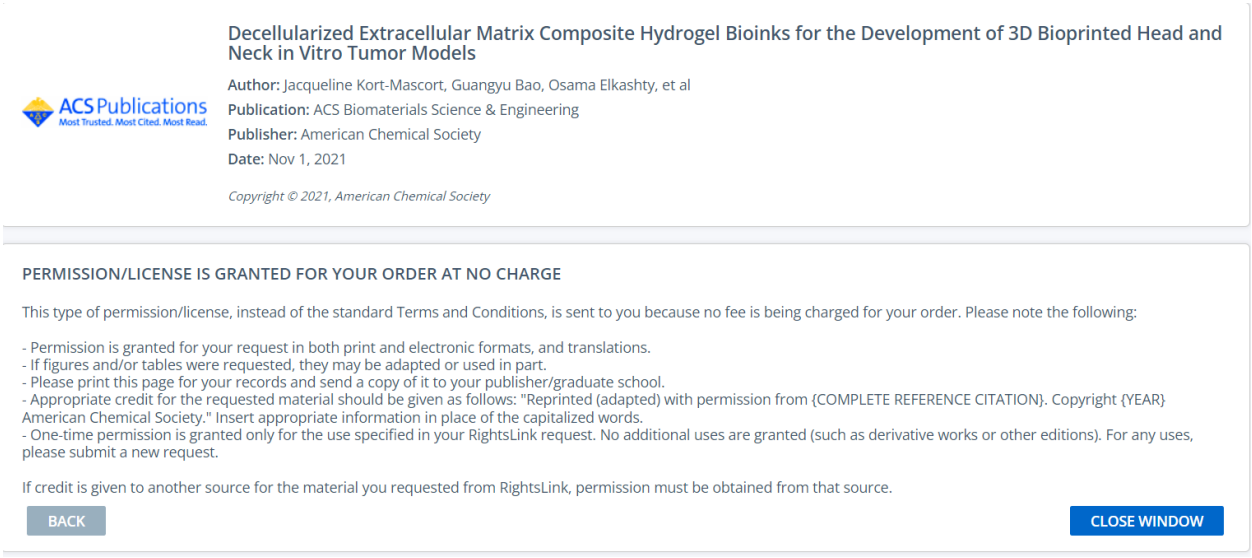

Decellularized Extracellular Matrix Composite Hydrogel Bioinks for the Development of 3D Bioprinted Head and Neck in Vitro Tumor Models

Author: Jacqueline Kort-Mascort, Guangyu Bao, Osama Elkashty, et al
Publication: ACS Biomaterials Science & Engineering
Publisher: American Chemical Society
Date: Nov 1, 2021

Copyright © 2021, American Chemical Society

PERMISSION/LICENSE IS GRANTED FOR YOUR ORDER AT NO CHARGE

This type of permission/license, instead of the standard Terms and Conditions, is sent to you because no fee is being charged for your order. Please note the following:

- Permission is granted for your request in both print and electronic formats, and translations.
- If figures and/or tables were requested, they may be adapted or used in part.
- Please print this page for your records and send a copy of it to your publisher/graduate school.
- Appropriate credit for the requested material should be given as follows: "Reprinted (adapted) with permission from {COMPLETE REFERENCE CITATION}. Copyright {YEAR} American Chemical Society." Insert appropriate information in place of the capitalized words.
- One-time permission is granted only for the use specified in your RightsLink request. No additional uses are granted (such as derivative works or other editions). For any uses, please submit a new request.

If credit is given to another source for the material you requested from RightsLink, permission must be obtained from that source.

BACK CLOSE WINDOW